Beattie, Allison Jane (2006) *Organised neural networks in culture.* PhD thesis.

http://theses.gla.ac.uk/1921/

Copyright and moral rights for this thesis are retained by the author

A copy can be downloaded for personal non-commercial research or study, without prior permission or charge

This thesis cannot be reproduced or quoted extensively from without first obtaining permission in writing from the Author

The content must not be changed in any way or sold commercially in any format or medium without the formal permission of the Author

When referring to this work, full bibliographic details including the author, title, awarding institution and date of the thesis must be given

Glasgow Theses Service
http://theses.gla.ac.uk/
theses@gla.ac.uk

Organised Neural Networks In Culture

Allison Jane Beattie

Submitted for the degree of PhD

October, 2006.

Centre For Cell Engineering,
Division of Infection and Immunity,
University of Glasgow,
G12 8QQ.

© Allison Jane Beattie 2006

Abstract

The nervous system is a collection of neural circuits that are both structurally and functionally organised within nervous tissue, and form connections to muscles and organs. The spontaneous electrical activity of neural networks seems to play an important role in the organisation and behaviour of the central nervous system (CNS). Although there exists much information regarding neuron behaviour, little is known about how these networks communicate to carry out their functional tasks. This is in part due to their complexity. The sheer number of cells that can comprise one such network, and the mass number of connections that can occur within this network, makes *in-vitro* studies of network behaviour difficult. Therefore a more simplified approach is required.

The aim of my research was to recreate simple, spatially organised neural networks in culture for the study of neural network behaviour. Spinal cord neurons were chosen as the biological model, as much is already know about spinal cord tissue circuitry *in-vivo*. These simple networks of cells were created by chemical patterning techniques (micro-contact printing (μCP)), and topographical guidance mechanisms.

μCP was used to test the hypothesis that alterations in network architecture could affect network behaviour. Changes in network structures were identified using immunocytochemical staining and scanning electron microscopy (SEM). Of the six patterns tested it was concluded that the *Jude* pattern did not satisfy the criteria required for a neural network. Cells failed to comply to the extreme angles of this design and so a hexagonal pattern was introduced. Dendritic architecture, of varying designs, was incorporated into these hexagonal networks with the aim of determining if variation in dendritic arborisation could affect network activity. An analysis of the result showed that cell morphology and connectivity was visibly altered, suggesting network characteristics were affected.

An attempt was made to create organised nerve cultures using micro-metric grooved patterns in poly-dimethylsiloxane (PDMS). The cellular response was determined by immunocytochemical staining and SEM imaging. Cells grown on micrometric topographical patterns did not align within the grooves as predicted. Therefore the effect of nano-metric pillared topography, created in poly-caprolactone, on nerve cell guidance was

investigated. In comparison to the flat material, this nanotopography reduced cell adhesion, although it was not completely non-adhesive. After 1 week cells were visibly aligning to the topography, at the micro- and nanometric level, and appeared to be growing longer processes compared to the cells grown on flat structures. This result suggests nanopillared topography has a promising future in nerve guidance studies.

The spontaneous electrophysiological activity of the cultured neural networks was investigated using multi-electrode arrays. Two devices, the flexible array and the planar array were used in this study. The aim was to compare the electrical activity of random networks with that of the spatially arranged cultures. Although random spinal cord cultures were characterised as displaying rhythmic firing patterns (which consisted of repeated spike bursts), no electrical activity was recorded from organised neural networks under the same conditions. Therefore the fundamental question, how does cell morphology and network architecture contribute to network behaviour remains unanswered. However, the author believes the methods for achieving this goal have been thoroughly investigated within this thesis and a conclusive result could be obtained in the near future if these are applied.

I hereby declare that all work presented in this thesis is my own, unless where otherwise stated.

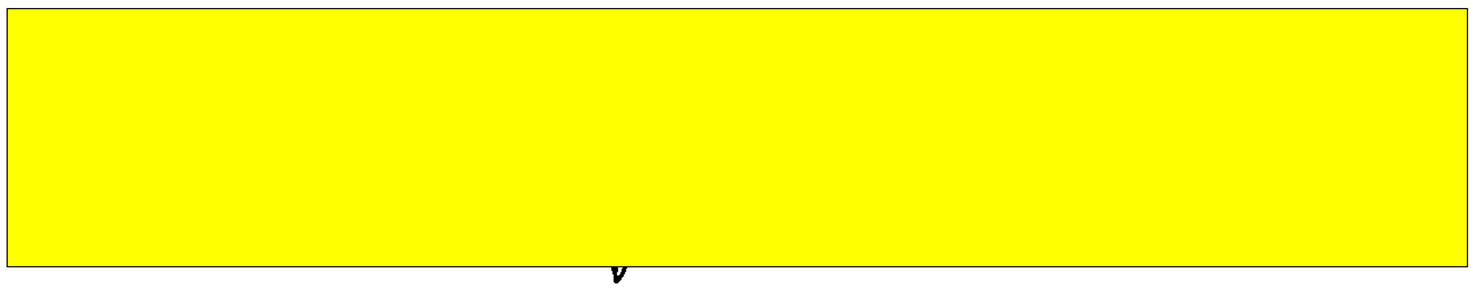

Allison Jane Beattie.

Acknowledgements

Not many have three supervisors. Fewer still have three great supervisors.

To Adam, I would like to thank you for feeding me coffee on those cold mornings when the lab was empty (except for the truly dedicated!!!), for not laughing (too much!) at my bad spelling and atrocious grammar, and for listening to my endless tales of highland dancing. I would also like to thank you for your encouragement and support, and for treating me as an equal despite the fact you were, quite literally, publishing papers before I was born!!!
To Chris, this work would never have been possible without *The Jude,* and now *The Judith.* You have been an inspiration to me throughout, always encouraging and always finding the positive, and most importantly, always making me smile with my favourite catch phrase *'Oh Goodie!'*.
To Mathis, this thesis could not have been produced without your continual help and support. I have learnt so much from you in past 4 years, and I hope our relationship has taught you a few things too.....hormonal PhD students will always use emotional blackmail to get you to, fix the printer, reset the microscope, sort the embosser, change the filter, fix the computer, load the programme, change the setting, update the software, download the picture, order the media. Thank you ;-> x.

When (or if) you read this thesis you will come across the name Rongyu Tang more than once. He is the other half, so to speak, of this project. Thank you Rongyu for sharing this experience with me, it would never have been the same without you. Our *School Trips* to the NeuroSilico meeting always had me in stitches with your funny tales of growing up in China. I hope one day our paths will cross again, but if not, I wish you health, happiness, and prosperity in the future. (*We did it, we got recordings!!!*)

Many thanks to those who have also contributed to this thesis; CCE technicians Andy, Anne and Gregor, thanks for all your help over the years, I will miss you guys sooo much! Mary Robertson and Sarah MacFarlane for their help with the fabrication work and SEM imaging, Margaret Mullin for preparing my samples, and to Sue Barnett and her lab for their help and support in the final months, especially Annette Sorensen for helping me obtain the wonderful images that are presented within (cheers Annette!!)

At CCE, I would like to thank Cath (who provided support and instruction at the start) and Matt (who provided support and instruction at the end), Lucia and Elena for teaching me the skills of coffee making (*no, add more coffee!*) and finally Osian, for his advice and masterly SEM skills (and his culinary delights) and, my Thesis Production Manager, Mairead, for her help, support, and words of advice and encouragement (*just write it!!!*). Cheers Maw!

I would also like to take this opportunity to thank Mary-anne (fellow dancing geek) and the McCreadie Girls (my dancing buddies); Amanda, Laura, Liza, Lee-anne, Kim, Terry and Doms (The Best Looking Dancers in Scotland!). Thank you all for welcoming me into your school, and making me one of the team. The long days in the lab were never as bad when I had a class to got to afterwards. CU @ Oban 2009!!!

And last but by no means least, I would like to thank my family.
To Mum and Dad, thank you so much for believing in me, and for telling me I can, when others have told me I can't. Not only has your emotional support helped me through this time but also your financial support for which I will always, always be grateful (I promise Dad, you will get your change!).
To Laurie, You are the best sister a girl could have! Thank you for letting me escape to your house in times of need (my second home), love ya babes!
To Stu (aka Dr.Miles), ha ha less than 4 yrs, beat ya!!! Now there are 2 of us (dumb blonde doctors), we must join forces and conquer the world!!!!
To Stan and Moira, Thank you for letting my steal your son away to Glasgow, and now Pittsburgh.

.....and finally.....

To My Darling Derek *(Honouree Member of CCE),*

It is now 2am on the morning of binding, Derek is checking each of the 4 thesis print outs, page for page, he has also painstakingly checked all the figures, and the tables, and the graphs, and the contents pages to be sure they match, never once complaining.

Thank you for listening to talk of nerve cell cultures night, after night; for not moaning when I woke you up in the middle of the night after a mammoth session typing, and for not complaining when I took the face of the you following morning when *you woke me up, getting ready for work*; for supporting me finically and mentally throughout, and for picking me up when I was down.

I could never have done this without you, and for that I am eternally grateful.

Allison x

(*We did it!!! Wooo Hooo!!)*

Table Of Contents

Chapter 2. Characterisation of Spinal Cord Cultures

Chapter 3. Micro-contact Printing to Create Neural Networks

Chapter 4. Investigation of Structure-Function Relationship in Neural Networks

Chapter 5. Nerve Cell Responses to Micrometric and Nanometric Topography

Chapter 6. The Application of Multi-electrode Recording Devices to Investigate Neural Network Behaviour

Chapter 7. Final Discussion

Figures Index

Chapter 4. Investigation of Structure-Function Relationship in Neural Networks

Chapter 5. Nerve Cell Responses to Micrometric and Nanometric Topography

(Chapter 5. continued...)

Chapter 6. The Application of Multi-electrode Recording Devices to Investigate Neural Network Behaviour

Graph Index

Tables Index

Abbreviations Index

Acronym	*Definition*
AA3.....	Proteolipid Protein Stain
AB	Antibody
ACM	Astrocyte Conditioned Media
Anti.B	Antibiotics Solution
AP	Action Potential
B27	B27 Media Growth Supplement
BSA	Bovine Serum Albumin
CAM	Cell Adhesion Molecule
C_4F_4	Carbon Flouride Gas Compound
CCE	The Centre For Cell Engineering
CNS	Central Nervous System
CO_2.....	Carbon Dioxide
Conc.	Concentration
DMEM	Dulbecco's Modified Eagle Medium
DNA	Deoxyribonucleic Acid
E14	Embryo (14 days into gestation)
ECM	Extracellular Matrix
EM	Electron Microscopy
FCS	Foetal Calf Serum
FGF	Fibroblastic Growth Factor
FITC	Fluorescein
GABA	Gamma-aminobutyric acid
GFAP.....	Glial Fibrillary Acidic Protein
HBSS	Hanks Balanced Salt Solution
H_2SO_4	Sulphuric Acid
HEPES	*4-(2-hydroxyethyl)-1-piperazineethanesulfonic acid*
H_2O_2	Hydrogen Peroxide
IBLS	Institute of Biomedical and Life Sciences
IgG	Immunoglobulin Class G
IgM	Immunoglobulin Class M
K^+	Potassium
ITS	Insulin Transferrin Selenite
MAP	Microtubule Associated Protein
µCP.....	Microcontact Printing
Mg^{2+}	Magnesium
MEA	Multi-electrode Array
MEM	Minimum Essential Medium
MT	Microtubule
Na^+	Sodium
NaCl	Sodium Chloride
NBA	Neurobasal A Media
NF	Neurofilament
NT	Neurotransmitter
P1.....	Postnatal (1 day old)

Abbreviations Index *(Continued)*

Acronym	*Definition*
PBS	Phosphate Buffered Salt Solution
PDMS	Poly-dimethylsiloxane
Pen /strep	Penicillin/Streptomycin Solution
PLL	Poly-l-lysine
PIPES	PIperazine-NN'-bis-2-ethane sulphonic acid
Qsil 215	Transparent Liquid Silicon Rubber
RO	Reverse Osmosis
RYT1	Etch Recipe
S.....	Serum
SEM	Scanning Electron Microscopy
SDS	Sodium Dodecyl Sulphate
SF_6	Sulphur Hexaflouride
TRITC	Tetramethyl Rhodamine Iso-Thiocyanate
UV	Ultra Violet
W/O	Without

Symbols Index

cm	Centimetres
dia	Diameter
°C	Degrees Celsius
°	Degrees
g	Grams
kD	Kilo Dalton
<	Less Than
L	Litre
>	More Than
µl	Microlitres
µm	Micrometres
ml	Millilitres
mm	Millimetres
mM	Millimoles
mV	Millivolts
M	Moles
n	nano
%	Percent
1°	Primary
rpm	Revolutions per minute
2°	Secondary
**	Significance at 0.01 Level of Probability
*	Significance at 0.05 Level of Probability
3x	Number of times treated (ie. three times)
V	Volts
Vin	Volts In
Vout	Volts Out
Vm	Membrane Potential

Chapter 1.

Introduction

1. General Overview

The term neuroscience covers a vast area of science and scientific research, from neuro-anatomy (the mapping of the fundamental structures of the brain and nervous system), behavioural neuroscience (the existence of memory, conscious thought and perception), to molecular and cellular function of nervous tissue (the molecular interactions that govern all of the aforementioned subjects). The knowledge and understanding that scientists and researchers have today in all of these different areas is credited to centuries of theoretical analysis and investigative research.

The first ever-recorded neuroscience experiment can be traced back to the time of the Egyptians, as archaeologists have discovered many mummified cadavers with cranial injuries of surgical precision (Kingsley 2000). The evidence of bone healing suggests that these incisions were preformed pre-death, and were the result of explorative experiments into the function of the brain, although the association of the brain with cognitive processing came much later on in history. It was first believed that the structure of the heart governed the process of mental thought and reason (teachings of Aristotle, 335 B.C), rather than the brain. However, investigation into the structure of the brain revealed its true identity, although identifying the mechanisms through which the brain carries out its function proved more challenging. There have been numerous attempts to theorise brain function. Some of the earlier theories, such as those of Galen (A.D.130-200), who believed the nerves, like blood vessels to be hollow, and that nervous systems communicated by the movement of liquid, now seem completely absurd, all have contributed in some way to providing the wealth of knowledge that now exists in today's academic society (Bear 2001). Almost all early experiments set out to prove or disprove testable conjectures of scientific contemporaries, which in turn lead to new opinions and speculations and so on, creating a driving force for scientific discovery. However, it has only been in the last 100 years, with advancements in technology and specialised research equipment that the study of neuroscience has really excelled, and now covers a broad field of scientific research including pharmacology, computational biology, developmental neurology, physiology and psychology. However, despite the personnel and finances that are dedicated to each of

these fields, there are still numerous questions that need answering, therefore even now, 5000 years on from the first-ever recorded neuroscience experiment, discoveries within the field of neuroscience are still to be made. This is most evident when one considers the plight of those affected by neurological trauma or those afflicted with neurodegenerative diseases, such as Alzheimer's or Parkinson's disease. Neurologists, Psychiatrists, Neurosurgeons and Neuropathologists, the different medical professionals who benefit from neuroscience research, may have the knowledge and know-how to control these disorders but they are unable to cure them. This is due to the lack of concrete evidence to explain the phenomenon of neural network plasticity, the ability of the cells that form the nervous system to continuously rewire, and the mechanisms underlying network function.

Although neural networks are found throughout the nervous system, they are most complex within the structures of the brain and spinal cord, the elements of central nervous system responsible for cognitive actions and motor control. Within each of these structures there exists many networks, where any given network, for example, may comprise of anything from 1000 to 20,000 cells, with one cell alone potentially connecting with over a thousand cells. It is this shear complexity of connections that has hampered the understanding of network function.

In this thesis an attempt will be made to develop a means to investigate the underlying principles of neural network function by recreating simplified circuits in culture. It is hypothesised that by drastically simplifying neural networks (by applying patterning techniques such as microcontact printing (μCP), described in Chapter 3, or structural topography, which is described in Chapter 5) we can eliminate the factor of complexity. By reducing the number of cells within a network, the synaptic modifications that occur within a network can be closely scrutinised for changes in synaptic strength and firing rates. However, it is proposed that to do this successfully it is essential that the network characteristics that exist *in-vivo*, such as network dimensions and cell morphology are represented in the pattern design. To investigate this theory, the network patterns used in this study will consist of varying geometric designs, with the aim of identifying the relationship between cell morphology, network structure, and behaviour and function. In the remainder of this chapter I will provide a historical review of relevant publications, then I will introduce the basic anatomy of neural networks, what drives network formation during development, and finally how networks communicate to convey their information.

2. Review of Relevant Literature

Creating Neural Networks

Although cell culture is an extremely useful tool for the study of cellular responses, many of the connections between neurons are lost during the dissociation procedure used to form primary cell cultures, providing little benefit when trying to investigate activity of multiple cells within a neural network (Detrait *et al.* 1998, Dodd *et al.* 1988, Potember *et al.* 1998). A number of early investigators set out to solve this problem by introducing engineering protocols into the study of neuroscience (Matsuzawa *et al.* 1996). The interface between biological systems and engineering materials has been the key element in the development of neuro-engineering (Cornish *et al.* 2002). In 1988, Kleinfield *et al.* conducted one of the first studies aimed at reconstructing the innate architecture of neurons in intact tissue, in cell culture conditions (Kleinfield *et al.* 1988). In order to produce an organised network of cells, Keinfield *et al.* first set out to investigate the adhesive properties of different substrate material available. They used photolithographic (Curtis *et al.* 1998) techniques, adapted from semi-conductor technology, whereby a surface is coated with photoresist, then exposed through lithographic mask with the desired pattern and developed to etch resist from exposed areas to define regions of the network pattern. Alkane chains were covalently bound to the open areas in the resist, by refluxing the substrates in alkyltrichlorosilane solution, to create regions of low cell adhesion. After plating, primary rat spinal cord neurons were maintained for up to 12 days, during which time phase contrast microscopy and immunocytochemistry analysis identified cells conforming to the underlying pattern.

This early example of combining silicon technologies and neurobiology produced conclusive results to support the use of such methods in creating organised cultures. However, subsequent studies were slow to follow, despite this being an intriguing and interesting study with plenty of scope for investigation. For example, since the smallest detail of the pattern to which cells conformed was only 50μm, it is surprising that studies aimed at investigating other geometrical patterns did not appear in the scientific literature thereafter. One explanation for the lack of similar studies around this time is that the techniques described in this paper are rarely available to most biologists. Therefore, research groups wishing to follow such procedures would require a close collaboration with

an electrical engineering department or an institute with etching facilities, something that has rarely been required for biological studies in the past.

The Centre For Cell Engineering, at Glasgow University, was founded based on this realisation; that to study the effect of manipulating cell substratum on cell behaviour would require a strong association between biological and engineering sciences. The work of A.S.G Curtis and C.D.W Wilkinson in the late 1980's (Clark *et al.* 1987) and early 1990's (Clark *et al.* 1990, 1991, Curtis *et al.* 1992, Wojciak *et al.* 1995) introduced the use of topographical guidance into cell studies. Exploiting the phenomenon of contact guidance (the alignment of cells to fibrous structures, Curtis *et al.* 1998), Curtis and Wilkinson (1998) explored various etching techniques to create cell culture substrates of varying topographies. The groove-ridge structure is a classical example of how structural changes in the culture surface can strongly influence the behaviour of cells. Cells including epitenon (Wojciak *et al.* 1995), heart fibroblasts, kidney cells, cerebral neurons (Clark *et al.* 1987, 1990), spinal cord neurons (Clark *et al.* 1993) and hippocampal neurons (Rajnicek *et al.* 1997) have been shown to align to a groove/ridge structure. Interestingly, the response recorded for each cell type depends entirely on the dimensions of the substrate topography. For example, spinal cord neurons *Xenopus laevis* will align in parallel to grooved structures 1μm wide, ranging from 14 to 1100 nm deep. However, under the same experimental conditions, hippocampal neurites will align perpendicularly (Rajnicek *et al.* 1997).

Although photolithography has provided a useful means of creating patterned substrates at the micrometer level, its use of harsh solvents and bases make it incompatible with many biological molecules, causing research groups to experiment with various other techniques (Clark *et al.* 1993, James 1998). Biologically important proteins such as laminin and fibronectin, are of particular interest to scientists as these proteins, unlike purely adhesive biomolecules such as poly-l-lysine, can induce specific cellular responses such as directed growth guidance and differentiation (Kam *et al.* 2001). As interest in biologically based neuronal processing increased, laboratories began to explore and devise new methods to obtain well-defined neuronal circuits in culture (Chang *et al.* 2003, Corey *et al.* 2003). In the late 1990's microcontact printing (μCP), a new method of producing patterned protein layers, was introduced which had specific importance to a number of emerging technologies including advanced tissue engineering, biomineralisation, DNA computing

and cultured neural networks (James 1998). μCP was the first 'soft lithography' and has revolutionised neural network biology today. This method of surface modification uses high relief elastomeric stamps, versatile cross-linking chemistry, commercially available reagents, and is constrained only by photolithographic techniques and surface chemistry (Cornish *et al.* 2002, Lauer *et al.* 2001a). As described in the introduction to Chapter 3, there are two main methods of μCP: chemisorption μCP and physisorptive μCP. Although these methods have not been directly compared within this thesis, there is already sufficient evidence within the scientific literature to support the method of choice: physisorption μCP. The series of publication by Vogt *el at* have shown physisorptive μCP is an effective method for creating adhesive patterns on a non-adhesive background (Vogt *et al.* 2005a, Vogt *et al.* 2005b, Vogt *et al.* 2003, Vogt *et al.* 2004, Vogt *et al.* 2005c). Using such methods defined neural networks can be maintained in culture for long periods of time. However, in all of these aforementioned publications, only simple linear network geometries have been considered. It is arguable that linear networks do not truly reflect the network arrangement that is found *in-vivo,* and that the dramatic alteration of cell morphology that occurs throughout such patterns can influence the network activity, and therefore network behaviour. In order to address this issue, I will consider geometric designs that incorporate neuron morphology into the network patterns.

Recording Network Behaviour

Creating neural networks is only part of the challenge that exists when trying to understand the behaviour of organised networks. Once networks have been created, changes in electrical activity between the cells of the network must be recorded, as these signals are significant to neuro-processing. Traditional electrophysiological recording systems, such as intracellular microelectrode recording, patch-clamp and voltage-clamp (see Introduction to Chapter 6) cannot be applied to such studies as they only to allow one cell or two cells to be recorded simultaneously. Multiple extracellular recording arrays, an essential criteria for recording network activity, have, however, been designed for this purpose.

The first multi-electrode array (MEA) systems appeared in 1980s as a means of monitoring the long-term activity of spontaneously firing networks. These first studies aimed to identify the changes in firing pattern that occur over time within a random network by maintaining dissociated cultures on MEA devices and recording activity over a number of

weeks (Droge *et al.* 1986). This work identified that spontaneous activity is not random but in fact can consist of bursting sequences occurring in consistent cycle periods, although consisting of varying degrees of regularity (Darbon *et al.* 2002). It has also been shown that these patterns can be altered by the chemical composition of the network environment (Gross *et al.* 1997). Further studies have gone on to investigate the relationship between rhythmic bursting patterns and pharmaceutical compounds, and it is now widely accepted that neural network dynamics can be altered by neurotransmitters and their blockers (Bracci *et al.* 1996, Chiappalone *et al.* 2003, Harsch *et al.* 1997, Selinger *et al.* 2004). This approach has lead to the intensive use of *in-vitro* cultured neurons, coupled to MEA devices as a biosensing system for neuropharmacological applications (Martinoia *et al.* 2005). However, although such studies have been beneficial for pharmaceutical development, they have failed to address the question of how the electrical activity of the network correlates to its underlying function. In this study I will use such devices to try and answer this question.

3. The Composition of Neural Networks

The neural networks that form the fundamental structures of the brain and spinal cord are in fact composed of a matrix of different cell types. These cells can be broadly categorised into two main groups; neurons, the cells the carry out CNS function, and glia, the cells that support them. However both these cell types can be further categorise into different cell sub-types based on their function or location in the CNS.

The Neuron

The smallest active unit of the nervous system is the nerve cell or *neuron*. In general, the main function of a neuron is to receive, transform and send information through a specialised signalling mechanism. Although there are different types of nerve cell, each with its own distinct morphology, all consist of three basic units: dendrites, cell body and axon (see Figure 1.1).

The Cell Body

Like all mammalian cells, the internal structures of the nerve cell are contained within a doubled layered phospholipid membrane, which consists of integral proteins that form channels, pumps and signalling complexes. The biophysical properties of the nerve cell membrane and cytoplasm leads to the development of a diffusion potential across the membrane, resulting in the inside of the nerve cell being negative in comparison to the outside. The movement of ions, and the charge distribution across the nerve cell membrane is an important feature when going on to consider the signalling properties of the neuron, as the resulting gradient is the driving force for signal transduction (described in more detail in section 4 of this Chapter: *Neuron Communication, Excitable Membranes*). The energy that is required to maintain this gradient is provided by the abundance of mitochondria within the cytoplasm. Also within the cytoplasm are the common cell structures of the Golgi apparatus, endoplasmic reticulum and nuclear membrane, as well as the fundamental structures of the cell cytoskeleton.

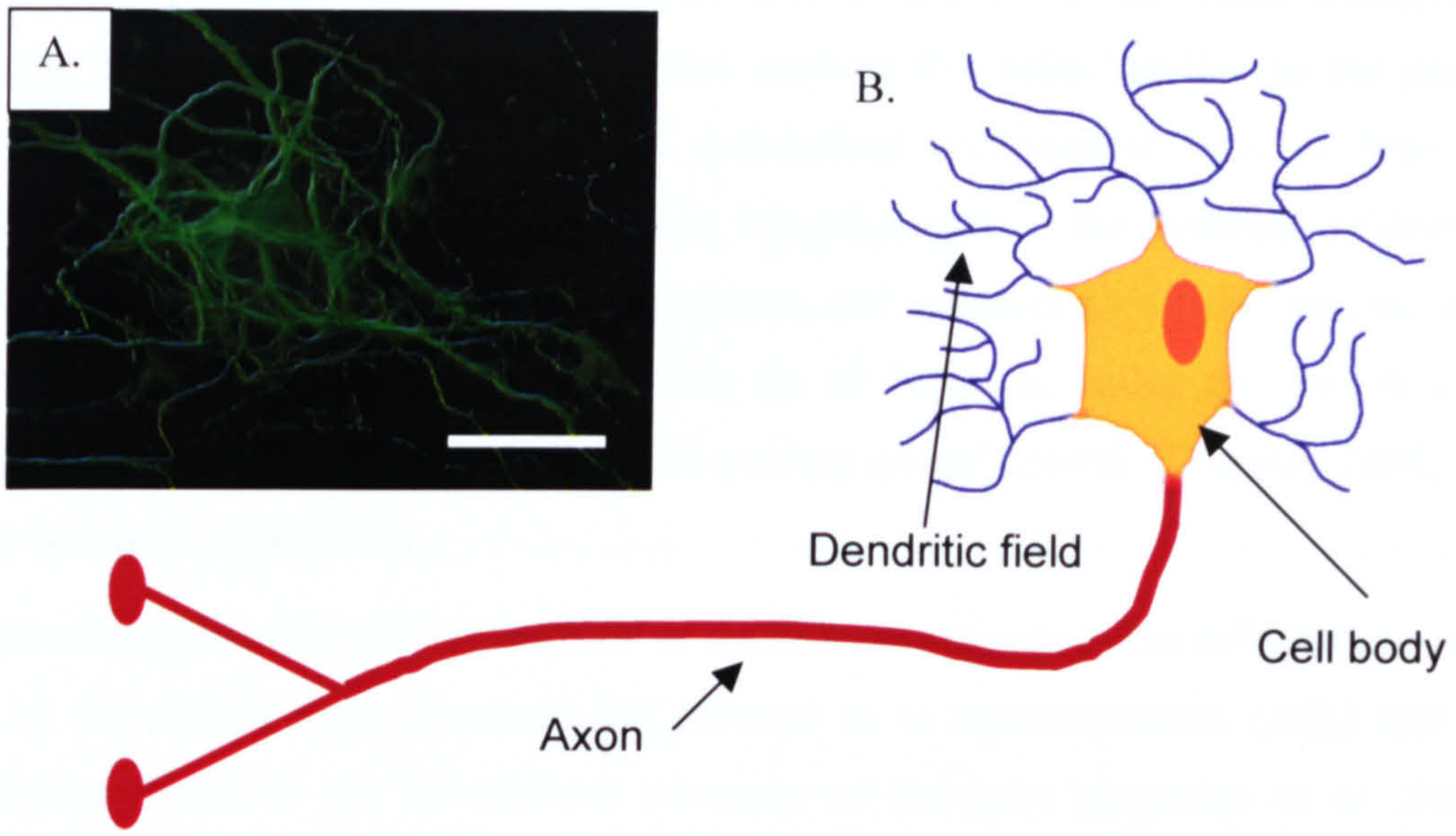

Figure 1.1. Image B is a schematic representation of a nerve cell showing the three fundamental structures which give this cell type its distinct morphology: cell body, axon and dendritic processes (which form a highly branched field surrounding the cell body). Image A is of a real neuron in-vitro, fluorescently labelled with cytoskeletal marker, ß-tubulin (scale bar is 50µm).

The cytoskeleton of a mammalian cell is a complex matrix of readily polymerising, and depolymerising protein filaments. The primary role of the cell cytoskeleton is to act as an internal scaffold to maintain the structure and shape of a cell, allow cell motility and internal transport. This structure is not completely rigid as the name suggests, but has a flexible composition, allowing a cell to adapt to the ever-changing external environment over time. However, the cytoskeleton is also involved in a diverse range of other activities. It is through the cytoskeleton that cell growth and motility are achieved, and the cytoskeleton also plays a fundamental role in cell division and cell polarity, although the exact role of the cytoskeleton depends on the cell type. In the nerve cell the cytoskeleton is responsible for maintaining neuronal morphology, as well as neuron function by playing a key role in the transport of substances and organelles from the cell soma to the distal regions of the axon (called the synaptic bulb), a circuital process for chemically mediated signal transmission (Brown 1991). The three major components of the cytoskeleton are actin filaments, microtubules and intermediate filaments (Alberts *et al.* 1994).

The actin filaments are the smallest of the matrix filaments, ranging from 5-8nm in diameter (Pannese 1994). These filaments form protein networks beneath the plasma membrane, and are linked to the exterior of the cell through transmembrane molecules called integrins and cadherins (Kingsley 2000). The extracellular integrin interprets the

cells surrounding environment. This information is relayed to the actin arrangement through the internal integrin binding site that anchors the actin bundles to the plasma membrane through their association with cytoskeletal components such as talin and vinculin. The binding and clustering of bound integrins leads to the assembly of docking molecules, and the development of focal contacts and adhesions. In the neuron, actin filaments are primarily located in the growing tip of the axon, called the growth cone, where their primary function is mediating and guiding axonal growth (Kingsley 2000, Luo 2002, Mallavarapu *et al.* 1999).

The intermediate filaments play a structural or tension bearing role in the cell (Alberts *et al.* 1994). In the neuron these filaments are referred to as neurofilaments (NFs) and are predominantly found in the cytoskeletal structure of the axon (Lavedan *et al.* 2002), although they occur in small numbers in the dendrites, where they are scattered in single units (Diaz-Nido *et al.* 1996). The exact role of NFs is still unclear, although there is now increasing evidence to suggest they are involved in maintaining axon diameter and stabilising axon branching (Letournel *et al.* 2006, Smith *et al.* 2006).

Tubulin is the monomeric compound of microtubules (MTs). However, in addition to tubulin, MTs also contain small amounts of other proteins called microtubule associated proteins (MAPs) and tau proteins (Alberts *et al.* 1994, Pannese 1994). In neurons microtubules are major determinants of the highly complex neuron morphology, in particular cell polarisation. There are a number of different isoforms of MAPs. During neuron development these play specific roles in the regulation of both axon and dendrites by accumulating at the site of future growth following the activation of internal signalling pathways in response to certain extracellular signals, including neurotrophic factors like nerve growth factor (NGF), and extracellular matrix molecules (ECMs) like laminin. In the mature neuron MAPs are differentially associated with each structure (Brandt 2001, Diaz-Nido *et al.* 1996, Levitan & Kaczmarek 2002). MAP-2, for example is located in neuron cell bodies and in dendrites but not in axons, whereas MAP-1 is found only in axons (Sanchez *et al.* 2000). Tau proteins, however, are distributed throughout the axon structure only and are not found in dendrites (Brandt *et al.* 2005). As well as providing structural support, MTs are also involved in axonal transport through their association with MT motor proteins by providing tracks for the transport of molecules from, and to, the cell body and the distal extremities of the cell (Chevalier-Larsen *et al.* 2006, Sanchez *et al.* 2000).

Dendrites

Protracting outwards from the cell body are thin spindle-like processes called dendrites. As the cell grows the dendrites continuously branch giving way to an elaborate field of fibres termed the dendritic tree. This has the effect of significantly increasing the surface area of the cell and therefore the area available for contact with other cells. The structure and arrangement of the branches within the tree formation vary from one cell to another, accounting for the physical differences in nerve cell morphology. On the surface of the dendrites are minute protrusions called dendritic spines, these are the synaptic inputs sites where a neuron will receive information from another cell. However the role of the dendrite is not only to receive information, some dendrites also possess the ability to transmit electrical signals to other cells.

The Axon

The axon, a thin tube-like process, up to 1m in length, originates at a cone-shaped protrusion of the cell body called the axon hillock. During axon outgrowth the terminal end of the axon is guided by a sensory, highly motile structure called the growth cone. The growth cone actively searches for, and then interprets the directional growth information present in the local extracellular environment. In the mature neuron the terminal end of an axon will hold a specialised region involved in signal transmission called the synaptic bulb. This appears as an enlarged area where the specialised secretary vesicles containing neurotransmitters, responsible for the chemical mediation of signal transmission, are located. Like dendrites, some axons are extensively branched, the branching most often occurring at the distal regions of the axon where the synaptic interaction sites are located. As with dendritic branching, this has the effect of increasing the area for cell-cell connectivity.

Types of Neurons

Neurons can be classified by their functional role in the CNS. Sensory neurons for example, convey information about the body's external environment (such as olfactory neurons, which process the sensation of smell), whereas other cells, such as motor neurons, relay commands issued by the higher centres of the brain. Some neurons only connect with other neurons, these are called interneurons, whereas sensory and motor neurons connect

with sensory receptors and muscles respectively. However, not all cells within the CNS can be categorised by their function as there are simply too many to label with a specific role. It is possible to identify neurons types instead by the molecules they secrete during chemically mediated signal transmission. For example if a cell releases a molecule that initiates activity in another cell, it is called an excitatory neuron, where as if this chemical suppresses the potential for excitation, the cell is called an inhibitory neuron (see section 4 of this chapter, *Neuron Communication, Chemical Excitation*). Neuron morphology can also provide information on cell function. Although, to a degree, no two neurons are structurally identical, there exists three fundamental nerve cell shapes; the bipolar neuron that has two main processes extending from its cell body (a single axon and dendritic process arise from the cell body, although both then branch significantly thereafter), the pseudounipolar neuron which has two axons, and the multi-polar neuron which has many processes extending from the cell body, although only one of these is an axon. Examples of the *in-vivo* shapes of different types of neuron are illustrated in Figure 1.2.

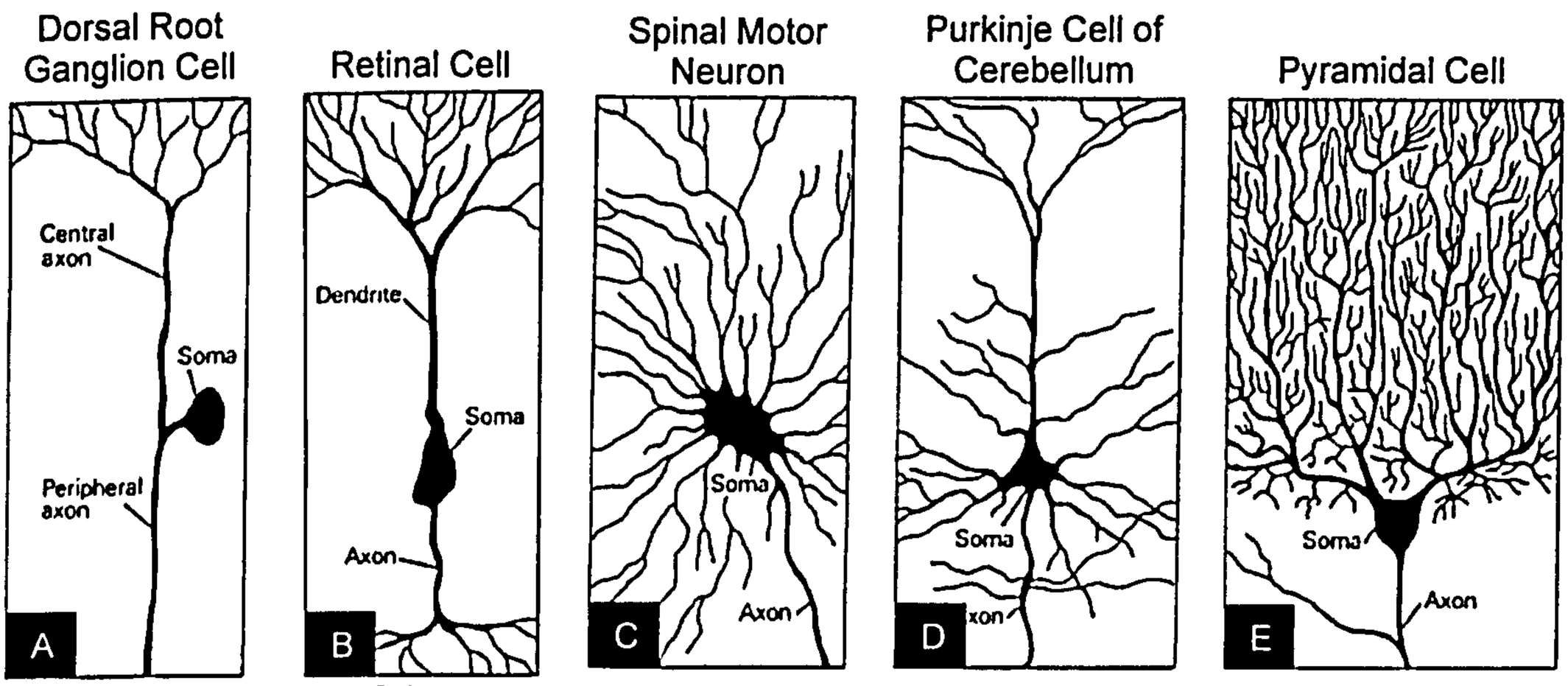

Figure 1.2. An illustrated example of the three types of neurons categorised by their basic morphology- as represented by a 2-dimensional projection. The dorsal root ganglion cell (A) is a pseudounipolar neuron found in the spinal cord, where one axon extends into the periphery and the other into the CNS. The retinal cell (B) is a bipolar neuron. The spinal motor neuron (C), purkinje cell (D) and pyramidal cells (E) are all examples of multipolar neurons. Image taken from Neurophysiology Of Vision (Court 1997)

The Glial Cells

Glial cells are the support cells of the nervous system, providing a chemically and structurally sound environment for neuronal growth. The term 'glial cell' in fact consists of a broad category of various subtypes (Jessen 2004, Pfrieger *et al.* 1996). Within the CNS

alone there exist 4 types of glia; astrocytes, oligodendrocytes, ependymal cells and microglia (Kufflerl *et al.* 1984); however, only the two main types, astrocytes and oligodendrocytes, will be considered in this general overview.

Astrocytes

The astroglia comprises a 'family' of related macroglial cells that express different morphological phenotypes with diverse and region-specific functions (Muller *et al.* 1995). This cell type is distinct in its morphology with wide radiating arms that interweave between neuronal cell bodies and surrounding fibres (Jessen 2004). The structural relationship between neurons and astrocytes has made this cell type a key area of study. Astrocytes are known to promote neuron adhesion and growth by providing a permissive surface for neurite attachment, although it is not clear which receptors are involved (Vernadakis 1996). Astrocytes also synthesise and secrete neurotrophic molecules, such as *glial cell derived neurotrophic factor* (GDNF) and *basic fibroblast growth factor* (bFGF), which also promote neuron survival and neurite proliferation (Levitan & Kaczmarek 2002, Muller *et al.* 1995). Although it has long been accepted that astrocyte-neuron co-existence is essential for neuronal development, only recently have astrocytes been recognised as playing a vital role in the regulation of dendritic pattern formation during CNS development (Abu-Akel 2003, Powell *et al.* 1997). Recent studies have shown that astrocytes derived from the local environment of the neuron stimulate dendritic growth, whereas target region-derived astrocytes preferentially stimulate axon growth (Le Roux *et al.* 1994, 1995).

Oligodendrocytes

Oligondendrocytes are most commonly found within the white matter of the CNS, although also exist within the grey matter (Kingsley 2000). In comparison to astrocytes, these cells are much smaller with a spherical cell body and fewer processes (Pannese 1994). In vitro, these processes are found wrapped around the sections of certain neuronal axons within the CNS, forming what is called a myelin sheath. The layered myelin acts as an insulator preventing current leakage. This has the effect of increasing the rate of signal transmission by allowing the electrical pulse, called the action potential (described in detail in section 4, *Neuron Communication*), to jump between the areas where myelination is absent, called the nodes of Ranvier.

3. Growth and Guidance of Neurons into Functioning Networks

The function of the nervous system depends entirely on the formation of specialised circuits, and is therefore dependent on the guidance cues that govern their formation. Axon growth and synapse formation are driven by combination of attractive and repulsive molecules present in the cell's environment. These molecules exist, either in the cell's immediate surroundings bound to the surface of an adjacent cell or the extracellular matrix, or as diffusible molecules secreted from distal locations. The fine balance of growth promoting and growth repulsive stimuli that a cell encounters during development is interpreted by the growth cone.

The Growth Cone

The growth cone is a highly motile, hand-like structure present that is the tip of an advancing axon. As an axon proliferates through the dense matrix of the extracellular space, the growth cone continuously searches and probes for long- and short-range guidance cues. The mechanisms through which growth cones are guided to their targets are often classified as chemoattraction (Figure 1.3, image A), chemorepulsion (B), contact-dependent attraction (C), and contact-dependent repulsion (D) (Mueller 1999).

Growth promoting cues can range from simply an adhesive substrate in an otherwise non-adhesive environment, to specific attractive signals, and repulsive stimuli. The growth cone responds to these guidance signals, and this response is mediated through the cytoskeleton of the cell, although the exact signaling mechanisms through which this occurs is not fully understood. The central core of the growth cone is an extension of the neurite process and is rich in microtubules that provide the structural support for axoplasmic transport, the specialised transfer of cell components, such as proteins and synaptic materials from the cell body to the extremity of the neurite (Lewis *et al.* 1992). Surrounding this central area is the lamellipodium, a region devoid of such mechanical structures but highly enriched in the contractile protein actin, a fundamental component of the cell's cytoskeleton (Luo 2002). Extending from this region are thin protrusions of the actin cytoskeleton called filopodia, see Figure 1.4 (Mallavarapu *et al.* 1999).

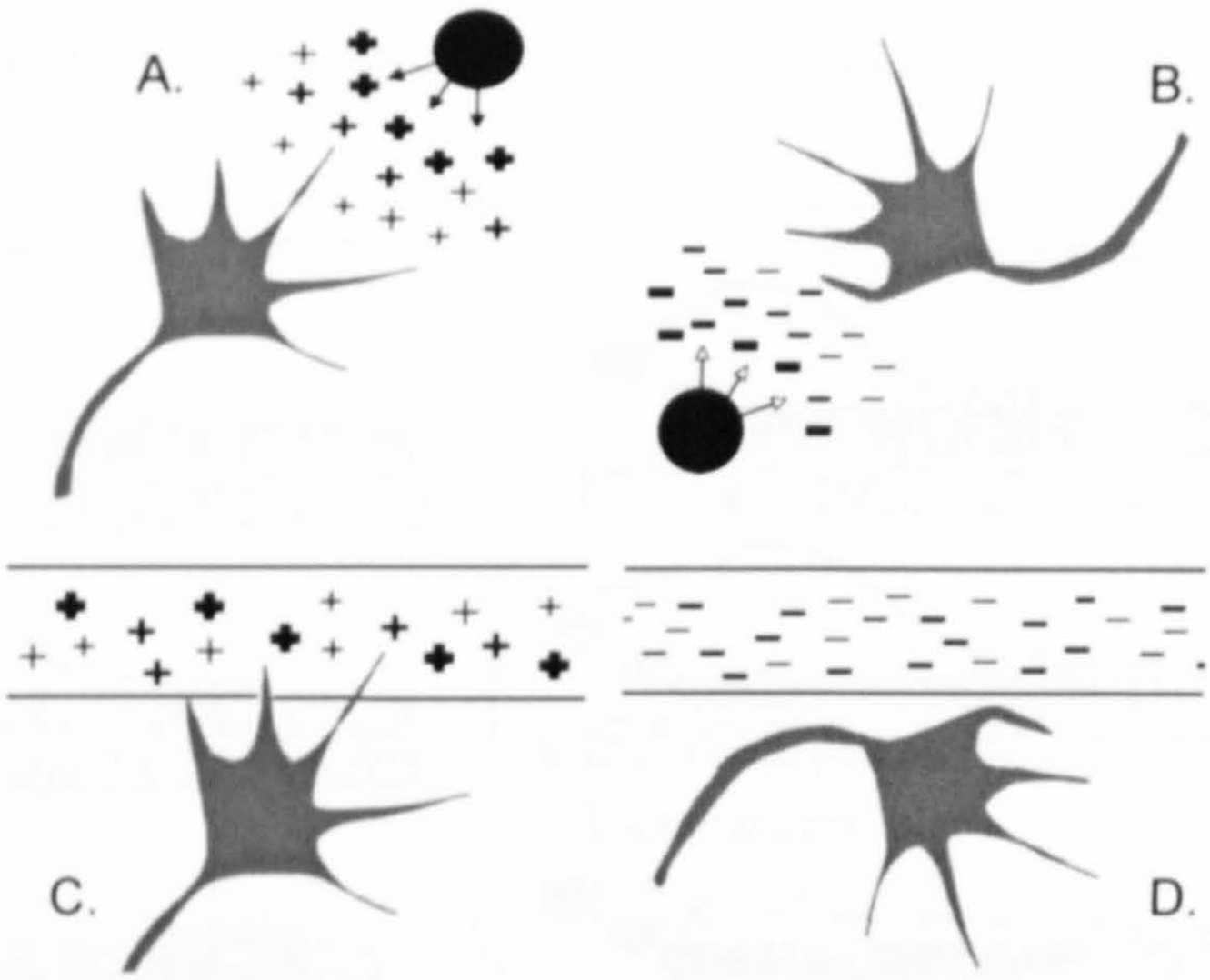

Figure 1.3. Schematic diagram showing the different stimuli that can effect growth cone guidance. Both attractive and repulsive chemical cues can exists diffusible molecules released into the extracellular space (A,B) or bound to a surface along which an axon migrates (C,D).

Figure 1.4. Schematic diagram showing the two types of cytoskeletal elements that predominate in the growth cone. Microtubules are found in abundance in the organelle-rich central domain (C), with some extending to the base of filopodia at the leading edge. The faster growing plus ends of microtubules are indicated (+). In the organelle-poor peripheral domain (P), actin filaments predominate, forming tight bundles in filopodia and a dense interwoven meshwork at the leading edge and in lamellipodia (Mueller 1999).

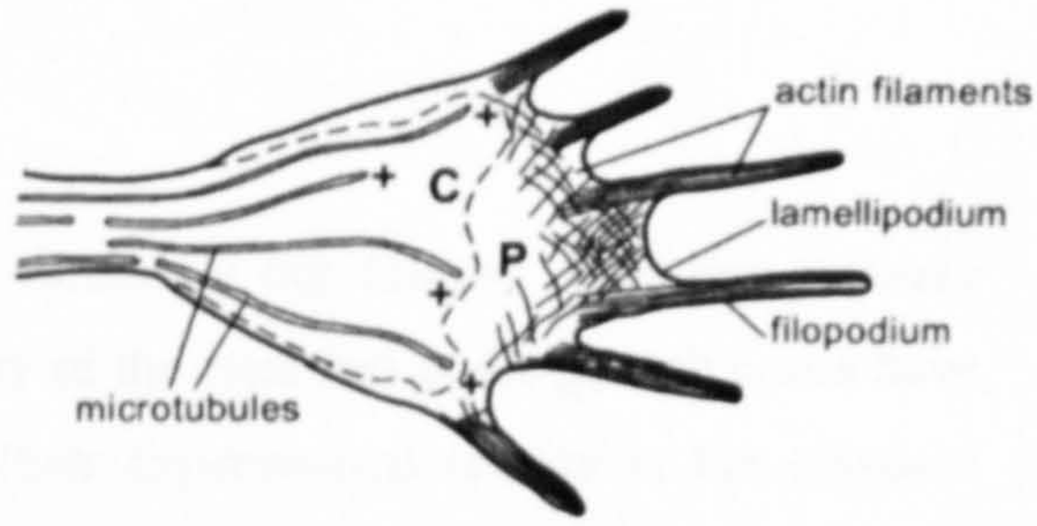

These dynamic structures of the growth cone repeatedly undergo cycles of extension and retraction, sampling the environment for guidance cues. The first insight into the relationship between movement of these structures and growth guidance came from work conducted by Forscher and Smith in 1988 (Dodd *et al.* 1988, Levitan 2002, Luo 2002, Mueller 1999, Suter *et al.* 1998). Using cytochalasin treatment coupled with high-resolution video microscopy they showed non-interacting growth cone actin filaments to move centripetally at rates of approximately 100 nm/s, a phenomenon they refer to as retrograde flow (see Figure 1.5). Studies have shown the rate of retrograde flow to significantly increase in advancing lamellipodia and filopodia, and to reverse direction during retraction. From close analysis of lamellipodia and filopodia recent research has

now identified a link between the intracellular network of the axon cytoskeleton, cross-linked membrane receptors and extracellular substrate interactions (Suter *et al.* 1998).

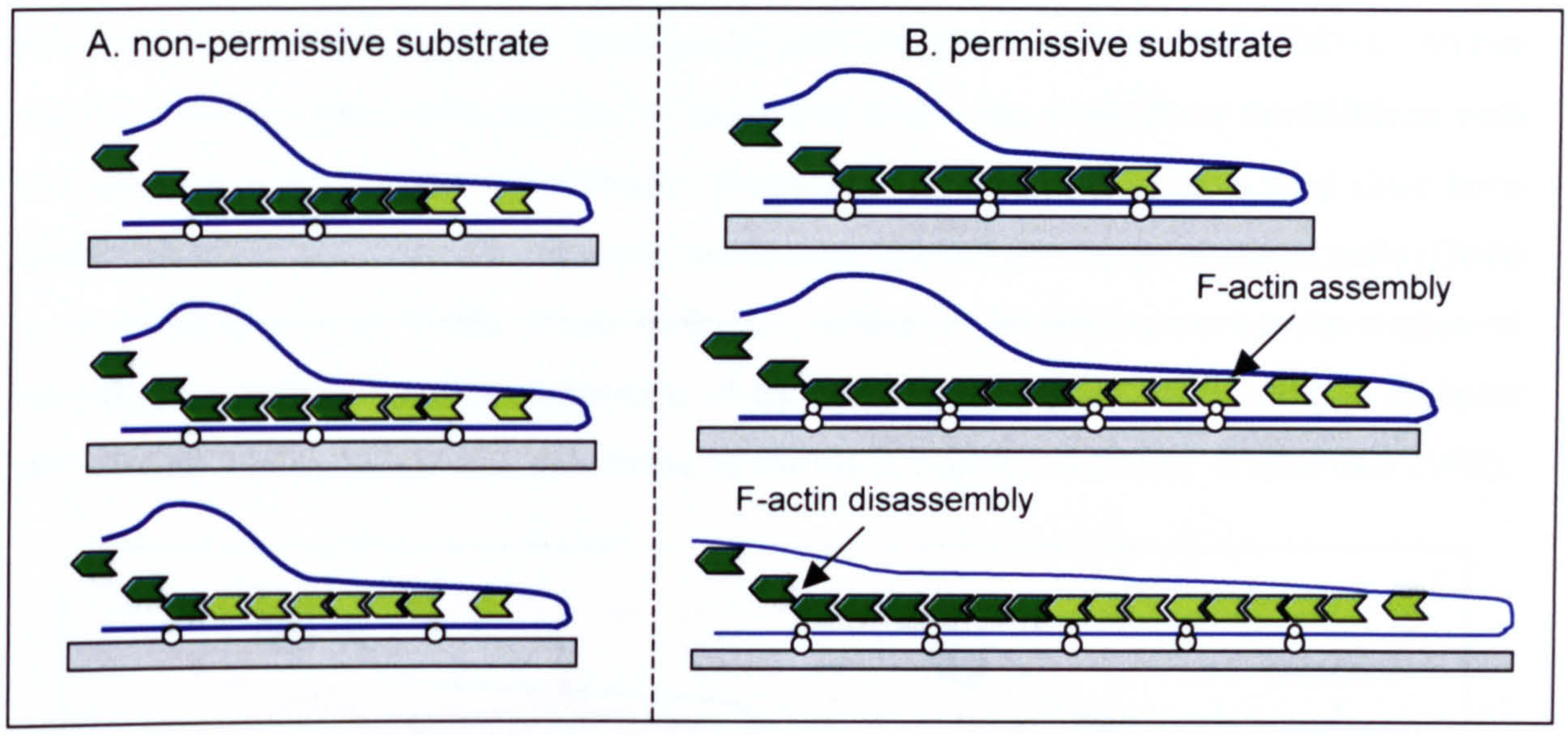

Figure 1.5. Diagram illustrating the assembly (shown in light green) and disassembly of F-actin (shown in dark green) that accounts for retrograde flow. When a growth cone encounters an adhesive substrate (B), the rate of actin depolymerisation decreases and the growth cone extends due to the continuous polymerisation of F-actin at the leading edge. If a cell encounters a repulsive stimuli the opposite occurs (A) (Levitan 2002).

Axon Guidance

The direction of axon growth does not occur randomly but follows a distinct pathway mapped out by the growth related signals. Many of the cues that guide growth cones have been revealed by cellular analyses that have their experimental origins in the classical observations of Ramon Y Cajal, Harrison and Spiedel in 1910 (Dodd *et al.* 1988). These early studies reported findings of axonal growth steered by physical interactions between neurons and other cell types *in-vivo* and *in-vitro*. It was first thought that neural epithelial cells surrounding pioneering axons were in some way involved in axonal growth, either signalling to the cell directly or by simply providing a permissive substrate for cell attachment. In recent years substantial progress has been made in the identification of the molecules in the neurons immediate environment that are involved in cell attachment and growth guidance, and of the neuronal cell surface receptors that recognise these molecules (Bixby & Jhabvala 1990).

Cell Surface Adhesion Molecules

Surrounding each cell, whether a nerve cell or neural epithelial cell, is a complex nanostructure rich in proteins that is the surface of adjacent cells and the extracellular matrix (ECM), which provides a structure for cell attachment (Curtis *et al.* 2001c). Within this environment there are a number of molecules which can form direct associations with the advancing axon, called cell adhesion molecules (CAMs). CAMs have long since been identified as the link between substrate attachment and cell growth in neuronal cells (Dodd *et al.* 1988, Suter *et al.* 1998). These molecules adhere the advancing axon to the surface of an adjoining cell, or cellular component of the extracellular space, by binding to receptor proteins present on the plasma membrane as shown in Figure 1.6 (Bixby & Jhabvala 1990).

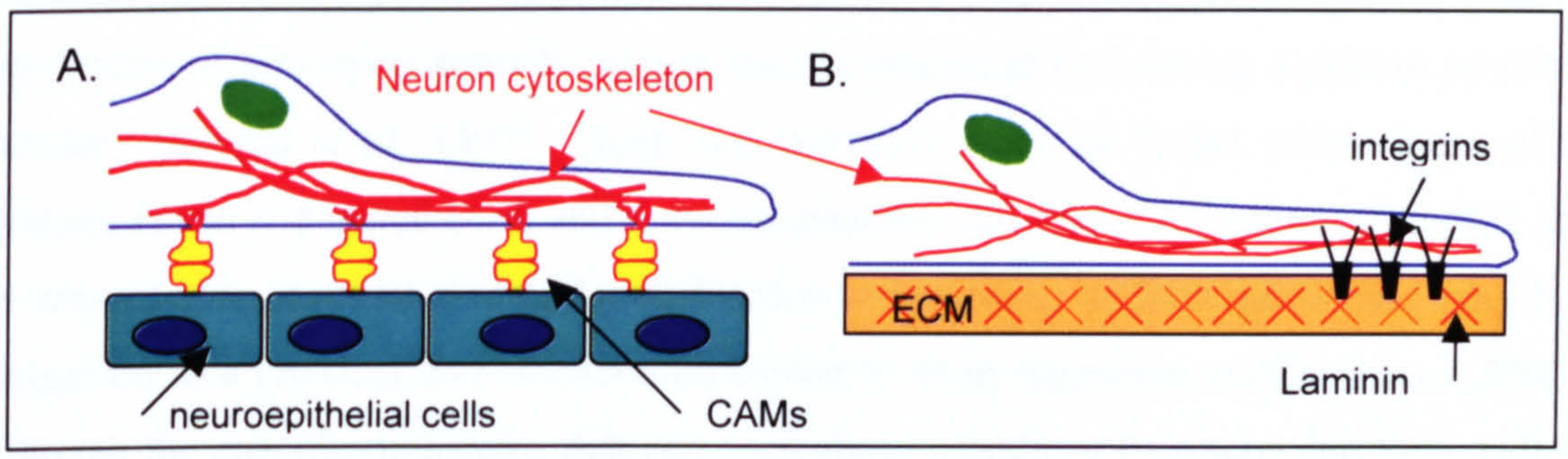

Figure 1.6. Image A is a schematic diagram showing the interaction between CAMs located on neighbouring cells, such as neuroepithelial cells. This association is mediated by homophilic interactions between surface molecules such as N-CAM or N-cadherin. Image B is a schematic diagram showing the association of the ECM glycoproteins, such as laminin, with receptor molecules which mediate their response, such as integrins. (Dodd et al. 1988).

The majority of CAMs are believed to cause cell-cell adhesion by binding to the same CAM on the adjacent cell. N-cadherin and N-CAM are the most abundant Ca^{2+}-dependent and -independent CAMs present on vertebrate nerve cells, promoting cell adhesion through homophilic mechanism. It is thought these molecules play an important role during early development, guiding axons through mesenchymal and epithelia environments that are devoid of other axons (Dodd *et al.* 1988). Once bound, CAMs increase the rate of retrograde flow through their intracellular link to the actin cytoskeleton. Although generally most CAMs only promote cell adhesion, extracellular matrix molecules, such as laminin and fibronectin, encode directional information (Engel 1992, Walsh *et al.* 1996). Laminin is a component of the extracellular matrix (ECM) that promotes axon elongation by interacting with axonal glycoproteins that are members of the integrin family (Dodd *et al.* 1988). The integrins are surface protein receptors, consisting of α and β subunits that

mediate cell adhesion to other cell surface- and ECM-glycoproteins. These surface receptors are considered of primary importance for cell attachment, with at least six different α/β combinations having been identified to bind to laminin (Engel 1992). It is through such transmembrane receptors that guidance information is fed to the actin cytoskeleton via complex signalling pathways (see Figure 1.7). Cell adhesion alone is not sufficient to guide neurons to their specific target, repulsive substrates also play an important role in axon guidance, a process referred to as contact-inhibition. Evidence for the existence of cell surface molecules that inhibit axon extension has come from a variety of *in-vitro* studies working with oligodendrocytes and astrocytes (Scholze *et al.* 1996, Theodosis *et al.* 2004). Although astrocytes overall have been shown to promote neurite extension and be an optimal substrate *in-vivo*, *in-vitro* studies suggest that certain selective populations of astrocytes actually restrict neurite extension by forming a growth inhibitory boundary (Powell *et al.* 1997). Such cell boundaries can be found within areas of the striatum, retina and spinal cord, and are most predominant after CNS injury. The glial scar, the area of glia accumulation and proliferation surrounding a CNS lesion, has long been recognised as a physical and biochemical barrier to axon regeneration (Chen *et al.* 2002a). Although the specific molecules that carry out these inhibitory functions and there cellular source are unknown, there is considerable cellular evidence to suggest that chondroitin sulfate protoeglycan (CSPG) and tenascins are involved (Chen *et al.* 2002b).

Secreted factors

As mentioned previously axon guidance is also influence by molecules that are secreted into the surrounding environment. These molecules play an important role in guiding cells from a distal location. Unlike cell adhesion molecules, guidance molecules do not promote mechanical adhesion, but act to steer the growth cone towards or away from their source depending on their chemotrophic properties. The first diffusible guidance molecules to be identified in the CNS were those of the netrin family, netrin-1 and netrin-2 (Aubert *et al.* 1995). Netrin-1, secreted from the floor plate of the developing spinal cord has a chemoattractive affect on commissural neurons, whereas trochlear motor axons interpret the same molecule as a repulsive factor (Guthrie 2001). Since the discovery of netrin, other important guidance molecules have been identified and characterised, including semaphorins and Slits. Semaphorins, which can also have both a repulsive or stimulatory effect on axon growth depending on their location in the CNS (repulsive response exerted

by binding with plexin or NP1 receptors, whereas (semaphorin 7a) association with integrins promotes axon outgrowth), can exist as both soluble factors or membrane bound molecules (Pasterkamp *et al.* 2003). Many cells, including sympathetic, motor, cerebellar, hippocampal, olfactory, corticospinal and dorsal root ganglion neurons, respond to this large family of guidance molecules (Grunwald *et al.* 2002). The Slit family of guidance molecules are expressed by the midline glial cells, and act as long-range chemorepellents for axons via the Robo receptor (a transmembrane glycoprotein which has a structural homology with a number of CAMs) (Hivert *et al.* 2002). The robo guidance system is an excellent example of how cascades of growth related factors are essential for the direct control of axon growth. In the developing spinal cord, axons are attracted to the midline by netrin. However once cells cross the midline they begin to express high levels of Robo on their growth cones, preventing them from re-entering this area. Like CAMs, guidance molecules also influence the growth cone through second messenger signalling pathways. One of the most defined second messenger system involved in neuronal growth are the Rho GTPase pathways, RhoA, Rac and Cdc42 (Grunwald *et al.* 2002, Luo 2002).

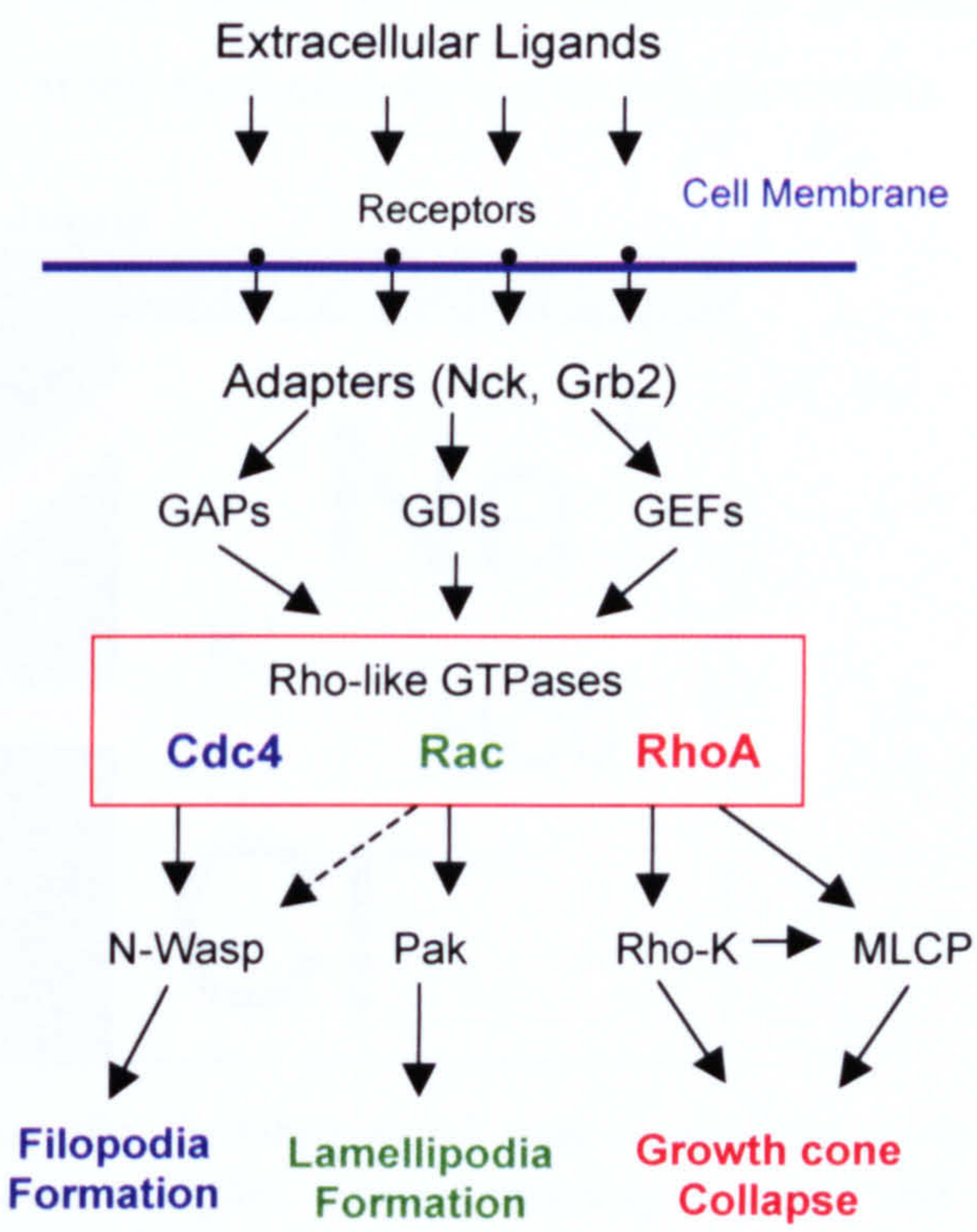

Figure 1.7. Schematic diagram illustrating the signal transduction pathways in growth cones. Extracellular guidance cues activate growth cone receptors, which in turn interact with protein scaffolds (the adapters Nck or Grb2) or directly activate GTPase-activating proteins (GAPs), guanine nucleotide dissociation inhibitors (GDIs) or guanine nucleotide exchange factors (GEFs). Activated, GTP-bound, Rho-like GTPases stimulate filopodia and lamellipodia formation or growth cone collapse by activating Rho-Kinase (Rho-K) or myosin-light chain phosphatase (MLCP)(Mueller 1999).

4. Network Communication

Excitable Membranes

Neuronal signalling depends entirely on rapid changes in the electrical potential difference across nerve cell membranes. The propagation of such electrical impulses throughout the nervous system is caused by current flow in and out of the cell, carried by ions both positively and negatively charged that are present in the cells immediate environment. The properties of the nerve cell membrane is the key to signal transmission within nervous tissue. Every neuron has a separation of charge across the membrane, with an excess of positive charges outside the cell and an excess of negative ions within the cell when the cell is at rest. This electrical gradient is maintained by the lipid bilayer of the cell, the composition of which makes it almost, but not entirely, impermeable to passive ion movement. As well as an electrical gradient, there also exists a chemical gradient across the nerve cell membrane, with the intracellular concentration of K^+ being much greater than that of the extracellular fluid and the opposite being true for the concentration of Na^+ (see Figure 1.11). Together these driving forces create the *electro-chemical gradient*, the governing force controlling the direction of ion movement across the cell membrane.

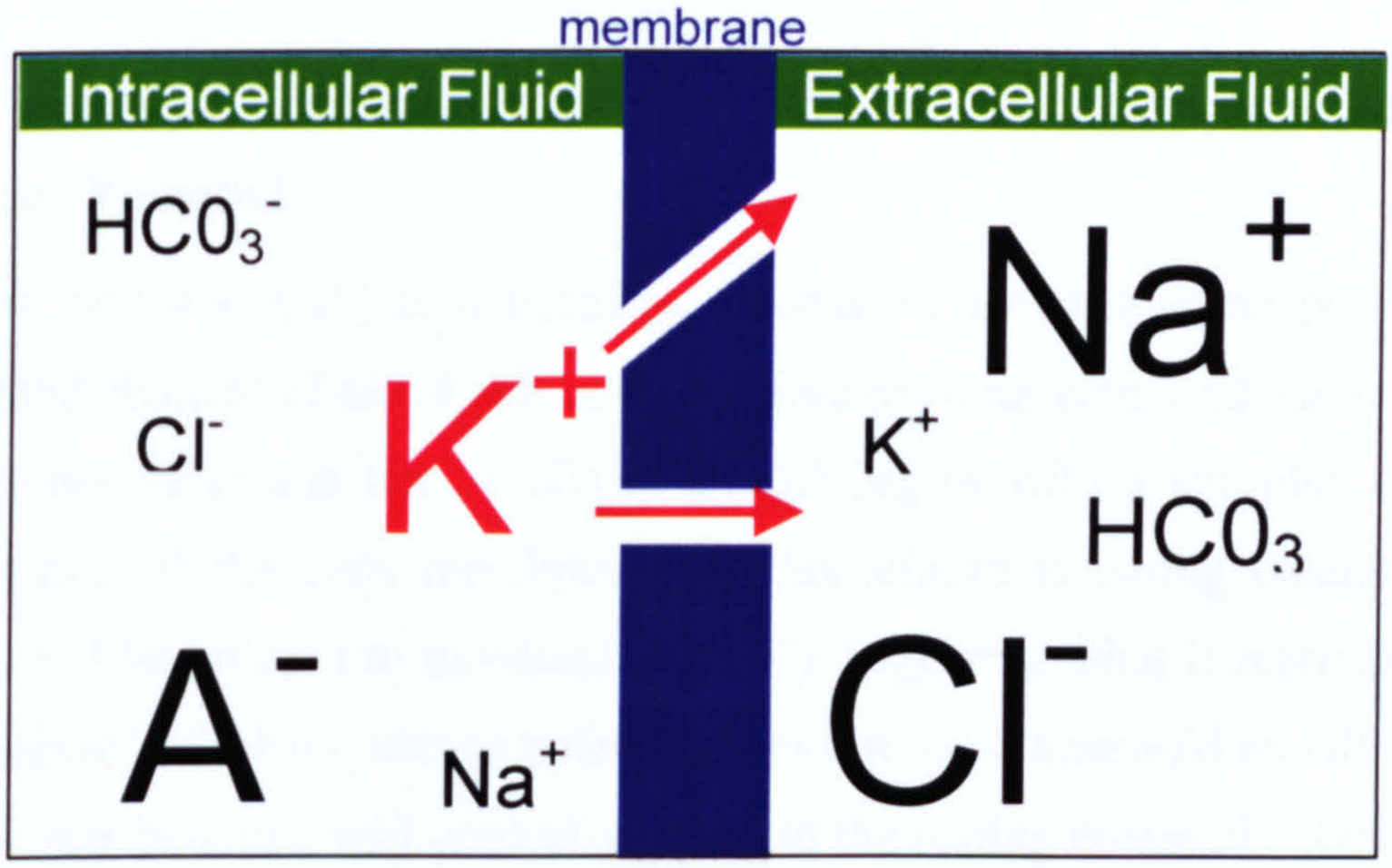

Figure 1.8. Schematic diagram showing the distribution of ions across the nerve cell membrane. The intracellular fluid contains a higher concentration of K^+ ions and large anions (A^-) separated from the extracellular fluid containing a high concentration of Na^+ and Cl^- ions by the cell membrane, which is permeable to the diffusion of K^+ ions but not Na^+, Cl^- and A^- (Roll & Trevesa 1998).

At rest, when the cell is not engaged in signal transmission, ions move across the cell membrane through non-selective ion channels present in the cells membrane. At first ions

will obey their concentration gradient, in the case of K^+ diffusing from inside the cell to the extracellular fluid. When a positive ion moves out of the cell it creates a displacement of charge across the membrane. If diffusion persists, the inside of the cell will become more negative resulting in a voltage gradient across the membrane. As the voltage gradient increases the rate of diffusion will decrease until a point where the electrical gradient will oppose the concentration gradient and ions will no longer move across the membrane. The voltage at which this happens for any given ion is called the *equilibrium potential* (Levitan 2002). However, all ions crossing the nerve cell membrane are never quite at equilibrium but are maintained at a steady state, referred to as the *resting membrane potential* (Vm), approximately –70 mV in value and defined as *Vm = Vin – Vout*. The resting membrane potential is the crucial factor governing cell-cell communication. When a nerve cell is stimulated, the resultant activation causes a change in membrane potential. These changes may be abrupt or slow, brief or long lasting, depending on the stimulus but the mechanism of potential change are fundamentally the same (Brown 1991). They always involve a change in the permeability of the membrane to ions. These shifts are conducted through ion-specific channels, whose openings are triggered by a variety of stimuli, some of which respond to changes in voltage, the so-called *voltage-gated* channels, while others are opened by binding of a ligand to the channel, the so-called *ligand-gated* channels.

The Action Potential

An action potential (AP) is a transient reversal of the membrane potential, and is the fundamental element of nerve cell, and therefore network communication (see Figure 1.9). The sequence of events that results in an AP begins with a stimulus that brings about depolarisation of the cells membrane. If this stimuli is strong enough the membrane potential will be brought to threshold (-55mV), triggering what is referred to as an '*all or none response'* (if the membrane potential does not reach threshold no AP will be fired, and the membrane potential will gradually return to the resting potential). Once the membrane reaches threshold the voltage-gated sodium channels begin to open, resulting in an influx of sodium ions along their electro-chemical gradient. As the membrane potential becomes less negative more sodium channels open in a positive feedback fashion, however once the inside of the cell reaches +40mV these channels become inactivated. At the same time as the Na^+ channels close, voltage-sensitive potassium channels open, resulting in an outward movement of K^+ ions down their concentration gradient. As the positively charged

potassium moves out of the cell, the membrane potential gradually becomes negative again to a point where it is less negative then the resting membrane potential (approximately –95mV). This is called hyperpolarisation and when the membrane potential reaches this value the voltage-gated potassium channels close, allowing the non-selective diffusion of K^+ ions to return the membrane to its resting potential (Kendal *et al.* 2000).

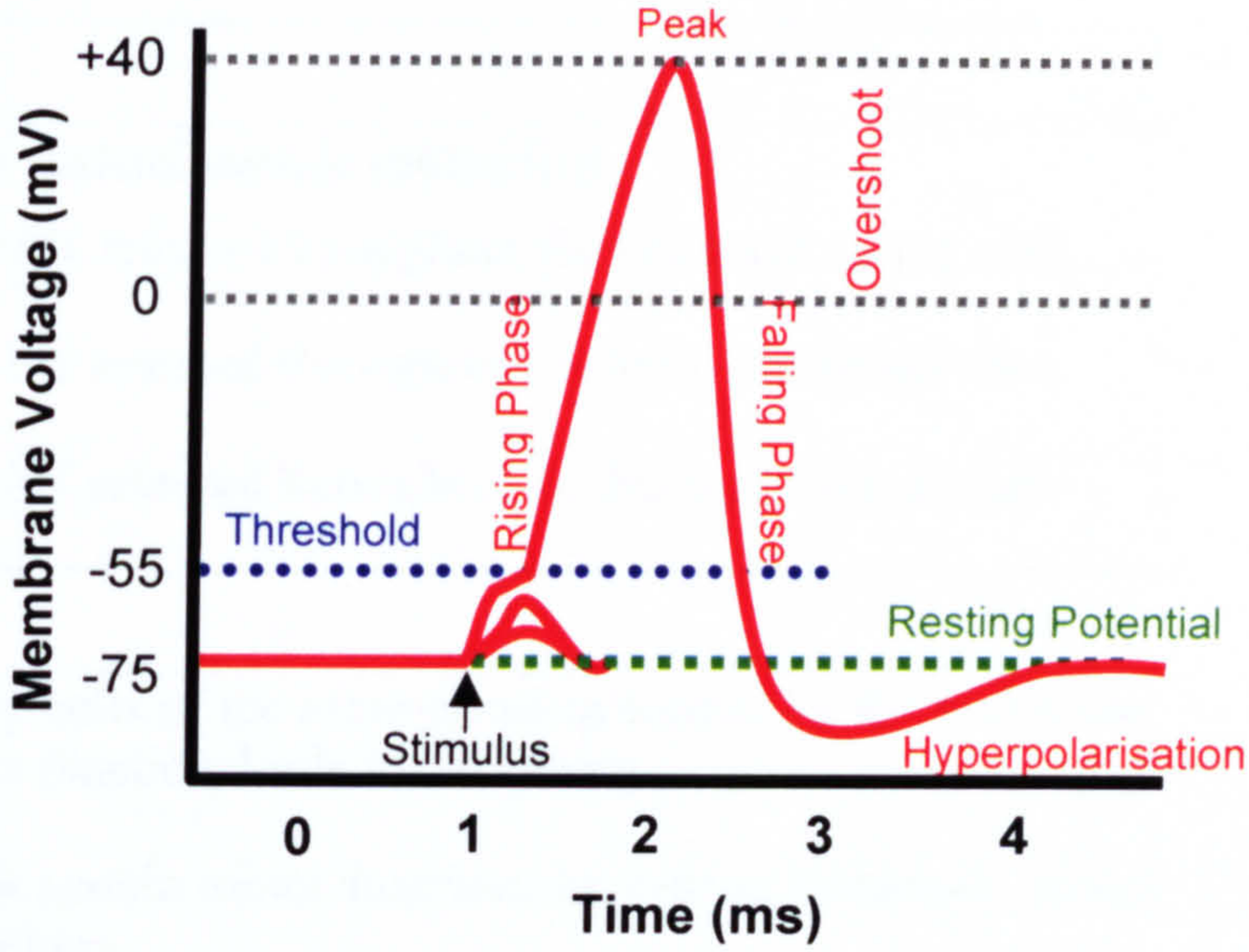

Figure 1.9. Schematic diagram illustrating the various components of an action potential. It should be noted that hyperpolarisation ensures the signal can only travel in one direction by preventing this area of the axon from reaching threshold by a backward propagating signal (Bear 2001).

Chemical Excitation

Action potentials are propagated in a uni-directional fashion, always travelling away from the cell body due to the refractory phase of the membrane following an AP. When the AP's reach the terminal point of the axonal process, called the synaptic bulb, the information carried encoded in the AP frequency is retransformed into an amplitude modulated signal. The resulting change in membrane potential activates a series of events, which results in the release of specialised neuro-chemicals, called neurotransmitters (NTs), from vesicles within the synaptic bulb. So far twenty NTs have been identified, some of which are listed in Table 1.1 (Holmes 1990). There are four types of NTs: the small molecule neurotransmitters (SMNTs), monoamines, peptides and the gases. The SMNTs are the most common neurotransmitters in the CNS, glutamine being the most common excitatory and, glycine and GABA being the most common inhibitory (however, it should be noted that the nervous system is also influenced by numerous neuro-hormones) (Kingsley 2000). Once released, the NTs diffuse across the synaptic cleft (the space between the cells where chemically mediated signal transmission occurs) and bind to specific receptors on the next cell, as shown in Figure 1.10. The site of contact between two nerve cells is called a synapse. The cell transmitting the signal is referred to as the presynaptic cell, and the cell receiving it is known as the postsynaptic cell. If the presynaptic cell is excitatory, the NT

released will bring about an excitatory postsynaptic potential, which triggers AP firing in the postsynaptic cell. If the presynaptic cell is an inhibitory neuron, the NT causes the membrane to *hyperpolarise* preventing the firing of an action potential. The existence of both excitatory neurones and inhibitory neurones in the central nervous system is a fundamental feature in network circuitry.

SMNT	**Function**
Ach	Initiator of skeletal muscle contraction.
Glutamate	Excitatory NT released throughout the brain and spinal cord.
GABA	Inhibitory NT released throughout the brain and spinal cord.
Glycine	Inhibitory NT released throughout the brain and spinal cord.
Monoamines	**Function**
Norepinephrine	Secreted by cells of the *locus ceruleus* located in the mid brain, however its functional role is not known.
Dopamine	Involved in certain motor functions as well as behaviour, mood and perception.
Epinephrine	Released by sympathetic nerve fibres.
Serotonin	Released by cells of the brain stem. Although exact function unknown it has been implicated in regulator of sleep patterns.
Peptides	**Function**
met-enkephalin leu endorphin *ß*-endorphin	Involved in sensory pathways of pain.
Substance P	Thought to be a synaptic NT in the sensory pathways of pain and touch.
Gases	**Function**
nitric oxide	Secreted predominantly in the olfactory bulb and cerebellum, although its exact role in the CNS is unknown.

Table 1.1. Table listing examples of the four categories of neurotransmitters. In order for a chemical to be classed as a NT it must (a) be synthesised by neurons, (b) be released from the synaptic terminal as a result of electrical activity (c), and (d) bind to receptors on the postsynaptic site (Kingsley 2000).

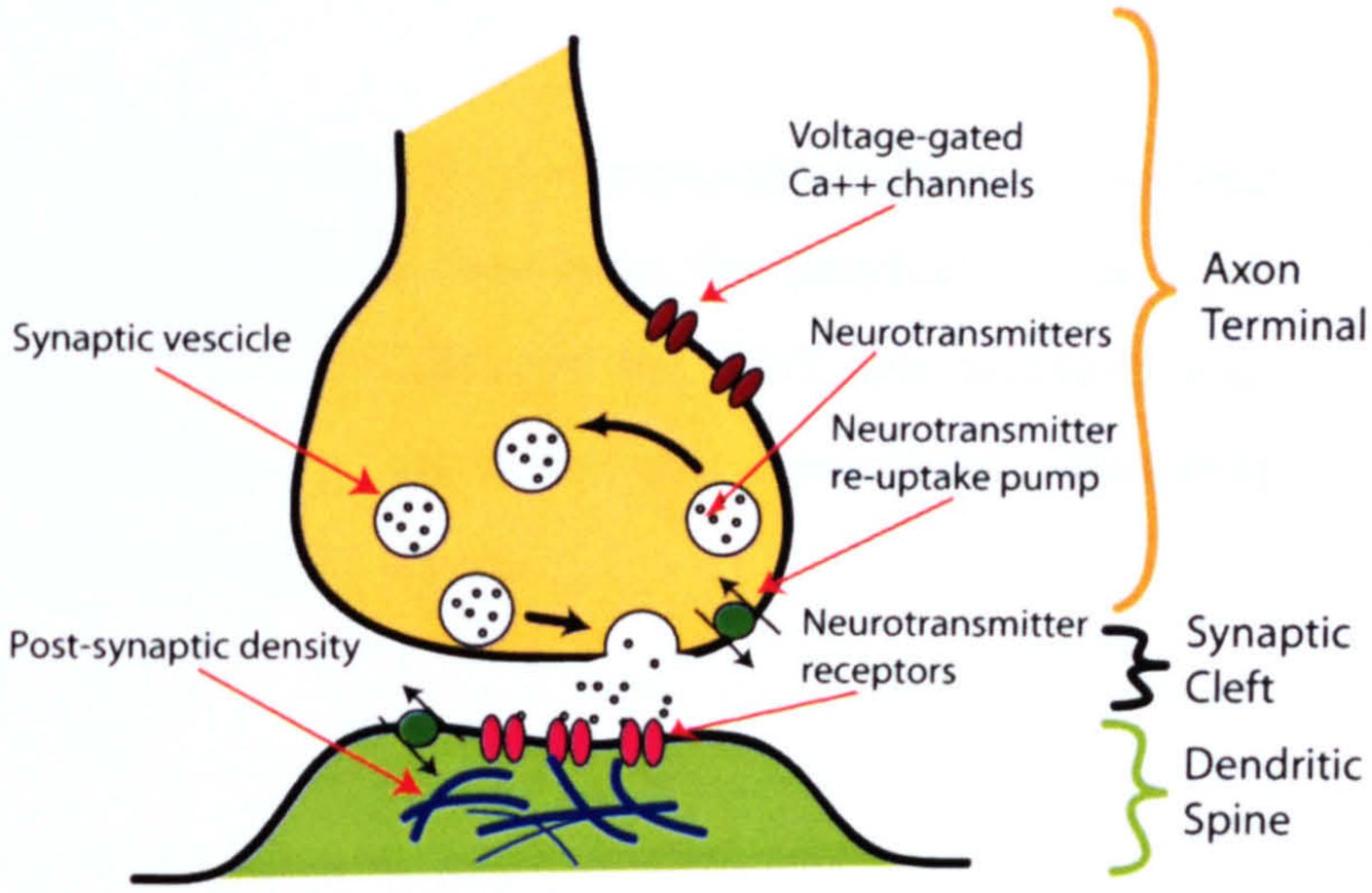

Figure 1.10. Schematic diagram illustrating the release of neurotransmitters (NTs) at the synaptic cleft. NT release is activated by an increase in intracellular calcium through voltage gated Ca^{2+} channels. The vesicles containing the NTs, must dock with the membrane of the presynaptic cell. The NTs then diffuse across the synaptic clef, then binds to postsynaptic receptors. The removal of the NTs (by diffusion, enzyme digestion or re-uptake) completes the chemical transmissions of the electrical signal. (Diagram taken form Wikipedia.org)

Electrotonic Excitation

Electrical synapses are the sites of neuron-neuron communication, where the electrical current from one cell passes directly to another via gap junctions (the site of close association between neighbouring cells). This is made possible by the presence of membrane spanning protein pores called connexins. These pores are large enough to allow ions and small molecules (~1-1.5kD) to pass from the cytoplasm of one cell to that of the other. Unlike chemical synapses, electrical synapses are not unidirectional and do not exhibit the distinct morphological structures of the chemical synapse shown in Figure 1.10. Therefore both cells involved can be either pre- or postsynaptic depending on the direction of signal transmission at any given time. When an action potential reaches the synapse the electrical current is transferred to the next cell by the movement of ions through the connexons to equalise the difference in membrane potential, thus the synapse is excitatory on the less depolarised neuron and inhibitory on the more depolarised neuron. The role of the electrical synapse is to transmit signals rapidly between cells and also to increase the synchrony of network activity.

5. Neural Networks

Inhibitory or excitatory synaptic connections have little behavioural significance on their own, however, when arranged into neural networks they form the backbone of network configuration. As described previously the structures of the CNS are arranged into specialised neural networks that may comprise millions of synaptic connections. However within these neural networks a hierarchy of circuitry exists.

Synaptic Circuits

The lowest level of network circuitry is the synaptic microcircuits (Roll & Trevesa 1998). These circuits may consist of a thousand neurons (relatively few when one considers the total number in the CNS) arranged into small patterns. Synapses can occur at variety of locations on a neuron as shown in Figure 1.11 below.

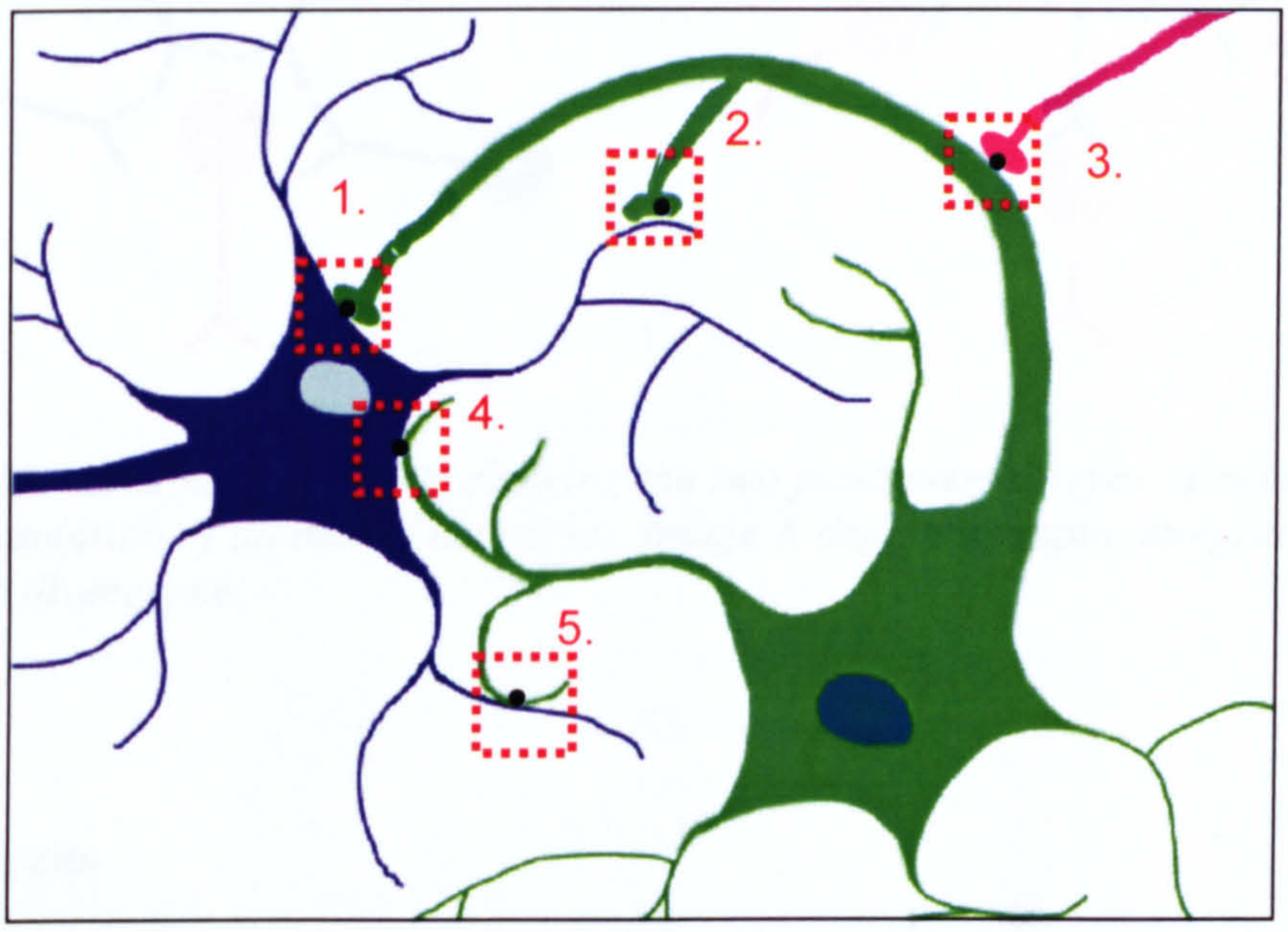

Figure 1.11. Illustration showing the various sites where a synapse can occur between neurons: axon-cell body (1), axon-dendrite (2), axon-axon (3), dendrite cell body (4) and dendrite-dendrite (5).

Axon-cell body, axon-dendrite and axon-axon are the most common locations for signal trnamission, although synapses have been reported to form between dendrites, and at dendrite-cell body sites. It is the existence of these multiple synapse sites that account for the complexity of even the simplest of microcircuits. The two basic types of microcircuits are called convergent and divergent networks (see Figure 1.12). *Synaptic integration* has

the effect of summating signals from various cells. For example, a single connection between a presynaptic and postsynaptic neuron may not be enough to bring a cell to threshold and fire an action potential. If however this postsynaptic cell was innervated by more than one cell, it could be that all inputs are required to bring the receiving cell to threshold, a process called *spatial summation*. The excitatory activity of a participating cell, however, can be switched off by a presynaptic inhibitory connection, a process called *presynaptic inhibition*. *Synaptic divergence* refers to the expansion or amplification of a signal. In this case one neuron connects with a number of different cells. Microcircuits are arranged in a variety of different ways throughout the CNS to form larger complex network arrangements, called *local circuits*.

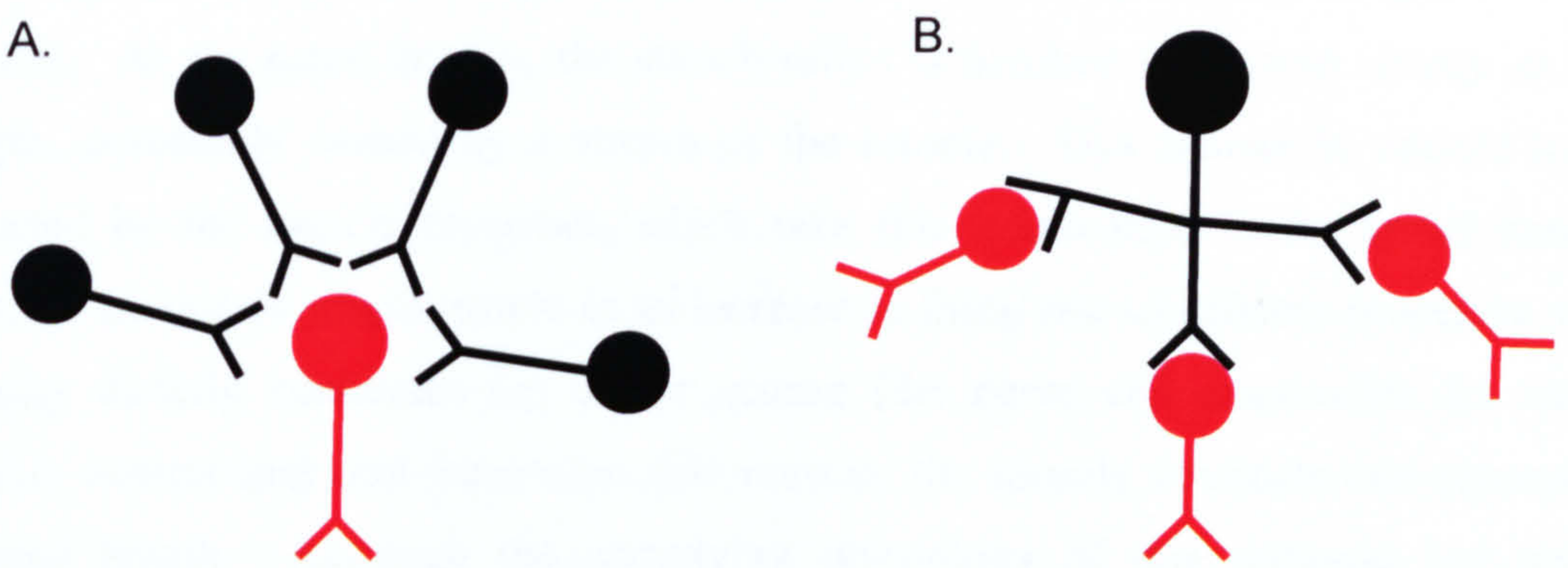

Figure 1.12. Schematic diagram showing the two fundamental types of microcircuitry that are the foundation of all neural networks. Image A depicts synaptic integration, and image B synaptic divergence.

Local Circuits

Local circuits are the networks that exist within a specific region of the CNS. The complexity of this type of circuitry depends on its function, for example, the local circuitry of the hippocampus (the area of the brain involved in memory) is far more complex than the local circuitry of the spinal cord, which contains the most simplest circuitry in the mammalian CNS. A great deal of information about synaptic organisation of the CNS has come from studies on the spinal cord local circuitry. The neurons of the spinal cord are arranged to form a variety of simple neural networks called reflex arcs.

The Stretch Reflex

Spinal reflexes offer some insight into the signal modulations that occur within neural networks. Such reflexes are a result of an internal feedback control system between sensory organs of the body (proprioreceptors, nociceptors, mechanoreceptors) and the nerve circuitry of the spinal cord. These circuits regulate the coordinated action of muscles, connected to the spinal cord via afferent and efferent nerve fibres. Several reflex networks exist but only the stretch reflex will be considered here.

The stretch reflex is a monosynaptic reflex that provides automatic regulation of muscle length. Information regarding the resting length of a skeletal muscle is continuously fed to the brain by the constant firing of afferent fibres activated by sensory receptors within the muscle. As the name implies, the stretch reflex is invoked by a rapid change in muscle length, potentially caused by a stretch of the muscle. This change in muscle length is detected by the muscle receptors, which take this information to the spinal cord. An increase in muscle length results in an increase in firing rate of afferent processes and this activity directly stimulates the motor neuron (the nerve cell responsible for initiating muscle contraction) that innervates this muscle, the muscle contracts and returns to its optimal length. Although the underlying physiology of this response has not been described, the important point to consider is that networks communicate their information by altering the firing activity of the neurons involved.

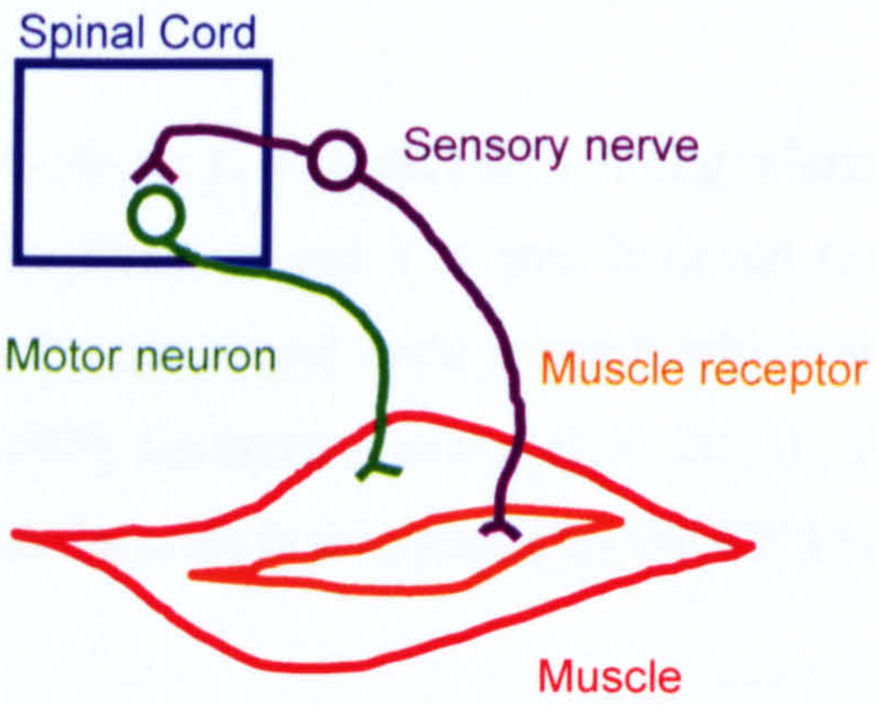

Figure 1.13. Schematic diagram illustrating the monosynaptic stretch reflex. When the muscle is stretched, the muscle receptor detects the change in length and signals this change to the spinal cord by increasing the firing rate of the sensory neuron. The sensory neuron directly innervates the motor neuron, causing this neuron to fire, this in turn activates the muscle and the resulting contraction returns the muscle to its starting length.

Neural Network Dynamics

Although neural networks can be activated by sensory receptors as described in the preceding section, there are also many areas within the CNS that exhibit neuronal activity in the absence of such stimuli. The activity within these neural networks is generated by endogenously active cells, called *pacemaker* cells. These cells control the network activity by establishing a firing pattern. There are two types of activity expressed by these spontaneously active cells; constant firing, where the pacemaker cells are firing continuously at a constant rate, or rhythmic firing, when the cell fires in rhythmic bursts (Latham & Richmond 2000). In each case the firing patterns can be modified by the presence of various excitatory or inhibitory neurons within the network, and by the ever changing synaptic connections that can occur over time.

Rhythmic firing activity is most commonly observed in the spinal cord during locomotor activity (Capaday 2002, Darbon *et al.* 2002). During walking the flexor and extensor muscle units of the limbs are repetitively excited and inhibited, resulting in a forward progressive movement of the body. Central pattern generator (CPG) is the term given to the spinal networks that can generate patterns of rhythmic activity for locomotion, even in the absence of external feedback or supraspinal control (Lacquaniti *et al.* 1999). This walking reflex originates from the motor neurons, however it is the presence of inhibitory and excitatory interneurons within the circuitry that regulates the network activity (Phillips *et al.* 1995).

There is now significant evidence to suggest that a strong relationship exists between firing pattern and neural network function and it is now believed that deviations in these basic activity patterns accounts for the neural code through which all functions of the CNS are governed (Darbon *et al.* 2002, Gutierrez-Galvez *et al.* 2003). Although the code has been identified the way in which the code is interpreted by the CNS is still to be determined.

Justification of Experimental Approach

Spinal Cord Neurons

The signalling events that occur between individual nerve cells has been thoroughly characterised, yet it is still unclear how networks of multiple cells use these mechanisms to communicate the quantity of information that is processed by the CNS. Within this vastly complex tissue, some circuits have been identified with regards to the cells that form them, their functional roles, and the signalling modulations that they interpret. The reflex circuitry of the spinal cord is the most understood in this context and it is for this reason spinal cord neurons were chosen as the biological model in this study. However, these circuits only represent a fraction of all those within the spinal cord, and the CNS, and therefore the majority of networks remain uncharacterised with regards to their cellular composition, firing patterns, and functional contributions to neuronal processing. It is for this reason I will investigate the network activity of dissociated spinal cord neurons, with the aim of identifying the signalling patterns that exists within such networks, the mechanisms that bring about alterations in activity, and how the network interprets such changes.

Defined Networks of Neurons

It is evident from histological studies of the CNS tissue that organisation plays an important role in network structure. However, the correlation between organisation and network function has not yet been determined, nor has the role of cell morphology in this context. It is for this reason that cells will be grown on various patterned networks, which will attempt to maintain some structural integrity that exists in the original tissue source, albeit of a 2-dimensional arrangement.

Multi-electrode Recording Devices

As described previously, individual nerve cells communicate via electrical and chemical mechanisms; however, networks communicate in terms of signal trends. It is for this reason neural network behaviour will be investigated using multi-electrode arrays (MEAs). These devices are best suited for this study as the activity of multiple cells can be recorded simultaneously. It is anticipated that by using the combination of experimental techniques outlined in this section, one can begin to investigate the phenomenon of neural network dynamics *in-vitro* and ultimately break the *neural code* of nervous tissue.

Chapter 2.

Characterisation of Spinal Cord Cultures

Abstract

The optimal culture techniques and growth conditions to produce healthy dissociated spinal cord cultures were investigated, with the aim of developing a method that would guarantee the ability to reproduce results. The suitability of the various techniques was determined by immunocytochemical staining for various nerve cell markers, from which cell survival rate could be distinguished. Results showed that both embryonic and postnatal spinal cord neuronal cultures could be maintained under similar growth conditions. However variations in the dissociation and plating techniques were required. The cultures produced met the criteria required for studying neural network characteristics, as cells were forming neural networks that were expressing synaptic proteins, and these cells could be maintained for long periods of time (5 weeks in culture, for postnatal cells, and 3 weeks in culture for embryonic cells).

Introduction

The desire to understand more about mammalian cell function, growth and behaviour led to the development of primary cell culture techniques in the early 20th Century (Banker & Groslin 1998). Over the years these methods have been modernised, introducing 'designer' growth supplements and media 'cocktails', specially engineered to ensure the survival and maintenance of a specific cell type. However, the basic methods of extraction, cultivation and growth remain unchanged. Unlike the culture of cell lines, primary cell culture provides a closer association to the original tissue source, as cells in this case have not been subjected to periods of continuous growth, during which time cell characteristics can change and may become quite different from those found in the starting population. However cultivation of a mass tissue type does have its drawbacks; it is almost impossible to completely isolate one cell type, with the culture almost always consisting of a mixed population of cells. With some mammalian cell types, such as fibroblasts, proliferation over time will guarantee a pure cell population. However, this is not the case with a neuronal culture. Mature nerve cells do not have the ability to proliferate or regenerate in the brain or once extracted from the parental tissue as in *in-vitro* studies, making primary cell culture the only choice for cultivation of a nerve cell population (Brewer 1997). Once in culture the nerve cell population will not increase, but will most likely decrease due to neuronal cell death caused by insufficient levels of growth supplements, or the proliferation of other cell types that co-exist within the nervous tissue (Orike *et al.* 2001). However, once cells have been dissociated it is possible to enrich the nerve cell population, either by suppressing the growth of diving cells by using antimetabolitic agents such as cytosine arabinoside (Ara-C), which inhibit DNA synthesis (Ai *et al.* 2003, Cornish *et al.* 2002, Haastert *et al.* 2005, Ullian *et al.* 2004), or by using a specific culture method that exploits the different adhesive properties of the various cell types within the culture (Banker & Goslin 1998, Parsons *et al.* 1995). In any case if one is going to use primary nerve cell cultures as a biological model, it essential that the cultivated cells are correctly identified as neurons to ensure future results are relevant.

The identification of neurons by use of phase contrast microscopy is possible as some have distinct morphological characteristics. However, when growing in dense cultures, even to the trained eye of an expert, it is very difficult to determine individual nerve cells without some sort of specific labelling. In the early years of neurobiology the first anatomists

identified neurons in the densely packed tissue of the brain using methods such as silver staining, the most famous of those being the Nobel Prize winning work of Ramon Y Cajal (Andres-Barquin 2002). However, only in the last 30 years or so have new methods for axonal tract tracing and cell labelling revolutionised neurobiology (Kobbert *et al.* 2000). The most common method used today to identify neurons (or other mammalian cells for that matter) is immunocytochemistry, the use of antibodies to identify antigens in living or fixed cells. Like all cells, neurons contain a dense network of filamentous proteins that form the cytoskeleton. However, some of these proteins are neuron-specific, such as neurofilaments and neuronal specific isoforms of tubulin, and are therefore not present in any other cell type. By using markers against these unique proteins, the nerve cell population can be identified and distinguished from other cell types within the cell culture, ensuring that the cells being grown are in fact neurons. Not only can one determine the cell type by these means but also identify the different structures of neuron morphology. Neurofilaments and tau proteins for example, are predominantly located in the axons of neurons and rarely found in dendrites, whereas MAPs, although also present in axons are primarily found in dendrites (Brandt *et al.* 2005, Diaz-Nido *et al.* 1996, Pannese 1994). This method of cytoskeletal labelling can also be applied to distinguish the glial population of a culture, as this cell type has a unique intermediate filamentous protein called glial fibrillary associated protein (GFAP) (Kingsley 2000).

Summary

In this chapter the methods used to develop a neuron rich culture from spinal cord tissue are described. Although previous studies at the Centre for Cell Engineering (CCE) had used primary neuronal cultures, this project was the first to use spinal cord tissue as a biological model. Therefore it was necessary to investigate and develop optimal conditions for isolating and maintaining this cell type. In the beginning cells were isolated from postnatal (P1-P3) Sprague Dawley rat pups and cultures were quantified using immunocytochemical staining techniques. However, during the production of this thesis, for unknown reasons, cell survival rates diminished resulting in a move towards embryonic cultures. Again growth conditions were investigated and cell populations were characterised by immunocytochemistry.

Materials and Methods

Media and Solutions

All the basic media and solutions used in this chapter are listed in *Appendix I: Media, Reagents and Solutions*. Where volumes are given, the total volume of the solution is the sum of those stated. Where the ingredient weight is given, the material has been dissolved in reverse osmosis (RO) water, unless otherwise stated. Alterations made to any solution after preparation is noted in the procedure descriptions.

A. Established Methods

A.1. Primary Postnatal Spinal Cord Culture

Substrate Preparation

Glass cover slips (13mm dia, VWR International) were cleaned in Caro's acid (3 parts sulphuric acid, 1 part 30% hydrogen peroxide) for 15 minutes, washed three times (3x) in sterile RO water before being stored in 70% ethanol until required. To remove all traces of ethanol, cover slips were stored in sterile RO water for 48 hours, then blow-dried with sterile particle-free compressed air and then kept in the oven at 60°C overnight. Cover slips were incubated in 1μg/ml sterile filtered poly-l-lysine (PLL)(Sigma, Poole, UK) for 1 hour. The culture vessel for these experiments was a 12 well plate.

Spinal Cord Dissection and Preparation

For each culture session, four neonatal Sprague Dawley rat pups aged between 1-3 days (supplied by Biological Services, Glasgow University) were killed by barbiturate overdose according to Home Office guidelines. Each pup was pinned face down on a dissection board, then washed in 70% ethanol to minimise contamination. An incision was made from head to tail, the skin was peeled back to reveal the musculature of the spine, which was then scraped away (using No.10 scalpel blade) to expose the vertebrae. Using a fresh scalpel blade the exposed dorsal vertebrae were removed by gently scraping with the blade, this time from tail to head, several times over the spinal column. All remaining bone fragments were removed using fine dissecting tweezers. The exposed spinal cord was isolated free from the dorsal root ganglia and transferred to a sterile Petri-dish, containing

sterile HEPES saline (kept at 4 °C), to remove remaining erythrocytes, connective tissue and meninges. Once all tissue was dissected, the collected spinal cords were transferred to a separate sterile glass Petri-dish where they were finely minced (fragments measured less 1mm^2) before being dissociated by cell isolation method C (see Method Development- *Cell Isolation* for descriptions). Five millilitres of 10% foetal calf serum (FCS) solution was added to stop enzymatic digestion; cells were then centrifuged at 800g for 4 minutes and the pellet resuspended in growth media. All remaining tissue fragments were dispersed by triturating the cell suspension approximately 10x using a sterile Pasteur pipette of decreasing bore size (the tip bore was reduced in diameter using a Bunsen flame). Cells were plated for 30 minutes in a tissue culture flask to reduce the glial population of the culture by differential adhesion. The supernatant containing the neuron-rich population of cells was again centrifuged (800g for 4 minutes) and resuspended, counted, then diluted to the required plating density. Cells were allowed to adhere for 1 hour (see Method Development- *Removal of Debris* for methods employed) before 2 ml (although volume varied depending on the culture vessel used) Growth Media (Media A: 98 mls NBA, 2mls B27, 1ml Glutamax, 1ml pen/strep) was added, following which the culture was maintained at 37°C in 5% $C0_2$, with Growth Media changed every 5 days.

Immunocytochemical Staining

Cells and cover slips were washed 3x with 1x phosphate buffered salt solution (PBS) (warmed to 37°C), then fixed with 4% formal saline at 37°C for 15 minutes. The cells were then incubated for 5 minutes at 4°C in permeabilisation buffer (added at room temperature), then in blocking solution (sterile filtered) for 5 minutes at 37°C. From the various blocking solutions tested (see Method Development- *Blocking Solutions*), solution D produced the best results, and was therefore the solution of choice for the following experiments (see Table 2.4 for solution composition). Primary antibodies were diluted to working concentration with blocking solution to a volume allowing approximately 100μl of antibody to be added to each cover slip. Cells were incubated in primary antibodies for 1 hour at 37°C after which a series of 5 minutes washes with Tween 20 buffer ensured that all traces of primary antibody had been removed. This process of antibody incubation and removal was repeated for the secondary antibody, diluted to working concentration in blocking solution, 100μl per cover slip, 1 hour incubation at 37°C, 3x for 5 minutes wash in Tween 20 buffer solution. To ensure antibody solution did not evaporate during the 1 hour

incubation period, cover slips were transferred to a water vapour saturated immunohistochemistry incubation chamber before being stored in the hot room. Excess washing solution was removed from each cover slip before being mounted (cells down) onto 50μl of mounting Vector (with or without nuclei stain) (Vector Laboratories, Ltd., Peterborough, UK) then sealed with clear nail varnish.

A.2. Primary Embryonic Spinal Cord Culture

The methods described in this section are based on those used in the Department of Glial Cell Biology (Beatson Laboratories, Glasgow University), which have been adapted to suit this study.

Substrate Preparation

Thirteen millimetre diameter glass cover slips were sterilised by autoclaving. Cover slips were coated with sterile filtered PLL (Sigma, Poole, UK) overnight at 37°C. Before being used cover slips were washed 3x in sterile RO water to remove all traces of unbound PLL. The culture vessel used in these experiments was a small Petri dish into which three cover slips were placed.

Cell Preparation

Pregnant (E14) Sprague Dawley rats were sacrificed by CO_2 overdose as approved by the Home Office. Before removing the embryonic sacs, it was necessary to wash the abdomen of the adult rat thoroughly in 70% ethanol to reduce contamination. The isolated embryo sacks were collected in HBSS w/o Ca^{2+} and Mg^{2+} (Gibco, Paisley, UK, previously stored at 4°C). Embryo dissection took place in a sterile Petri dish containing HBSS w/o Ca^{2+} and Mg^{2+}. The embryos were removed from the amniotic sac using fine dissecting forceps then transferred to a fresh Petri dish containing HBSS w/o Ca^{2+} and Mg^{2+}. Each embryo head was removed using dissecting scissors; this also removed the musculature surrounding the neck, allowing easier access to the spinal cord tissue. The white column of the spinal cord tissue was exposed by gently removing each covering tissue layer cover using fine dissecting forceps. The cords were removed and placed in a fresh Petri dish containing HBSS w/o Ca^{2+} and Mg^{2+} and the meninges removed. Cords were collected in the lid of a sterile Petri dish and all remaining solution removed, cords were then chopped into

fragments measuring less than 1mm^2 using a sterile scalpel blade. Cells were isolated by enzymatic digestion in 2ml trypsin solution for 20 minutes at 37°C. Cell digestion was stopped by adding 2mls SBTI-DNAse solution. The cell suspension was gently triturated with a sterile wide bore Pasteur pipette, then centrifuged at 800g for 5 minutes. The cell pellet was re-suspended in plating media then triturated gently; all non-dispersed tissue was allowed to settle before being discarded. Cells were then plated at the required plating density. After allowing cells to settle and adhere for 2 hours under culture conditions (5% CO_2, 37°C), all plating media was removed and exchanged with 1ml serum-free growth media containing 98 mls NBA, 2mls B27, 1ml Glutamax, 1ml pen/strep (Media A, all reagents from Gibco). Cells were maintained in 5% CO_2 atmosphere at 37°C, with 50% of the culture media being changed every 4 days.

Immunocytochemical Staining

Cells were washed 3x with 1x PBS (warmed to 37°C), fixed with 4% formal saline at 37°C for 15 minutes, then incubated in permeabilisation buffer (0.5% Triton X100) for 15 minutes at room temperature. All antibodies were diluted to working concentration with a modified PBS solution (0.3 M NaCl PBS, 0.3% Triton X100), all primary antibodies were incubated overnight at 4°C, and all secondary antibodies at working dilution 1:100 for 1hour at 37°C. After each stage of antibody incubation, cells were washed gently 3 times in 1x PBS. Cultures were characterised using the following cells markers: neuron specific Mouse Anti-β-tubulin III (IgG_{2b}) (1:100, Sigma), the synapse marker Synaptophysin (1:100, Santa Cruz Biotechnology, Santa Cruz, USA), axon specific Smi31 (1:1500, Sternberger Monocolonals, Maryland, USA), the glia marker Rabbit Anti-Glial Fibrillary Acidic Protein (GFAP) (1:100, Dakocytomation, Glostrup, Denmark) and oligodendrocyte marker AA3 (1:10, hybridoma supernatant kindly donated by Dr. Sue Barnett, Beatson Laboratories, Glasgow), used in conjunction with secondary antibodies; FITC goat anti-mouse IgG_{2b} and TRITC goat anti-rabbit (both from Cambridge Bioscience, Cambridge, UK), Cascade blue goat anti-mouse IgG_1 and Cascade blue goat anti-rabbit (both from Molecular Probes, Paisley, UK) and TRITC goat anti-rat IgM (Cambridge Bioscience), respectively. All fluorescence images were taken using a Evolution QEi camera (MediaCybernetics, Berkshire, UK), mounted onto a Zeiss Axiovert 200M microscope (Zeiss Ltd, Hertfordshire, UK) and captured using Image Pro-Plus (MediaCybernetics) acquisition software.

B. Method Development

B.1. Primary Postnatal Spinal Cord Culture

Cell Isolation

The 3 different isolation methods used to produce a single cell suspension are summarised below:

Method		Description
A	Enzymatic digestion only	Chopped tissue was incubated in 5ml 0.25% trypsin solution at 37°C for 20 minutes.
B	Mechanical dissociation only	Chopped tissue was triturated approx. 20x with Pasteur pipettes of decreasing pore diameter.
C	Enzymatic + Mechanical (A+B)	Method A followed by Method B

Table 2.1. Table summarising the methods used to produce a single cell suspension.

Removal of Cell Debris

Following initial cell plating the following methods were used in an attempt to reduce cell debris within the cell culture:

Method		Description
A	No removal	Once plated cells were maintained in culture for 4 day until 1st media exchange.
B	Shaker plate	Cells were allowed to adhere for 1 hour, then placed on a shaker table at the lowest possible speed for 30 minutes.
C	Manual panning	Cells were allowed to adhere for 1 hour, then gently swirled for 5 minutes by hand and growth media exchange. This step was repeated 3 times.
D	Media exchange	Cells were allowed to adhere for 1 hour, then growth media was exchanged 3 times.

Table 2.2. Table summarising the methods used to reduce cell debris.

Growth Media

The various growth media tested are listed in Table 2.3. The figures given indicate the volume (ml) added (see Abbreviations for short form).

A		B		C		D		E	
Hams F12	93	MEM	27.6	NBA	95	NBA	96	NBA	98
Anti.B	2	Anti.B	2	Anti.B	3	Anti.B	2	B27	2
FCS	5	FCS	3	FCS	2	B27	2	Glutamax	1
				FGF	0.01			Pen/strep	1

Table 2.3. Table listing the 5 different compositions of growth media tested with postnatal spinal cord neuronal cultures.

Blocking and Permeability Solutions

Five different blocking solutions for fluorescent protein imaging were used to produce the optimum fluorescent imaging results. The solutions tested are listed in Table 2.4 (see Abbreviations for short form).

A	B	C	D
4% BSA 0.2% Triton X100	5% Goat Serum 0.2% Triton X100	0.5% BSA 0.1% Triton X100 10% FCS	1% BSA 1% Triton X100 5% Goat Serum

Table 2.4. Table listing the 4 different compositions of blocking solutions tested. Each solution was made to a total volume of.100ml using 1x PBS salt solution.

B.2. Primary Embryonic Spinal Cord Culture

Growth Media

Four growth media compositions were tested: Neural Basal A (NBA) media (98 mls NBA, 2mls B27, 1ml Glutamax, 1ml pen/strep), NBA plus astrocyte-conditioned media (ACM), NBA plus horse serum, and finally NBA plus ACM with horse serum. The ACM media was removed from astrocytes cultures (maintained in DMEM, supplemented with L-glutamine) after 5 days. Table 2.5 describes the methods used to remove serum-containing plating media.

Media		Description
A	NBA	All serum containing plating media was removed, cells were gently washed in HBSS to remove all traces of serum. 1ml of NBA media was added and cells returned to culture.
B	NBA + ACM	All serum containing plating media was removed, cells were gently washed in NBA to remove all traces of serum. 0.5ml of NBA media and 0.5ml of ACM was added and cells returned to culture
C	NBA + S	Serum containing plating media was not removed. 1ml of NBA media was added and cells returned to culture.
D	NBA + ACM + S	Serum containing plating media was not removed. 0.5ml of NBA media and 0.5ml of ACM was added and cells returned to culture

Table 2.5. Table describing the methods used to exchange the plating solution for growth media and the resulting media composition.

Differential Adhesion

The use of differential adhesion as a means of reducing the glial population of the embryonic culture was tested. Following emzymatic digestion and mechanical dissociation, cells were resuspended in plating media (see Appendix), transferred to a culture flask and maintained for 1 hour in culture conditions (37°C, 5% CO_2).

Results

A. Established Methods

A.1. Primary Postnatal Spinal Cord Culture

Classification of Cell Population

The population of cell types within the culture of postnatal spinal cord tissue was investigated using double labelling fluorescence microscopy. Cells, plated at 1000 cells/mm^2, were cultured for 7 days on 13 diameter cover slips then fixed and double stained for GFAP, a cytoskeletal filament only present in glial cells, and β-tubulin, a neuron specific isoform of tubulin. Cell counts were calculated from 10 images taken at random from 5 different samples. Results showed 40 % of the cells stained positive for GFAP, where as 60% of cells stained positive for β-tubulin (see Graph 2.1).

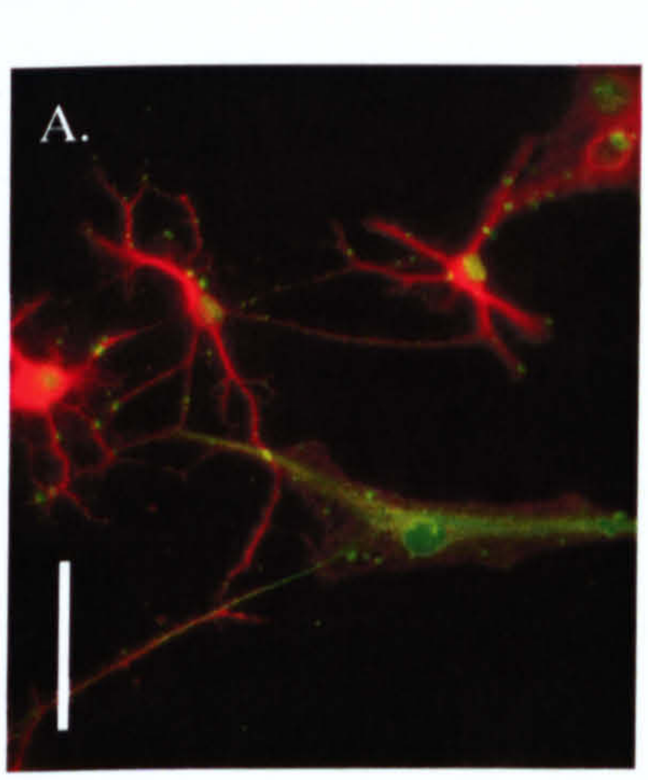

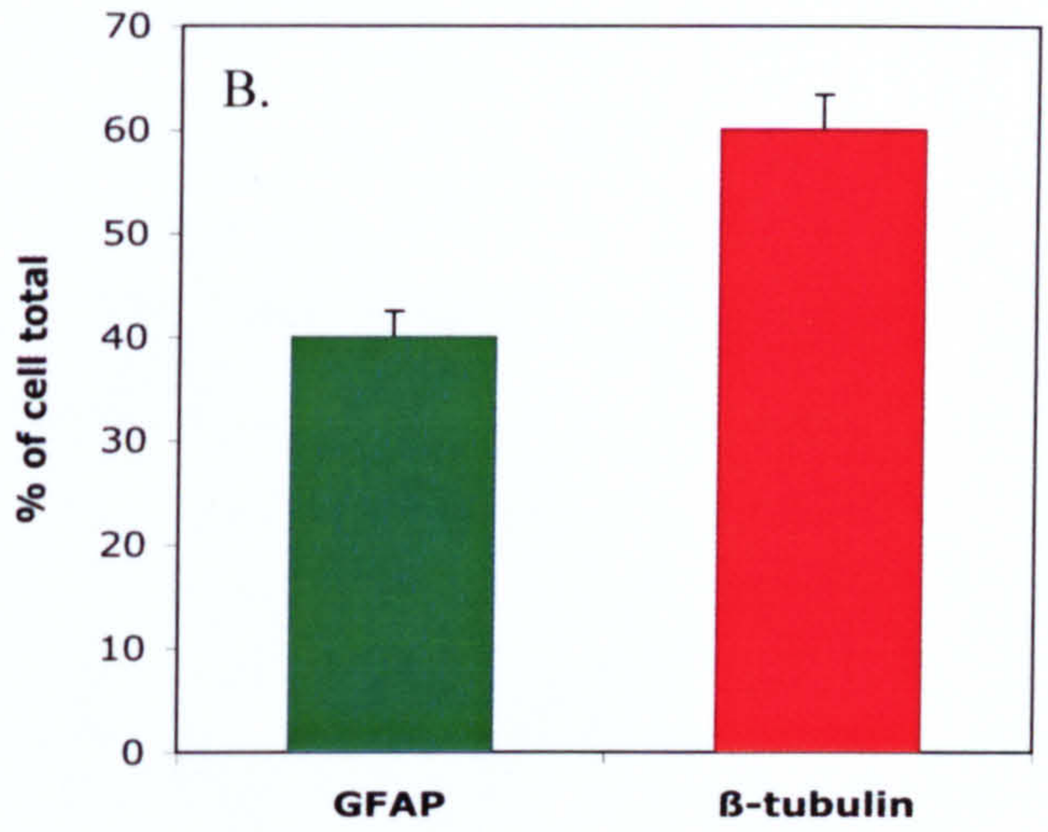

*Figure 2.1. (A) Double staining of postnatal spinal cord culture for the neuronal cytoskeletal marker **ß-tubulin** and glial cell marker **GFAP**, following 1 wk in culture. Scale bar is 50µm.*

*Graph 2.1. (B) Graph showing the percentage of total cells within postnatal spinal cord tissue culture which stained positive for **GFAP** and **ß-tubulin**, following 1wk in culture. Results and mean value ± standard deviation*

Percentage of GABA-ergic Inhibitory Neurons

The population of inhibitory neurons within the culture was considered. Cells were fixed and stained for GABA antibody, (a marker for inhibitory amino acid neurotransmitter GABA in cell bodies, axons and terminals of GABA-ergic neurons) after 2 weeks and 5 weeks in culture. Twenty random images were taken from five different samples at each time point and analysed as shown in Figure 2.2. The phase contrast image (A1, B1) was used to count the total cell number for any field of view. The corresponding fluorescence image was superimposed over this allowing the number of GABA-ergic cells to be counted and thus calculated as a percentage of the total number of cells. After 2 weeks only 5% of the culture population stained positive for GABA, compared to 12% after 5 weeks (see Graph 2.2.B). However, if the total number of cells counted is considered, no difference in the number of GABA-ergic neurons was found between the two time points. In fact the total number of cells that did not stain for GABA had fallen from 998 to 445 cells (see Graph A), accounting for the difference in the percentage of GABA neurons shown in Graph B.

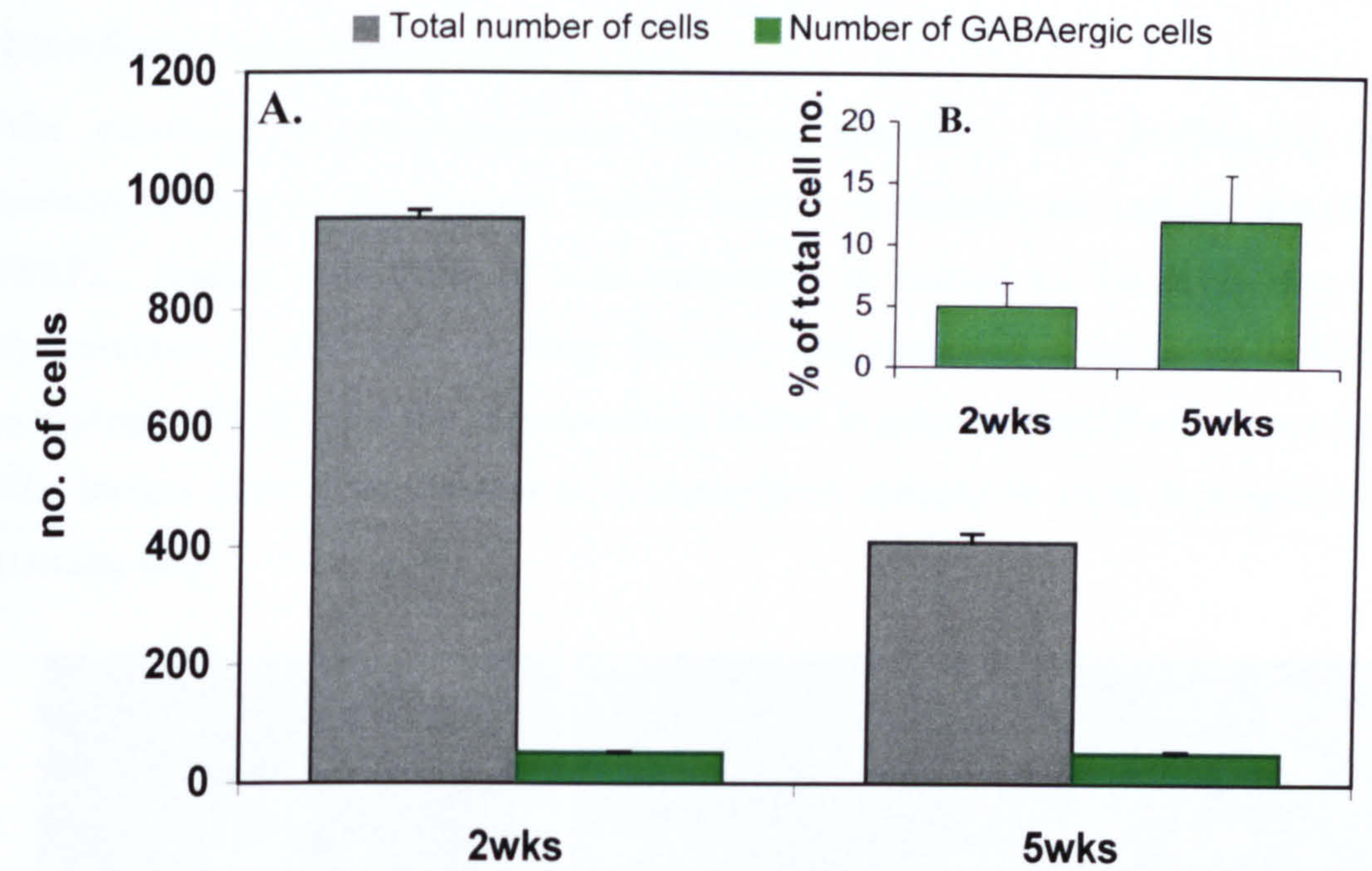

Graph 2.2. Graph A shows the number of cells stained positive for inhibitory neurotransmitter GABA in relation to the total number of cells counted after 2 weeks and then 5 weeks in culture. Graph B showing this result as a percentage of cell number. Results are the mean value ± standard deviation.

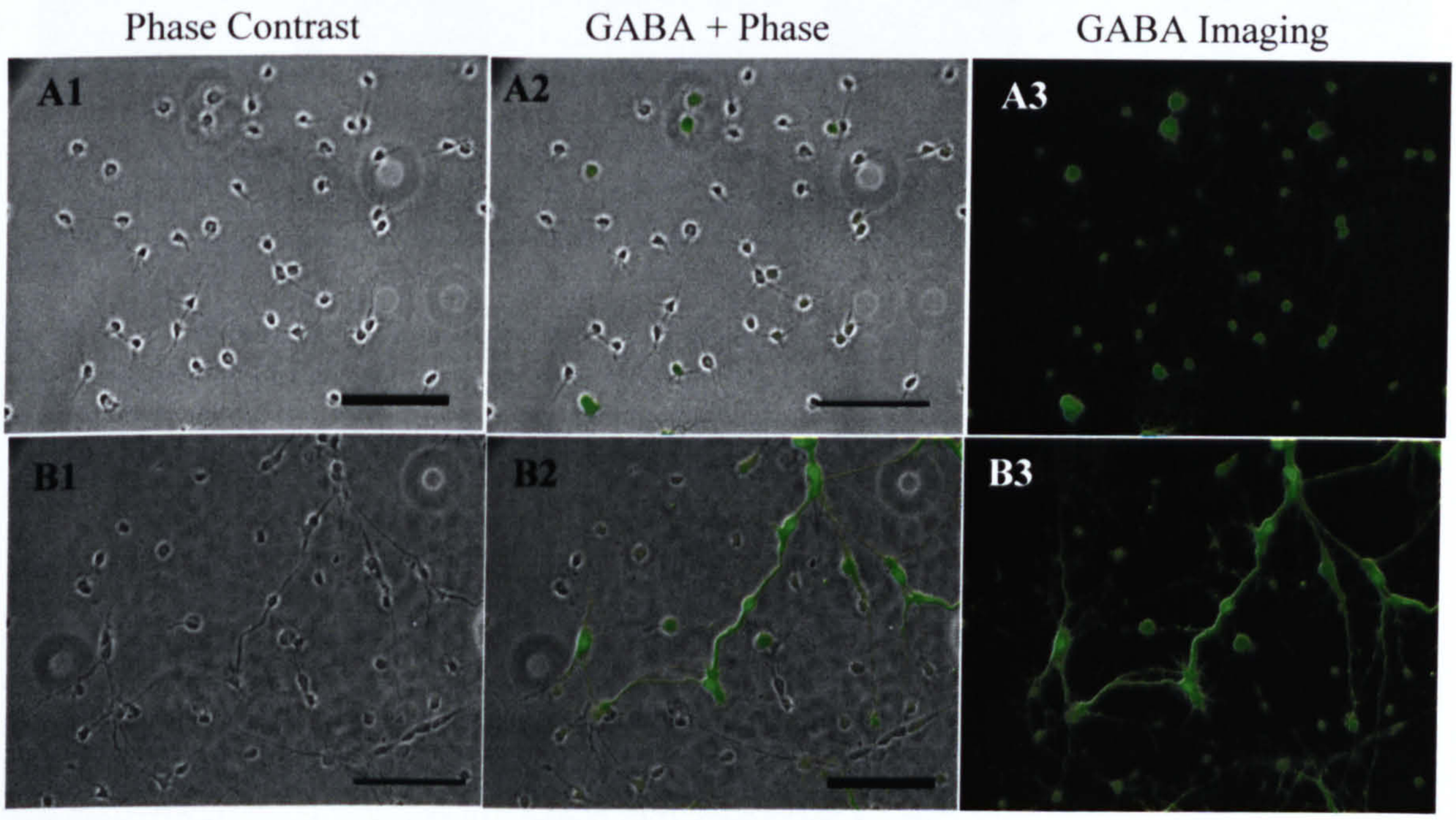

Figure 2.2. Postnatal spinal cord neurons following 2 weeks (figure set A) and 5 weeks (figure set B) in culture fixed and stained for GABA. Images showing phase contrast microscopy (A1, B1) and corresponding fluorescence image (A3, B3). Statistics were calculated from the fluorescence-phase overlay (A2, B2). Scale is 100 μm and is the same for all images.

Identification of Synaptic Activity

The existence of neurotransmitter releasing apparatus was investigated by double immunostaining for the synaptic vesicle marker, synaptophysin and the dendritic marker MAP2. Images were taken of cells maintained in culture for 16 days. The results are fluorescence micrographs showing; the raw, non-enhanced labelling of MAP2 (A) and synaptophysin (B), and the corresponding colour overlay of both fluorescence images (C). The images show a localisation of synaptophysin staining to areas highlighted by MAP2 staining only.

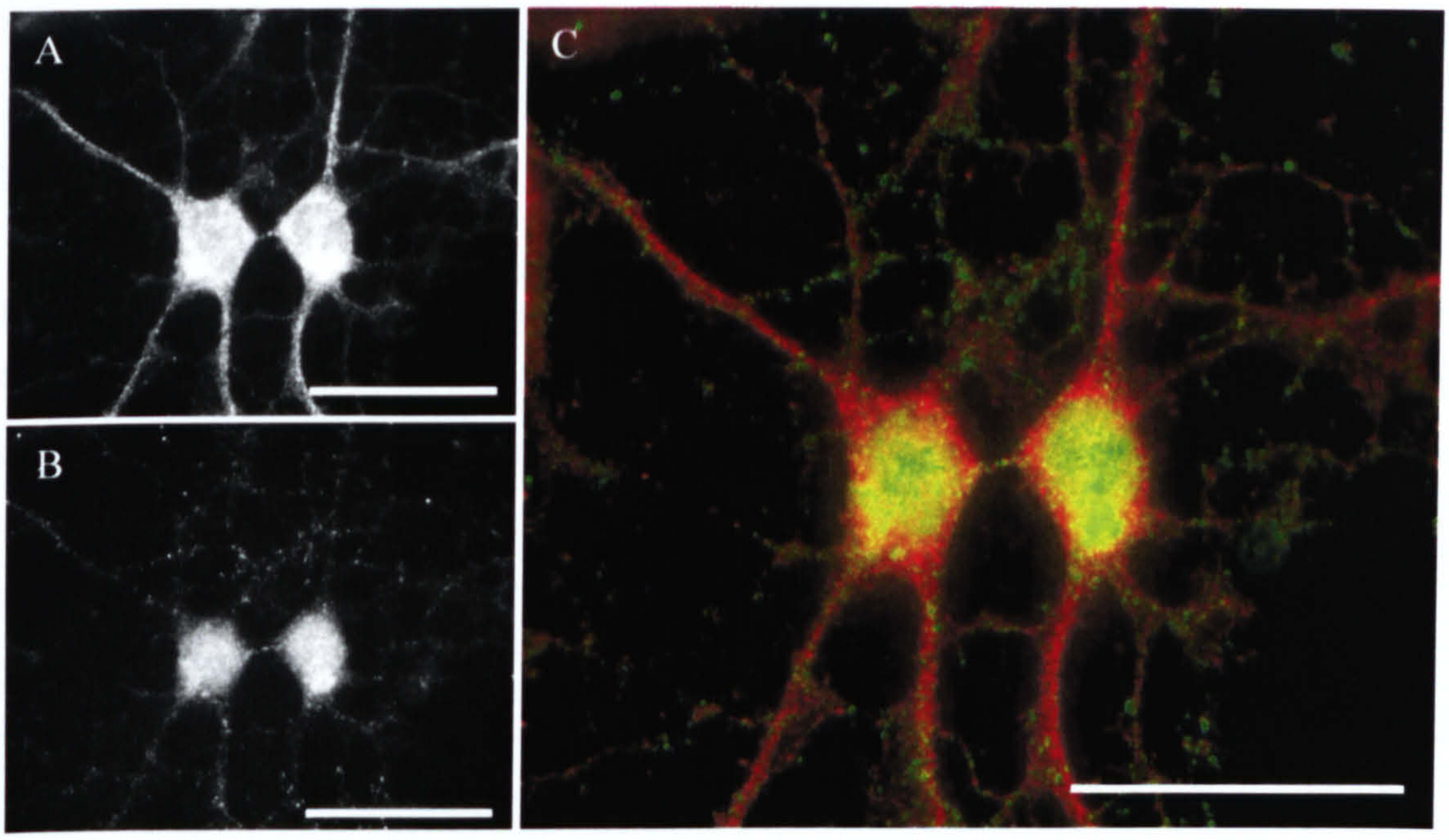

*Figure 2.3. Postnatal spinal cord neurons double stained for **MAP2** and neurotransmitter vesicle marker **synaptophysin**. Image A & B show raw unedited micrograph of MAP2 and synaptophysin, respectively. Image C shows colour overlay. The scale bar is 50μm in all images.*

A.2. Primary Embryonic Spinal Cord Culture

Classification of Cell Population

The population of cell types within cultures of embryonic spinal cord tissue was investigated by use of triple immunocytochemistry. Cell populations were compared at plating densities of 6000, 8000 and 10,000 cells/mm^2 following 1 week and 2 weeks in culture. Cells were fixed and stained for β-tubulin, a neuron specific cytoskeletal marker, GFAP, a glial cell marker and AA3 a marker for late oligodendrocytes. Five images were taken at random from a total of 5 samples, examples of which are presented in Figures 2.5-2.7 (in each case figure set A shows cells after 1 week, and figure set B after 2 weeks in culture) and the results, measured as percentage of total cell number per field of view, are presented in Graph 2.3.

A) 6000 cells/mm^2

After 1 week in culture 70% of the total cell population stained positive for β-tubulin, with only 10% and 20% of cells staining positive for the glial cell markers AA3 and GFAP respectively. However after 2 weeks glial proliferation and neuronal cell death resulted in a dramatic change in cell culture population, with 45% of cells staining positive for GFAP and less than 20% staining positive for neuronal marker, β-tubulin.

B) 8000 cells/mm^2

The population of β-tubulin cells dropped by only 10% following 2 weeks in culture, and the glia population only increased by 5%.

C) 10,000 cells/mm^2

Following 1 week in culture the glial populace accounted for only 10% of total cells counted, however this increased to 30% after 2 weeks. The opposite was true for the neuron population, with 50% of cell staining for β-tubulin after 1 week, dropping to 30% after 2 weeks.

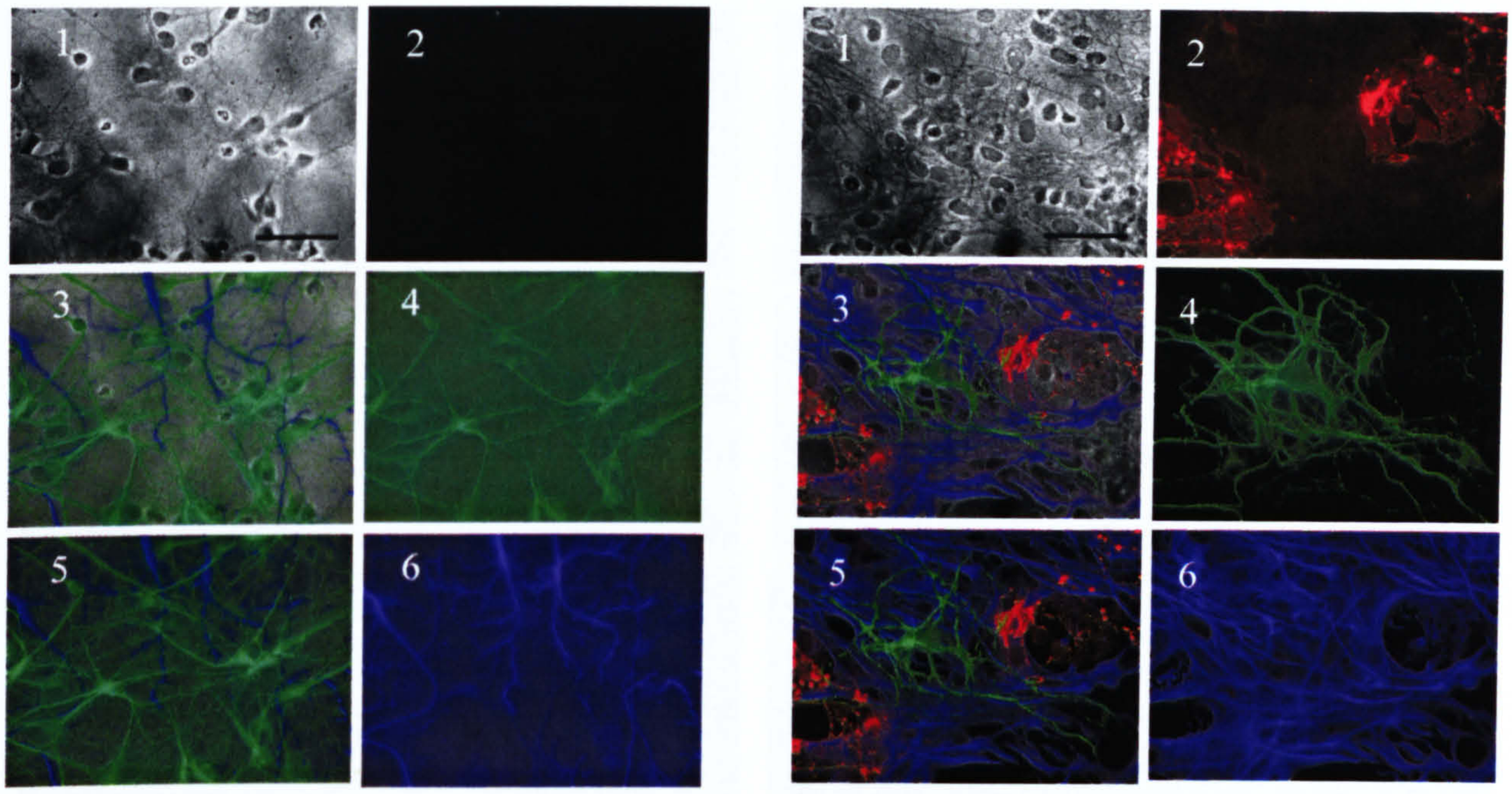

*Figure 2.4. Fluorescence images showing embryonic (E14) spinal cord neurons plated at 6000 cells/mm^2 following 1wk in culture (figure set A) and 2wks in culture (figure set B). Cells tripled labelled for **AA3** (2), **ß-tubulin** (4) and **GFAP** (6). In both figure sets image 1 shows phase contrast micrograph, image 3 phase and fluorescence overlay, and image 5 the triple stain composite. The scale bar in image 1 of each figure set is 50µm and is the same for all images.*

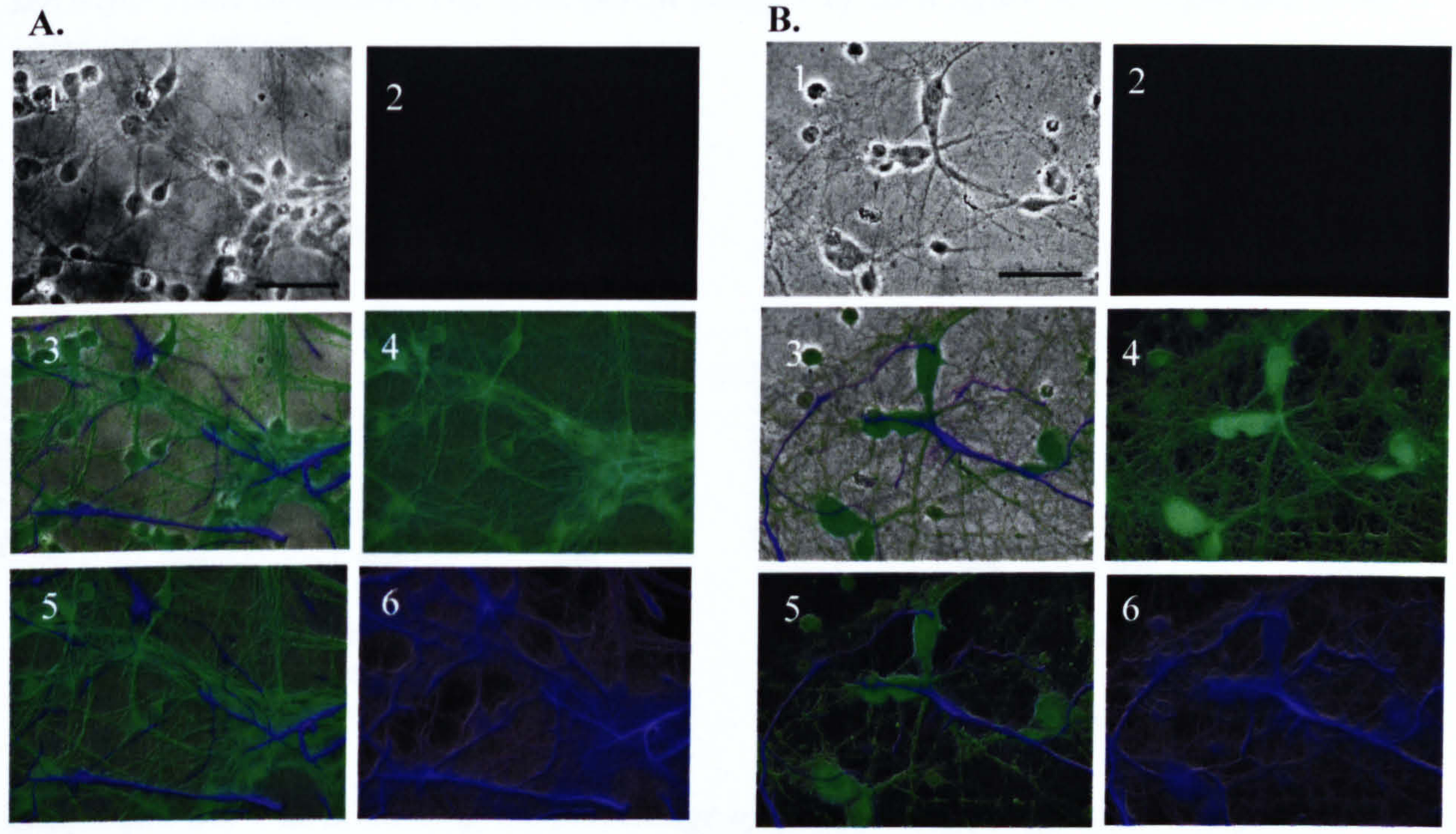

*Figure 2.5. Fluorescence images showing embryonic (E14) spinal cord neurons plated at 8000 cell/mm^2 following 1wk in culture (figure set A) and 2wks in culture (figure set B). Cells tripled labelled for **AA3** (2), **ß-tubulin** (4) and **GFAP** (6). In both figure sets image 1 shows phase contrast micrograph, image 3 phase with fluorescence overlay, and image 5 the triple stain composite. The scale bar in image 1 of each figure set is 50µm and is the same for all images.*

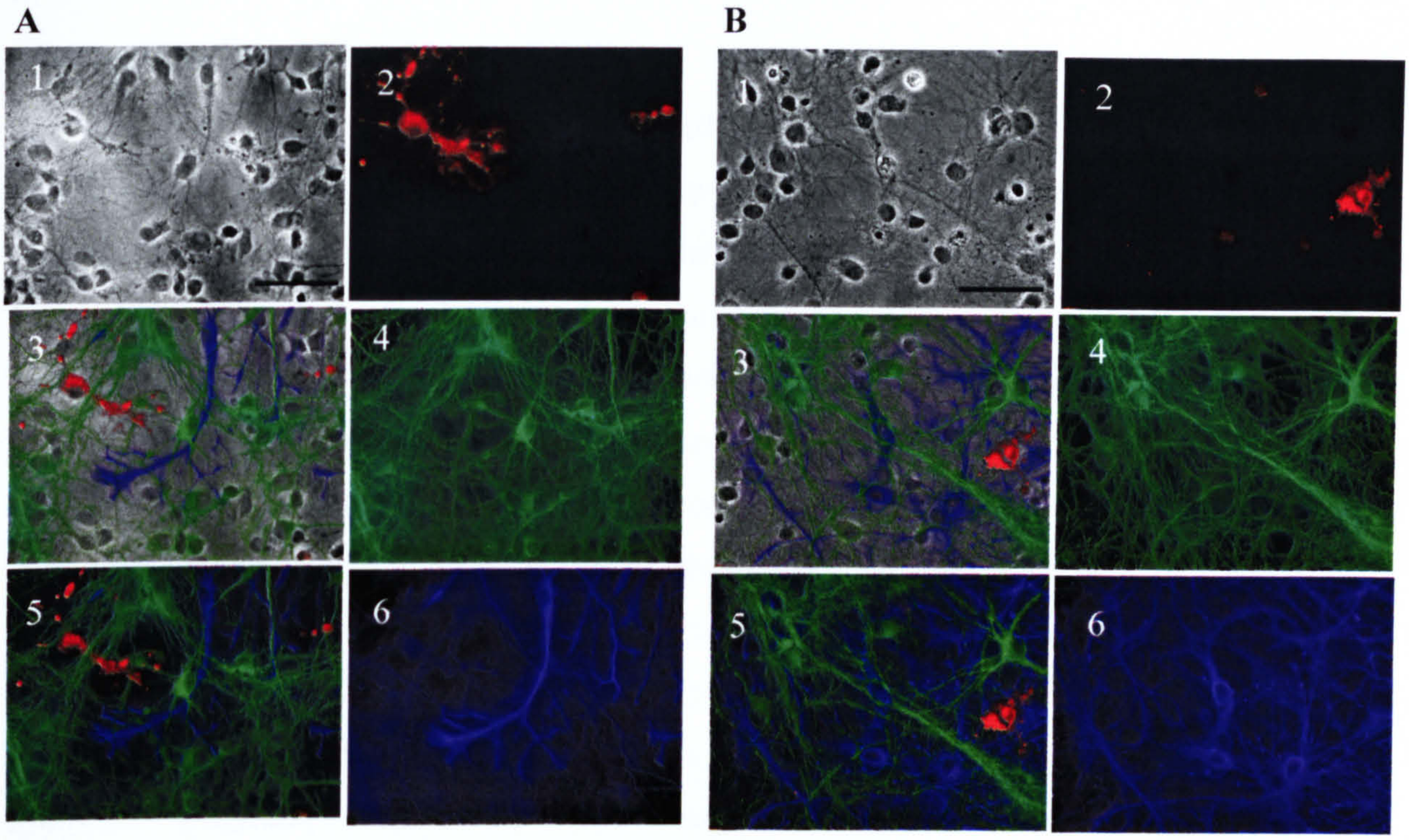

*Figure 2.6. Fluorescence images showing embryonic (E14) spinal cord neurons plated at 10,000 cell/mm² following 1wk in culture (figure set A) and 2wks in culture (figure set B). Cells tripled labelled for **AA3** (2), **ß-tubulin** (4) and **GFAP** (6). In both figure sets image 1 shows phase contrast micrograph, image 3 phase with fluorescence overlay, and image 5 the triple stain composite. The scale bar in image 1 of each figure set is 50µm and is the same for all images.*

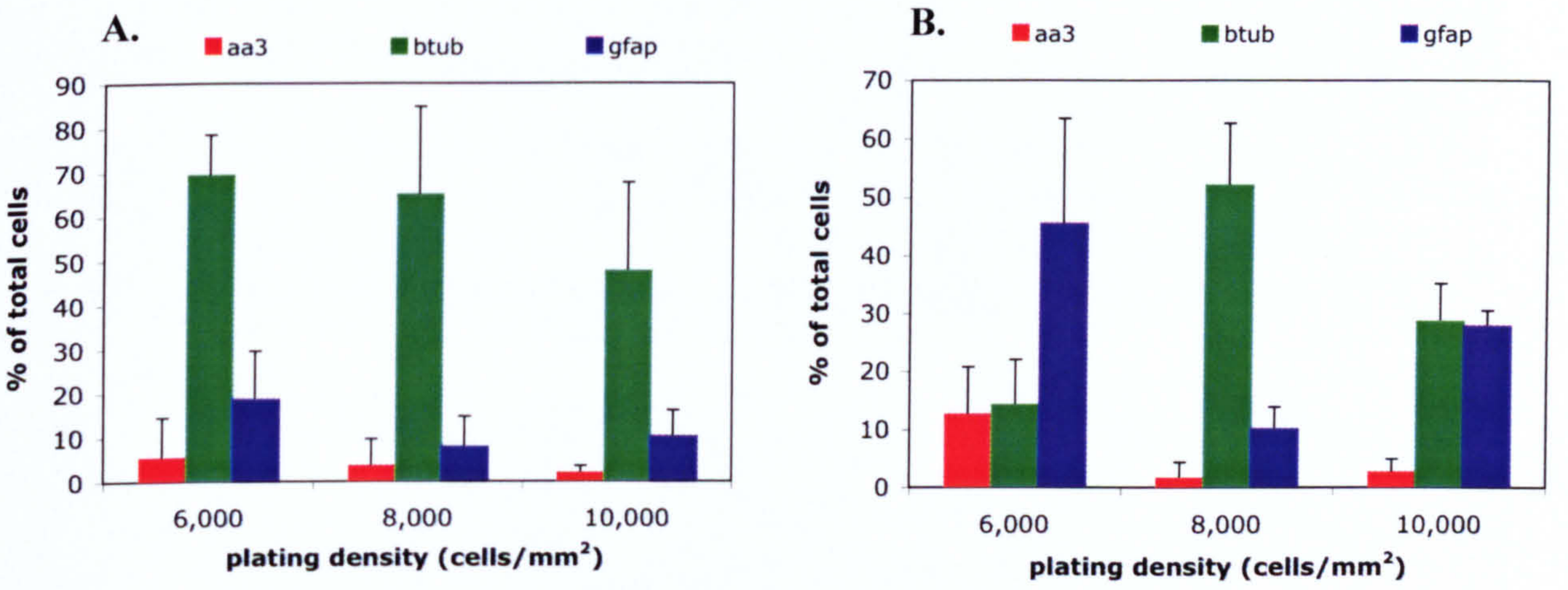

*Graph 2.3. Bar charts showing the percentage of cells stained positive for **AA3**, **ß-tubulin** and **GFAP** at each plating density, 6000 cells/mm², 8000 cells/mm² and 10,000 cells/mm², after 1 week (A) and 2 weeks in culture (B). Results are the mean value ± the standard deviation.*

Characterisation of Neural Networks

The aim of this study was determine what effect plating density had on neural network configuration, with regards to synapse formation and axon development. Cells grown at plating densities 6000, 8000 and 10,000 cells/mm^2 were fixed and tripled stained for β-tubulin, Smi 31 and synaptophysin, and compared after 1 week, and 2 weeks in culture. At each time point and for each density, five fields of view, selected at random from five different samples, were used to assess the formation of neural networks. The result are presented in Figure 2.7, and show the fluorescence micrographs of the three stains combined. Cultures grown for only 1 week showed no evidence of phosphorylated axons regardless of the density at which they were seeded. Only in cultures that had been maintained for 2 weeks were axons staining positive for Smi 31. However at both time points synaptophysin staining was evident in all samples. In cultures plated at 6000 cells/mm^2 individual cells bodies were easily identifiable, as were the surrounding innervating axons and dendritic processes. At plating densities 8000 and 10,000 cells/mm^2, the neural networks were much more dense, making it difficult to track the path in a particular process or axon.

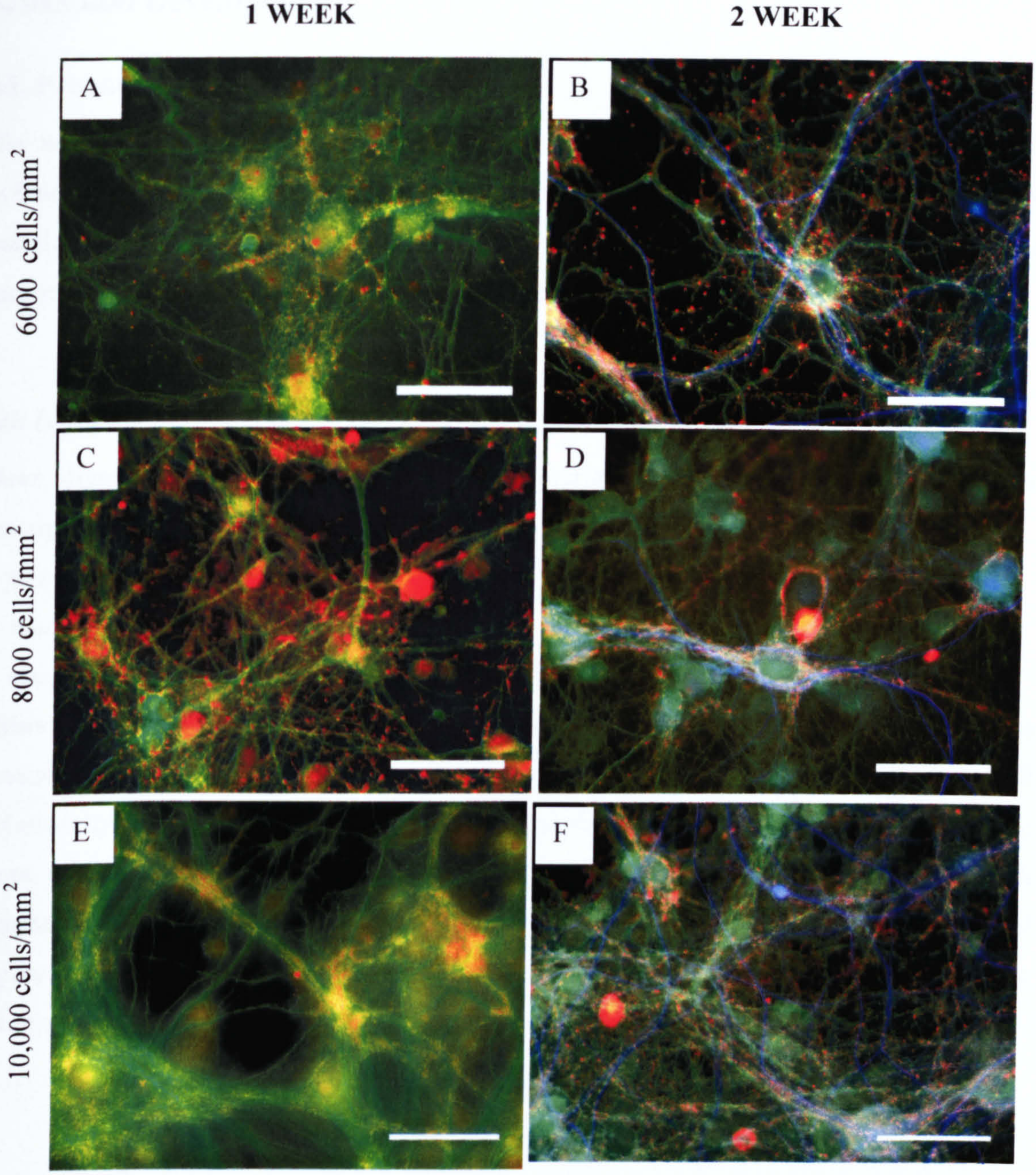

Figure 2.7. Fluorescence images showing embryonic (E14) spinal cord neurons tripled labelled for ß-tubulin, synaptophysin and Smi 31 at; 6000 cells/mm^2 following 1wk (A) and 2wks in culture (B), 8000 cells/mm^2 following 1wk (C) and 2wks in culture (D) and 10,000 cells/mm^2 following 1wk (E) and 2wks in culture (F). Scale bar in each image is 50µm.

B. Method Development

B.1. Primary Postnatal Spinal Cord Culture

The work presented in this section aimed to develop and optimise the tissue culture techniques used to isolate primary postnatal spinal cord neurons. Various dissection techniques, digestion methods and Growth Medium have been tested throughout the duration of this thesis. Results are based on observations made during diagnostic testing.

Cell Isolation

Three digestion methods were tested (see Materials and Methods- *Cell Isolation* for descriptions):

- enzymatic digestion only
- mechanical dissociation only
- enzymatic directly followed by mechanical dissociation.

Although isolation by enzymatic digestion had the desired effect of breaking down the connective tissue, the cell suspension was predominately composed of cell aggregates. Cell isolation by mechanical dissociation only, produced the same result, however in this case more cell debris was evident. Of the three methods tested, the combination of both enzymatic and mechanical digestion proved most successful, with fewer cell aggregates and higher concentrations of living, suspended cells. However cell debris remained a compromising factor. Results are summarised below in Table 2.6.

Method	Cell Aggregates	Single Cells	Cell Debris
A	+ / +	– / –	+ / –
B	+ / +	– / –	+ / +
C	– / –	+ / +	+ / –

Table 2.6. Summary table of qualitative observations of cell suspension made after cell isolation procedure. A quantitative analysis is given where +/+ indicates 'abundant', +/– 'evident', and –/– 'infrequent'.

Plating Density

It was necessary to grow cells at an optimal density that would allow for the identification of individual cells without compromising cell survival. The following densities were chosen; 100, 1000 and 5000 cells/mm^2. Cells plated at the lowest density tested (100 cells/mm^2) could not be maintained at the even distribution observed initially after plating. It was noted that after 72 hours in culture, cells would begin to actively migrate toward one another and formed aggregates, those cells that did not and remained isolated, would not survive (see Figure 2.8). On average, cells plated at this density showed no defining structural morphology and could not be maintained longer than 7 days in culture. Cells grown at 1000 cells/mm^2 appeared healthier, with longer processes evident, fewer aggregates forming, and with an even cell body distribution across the culture substrate. Cells plated at this density could be maintained for up to 3 weeks in culture conditions if sterility was not compromised. At a plating density of 5000 cells/mm^2 cell bodies were easily identifiable, however due to the increased concentration cell clumping would occur.

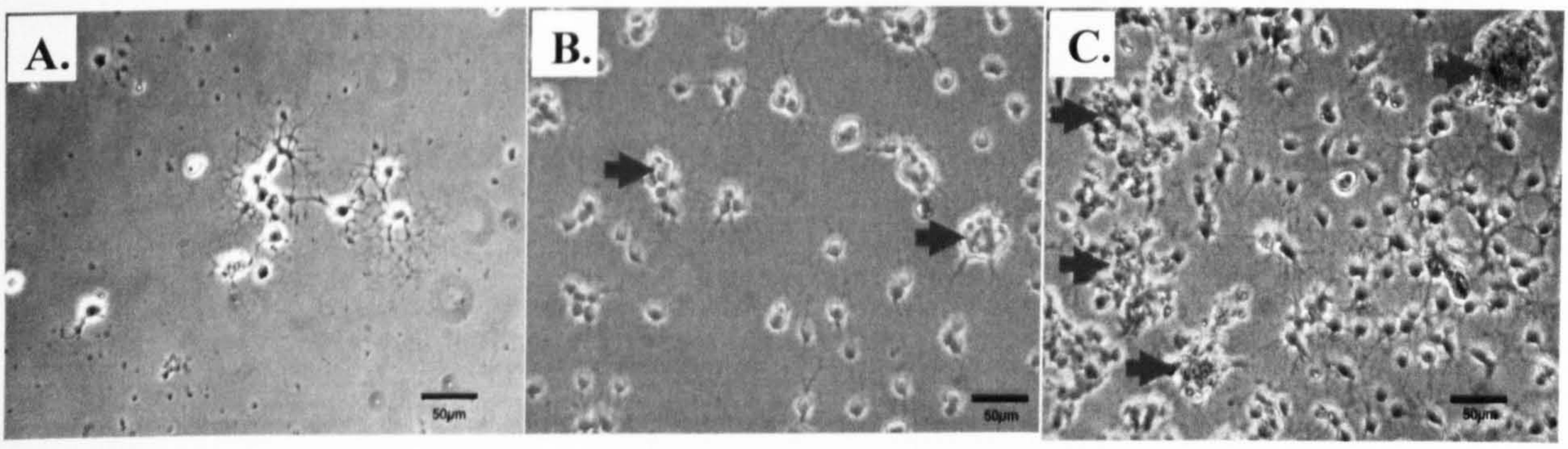

Figure 2.8. Spinal cord neurons at various plating densities; 100 cells/mm^2 (A), 1000 cells/mm^2 (B) and 5000 cells/mm^2 (C) following 7 days in culture, arrows indicate cell aggregates.

Removal of Cell Debris

Cell death was observed if debris, resulting from cell isolation, remained within the culture after cell plating. Therefore, steps had to be taken to remove this without affecting cell survival (see Materials and Methods- *Removal of Cell Debris* for method descriptions). The results are summarised in Table 2.7.

Method	Result Description	Result Summary
A	Cell death occurred after 24 hrs.	– / –
B	Although this method proved effective in removing debris, the shear force of the medium on the shaker plate detached partly adhered cells from the culture substrate.	+ / –
C	This method reduced cell debris without affecting adhered cells, however the exact force exerted on the cells could not be controlled.	+ / –
D	This method reduced Reduced cell debris without affecting adhered cells	+ / +

Table 2.7. Table of results summarising the affect of cell debris removal method on cell culture. A quantitative analysis is given where +/+ indicates an 'abundance' of healthy cells, +/– 'evidence' of healthy cells, and –/– an 'infrequent' number of healthy cells.

Blocking Solution

Four blocking solutions, of various compositions (see Materials and Methods-*Blocking Solutions*) were tested, with the aim of optimising immunocytochemical imaging. Results are from observations made following immunocytochemical staining with microtubule associated protein II (MAP2) antibody.

Fluorescence images in conjunction with blocking solution A showed non-specific binding of primary antibody based on morphological observations of labelled cells (Figure 2.9.A). Blocking solution B (Figure 2.9.B) showed similar results; all cells appeared to be labelled, with no evidence of neuronal structure. The neuron population of the cell culture could not be reliably identified using either blocking solution A or B. The use of blocking solution C significantly improved the quality of fluorescent stain and subsequently the images captured (Figure 2.9.C). Labelled cells displayed morphological characteristics associated with nerve cells structure, with no evidence of non-specific antibody binding. Of the four solutions tested, blocking solution D produced the best results. Cell bodies and cell structure were easily identified with no non-specific binding evident. Solutions C and D were also tested in double antibody labelling experiments, with primary antibodies against GFAP and β-tubulin. Although non-specific binding did not occur in each case, images taken of cells stained using solution D (see Figure 2.9.F) displayed less background labelling, as well as fewer antibody aggregates, making them more defined. The observations described are summarised in Table 2.8.

Solution	Result Description	Result Summary
A	Background labelling and non-specific binding abundant.	– / –
B	Background labelling and non-specific binding evident.	– / +
C	Reduced background labelling and no non-specific binding evident	+ / –
D	No Background labelling and no non-specific binding.	+ / +

Table 2.8. Table of results summarising the effect of blocking solution composition on fluorescent imaging where +/+ indicates 'excellent', +/– 'good', –/+ 'poor' and – / – 'bad'.

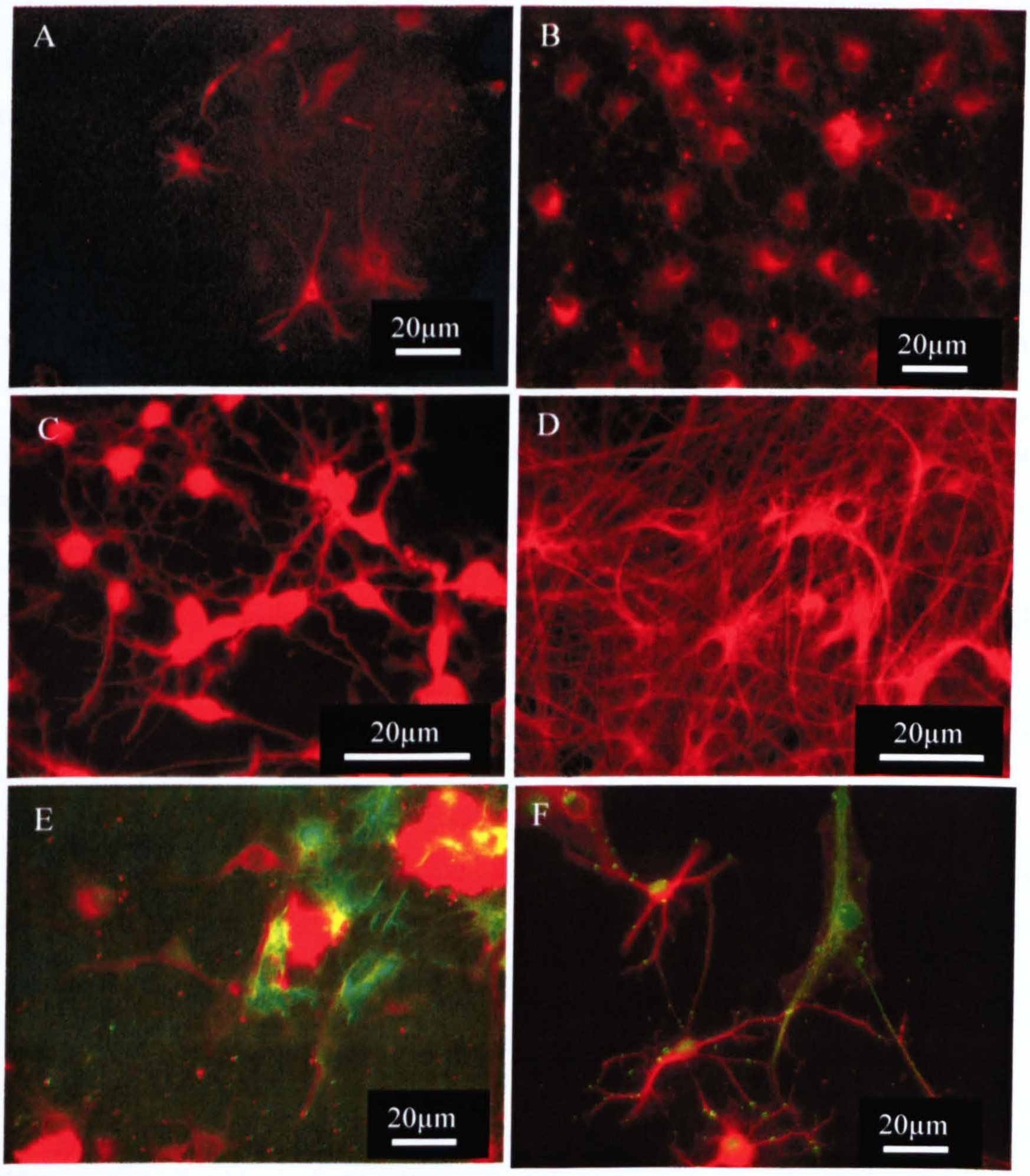

*Figure 2.9. Immunocytochemical microscopy of postnatal spinal cord neurons. Images A-D show cells fixed and stained for microtubule associated protein II (**MAP 2**) following incubation in blocking solution A-D (image label corresponding to blocking solution composition). Images E and F show cells fixed and double stained for glial fibrillary associated protein (**GFAP**) and **ß-tubulin** following incubation in blocking solution C (image E) and D (image F).*

B.2. Primary Embryonic Spinal Cord Culture

The results in this section were used to optimise the culture conditions for the survival of low-density embryonic spinal cord neurons.

Growth Media

Embryonic spinal cord neurons were grown on 13 diameter cover slips for 2wks, in the following culture media: 'NBA' (A), 'NBA + ACM' (B), 'NBA + S' (C) or 'NBA + ACM +S' (D) (see Section B.2, Materials and Methods for media descriptions). The effect of Growth Media composition on neuron survival and glial proliferation was investigated by means of fluorescence microscopy. Cells were fixed and triple labelled for Smi 31 (phosphorylated neurofilament marker), AA3 (mature oligodendrocyte marker) and GFAP (glial cell marker). Five images were taken at random from five different samples grown under each condition, and the results are based on observations made (see Figure 2.10). Cells grown in Growth Media A (NBA only) appeared to have more axons staining positive for Smi 31, in comparison to cells maintained in either Growth Media B, C or D (Figure 2.10, image set 2). Cultures maintained in media A, B and D were highly abundant in GFAP positive cells (Figure 2.10, A1, B1 and D1). However, the composition of Growth Media A and D did not appear to support oligodendrocyte proliferation (Figure 2.10, A3, B3). Growth Media C did not support glia proliferation, with the population of GFAP positive cells being greatly reduced in comparison to the other samples. However, this media was sufficient for oligodendrocyte growth. These results are summarised in Table 2.9.

Media	GFAP	Smi 31	AA3	Summary
A	+ / +	+ / +	– / –	**+ / +**
B	+ / +	+ / –	+ / –	**+ / –**
C	+ / –	+ / –	+ / +	**– / –**
D	+ / –	– / –	+ / –	**+ / –**

*Table 2.9. Table of results summarising the effect of growth media composition on nerve cell culture as determined by immunocytochemical labelling with antibodies against **GFAP**, **Smi 31** and **AA3** where +/+ denotes 'excellent', +/– 'good' and –/– 'poor'. For each antibody a quantitative analysis is given where +/+ indicates 'abundant', +/– 'evident' and –/– and 'infrequent' presence of antibody staining.*

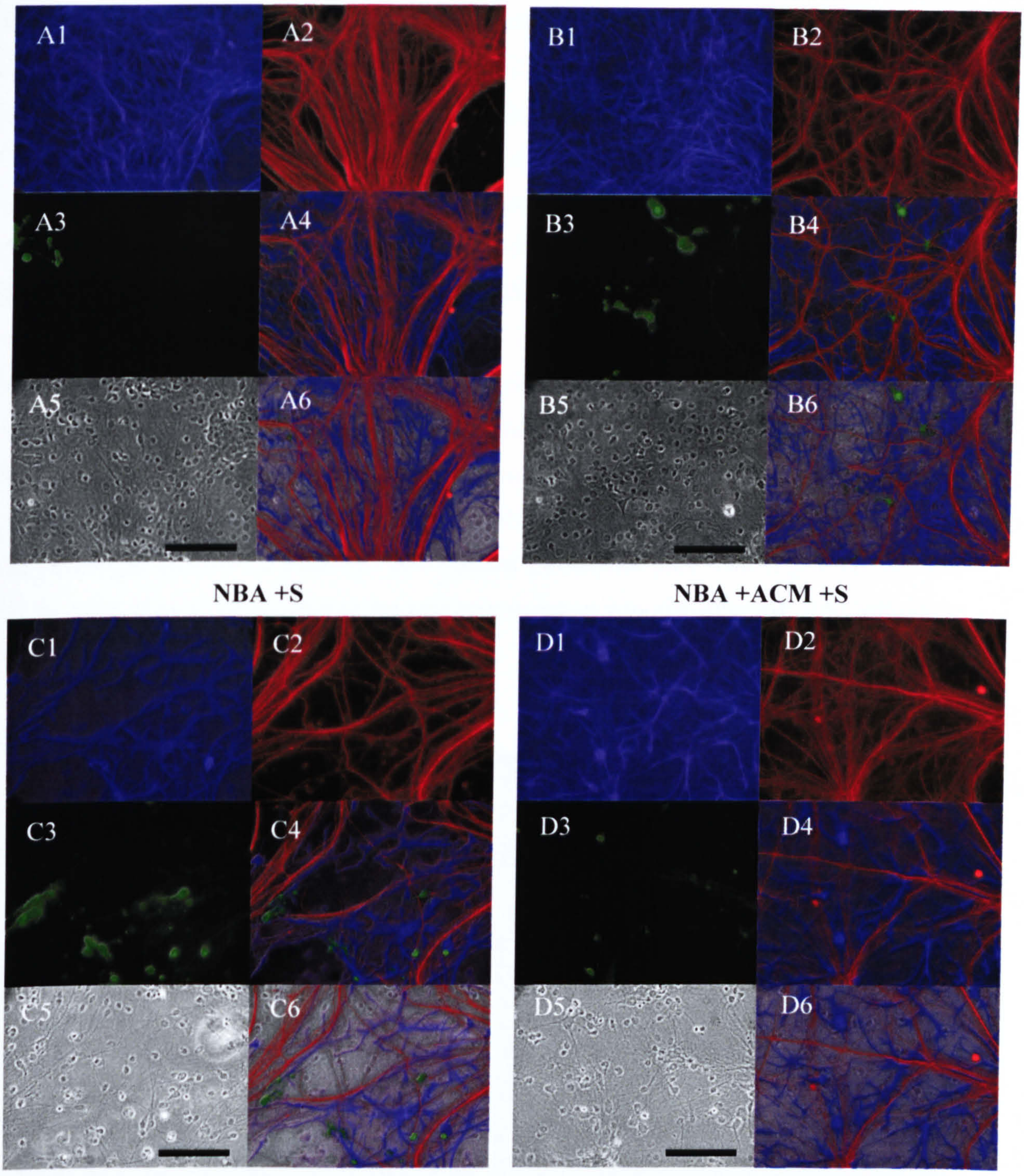

*Figure 2.10. Fluorescence images showing embryonic (E14) spinal cord neurons plated at 12,500 cells/mm^2 following 2 weeks in culture. Cells tripled labelled for **GFAP**, **Smi 31** and **AA3**. Figure sets shows cells maintained in various growth media; A: NBA only, B: NBA + ACM, C: NBA + S, D: NBA + ACM + S. In each figure sets image 1, 2 and 3 show the fluorescent micrograph of each antibody (**GFAP**, **Smi 31** and **AA3** respectively) and image 4 a compilation of these three images. Image 5 shows the corresponding phase contrast micrograph, and image 6 phase with fluorescence overlay. The scale bar in each phase image is 100µm; this is the same for all other images.*

Differential Adhesion

The effect of differential adhesion on the population of glial cells was considered. Embryonic spinal cord neurons were plated at 12,500 cells/mm^2 on 13 diameter cover slips and maintained in culture for 2wks. After this time cells were fixed and labelled for GFAP, a glial cell marker (see Figure 2.11.A1 and 2.11.B1), Smi 31, phosphorylated neurofilament marker (A2, B2) and AA3, a marker for mature oligodendrocyte (A3, B3). Figure 2.11 shows the fluorescence micrograph for each antibody staining, the colour compilation (A4, B4), corresponding phase contrast image (A5, B5) and phase-fluorescence overlay (A6, 61) for each experimental condition. The area of surface coverage was calculated by thesholding each image, calculating the area of pixels highlighted, and the results presented as a percentage of the total area available. It was noted that following differential adhesion the surface area stained positive for GFAP had reduced by 10% (see Graph 2.4), suggesting the use of this procedure had reduced the initial glial population of the culture. However the process of differential adhesion also reduced the surface area stained positive for Smi 31, from 46 % to 33%, suggesting the neuron population was also affected. The difference in oligodendrocyte proliferation was negligible.

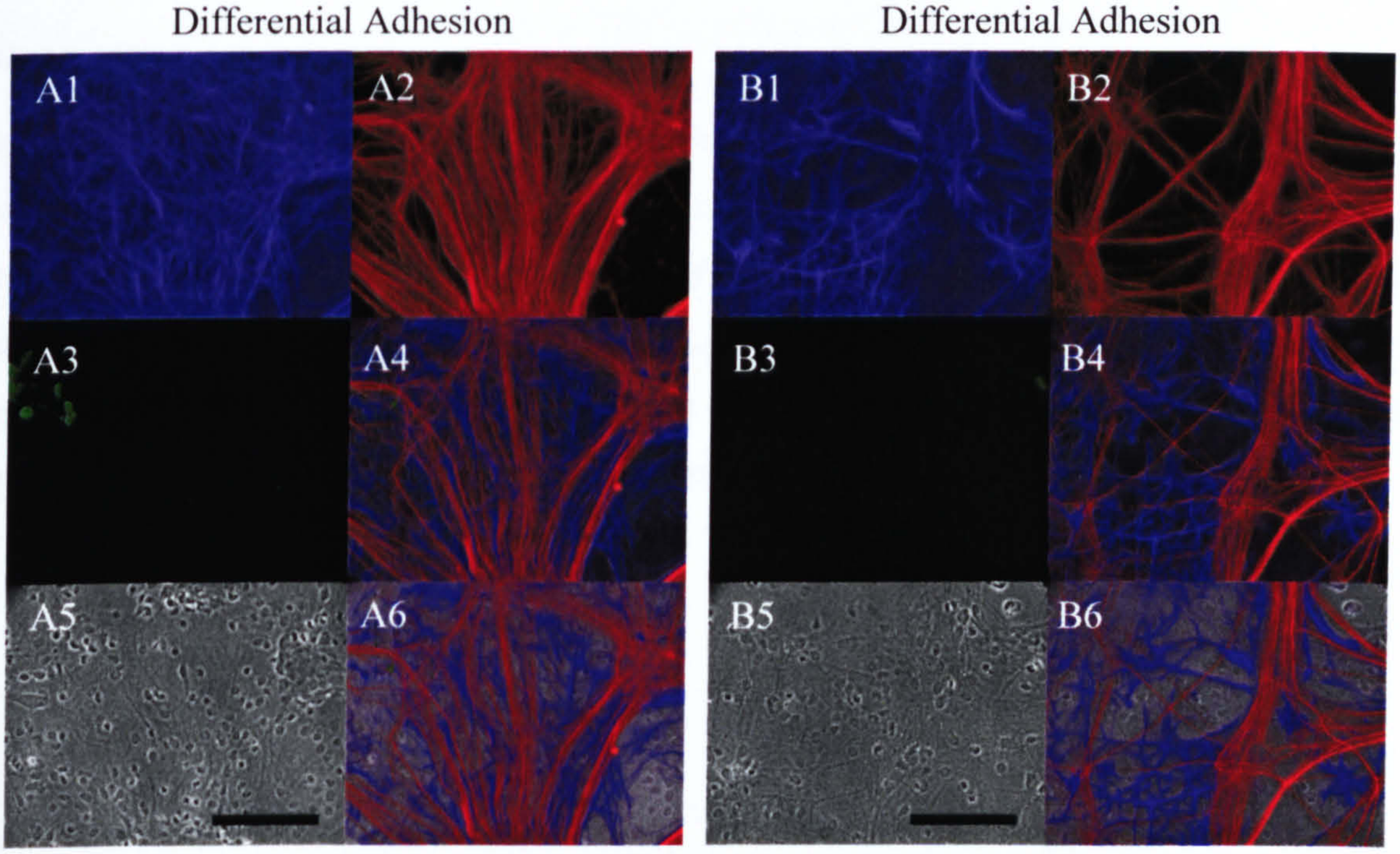

*Figure 2.11. Fluorescence images showing embryonic (E14) spinal cord neurons plated at 12,500 cells/mm^2 following 2 weeks in culture. Cells are tripled labelled for **GFAP** (image 1), **Smi 31** (image 2) and **AA3** (image 3), image 4 is a compilation of the three stains, image 5 is the phase micrograph and image 6 is phase with fluorescence overlay. Figure set A shows cultures without differential adhesion, and set B shows images of cultures having been subjected to the differential adhesion procedure. The scale bar in each phase image is 100µm; this is the same for all other images.*

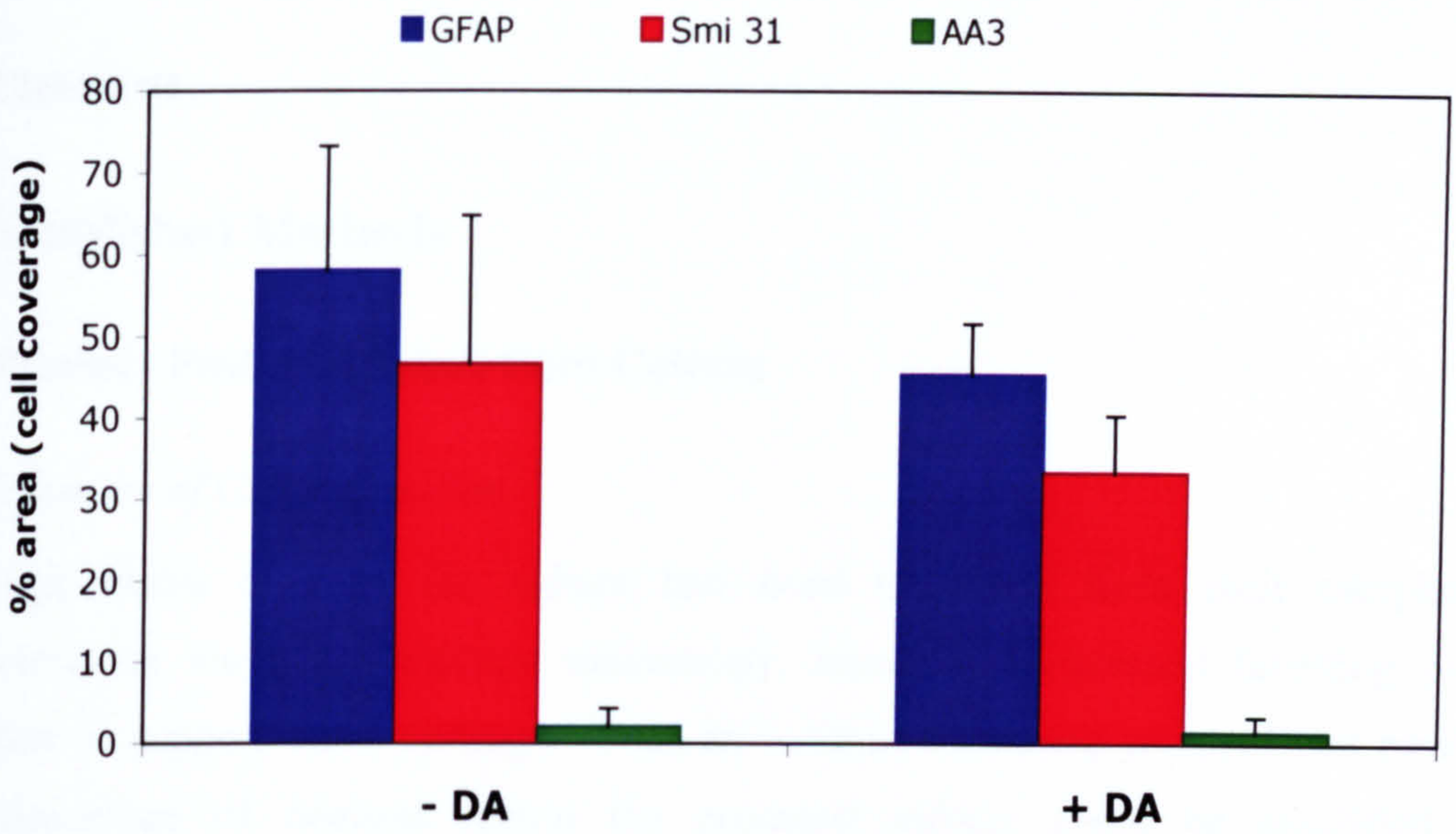

*Graph 2.4. Graph showing the effect of no differential adhesion (-DA) v's differential adhesion (+DA) on percentage of surface area covered by **GFAP**, **Smi 31** and **AA3** positive staining on substrates of 2wk old embryonic spinal cord cultures. Results are mean ± standard deviation.*

Summary

The results demonstrate that the methods developed and described in this section are sufficient to continuously produce a viable neuron population of both primary postnatal and embryonic spinal cord neurons. Cultures of both have been successfully grown and maintained, as shown by immunocytochemical staining. After 2 weeks in culture, cells appear to be forming highly connected neural networks, this evidence supports the use of this biological model for the study of neural network behaviour.

Discussion

A. Established Methods

A.1. Primary Postnatal Spinal Cord Culture

Classification of Cell Population

Although nerve cells in the culture had been identified from their morphological characteristics via phase contrast microscopy, immunocytochemical labelling provided evidence to support these findings. Once an optimised staining protocol was established the percentage of neurons within the postnatal culture could be identified. The fluorescently labelled images showed that 60% of the cells stained positive for the nerve cell marker *ß*-tubulin, suggesting the cell isolation techniques and cultivation protocol was successful in establishing and maintaining a substantial nerve cell population. An attempt was made to identify the different sub-classes of neurons that exist within spinal cord tissue, such as motor neurons, which innervate skeletal muscle fibres, and inhibitory or excitatory interneurons which are found within neural networks (Berg & Fischbach 1978) (see Chapter 1, Table 1.1 for a description of neuron classification based on neurotransmitter release), using immunocytochemical staining. Nerve cells are categorised by their secretion of either excitatory or inhibitory neurotransmitters, and the subsequent effect they have on signal transmission. When working with this tissue it was necessary to identify the population of these different cell types, especial those of inhibitory action, as a culture over populated with inhibitory cells would have a suppressing effect on network activity, and would therefore be detrimental to the investigation of spontaneous network activity. Immuno–labelling with anti-GABA found cultures to contain 5% inhibitory neurons after 2 weeks, similar to those previously published by studies investigating network behaviour (Wagenaar *et al.* 2005). Although this fraction increased to 12 % after 5 weeks, this change in nerve cell population was in fact due to cell death. Therefore, these results were not of any great concern, as it is highly unlikely cells would be used for experiments after 4 weeks. Although this study provided conclusive results with regards to GABA-ergic neurons, immuno-labelling, with other antibodies, was not successful suggesting other methods (such as intracellular recording) should be used in conjunction with labelling studies in the future.

Despite attempts to reduce the glial population of the culture by differential adhesion, 40% of cells cultures stained positive for the glial cell marker GFAP. Although this percentage would only increase over time due to cell proliferation, it was decided not to introduce anti-mitotic drugs for fear of reducing the neuron cell counts.

Identification of Synaptic Activity

When working with a primary neuron culture, regardless of the tissue source, it is essential that cells are not only maintained in a growth-promoting environment but that this environment is also supportive of nerve cell function. The specialised junctions through which neurons communicate are formed by the close assembly, and tight attachment, of pre- and post synaptic specialisations (Biederer *et al.* 2002). Basic observation of cells via phase contrast microscopy might give the impression that cells are interconnected, as cell processes can appear dense and entwined, suggesting synaptic connections are being made. However only by performing investigative microscopy techniques, such as transmission microscopy (TEM) or immunofluorescence microscopy, can synapse formation be correctly identified. Once the presence of synapses has been established, the functionality of these structures must also be determined. In this experiment cells were doubled labelled for dendrite specific marker MAP2 and synaptic vesicle marker synaptophysin. It was hypothesised that since the majority of synaptic formations are of the axon-dendritic variety that the correlation between these two stains would give a reliable indication of synapse location. The resulting fluorescence images show that the synaptophysin labelling directly correlated to the dendritic morphology, suggesting synaptophysin expressing is occurring at synaptic junctions. The relationship between these images also proves the synaptophysin labelling to be real, and not a result of antibody aggregates forming. Although images show cells after 16 days, cells were found to be synaptically active after 1 week. However, the types of synapses being formed has still to be identified.

A.2. Primary Embryonic Spinal Cord Culture

Classification of Cell Population

Although the population of neurons was shown to significantly decrease after 2 weeks in cultures plated at 6000 cells/mm^2, cells that did survive were shown to be well developed with healthy processes evident (see Figure 2.4.B). The reduced number of neurons was a

not a major concern, as for the study of neural networks a culture low in neuron numbers is preferential. The fact that neurons were surviving at such a low density suggested that the creation of a neural network of relatively few cells would be possible using this plating density and the growth conditions used to culture these cells.

Characterisation of Neural Networks

Neural network formation was identified by triple staining for β-tubulin, synaptophysin and Smi 31, a marker of phosphorylated neurofilament proteins present in the axons of mature neurons (Letournel *et al.* 2006). Ideally, this triple staining study, which aimed to identify axonal growth and dendritic morphology in random networks, should have incorporated dendritic marker MAP2 with axonal SMi31. Unfortunately, comprehensive results could not be obtained from triple staining with MAP2. Therefore, MAP2 was substituted for β-tubulin, which is present in both axons and dendrites. Using this combination of markers can limit the quality images obtained, as cross-labelling will ultimately occur. From the results shown in Figure 2.7 it was noted that axons were only evident in 2 week old cultures, although the synaptophysin staining suggests cells were capable of forming active synapses after 1 week. In each case cells were forming highly connected neural networks. However, at the lowest plating density (6000 cells/mm^2) individual cell bodies were evident, as were the innervating processes (see Figure 2.7.B) in comparison to cultures plated at 8000 and 10,000 cells/mm^2.

B. Method Development

B.1. Primary Postnatal Spinal Cord Culture

Although the Centre for Cell Engineering had used primary neuronal cultures as a research tool in previous research projects, this was the first time cells had been prepared from spinal cord tissue. It was therefore necessary to develop and optimise a standard protocol that would allow for the culture of a low density, single cell suspension of spinal cord neurons with minimal glia proliferation.

Cell Isolation

The central nervous tissue of the postnatal rat pup is wrapped in a dense connective tissue, and contains a very well developed network of already specific synaptic connections,

making the cell isolation process difficult. As cells were to be used for network analysis studies, where the connection between individual cells is highly regulated, it was essential that cell cultures were derived from single cell suspensions. The presence of tissue fragments or cell aggregates would not only compromise the success of cell survival, but also interfere with experimental investigation by potentially blocking the specific cell adhesion sites in the network patterns that have been designed for the study of network behaviour. Three methods of cell isolation were tested with the aim to develop the best method that would produce the purest cell suspension. The first (A) involved enzymatic digestion only, where the chopped tissue was incubated in trypsin solution for 20 minutes. Although this method did successfully break down the connective tissue, a single cell suspension could not be obtained. The second method (B) relied on mechanical forces to isolate the cells by sequential trituration. However, large tissue fragments were predominant in both preliminary isolation methods A and B, suggesting that a combination of both methods (isolation method C) was required (Although this may seem obvious, it was necessary to test both isolation methods individually in order to determine which, if any would produce a single cell suspension). The introduction of method C reduced the number of tissue fragments dramatically, although over-trituration of the cell suspension would result in a suspension of cell debris rather than individual cells.

Plating Density

The main function of nerve cells is to make decisions: i.e. to engage in neuronal integration; therefore the formation of functioning synaptic connections is a main priority of this cell type. During early development neuron projections must locate their desired target while manoeuvring through a diverse and ever changing 3-dimensional environment. The navigation of these developing axons is facilitated by the presence of guidance cues such as axonin-1, either secreted into the local environment or expressed on the surface of neighbouring cells (Grunwald & Klein 2002, Stoeckli *et al.* 1991). Cells that do not reach their target are eliminated; otherwise network malfunctions would occur across the whole CNS (Dodd & Jessell 1988). Therefore, if these strong growth-promoting signals are not available for growth stimulation in *in-vitro*, cells cannot survive. This was evident in cell cultures plated at a low density. Initially after plating cells appeared to be phase bright and healthy, although sparsely distributed across the culture substrate. However after 24 hours mostly all cells had died; only those that by chance had adhered in close proximity to another cell managed to survive, although these cells could not be maintained longer than,

on average, 3 days. As the plating density was increased the percentage of cells surviving past this initial plating period also increased. These cells were much healthier in appearance, with axonal outgrowth evident. Cells plated at the highest density could also be maintained for longer periods of time. If required cells could be grown for up to 5 weeks, although glial cell proliferation reduced the ability to observe individual cells.

Removal of Cell Debris

Even after the optimisation of the cell isolation technique, cell debris was still a factor affecting nerve cell survival. If the debris were allowed to settle and adhere to the culture substrate along with the cell population, cell death would occur after 24 hours. This is most probably due to the toxins released into the culture environment and inability of nerve cells to produce sufficient levels of antioxidants (Brewer & Cotman 1989). Various methods of removing debris from the cell culture were attempted. However, the presence of the fine particulate matter was a limiting factor in the success of this operation. It was hypothesised that the application of shear force would pull the particles together into the centre of the culture vessel. However it was not possible to apply enough force to have this effect without dislodging the cells already adhered, either by using a speed-controlled shaker table, or by agitating the culture by hand. The only way to successfully remove the debris was to exchange the growth media several times after initial plating.

B.2. Primary Embryonic Spinal Cord Culture

Investigation of Growth Media Composition

Neuron survival *in-vitro* is a major issue when working with primary neuron cultures. These cells are very difficult to maintain due to the aggressive dissociation techniques and also because they require an optimal growth promoting environment which must be precisely controlled. Brewer *et al* have established a widely accepted system for maintaining primary cultured embryonic neurons, by substituting normal growth media components, such as serum and insulin, for an optimised serum-free supplement called B27 (Gibco) (Brewer *et al.* 1993). As this research was conducted solely on primary embryonic hippocampal cultures, it was necessary to establish if the same method would be suitable for embryonic spinal cord cultures. The methods described in this chapter for isolating and growing embryonic spinal cord cultures have been adapted from those used in the

laboratory of Dr. Sue Barnett. The methods and growth conditions used by this group have been developed to support oligodendroctye growth by supplementing the growth media with ACM and horse serum. As the survival of glia was not a priority for this study, an optimal growth media that would support neuron survival without promoting glial proliferation, was investigated. Of the four media compositions tested it was decided that NBA media, containing 98 mls NBA, 2mls B27, 1ml Glutamax, 1ml pen/strep, was the most suitable as the neuron population was supported (as determined by Smi 31 fluorescent labelling) but not oligodendrocytes (see Figure 2.10).

Effect of Differential Adhesion

Although some studies use anti-mitotic drugs to reduce the glial population of their cultures, a less toxic approach called differential adhesion was investigated. This method had been used with success in the cultures of postnatal cells. However it proved to have little effect on the percentage of each cell population within the embryonic cultures, but did appear to reduce the overall number of cells to survive. It is hypothesised that the extra time required, and the disruption to the cells during this culture method was having a detrimental effect on neuron survival as the area covered by Smi 31 staining was reduced after differential adhesion methods had been employed. The difference in glial population was not sufficient to compensate for the reduced neuron population; therefore this method was not used in future experiments.

Conclusion

Dissociated cultures of postnatal spinal cord neurons were intended to be used throughout the course of this thesis and therefore considerable attention was applied to establishing an optimal protocol for their use. However, due to unforeseen problems in cell survival rates it was necessary to turn to embryonic cultures and establish a suitable culture system to ensure cells cultured were in fact neurons, and that these cells could be maintained in healthy cultures for long periods of time. Immunocytochemical staining results proved viable nerve cell cultures were repeatedly being produced by the methods described in this chapter. Cells were healthy and forming chemically active networks, meeting the criteria required for investigating neural network behaviour.

Chapter 3.

Micro-contact Printing to Create Neural Networks

Abstract

In this chapter the methodologies used to establish an optimal protocol suitable for the investigation of the effects of network geometry on neuron behaviour are described. Physisorption micro-contact printing (μCP) and chemisorption μCP methods were tested as were stamp fabrication methods and the biocompatibility of various stamping polymers. Preliminary studies showed that aligned neural network could not be produced by stamping non-adhesive proteins by chemisorption μCP methods. Network formation was only observed by μCP an adhesive biomolecule onto a cell repellent substrate by physisorption μCP.

Introduction

Micro-contact printing (μCP) is a relatively new method of cell engineering that has developed over the last decade to become a reliable and versatile surface modification method with a wide variety of applications. Referred to also as 'soft lithography', this technique was first developed as an extension to micro-electronics fabrication technology (Cornish *et al.* 2002). More importantly in this context μCP has been used to create geometrical patterns of chemical contrast on biologically compatible substrates, with the aim of introducing 2-dimensional structural organisation into cell culture. The use of cell adhesive and growth-promoting molecules in juxtaposition with substrates of less permissive qualities has the affect of limiting cell adhesion to a preferential area. The creation of such structures by μCP involves first fabricating a patterned silicon master dye by photolithographic and etching techniques, from which a poly(dimethylsiloxane) (PDMS) elastomer polymer replica is formed by in-situ polymerisation. Referred to as a polymer 'stamp', the topographical patterned stamp is loaded with a biomolecule solution, the surface dried, and then brought into contact with a substrate creating a replica of the original pattern in chemical form. The biomolecules in the inking solution adhere to the substrate by chemisorption or by physisorption.

Chemisorption

The original method of μCP developed by George Whitesides' laboratory was based on the binding of protein molecules to a structure by printing alkanethiols onto gold substrates (Kane *et al.* 1999). This approach is referred to as chemisorption, distinguished by its use of chemical bonds, such as covalent bonding or ionic bonding, to immobilised biomolecules on the surface of a substrate et (Smith *et al.* 2004). Although this method has been modified by various groups worldwide the underlying principle remains the same (Chang *et al.* 2003). All protocols begin with the fabrication of a silicon master, from which a stamp is created. Once removed from the master, the stamp is incubated with the desired protein, before being transferred to an aminosilane-activated cover slip, where the protein is cross-linked to the receiving substrate (see Figure 3.1). Because biomolecules, such as laminin or fibronectin, are actively bound to the surface by strong chemical bonds, this approach has proven very successful in maintaining surface modification over a long period of time (Branch *et al.* 2000).

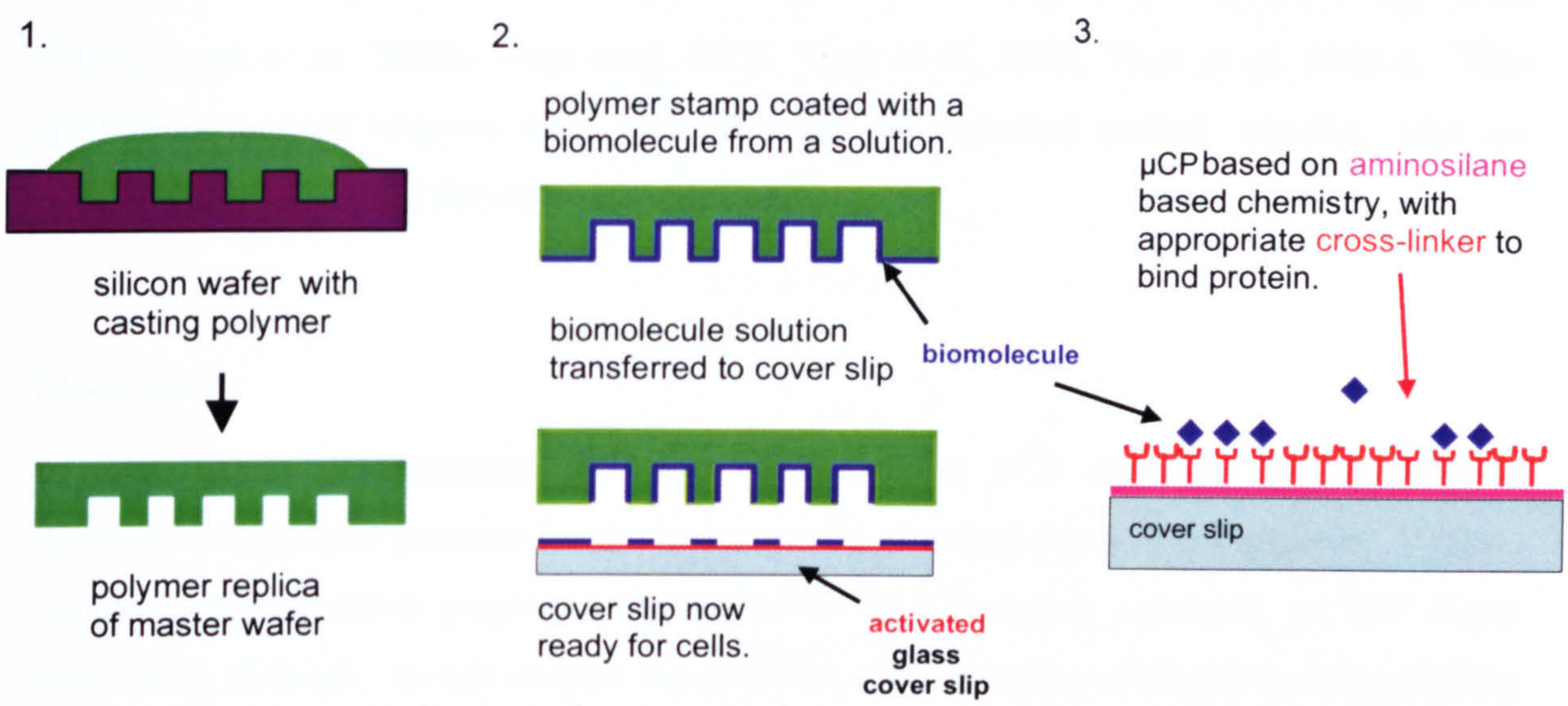

Figure 3.1. Schematic diagram showing step-by-step methodology of chemisorption micro-contact printing (µCP). Step 1 illustrates replication of the master pattern in polymer, step 2; biomolecule (blue) loading and pattern transfer, step 3; amino-silane cross-linker chemistry of activated cover slip (arrow indicates bound biomolecule).

Physisorption

Physisorption μCP, unlike the chemisorption μCP, does not involve covalent chemical binding of the biomolecule or protein to a surface, whether it be an activated cover slip or otherwise. This method relies solely on the adsorption properties of the biomolecule itself by exploiting weak intermolecular forces that may exist between the biomolecule and the substrate, such as van der Waals forces or hydrogen bonding (Ramrus & Berg 2006).

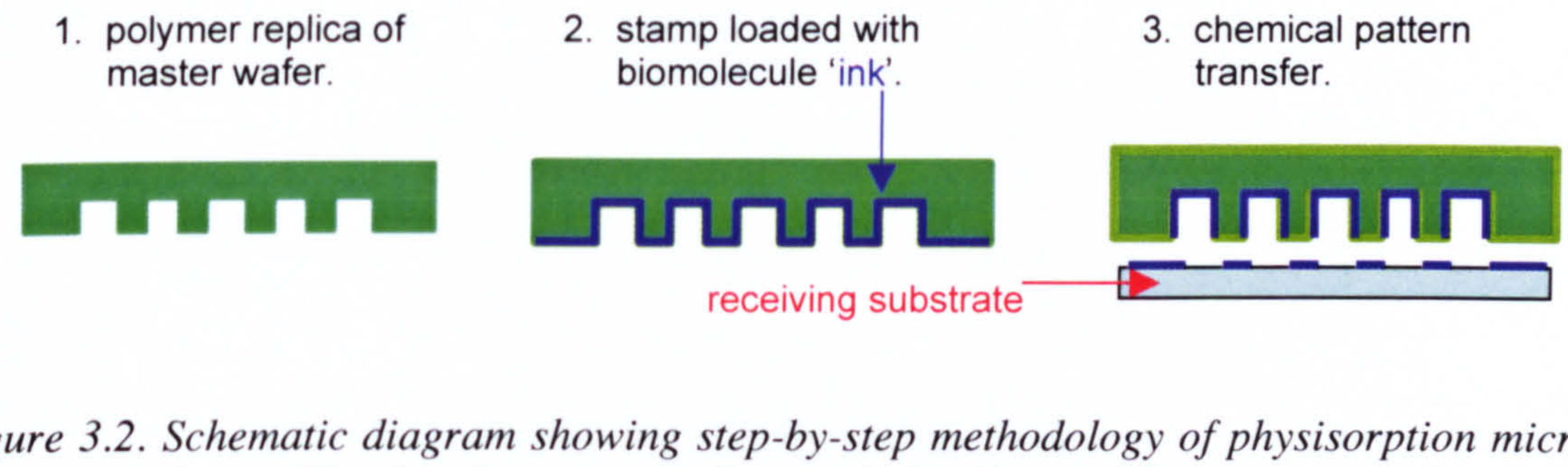

Figure 3.2. Schematic diagram showing step-by-step methodology of physisorption micro-contact printing (µCP). 1. polymer stamp, 2. protein loading and 3. pattern transfer.

As with the previous μCP method described, physisorption μCP begins with the fabrication of a polymer stamp from a silicon master. The stamping polymer is incubated in a biomolecule solution, which is then transferred to substrate surface, by simply applying slight pressure when stamping. Most often with this approach, a highly hydrophobic

material, which repels cellular adhesion, is used as a background substrate (Vogt *et al.* 2005a, Vogt *et al.* 2005b, Vogt *et al.* 2003, Vogt *et al.* 2004, Vogt *et al.* 2005c). This simplified method requires only this one step of chemical pattern transfer, with no specialised treatment of the substrate required.

Summary

In this chapter physisorption μCP and chemisorption μCP methods will be used to determine an optimal protocol for the investigation of neural network compliance. Various commercially available polymers will be tested as a stamping substrate, as will stamp fabrication methods. In this chapter the different concentrations of the biomolecule inking solution will also be considered.

Materials and Methods

This section describes the methods used to create chemical patterns of adhesive or non-adhesive proteins via microcontact printing (μCP) methods. Two methods are described, chemisorption and physisorption plus supporting development methodologies in Section B. The solutions not described within the text are listed in the appendix *Media, Reagents and Solutions*.

A. Established Methods

Fabrication of the Master Die on a Silicon Wafer

Rongyu Tang (Department of Electronics and Electrical Engineering, Glasgow University) designed and fabricated all the photomasks used to create network patterns in silicon. Both the author of this thesis and Rongyu Tang contributed to the fabrication of patterned silicon wafers unless otherwise stated. The mask pattern was created on a 4 inch silicon wafer using an MA6 mask aligner (SÜSS MicroTech Inc, Vermont, USA). The dry etch process was performed by technical staff within the Bioelectronics division of the Department of Electronic and Electrical Engineering (Glasgow University) in a STS Deep Etcher using an un-switched mixture of SF_6 and C_4F_4, called 'RYT1'. This etch recipe was developed by Rongyu Tang and was used to etch all structures prepared for this study. A detailed protocol of the methods used is listed below.

Cleaning and Photolithography

1. Clean 4 inch silicon wafer by sonicating in Opticlear, then acetone and finally methanol for five minutes. After each stage, rinse wafer with RO water and then blow dry with particle free nitrogen following final rinse.
2. Bake the wafer 100 °C for 15 minutes.
3. Spin an even layer of hexa-methyl-disiloxane primer and then Shipley S1818 (Shipley, Marlborough, MA, USA) on sample at 4000 rpm for 30 seconds (see Figure 3.3, diagram a).
4. Bake at 90 °C for 30 minutes or alternatively bake on a hotplate at 90 °C for 5 minutes.
5. Let the sample cool down to room temperature.
6. Load network pattern mask into mask aligner (SUSS MicroTec MA6) and expose sample to UV light for 5 seconds (200 Watt Hg) (Figure 3.3.b).

7. Develop the sample in Microposit® concentrate (ammonium hydrogen phosphate developer for positive resists) and RO water solution (1:1) for 60 seconds.

Dry Etching

Dry etch wafer with recipe RYT1 in ICP (Inductively Coupled Plasma) for seven minutes (see Figure 3.3.c). This creates the network pattern, with the track standing proud of the silicon (Figure 3.3.d).

Recipe specifics of RYT1:

1. Flow rate: C_4F_8/SF_6 = 50 sccm/40 sccm
2. Chamber pressure: 10 mTorr
3. Table temperature: 20 °C
4. Coil Power/platen power: 600 W/10 W
5. Process time: 5 μm/7 mins
6. DC self bias: 610 V

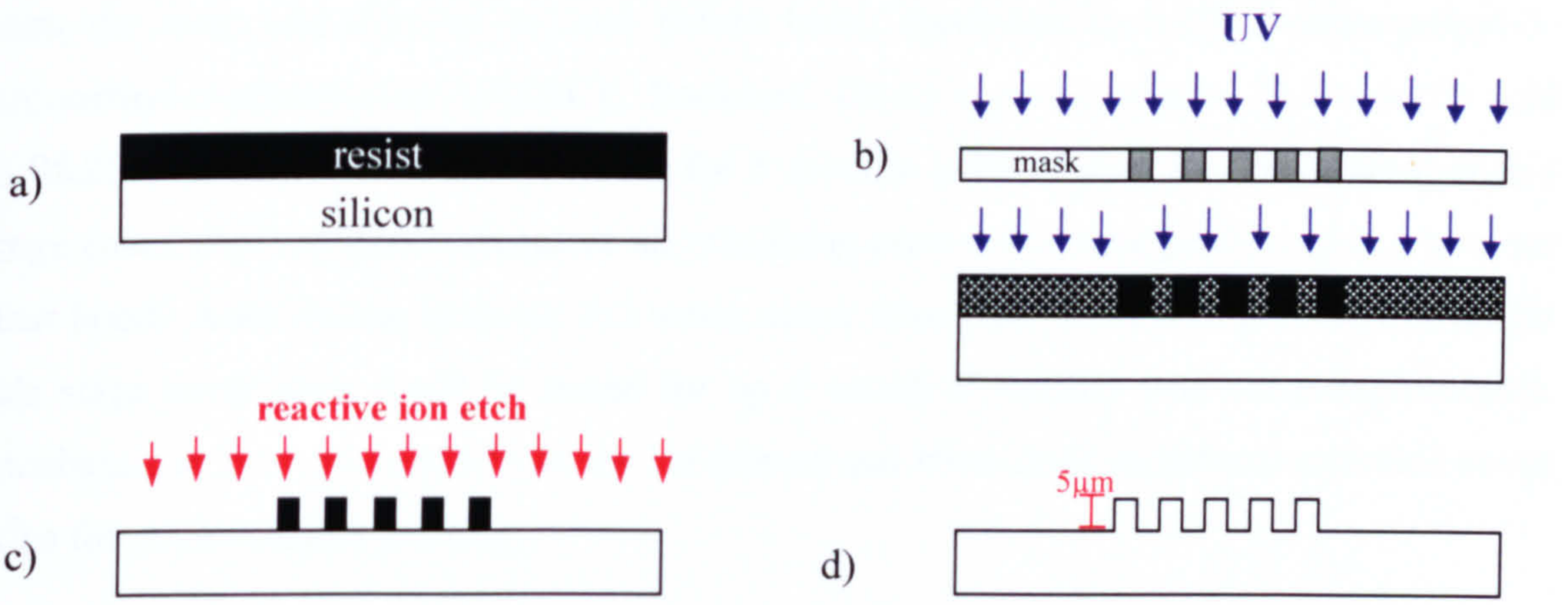

Figure 3.3. Schematic diagram showing the fabrication process of a network pattern in silicon. The silicon is coated with resist (a), which is then exposed to UV (b), leaving the undeveloped resist (c). The substrate is then dry etched to create a topographical representation of the original mask 5μm in depth (d).

Biological Solutions

The various protein solutions used in this chapter included; albumin, laminin and Poly-lysine (PLL) all of which were purchased from Sigma (Poole, UK). Albumin and laminin were diluted in sterile filtered 1x PBS to concentrations of 4μg/ml, 8μg/ml or 12 μg/ml (for

albumin), and 25 μg/ml (for laminin). Poly-l-lysine (molecular weight 70,000) was diluted in sterile filtered RO water to concentrations of 1 μg/ml, 10 μg/ml or 25 μg/ml.

Nerve Cell Culture

Only postnatal (P1) spinal cord cultures were used. For method descriptions see *Chapter 2, Primary Postnatal Spinal Cord Cultures, Established Methods.*

i) Chemisorption Microcontact Printing

Cover slip Activation

Cover slips were washed in Caro's acid (3 parts sulphuric acid (H_2SO_4) to 1 part 30% hydrogen peroxide (H_2O_2) for 15 minutes, then rinsed in RO water before being incubated in 0.5 M NaOH for 20 minutes. After incubation all cover slips were rinsed in sterile RO water, blow-dried, then transferred to an oven for 1hr at 75°C. Cover slips were removed from the oven and allowed to cool before being incubated in 0.1% 3-aminopropyl-3-aminoethyl-triethoxysilane (PIERCE, Rockford, USA) in acetic ethanol (0.5% acetic acid in 95.25% ethanol 3.25% water, stirred for 5 minutes prior to use) for 15 minutes; at this stage cover slips are sterile, therefore all remaining procedures were performed in a laminar flow hood. After rinsing in sterile RO water, cover slips were dried with particle free air (at this stage cover slips could be stored for up 1 month if sterility was not compromised). Incubating in 2.5% gluteraldehyde for 1hr (rinsed and blow-dried as before) activated cover slips for micro-contact printing.

Protein Loading and Pattern Transfer

Prior to protein loading all stamps were sterilised in 70% ethanol, rinsed thoroughly with RO water and blow dried with particle-free air. Stamps were incubated in protein solutions at varying concentrations for 1 hour to allow weak ionic bonding to occur between stamp and protein. After protein "inking" stamps were rinsed in sterile RO water and blow-dried before being placed (pattern down) on the receiving substrate for 1hr. The remaining exposed gluteraldehyde binding sites were blocked by incubating cover slips in 1M Tris ethanolamine·HCL (pH 7.4) for 1hr. Stamped substrates were stored in HEPES solution (see *Media, Reagents and Solutions* Appendix for solution details) containing Gentamycin

(1:1000) at 4°C overnight to prevent the growth of any bacterial infection (James *et al.* 2004).

Immuno Staining

Stamped substrates were rinsed twice in 0.1%BSA/PBS (1x) to block any unspecific binding sites. The primary antibody (anti-laminin produced in rabbit) (Sigma) was diluted to a working concentration of 1:40 with the BSA/PBS solution. Substrates were incubated in primary antibody for 40 minutes at 37°C, washed (3x for 5 minutes) in Tween 20 washing buffer (see *Media, Reagents and Solutions* Appendix) before adding the secondary biotinylated antibody (Vector Laboratories, Ltd., Peterborough, UK) at 1:50 dilution. The secondary antibody was left on for 1hr, removed with series of 5-minute rinses before adding the fluorescent marker (1:50 Texas Red- streptavidin diluted in BSA/PBS) (Vector Laboratories, Ltd.) for 30 minutes at 4°C. Before final mounting, substrates were washed three times in Tween 20 buffer to remove any unbound antibody.

Coomassie Blue Staining

Cells were washed in 1x PBS (warmed to 37°C prior to use) to remove all traces of growth media then fixed with 4% formal saline at 37°C for 15 minutes. Cells were incubated in Coomassie blue (a non-specific protein stain) for 5 minutes then rinsed with RO water (3x 5 minutes).

ii) Physisorption Microcontact Printing

Protein Loading and Pattern Transfer

Prior to protein loading all stamps were sterilised in 70% ethanol, rinsed thoroughly with RO water, then incubated in 10% SDS for 10 minutes (Chang *et al.* 2003, Vogt *et al.* 2003, Vogt *et al.* 2004). Stamps were then washed 3 times in sterile RO water, blown dry in particle-free nitrogen flow, then incubated in a biomolecule solution for 1 hour (kept on ice during incubation). Following biomolecule *'inking'*, stamps were slowly blown dry with a particle-free nitrogen flow, ensuring the biomolecule solution was maintained on the stamp surface for as long as possible. Once dried stamps were inverted onto the bed of a sterile polystyrene Petri dish, with slight thumb pressure applied for 20 seconds. The stamped area was highlighted on the reverse side of the Petri dish using a permanent marker pen.

B. Method Development

Fabrication of Polymer Stamp

Various fast curing commercially available poly-dimethylsiloxane (PDMS) polymers were used to create negative replicas of a patterned silicon wafer. The polymer preparation steps were as follows:

a) *MicroSet* (Microset Products Ltd, Warwickshire, UK) was supplied in a double barrel gun format. This automatically mixed the polymer at a ratio of 1:1 with the curing agent during dispensing. No suction step was used with this polymer. Once mixed this polymer was used immediately.

b) *Qsil 215* (ACC Silicones, Sommerset, UK), also supplied in a dispensing gun, was mixed with curing agent at a ratio of 1:10, then placed in a vacuum chamber for 20 minutes to remove all dissolved gases (this treatment reduced bubbles formation during curing). Once mixed the polymer/curing agent mixture could be stored for up to 5 days at -20°C, or used immediately.

c) *Sylgard 184* (Dow Corning, Coventry, UK) was stirred for 5 minutes before being mixed with curing agent at a ratio 1:10 (wt/wt). The uncured polymer solution was placed in a vacuum chamber for 20 minutes. Once mixed and degassed the uncured polymer could be stored for up to 5 days at -20°C, or used immediately.

The methods of stamp fabrication for each polymer are described in Table 3.1. Three fabrication methods were tested. Methods A and B were used to fabricate all three polymer stamps (Sylgard 184, Qsil 215 and MicroSet stamps). However Method C was used to fabricate only Sylgard 184 and MicroSet stamps as the Qsil 215 product was discarded following an unsuccessful protein transfer result.

Polymer	**Fabrication Method**
Sylgard 184 MicroSet Qsil 215	**A.** Approx. 2ml was dispensed onto the master, then backed with a microscope slide (supported by cut sections of cut microscope slides). Incubated for 24hrs at 60°C .
	B. Approx. 50µl was dispensed onto master, backed with a 13 mm diameter cover slip (no supports were used). Cured on a hotplate for 2 minutes at 95°C.
Sylgard 184 MicroSet	**C.** Pipette tips (1ml or 5ml) were used as a casting mould. Approx. 200µl was first dispensed into mould and cured for 2hrs at 120°C. 50% of remaining cast volume was filled and cured overnight at 75°C.
MicroSet	**D.** Approx. 2ml was dispensed onto master (no backing was used). Cured on a hotplate for 2 mins at 95°C.

Table 3.1. Summary of stamp fabrication techniques.

Results

B. Established Methods

Albumin Patterning

The first μCP experiments were based on the hypothesis that better cell compliance would be obtained by stamping patterns of a non-adhesive biomolecule on a cell-adhesive substrate. Albumin was chosen as a protein which, is generally believed to be non-adhesive to cells (Detrait *et al.* 1998). Figure 3.4 shows an SEM image of the stamp pattern used in this experiment. The stamp is a flat structure, where grooved define the network pattern. The red shaded section highlights the area of albumin, which will be transferred during μCP and the yellow tracks indicate the grooved pattern which will not transfer albumin as shown in Figures 3.1 and 3.2. Based on discussions with Professor Curtis it was decided that a concentration of 2μg/ml albumin would be required to create a protein monolayer. However, preliminary results (not shown) proved this concentration to be insufficient in reducing cell adhesion. A starting concentration of 4μg/ml was decided and compared to the effects of higher concentrations of 8μg/ml and 12μg/ml albumin. Albumin patterns were stamped onto 13mm diameter cover slips as described in the methods section of this chapter. Postnatal (P1) spinal cord neurons were plated at 10,000 cells/mm^2 onto each construct and maintained in culture for 7 days. Cells were fixed and stained with Coomassie blue, then observed at low magnification.

Figure 3.4. Scanning electron micrograph showing PDMS stamp structure and network pattern used in albumin concentration experiment. Red shading highlights area of albumin loading and subsequent transfer. Yellow outline indicates the grooved pattern where the stamp will not be in contact with the receiving surface and therefore no protein transfer will occur resulting in a area of preferential cell adhesion. Note scale bar 200μm.

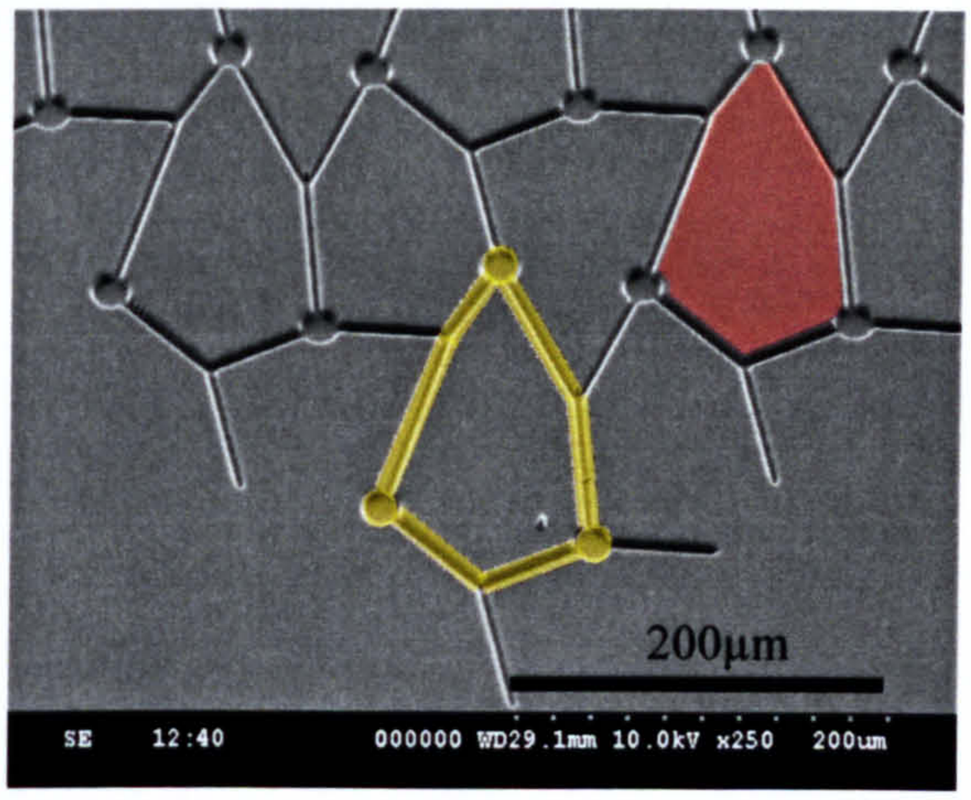

The results shown in Figure 3.5 are images of albumin stamped structures fixed and stained with Coomassie blue. Five images were taken at random from five different samples of each experimental albumin concentration, 4μg/ml, 8μg/ml and 12μg/ml. On each sample there was a distinctive border where cell adhesion and growth would change significantly indicating the stamped region of the substrate, and thus making it possible to correctly identify the section for analysis. All images were processed by calculating the area of the stamped region within a field of view, thresholding this area, then calculating the percentage of pixels highlighted by Coomassie Blue staining (see Figure 3.6). This provided a means for calculating the area of surface coverage by cell adhesion within the stamped site. The results are shown in Graph 3.1 and summarised in Table 3.2. On samples stamped with 4μg/ml albumin cell clumping was evident, with more than 25% of the surface area covered by cell adhesion as indicated by Coomassie blue staining. Due to the high concentration of adhered cells at this albumin concentration, no pattern compliance was observed, as very few individual cell bodies could be identified (see Figure 3.5, image B). Substrates stamped with 8μg/ml albumin had less than 10% of the surface area available covered by adhering cells. This proved significantly less than both the control area free of albumin and samples stamped with 4μg/ml albumin ($p< 0.001$, as determined by Student's *t*-test). Although individual cell bodies were evident on the samples stamped with 8μg/ml, the cells did not comply to the *Jude* pattern, neither the node adhesion sites nor the connections between them. This was also true for samples stamped with 12μg/ml albumin, with less than 5% of the total surface area covered by adhering cells. Although these values were less than those measured for areas stamped with 8μg/ml albumin, this difference did not prove to be statistically significant. All statistical results are summarised in Table 3.2.

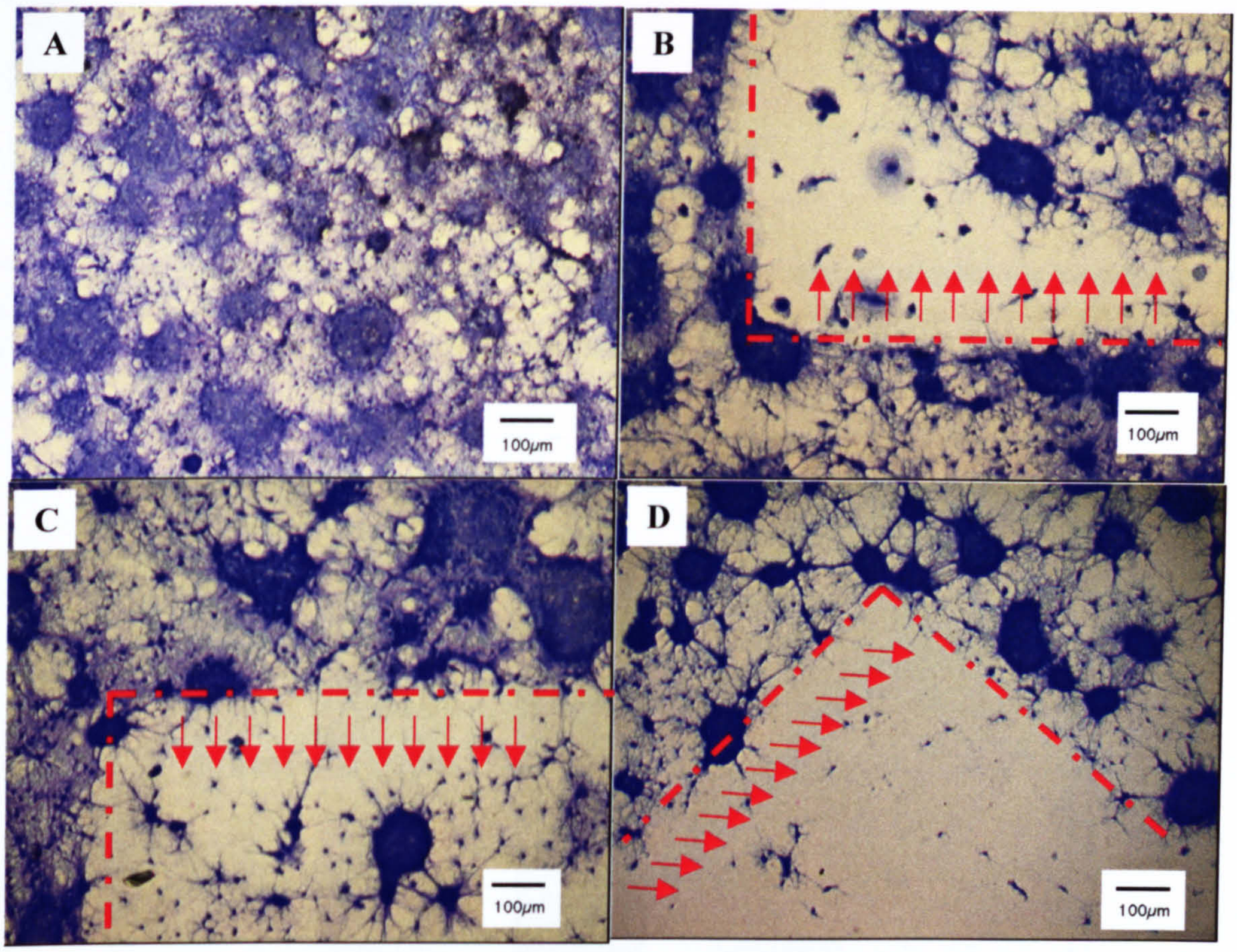

Figure 3.5. Images showing cell coverage of postnatal (P1) spinal cord neurons on μCP patterns of varying albumin concentration: 4 μg/ml (B), 8 μg/ml (C) and 12 μg/ml (D) fixed then stained with commassie blue. Images B, C and D show stamp boundary (shown in red), image A shows unstamped area. Arrows point inwards to stamped area. The scale bar in each image is 100μm.

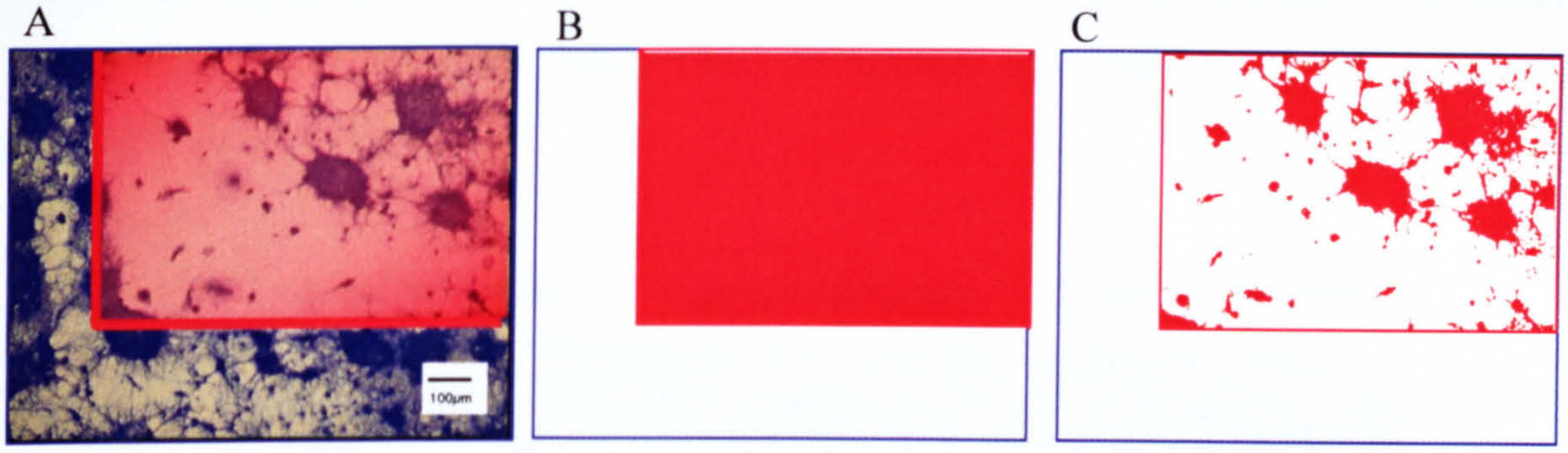

Figure 3.6. This series of images shows the process used for calculating the percentage of surface area covered by adherent cells. Image A shows stamped area (shaded red), B area available for adhesion (100%), and C thresholding of area stained for Coomassie Blue.

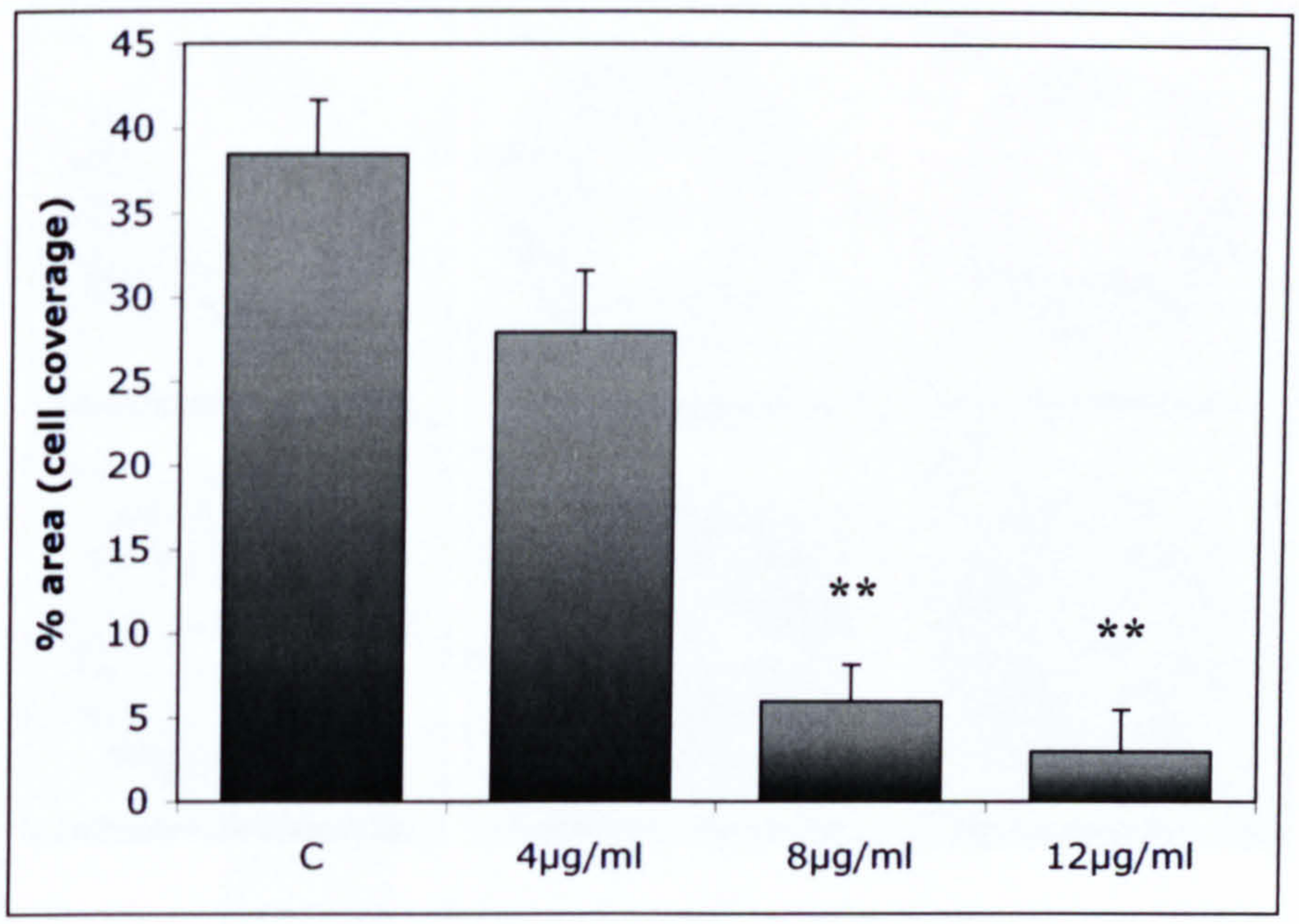

*Graph 3.1. Showing % of area covered by adhering cells on control area (C) and stamped areas of 4 µg/ml albumin, 8 µg/ml albumin and 12 µg/ml albumin, following 7 days in culture. Results are mean ± standard deviation, calculated from 5 samples. ** denotes a significant difference from the control as determined by Student's t-test ($p<0.001$).*

	4µg/ml	8µg/ml	12µg/ml
C	$p>0.01$	** $p<0.001$	** $p<0.001$
4µg/ml		** $p<0.001$	** $p<0.001$
8µg/ml	** $p<0.001$		$p>0.01$
12µg/ml	** $p<0.001$	$p>0.01$	

*Table 3.2. Summary of statistical significance between each sample (like for like comparison shaded in grey) as determined by Student's t-test. ** denotes significance at the 0.001 level of probability.*

During this experiment it was noted that cell coverage within the stamped area varied between samples of the same field. These differences were catalogued and are shown below in Figure 3.7.

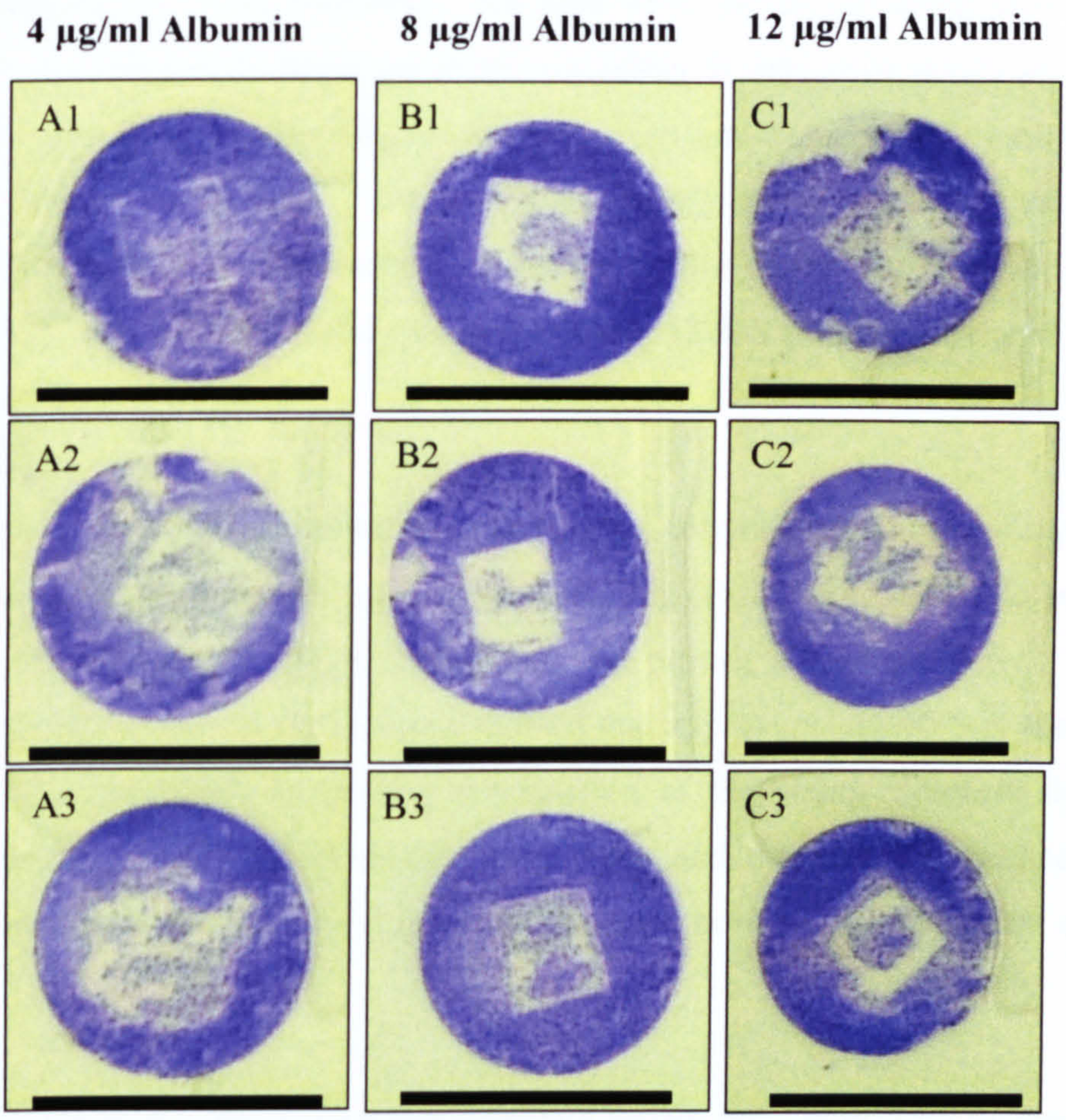

Figure 3.7. Results are overview photographs of 13 diameter cover slips with commassie blue stained P1 spinal cord neurons (10,000 cells/mm^2 density) following 7 days in culture. Images show cell coverage on samples stamped with 4µg/ml (A1-3), 8µg/ml (B1-3), 12µg/ml (C1-3) albumin. Scale bar is 13mm.

Evaluation of Protein Transfer

The stamping properties of commercially available poly-dimethylsiloxane (PDMS) polymers, Sylgard 184 (Dow Corning), Qsil 215 (ACC Silicones Ltd) and MicroSet (Microset Products Ltd) were compared. All tests were carried out using μCP method 1 (chemisorption). The aim of this experiment was solely to determine which polymer was best suited for transferring a biomolecule protein. Laminin, and therefore anti-laminin as the primary antibody, was used to evaluate the accuracy and extent of pattern transfer. Results are from fluorescent microscopy images highlighting the transfer of laminin (anti-laminin labelled with FITC secondary antibody) using PDMS polymers Sylgard 184, Qsil 215 and MicroSet.

A) Sylgard 184

The first stamp structure to be tested was the Sylgard polymer fabricated from a grooved silicon master. The results from the fluorescent staining (Figure 3.8) show this polymer to be a highly effective tool for μCP, transferring the protein almost perfectly. However further analysis of the overall surface area showed that approximately 40% of the stamped region was "over-stamped", suggesting deformation of the stamp structure during the stamping process. New Sylgard stamps were made and the process repeated, paying particular close attention to maintaining stamp integrity, however, better results could not be obtained.

B) Qsil 215

Qsil 215 was clearly the worst stamping substrate tested, with over 40% of the stamped area showing pattern distortion (Figure 3.9). Analysis of the fluorescent staining revealed some areas of the stamped substrate to be devoid of any protein transfer. No further experimentation was conducted using this polymer.

C) MicroSet

The MicroSet Stamps were fabricated in both grooved and ridged formation. Results showed MicroSet to transfer the protein pattern over the entire stamped region; this was the only stamp to do so (Figure 3.10). However, on closer analysis of the results from the ridged stamp, it was evident that the protein pattern had not been successfully maintained. Over the whole stamped region the laminin solution had appeared to accumulate at the edge at the ridge feature of the stamp, creating a halo effect on transfer (Figure 3.10.B).

Figure 3.8. Evaluation of protein transfer from Sylgard stamp (ridges stamp fabricate from grooved master). Area of protein transfer shown by red fluorescence. Arrows indicate region of " over-stamping"(B, C).

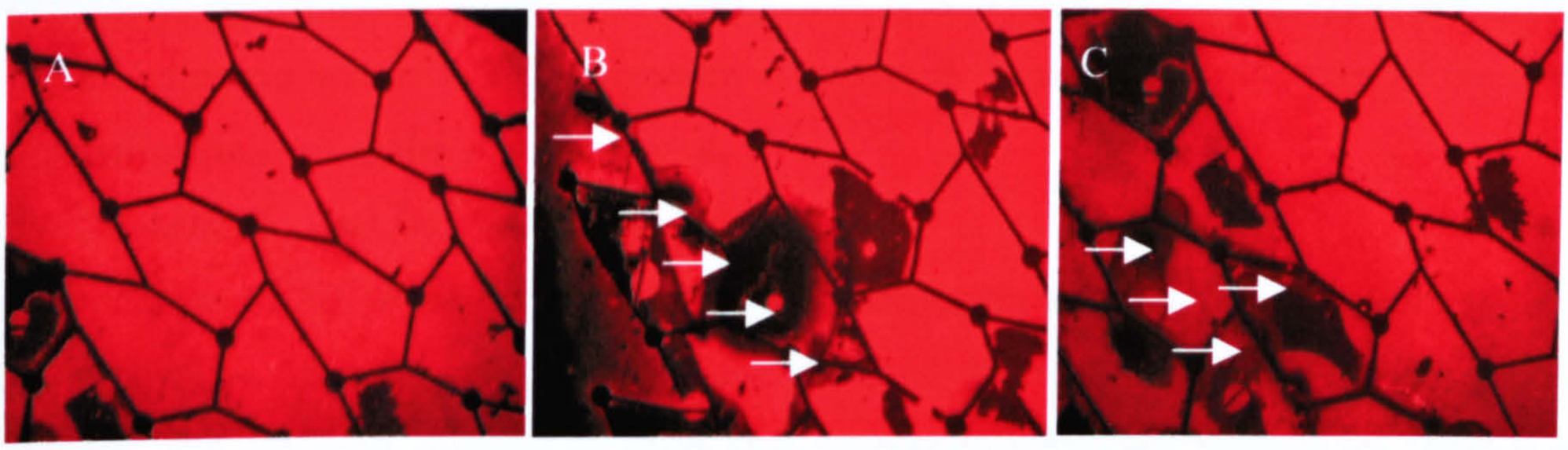

Figure 3.9. Evaluation of protein transfer from Qsil 215 stamp (grooved stamp made from ridged master). Area of protein transfer shown by red fluorescence. Arrows indicate areas where pattern is defective (B, C).

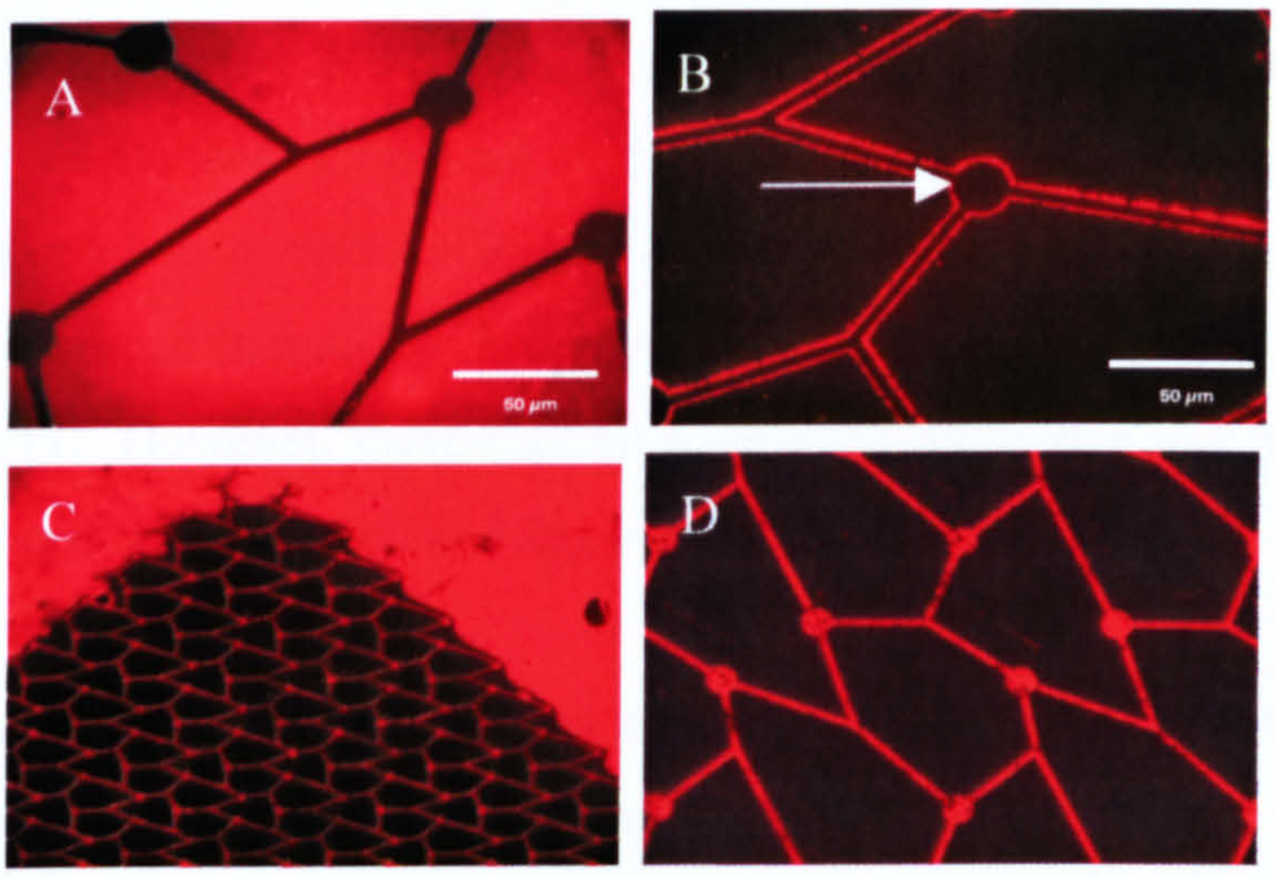

Figure 3.10. Evaluation of protein transfer from MicroSet stamp (grooved stamp, A and ridges stamp B, C, D) Red area highlighted the extent of protein transfer. Arrow shows halo effect following protein transfer from ridged stamp (B). Images C & D are of stamp results following increased drying time (ridge stamp).

Biocompatibility of Polymers Sylgard 184 and MicroSet

The biological compatibility of the polymers Sylgard 184 and MicroSet, with regards to pattern compliance, was considered. This experiment aimed to determine whether the varying chemical composition of the polymer in question had any adverse effect on cell growth and survival. To ensure no other chemicals could influence this result, the μCP method 2 (physisorption) was used here. Both polymer stamps were used to print varying concentrations of poly-l-lysine (PLL) solution (1, 10, 25μg/ml) on to a sterile Petri dish. Postnatal spinal cord neurons (P1) were plated at 10,000 cells/mm^2 and images taken after 48hrs in culture. Five phase contrast images of stamped areas were taken at random from 3 samples of each subject, 48 hrs after plating. The results have been categorised into effects on cell adhesion and survival, and pattern compliance. Statistical significance of the result was determined using the Student's *t*-test.

A) Cell Adhesion and Survival

Observations of the phase contrast microscopy images showed that a higher percentage of cells grown on Microset stamped substrates appeared darker in phase than those grown on Sylgard 184 stamped samples at each PLL concentration (This method of identifying healthy cells in culture was based on information presented in *Culturing Nerve Cells*, Banker 1998). This difference proved statistically significant using Student's *t*-test for PLL concentration 1μg/ml, although insignificant at 10 and 12 μg/ml PLL concentrations (results summarised in Graph 3.2 A). The polymer effect on cell survival was determined by comparing the number of cells adhered in each field of view. There were significantly fewer cells adhered to samples stamped with 1μg/ml PLL using the Microset polymer compared to substrates stamped with Sylgard at the same concentration, as shown in image A of Figure 3.11. However, there was no significant difference in cell adhesion between substrates stamped with 10μg/ml and 25μg/ml (see Graph 3.2 B).

B) Pattern Compliance

The relationship between polymer stamp and pattern compliance was investigated and the statistical significance of the result determined using Student's *t*-test. The percentage of cells following the pattern was calculated by superimposing the Jude pattern outline over the aligned cells (see Figure 3.11, image B) and the following parameters determined; i) soma-node compliance ii) soma located on interlinking tracks and iii) somas not complying to the pattern. At PLL concentration of 1μg/ml MicroSet proved to the least effective polymer stamp. Compared to Sylgard 184 stamped substrates, there was a significantly

lower percentage of cells bodies localised at the node adhesion site ($p < 0.05$) and following the pattern intersections ($p < 0.01$), with a significantly higher percentage of cells bodies (50%, $p < 0.01$) failing to comply to the pattern at all. Although a difference also existed between samples of stamped with 10μg/ml and 25 μg/ml PLL, these results did not prove significant.

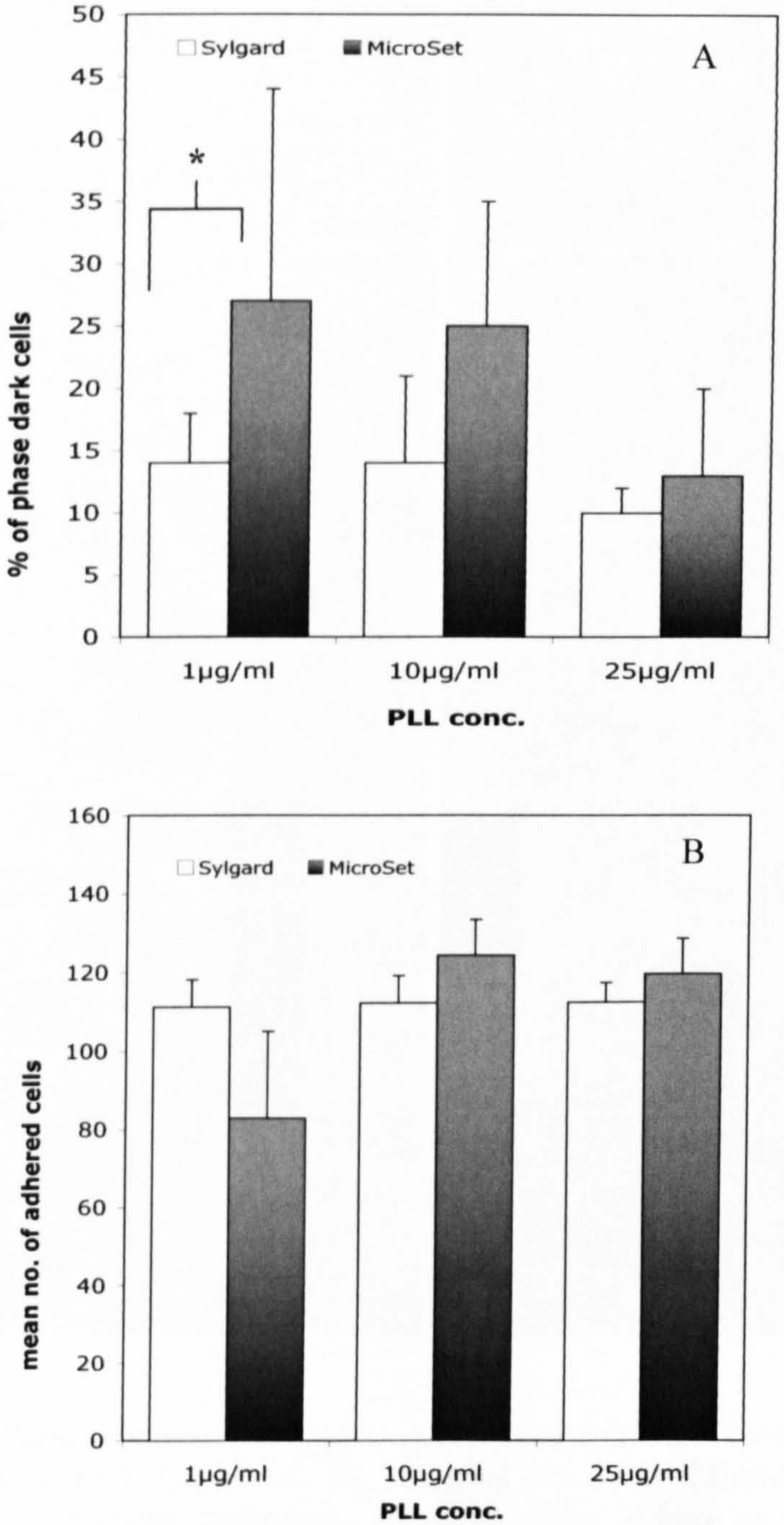

*Graph 3.2. (A) Showing percentage of phase dark cells observed on substrates stamped using polymers Sylgard or MicroSet. (B) Showing the mean number of cells adhered per sample (± SD). * denotes significance at 0.05 level of probability.*

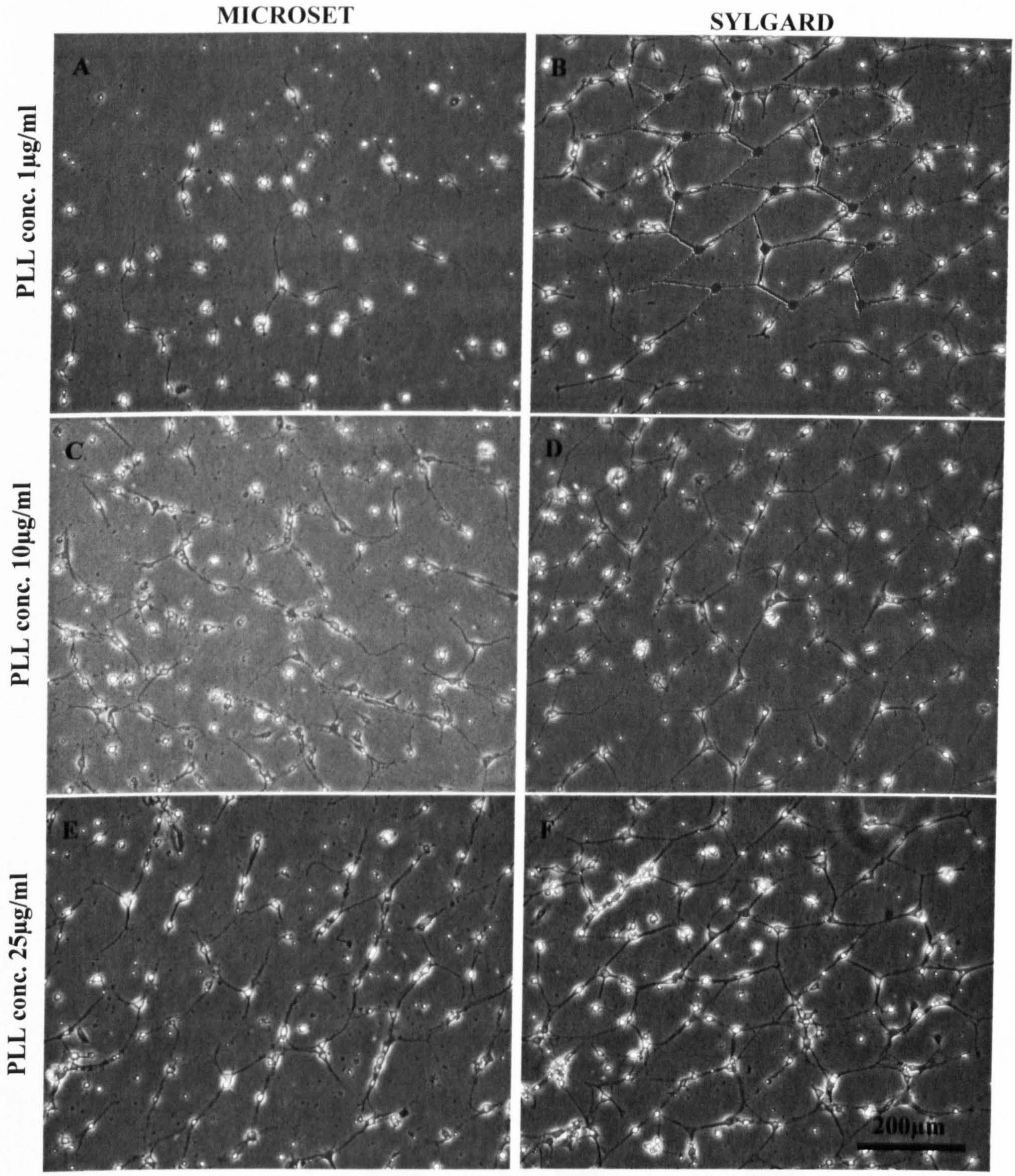

Figure 3.11. Phase microscopy images showing P1 spinal cord neurons grown on substrates stamped with 1µg/ml (A, B), 10µg/ml (C, D) or 25µg/ml (E, F) PLL using Sylgard or MicroSet stamp structures. Image B shows in blue an overlay of the stamp. This was used to measure cell compliance to the pattern. The scale bar is the same for all images.

A

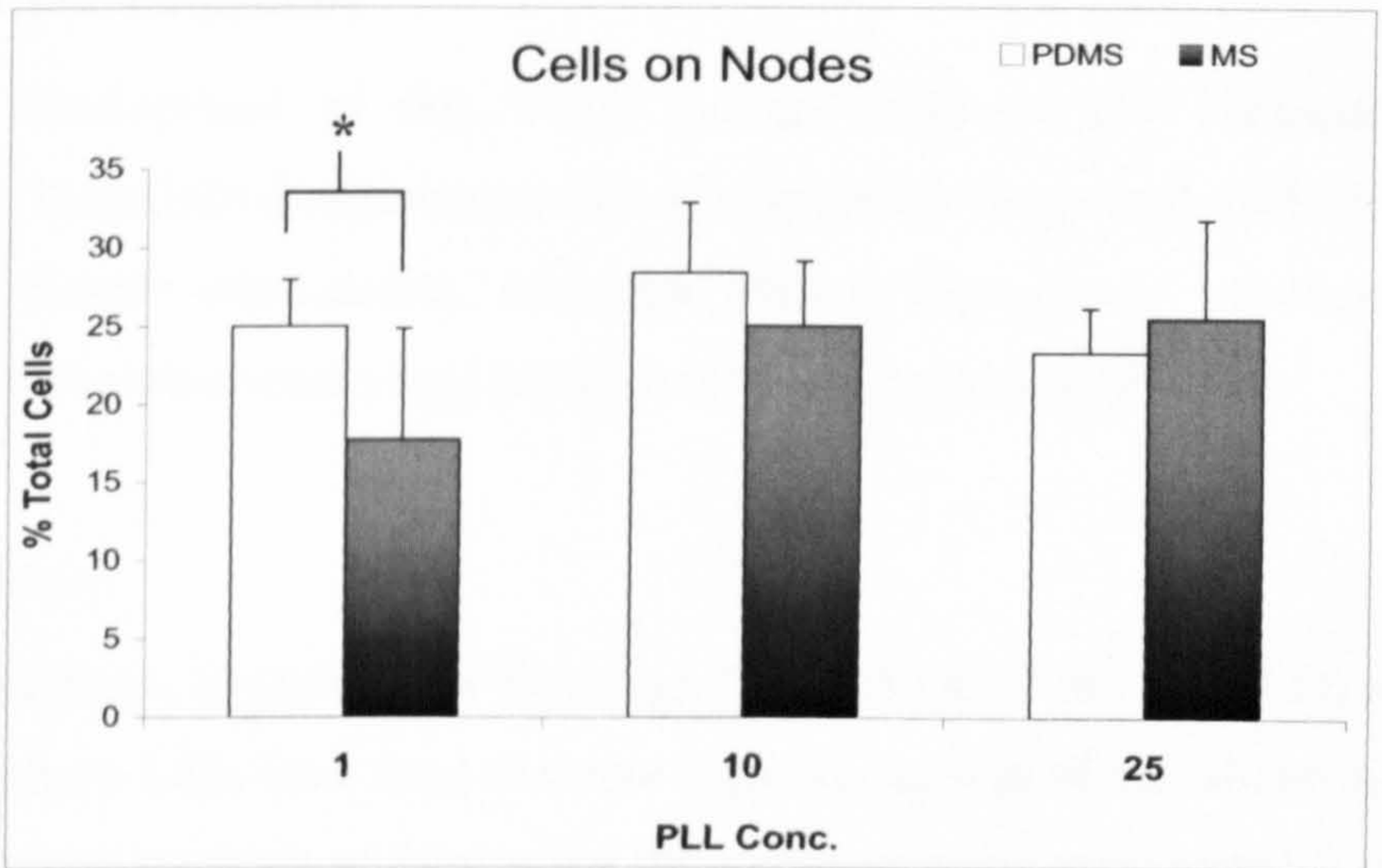

B

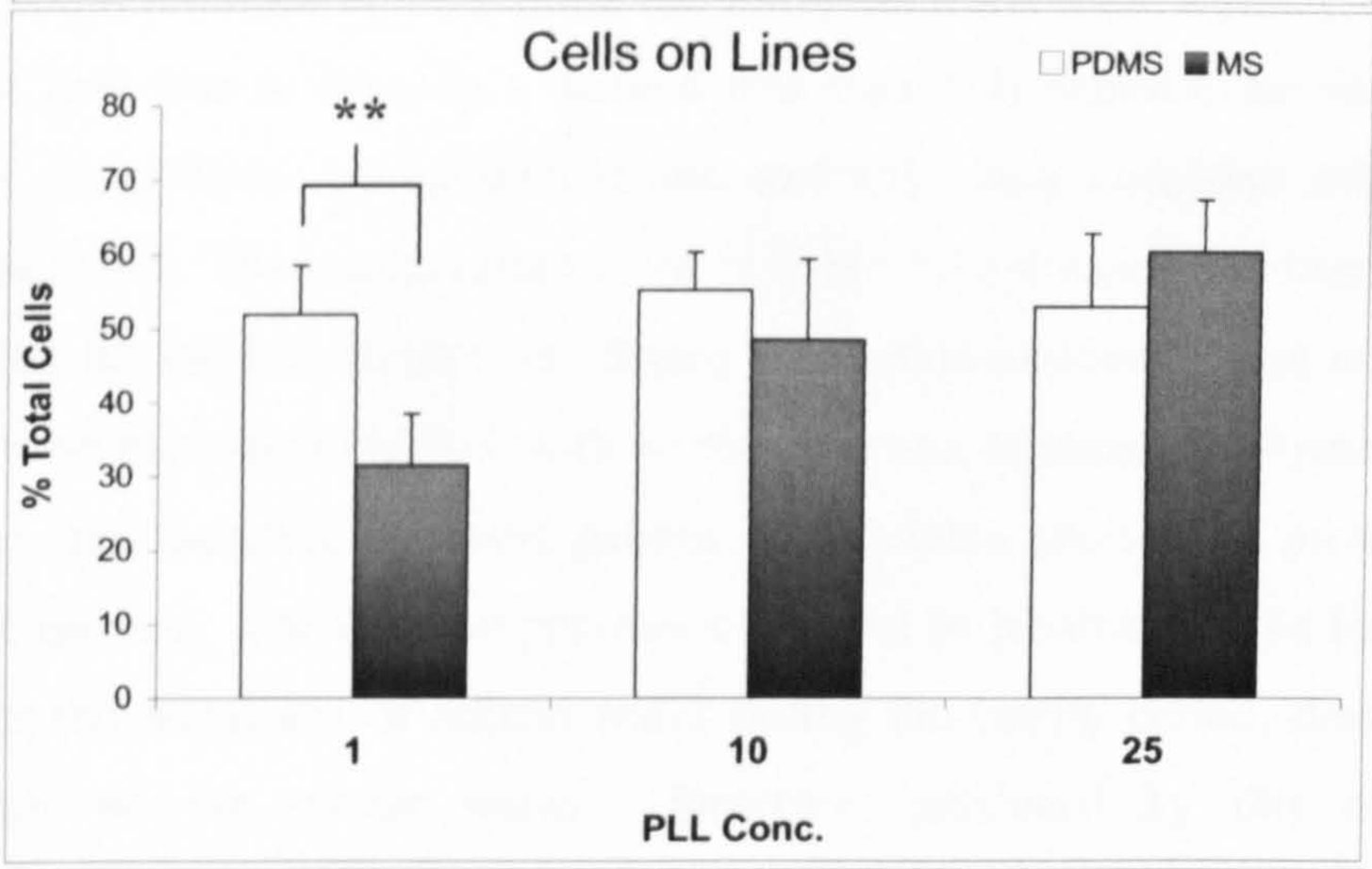

C

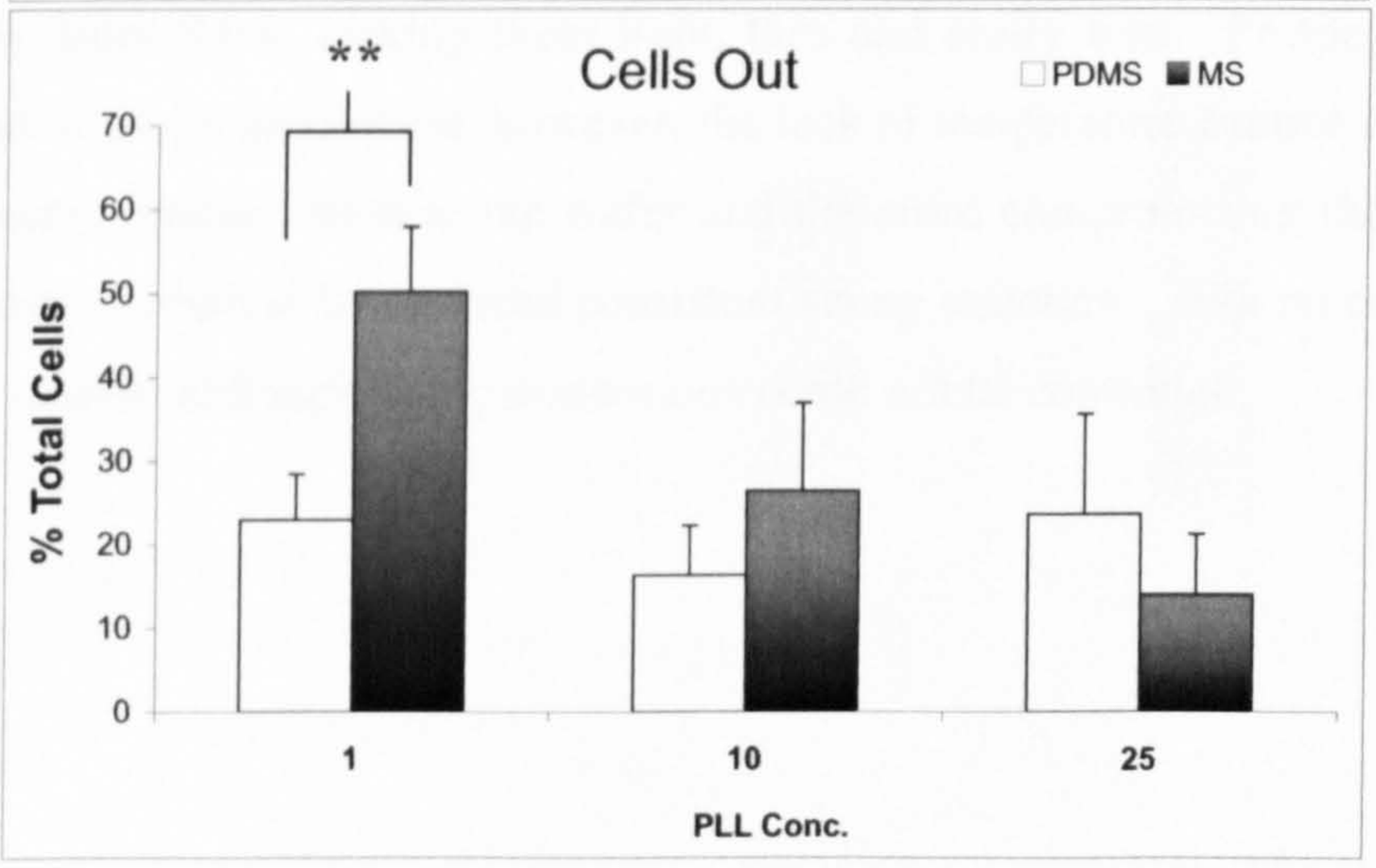

*Graph 3.3. (A) Graph showing % of total cells adhered to node sites of chemical patterns created by Sylgard (PDMS) or by MicroSet (MS) stamping, (B) % of total cells adhered to pattern intersections, (C) % of total cells failing to comply to the pattern. Results are mean ± SD, * denotes significance at 0.05 level of probability and ** at 0.01 level of probability.*

A. Method Development

During the development of this thesis various different μCP methodologies were investigated. These initial experiments aimed to establish an optimal method which would be used for further experiments. Although various biomolecule solutions and stamp modification techniques were tested not all results will be presented.

Stamp Fabrication

Fast curing polymers, Sylgard (Dow Corning), Qsil 215 (ACC Silicones Ltd) and MicroSet (Microset Products Ltd), were used to create negative replicas of the silicon wafer for μCP purposes. Various methods of fabricating the stamp structure were tested (see Table 3.3). The objective here was to develop a method that would; i) increase the life-time of the silicon wafer, ii) optimise stamp dimensions, and iii) retain structural integrity of the micrometric structure. The results summarised in Table 3.3 are based on observations made during and after the fabrication process. Stamp fabrication protocol C was noted to be the most efficient and consistent method, with no displacement of uncured polymer outwith the casting mould, and therefore the focal pattern. Fabrication protocol A proved to be the least effective method. The uncured polymer could not be localised to the focal area, and dispersed over the remainder of silicon wafer during the curing period, destroying other patterned areas on the master wafer. Structures produced by this method were approximately 3mm thick, making them light, thin and easily torn. Protocol B was the fastest method of stamp production, however, the lack of temperature control meant stamps over-cured easily, binding them to the wafer and therefore compromising the life-time of the silicon master. Method D produced consistent stamp structures, with no contamination of the silicon master, although stamp dimensions could not be controlled.

Fabrication Method	↑ Life-time of Silicon Wafer	Control of Stamp Structure	↑ Integrity of Stamp
A	– / –	– / –	+ / –
B	– / +	– / +	– / +
C	+ / +	+ / +	+ / +
D	+ / +	+ / –	+ / +

Table 3.3. Summary table of qualitative observations of stamp structure after fabrication by methods A, B, C and D (see Table 3.1 for fabrication descriptions). A quantitative analysis is given where +/+ indicates 'excellent', +/– 'good', –/+ 'poor' and –/– 'bad'.

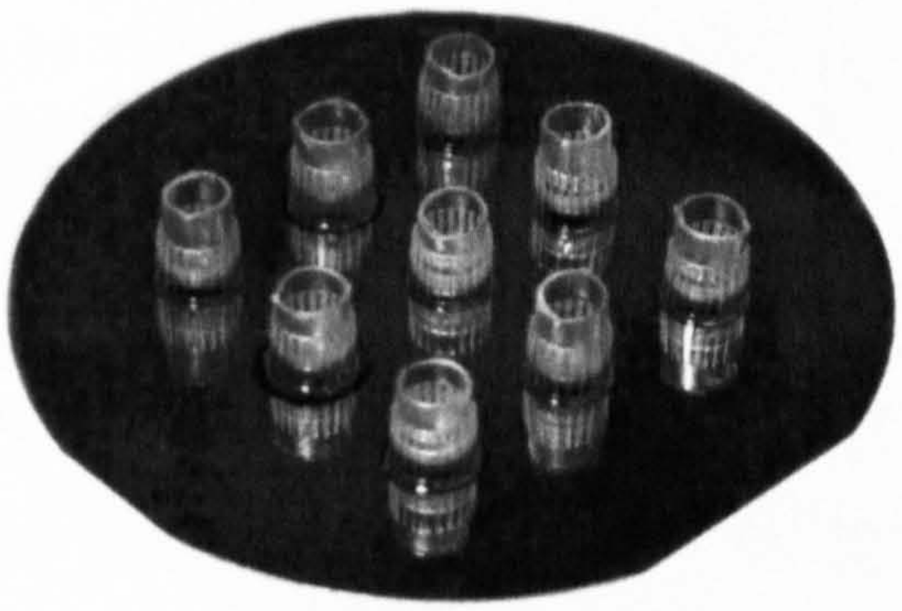

Figure 3.12. Photograph of 4 inch silicon wafer, showing casting mould made from modified 1ml pipette tips, as used in stamp fabrication method C.

Summary

Stamping with the non-adhesive protein albumin proved unsuccessful in creating organised neural networks by μCP. Of the three polymers tested it was concluded that Sylgard 184 was the best suited polymer as a stamp for μCP compared to the other polymers; not only did it accurately transfer the biomolecule inking solution but it also appeared to be more compatible with the neuronal cultures.

Discussion

A. Established Methods

Albumin Patterning

It was hypothesised that cell compliance to the chemical pattern would be best achieved by μCP with a non-permissive substrate. In this experiment the effect of 4μg/ml, 8μg/ml and 12μg/ml albumin concentration on surface coverage by cell adhesion was investigated. From Coomassie blue stained images it was evident that albumin was in fact a non-adhesive substrate that did not promote neuron growth. However the concentration of the albumin solution was the most important factor influencing this result. At a concentration of 4μg/ml, the difference in cell adhesion was only apparent at the stamp edge (see Figure 3.5.B). This distinct border at the stamp edge could be due to an accumulation of the biomolecule solution during stamp wetting. At the higher albumin concentrations of 8μg/ml and 12μg/ml albumin the percentage of surface coverage by cell adhesion was significantly lower than both the control samples, and those stamped with 4μg/ml. In both cases the cell concentration had reduced sufficiently, allowing single cell bodies to be identified. However, not one of the 5 different samples at either concentration showed any evidence of cells growing in a way that would suggest they were complying to the printed pattern. During this experiment it was noted that the overall cell coverage between samples of the same field varied significantly (see Figure 3.7). Based on this evidence it was concluded that the area of protein transfer required to produce a patterned network by non-adhesive chemical printing was too great, limiting the precise control of individual cell bodies and their neurite extensions. It was therefore decided that further experiments would be conducted by printing adhesive and growth-promoting biological substrates on to non-adhesive support materials.

Evaluation of Protein Transfer

The most commonly used polymer in μCP technology is the Dow Corning product Sylgard 184 (Chang & Gregory 2001, Lauer *et al.* 2001a, Schmalenberg *et al.* 2004, Scholl *et al.* 2000, Sgarbi *et al.* 2004, St John *et al.* 1997, Vogt *et al.* 2003, Wheeler *et al.* 1999). This experiment aimed to determine whether other commercially available PDMS polymers, Qsil 215 and MicroSet, could also be used for this procedure. The stamping properties of

the above mentioned polymers were compared to those of Sylgard. Although results showed Sylgard to be the most suitable polymer for μCP purposes, the fluorescence images (see Figure 3.8) showed this stamp structure to be highly susceptible to stamp deformation. Of the 3 polymers tested, structures stamped with Sylgard showed at least 40% of the stamped region to be 'over-stamped'. Scanning electron micrographs of the stamp used showed the defect not to be in the stamp structure itself, but to be occurring during the stamping procedure. It was concluded that these results are most likely to be caused by stamp 'buckling' or 'sagging' (see Figure 3.13), where the unsupported section of the pattern polymer structure collapses during stamping (Quist *et al.* 2005).

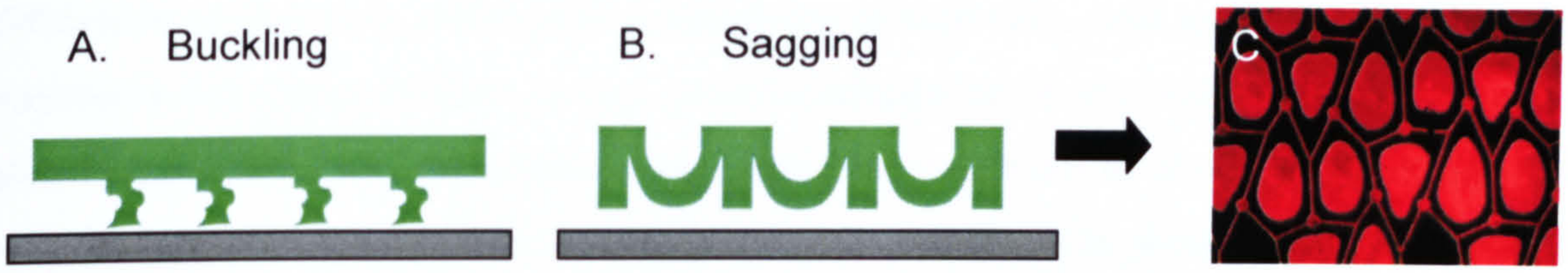

Figure 3.13. Schematic diagram showing the different types of stamp deformation that could potentially cause the result observed during the evaluation of pattern transfer experiment (A, B), and the corresponding fluorescent image illustrating this result (C).

To eliminate the occurrence of this type of stamp distortion in further experiments, the stamp fabrication methods were revised. Qsil 215, like Sylgard, is a clear PDMS curable polymer. However, its ability to transfer a protein pattern differed greatly. Samples stamped with this polymer were extremely distorted, with large regions of the patterns completely defective. Due to this result no further μCP experiments were conducted using this polymer material. MicroSet, unlike the other polymers tested, is distinct by its black, non-transparent appearance. This is due to the presence of black carbon fillers in its composition. The first fluorescence imaging results produced by stamping with a ridged MicroSet structure showed a distortion in the stamp structure to have occurred during stamp fabrication (see Figure 3.10.B). However, further SEM analysis showed this not to be the case. The only possible explanation for this effect could be that excess protein solution had accumulated at the edge of the ridged feature, possibly due to insufficient drying time. To test this hypothesis the stamping procedure was repeated, ensuring the stamp had completely dried before use. This had the effect of removing the '*halo*' feature

from future substrate stamping. Of the 3 polymers tested this was the only one to show a non-distorted, complete uniform transfer of biomolecule solution.

Biocompatibility of Polymers Sylgard and MicroSet

This experiment aimed to determine whether the carbon black fillers present in the composition of the MicroSet polymer would have a detrimental effect on the growth and survival of the neuronal culture. From phase contrast images of cells after 48hrs in culture (see Figure 3.11) it was evident that the use of MicroSet as a stamping polymer was affecting neuron survival. From observations of phase contrast images of each experimental condition it appeared that less cells were adhering to the MicroSet printed structures in comparison to structures printed with Sylgard stamps. Although, this difference proved to be statistically insignificant in each case, cells grown on the MicroSet structures did appear to have shorter, underdeveloped processes, with the majority of the population phase dark in appearance suggesting the composition of the MicroSet polymer was in fact having a detrimental affect on cell growth. On these samples there also appeared to be an abundance of debris-like particles, distributed across the culture substrate. Further SEM analysis of MicroSet stamped structures showed some polymer deposits to be transferred during the stamping. An investigation of cell compliance to the stamped pattern also showed MicroSet to be the least effective polymer, with almost 50% of the total cells adhered lying completely outwith the network pattern (at 1μg/ml PLL concentration). From these results it was concluded all μCP experiments would be performed using Dow Corning, Sylgard 184 as the polymer of choice.

B. Method Development

Stamp fabrication

The first stamp fabrication method (A) employed was based on those previously established at the Centre For Cell Engineering. This approach, however, had originally been developed to produce PDMS structures for the investigation of cellular responses to topography. The dimensions of the PDMS structures were essentially designed to work with cell culture, and were therefore unsuited for the repeated handling that occurs during μCP. Although the micrometric pattern structure was successfully replicated, the structure of the stamp itself was difficult to handle and was often destroyed after the first application. Creating stamps by this method also reduced the lifetime of the silicon wafer, as the modified glass supports

were not effective at containing the uncured silicone. During the required curing time, the polymer would spread over the entire wafer, not only destroying other patterns but also compromising the integrity of the stamp structure.

Method B was developed in an attempt to reduce polymer spreading during curing. It was thought that by bringing the silicon master and polymer construct into direct contact with a high heat source curing time would be reduced, therefore reducing the opportunity for polymer spreading to occur. The polymer stamps were cast on a hotplate reducing the curing time dramatically from 24 hrs to approximately 2 minutes. Although this method prevented polymer spreading, the limited control of the heat output often resulted in the undesired effect of moulding the stamp to the wafer. This effect was irreversible, resulting in the destruction of both the silicon master and the stamp structure.

The details of methods used to fabricate polymer stamping structures from silicon wafers are rarely described in the relevant scientific literature, with the exception being the publications of Lauer *et al.* and Vogt *et al.* (Lauer *et al.* 2001a, Vogt *et al.* 2003). In these publications the use of a polymer casting mould, in the form of an inverted Eppendorf tube, is described. This method was adapted using 1ml Gilson pipette tips, for 10 mm^2 patterns, and 5ml pipette tips for the larger patterns of 1cm^2 in size. The pipette tips were easily modified due to the pliable nature of the plastic (unlike the Eppendorf tube, which could

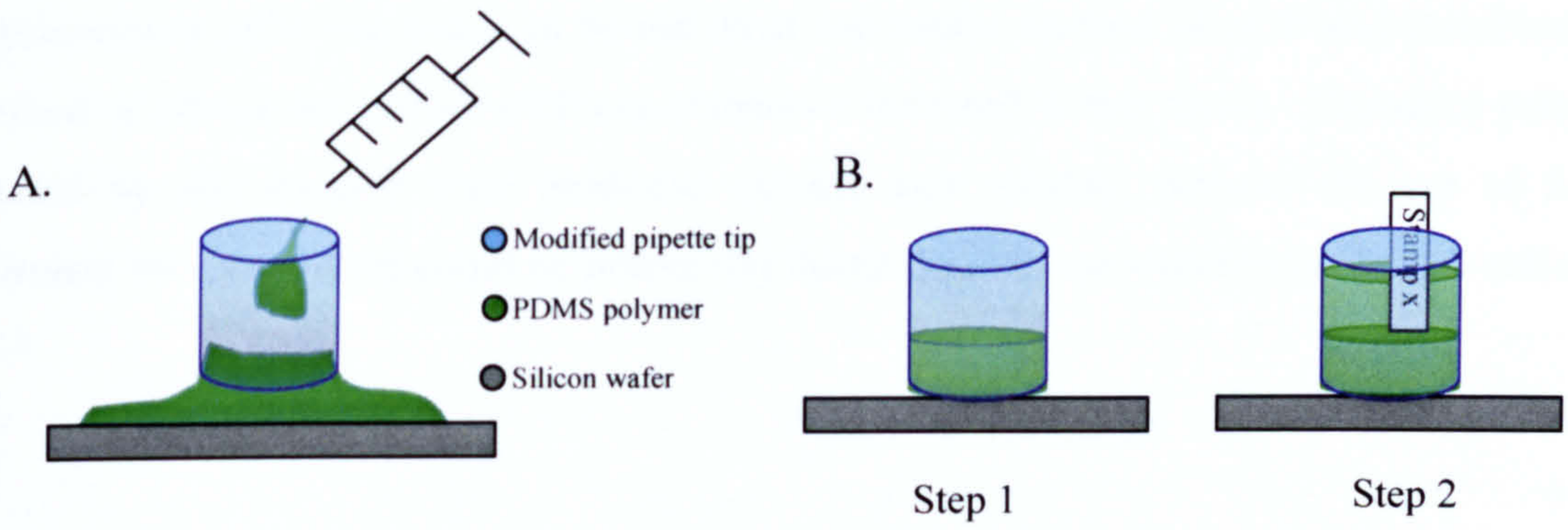

Figure 3.14. Schematic diagram showing problems encountered during fabrication method C (A). Diagram B shows the final 2 step process used to fabricate polymer stamps. Firstly approximately 1/3 of the mould was filled with polymer then cured, and then the remaining volume filled and again cured. Following the first step it was possible to add label in order to identify which silicon wafer it was cast from.

only be modified using a dissecting scalpel blade, this proved too dangerous to pursue). Using sharp scissors the dispensing tip of the pipette was removed, leaving 1.5 cm of the structure remaining and the tips inverted onto the silicon wafer with the cut end protruding.

The uncured polymer was loaded into a 5ml syringe to control distribution during dispensing. It was noted that if too much polymer was dispensed into to the stamp mould, the fluidic force of the uncured polymer would push the polymer through the mould, dispersing over the silicon wafer (see Figure 3.14. A), similar to effect noted during fabrication method A. From previous attempts at developing an optimal protocol it was known that the application of a high heat source would reduce this effect, therefore a new method (method C) was devised that would contain the polymer to the mould after initial dispensing, but without encompassing the effects observed in method B. Method C involved the stamp being cured in 2 stages, first at 120°C for 2hrs then at 75°C overnight. Increasing the curing temperature to 120°C, and reducing the polymer volume (approximately 200 μl) in the initial stages of curing had the effect of successfully inhibiting polymer spreading. During the second curing stage it was possible to add a stamp label, indicating stamp pattern details, without any effect on the micrometric pattern. Stamps produced by this method were of sound structure, could be easily handled and without difficulty could be distinguishable from one another.

Conclusion

Although physisorption μCP and chemisorption μCP have not been compared directly, physisorption μCP was found to be the most successful method of μCP and therefore the method of choice for further μCP experiments conducted in this thesis. Chemical patterns created by this method were produced quickly and reliably, without the use of harsh chemical solvents which could be potentially detrimental to the viability of the cell culture.

Chapter 4.

Investigation of Structure-Function Relationship in Neural Networks by μCP

Abstract

A structure-function relationship exists throughout nature. This is most evident in the CNS. However it is not known how cell morphology contributes to this partnership. The aim of this study was to determine whether variations in cell morphology would affect network characteristics. Six network designs were considered, three of which incorporated various dendritic morphologies. The patterns were introduced to the cultures using μCP techniques, and the effect investigated using immuncytochemical staining and scanning electron microscopy. Cell compliance was increased on patterns of hexagonal dimensions, and alignment most accurate on patterns consisting of 20μm node adhesion sites. Although the patterns that incorporated dendritic morphology did not appear to actually change the shape of individual neurons, they did appear to be having an affect of overall network characteristics as shown by synaptophysin staining and SEM imaging. These results suggest that this methodology could provide insight into the structure-function relationship of neural networks, although changes to the experiment design might need to be considered, as cell location within the pattern could not be precisely controlled.

Introduction

Throughout biology, there is a close relation between structure and function, evidence of which exists within the structure of neurological systems. Easily distinguishable from other cells types found in the body, nerve cells have a unique morphology comprising of a cell body, from which many neurite extensions protrude. These extensions can be categorised into dendrites, the neurites that contain the apparatus for receiving information, and the usually longer structure of the axon, which is responsible for transmitting those signals that arise from neurotransmitter release. Although vertebrate neurons share this common morphology, the elaborate dimensions of both axons and dendrites are systematically different between neuron classes and individual cells. Dendritic arborisations alone are highly branched, providing multiple interaction sites with neighbouring neurons of equally branched dimensions, and so on, creating a truly complex network arrangement. These neural networks are the underlying substrate for CNS function. However, the mechanism through which these cells and their intricate network configurations are maintained is poorly understood. It is now widely accepted that cell structure as well as the complex and varying network structure, is highly organised, suggesting it has adapted to serve a functional purpose (Uemura *et al.* 1995, van Pelt & Schierwagen 2004, van Pelt *et al.* 2001). Although studies using system modelling have shown that nerve cell morphology plays an important role in neuronal communication (van Ooyen *et al.* 2002, van Pelt & Schierwagen 2004, Vetter *et al.* 2001), it is this complexity that makes *in-vitro* studies more difficult. However, over the last decade there has been a significant increase in the transfer of micro-fabrication technology into the domain of biological research, providing a means through which the complex structure and organisation seen *in-vivo* can be replicated in the culture dish.

The positioning of cells in a defined pattern, whether by μCP or surface topography has the effect of introducing order into cultures of otherwise random spatial distribution. Using such techniques, small networks of fewer cells can be investigated. Many groups have opted for this approach, introducing linear or grid-like patterns, with nodal regions of varying dimensions for soma attachment, into their culture systems (Branch *et al.* 2000, Chang & Gregory 2001, Clark *et al.* 1993, Corey *et al.* 2003, Cornish *et al.* 2002, Craighead *et al.* 2001, Heller *et al.* 2005, James *et al.* 2000, Vogt *et al.* 2003, Wheeler *et al.* 1999). Although this has proved successful in actually reducing the number of cells in a

network, cell bodies have rarely been completely isolated and cell polarity is unidentifiable as many distinguishing features of the cell morphology are lost. Attempts have been made by some groups to introduce polarity into their networks, by modifying the geometric pattern to stimulate the growth of dendritic and axonal structures (Stenger *et al.* 1998, Vogt *et al.* 2004), they have failed to determine the exact geometric parameters required with respect to cell morphology and so these patterns still are of linear form (see Figure 4.1).

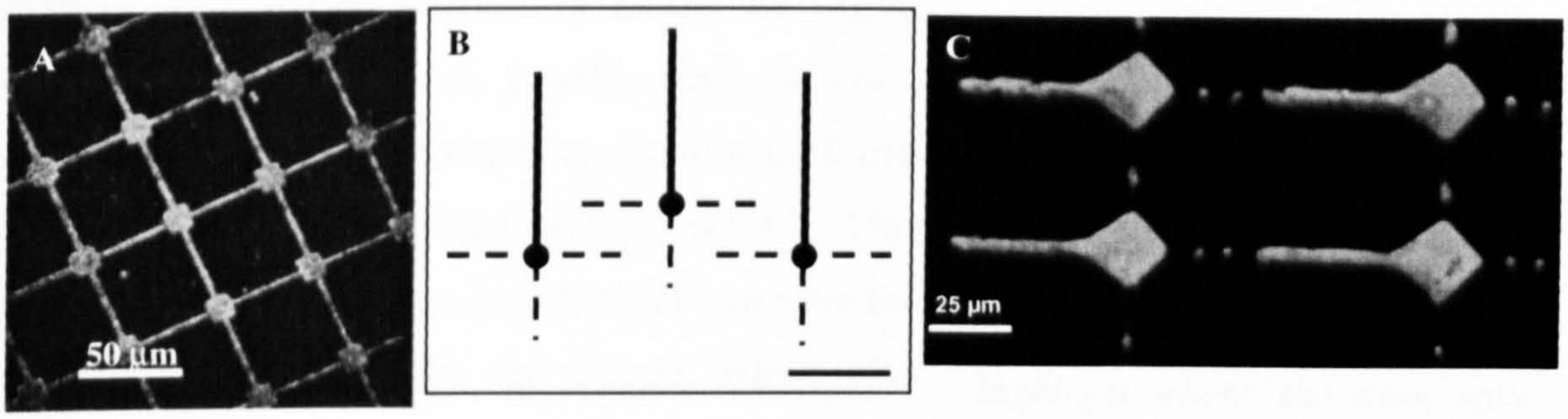

Figure 4.1. Image A is an example of a typical grid/linear pattern predominantly used in neural network studies (Fluorescence image of peptide transfer taken from Heller et al. 2005). Image B is a schematic diagram of the design used by Stenger et al. (1998) to introduce controlled polarity into neuron cultures (scale bar 100µm), and image B is an example of a similar geometric pattern used by Vogt et al. in a study of synapse formation and network behaviour (2004).

Cells complying to this type of pattern have limited growth opportunities and will predominantly exhibit a morphology quite different from that observed in random dissociated cultures or *in-vivo* studies. It is arguable that by drastically altering cell shape within any predetermined network in culture, it is quite possible that cell behaviour, and therefore network behaviour, is being modified (Ravenscroft *et al.* 1998). To test this hypothesis 6 network patterns of various geometric dimensions were designed and compared.

Network Patterns

Jude

This pattern was originally designed by Dr. Judy Wilkinson and is based on the computational aspects of signal processing in a neural network (Wilkinson & Curtis 1999). The pattern consists of soma attachment sites of 20μm diameter (the black circular node region) with interconnecting tracks of 5μm width. The angles incorporated into the design were estimated from a study of nodose ganglion cells conducted at CCE prior to this study (Wilkinson, C.D.W., not published). The average angle at which the axons first branched

was measured to be 60°±30°. From this data a pattern, capable of filling a 2-dimensional area was devised taking into consideration fabrication limitations. From the limited set of possibilities the *Jude* pattern was chosen, creating one unit or "tile", which is easily replicated. Unlike linear or grid patterns, this design provides a means for signal expansion over the network. For this pattern to work, it is essential that the proliferating axon of each cell follow the track indicated in blue in Figure 4.2. This axon must split at the first junction and innervate the cells as indicated by the red arrows, which also indicate the direction of signal transmission.

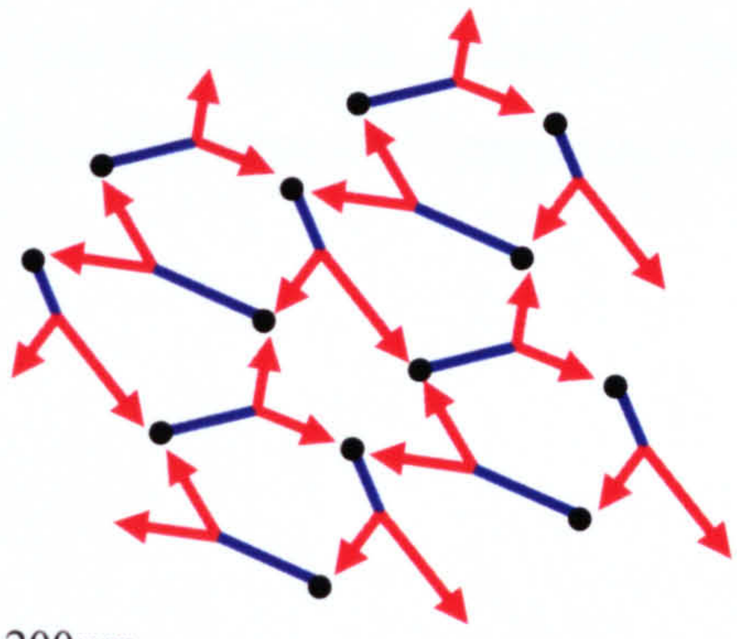

Figure 4.2. Expanding Pattern Design. The cell body is represented by the black circle. The blue line indicates the desired path of the developing axon, and the red arrows highlight where the axon splits and the subsequent direction of signal transmission.

Hexagon Patterns

This design was based on the hypothesis that the extreme, and unequal, angles at the track intersections in the *Jude* pattern would limit neurite adhesion, by creating an imbalance in the mechanical forces exerted on the cell body (Bray 1979). It was anticipated that once wandering neurites located their target, the tensile force between the primary cell and the connection would dislodge focal contacts that had been previously made along the chemical pattern. By introducing equal angles at the intersection sites, it was hypothesised that neurite compliance would be increased, as the force exerted on the process, and on the cell itself, would be of equal value. All hexagonal patterns (see Figure 4.4) consist of a soma adhesion site at every 2nd junction of 5μm width connecting tracks. The adhesion sites of 20μm (*hex 20*) and 40 μm (*hex 40*) were compared to nodal regions comprising of a sunflower design (*sun*), an oakleaf design (*oak*) and a lattice effect (*lattice*). The descriptive nodal designs (*sun, oak* and *lattice*) were aimed at introducing dendritic arborisations into otherwise constrained network. It was hypothesised that changing the morphology of the cells in the network would in effect alter the network activity.

Summary

This study will investigate the effect of varying network patterns, created by μCP techniques, on cell compliance and network formation. Fluorescence microscopy will be

used to identify the neuronal growth within the network and the synaptic activity of the network. Scanning electron microscopy will also be used to determine cell compliance to the chemical pattern.

Materials and Methods

Pattern Dimensions

Jude Pattern

Designed to be easily fabricated the *Jude* pattern consists of a repeating single unit composed of three individual tiles as shown in Figure 4.2. The lines are colour coordinated to highlight those that are the same, and from this it is possible to determine the position of the adjacent tile. One mask template was used to create all structures carrying the *Jude* pattern to ensure structures were of the same dimensions. Each node section is 20 μm, and the lengths of the connecting lines are as follows (see Table 4.1):

Line	Length	Line	Length	Line.	Length
1.	50 μm	6.	80 μm	11.	55 μm
2.	50 μm	7.	65 μm	12.	60 μm
3.	65 μm	8.	60 μm	13.	50 μm
4.	100 μm	9.	100 μm	14.	50 μm
5.	40 μm	10.	80 μm	15.	40 μm

Table 4.1. Table showing lengths of the interconnecting tracks forming the Jude pattern master template from which all other structures were made. The line number corresponding to the line label given in Figure 4.3. The node size in this pattern is 20μm.

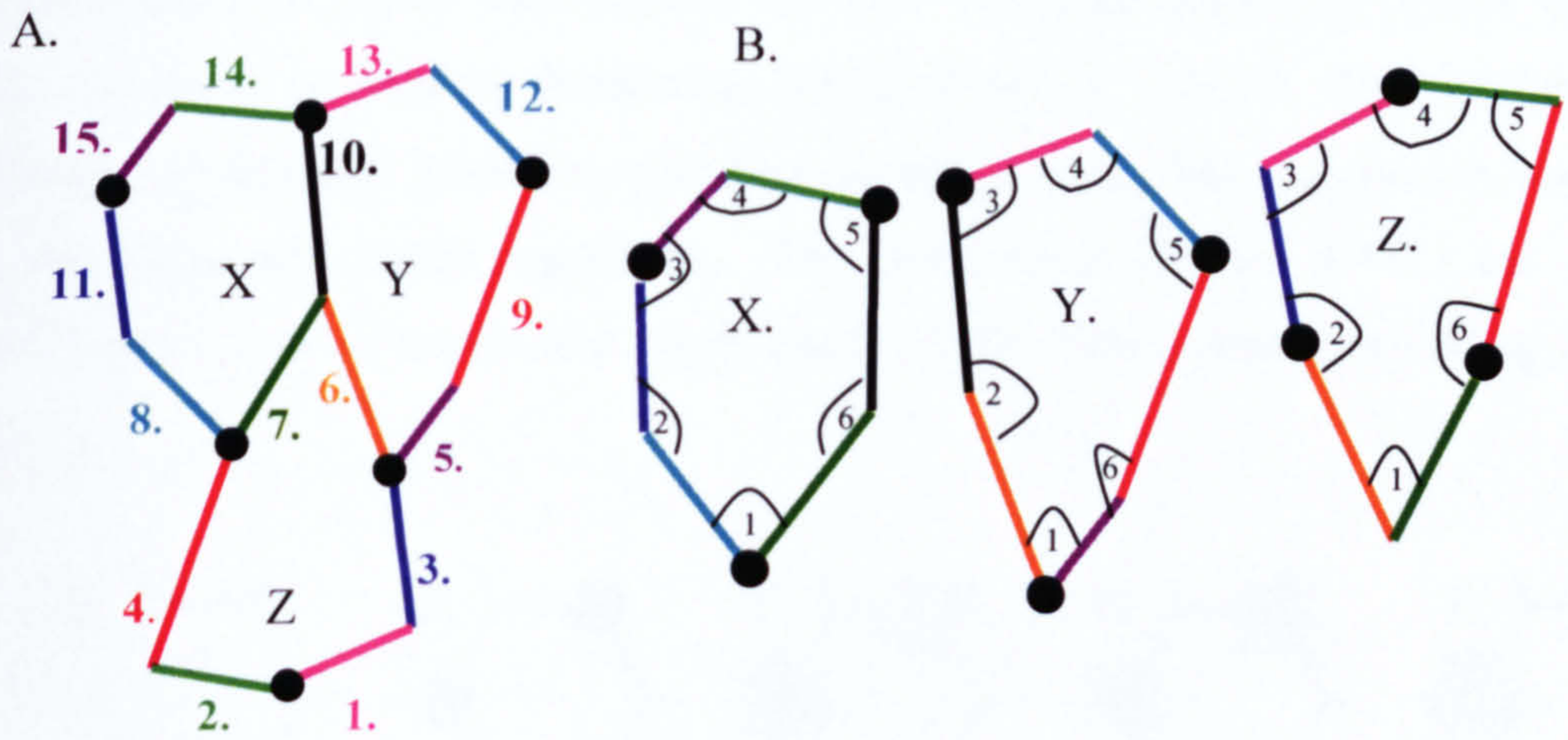

Figure 4.3. Schematic diagram illustrating the repeating unit of the Jude pattern (A). The colours are simply to highlight each wall within the pattern. The single unit consists of 3 individual tiles of different dimensions, labelled here as X, Y and Z (B). The six angles that create the each tile shape are listed in Table 4.2.

Each individual tile incorporates 6 different angles (see Figure 4.3.B). These angles are what gives the pattern its unique dimensions and are listed in Table 4.2.

Tile A		Tile B		Tile C	
Label	Angle	Label	Angle	Label	Angle
1.	70	1.	60	1.	50
2.	150	2.	160	2.	170
3.	140	3.	115	3.	100
4.	120	4.	110	4.	150
5.	100	5.	115	5.	80
6.	150	6.	165	6.	170

Table 4.2. Table showing the angles of each tile which together for the single repeating unit of the Jude pattern. There are 6 angles in each tile as labelled in Figure 4.2.B.

Hexagonal Patterns

All the hexagonal patterns used in this study were fabricated from the same network template with only the soma adhesion sites (node) varying between each pattern. The template consisted of a *'honey comb'* design, with each of the five sides measuring 5μm in width and 100μm in length. This length includes the soma adhesion site therefore if the node measures 20μm the connecting lines are 80μm, and if the node is 40μm the connecting lines are 60μm. All angles throughout the pattern measure 120°. The five hexagonal patterns are named according to their nodal design. *Hex 20* and *hex 40* have a circular node of 20μm and 40μm respectively (see Figure 4.4, image A and B). The three remaining pattern were developed with the aim of introducing dendritic architecture into the network. Each of these patterns has a design for dendritic growth surrounding the 40μm node. The patterns are named according to the shape the design represents. The *oak* pattern (Figure 4.4.C.) has 12 'oak leaf' structures, 13 μm in length and 10μm width (at the widest point), extending from the node site.

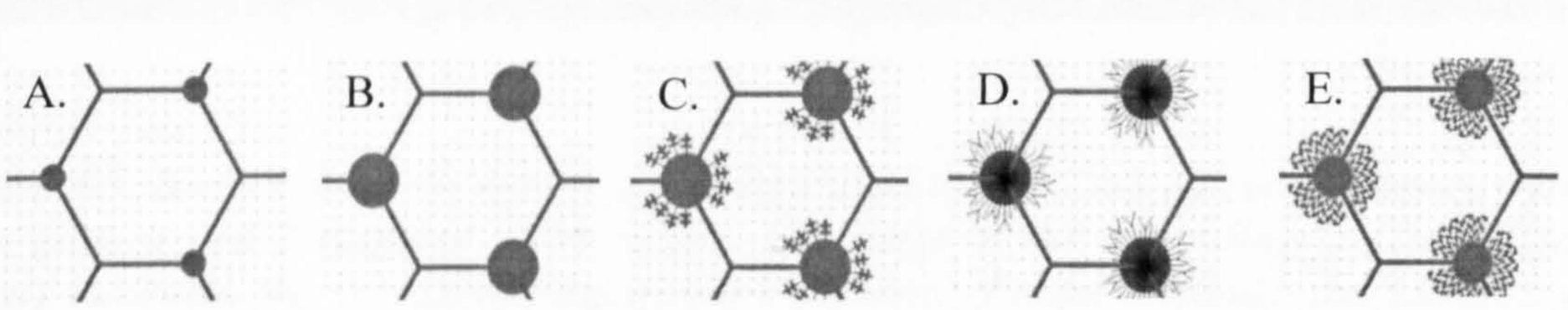

Figure 4.4. Images showing the varying nodal designs of hexagonal patterns hex 20 (A), hex 40 (B), oak (C), sun (D) and lattice (E).

The node of the *sun* pattern (Figure 4.4.D.) is based on a sunflower shape, with micrometric line structures, 2μm in width, with length (ranging to a maximum of 15 μm), radiating from the node site. The node of the *lattice* pattern is surrounded by a trellis-like structure protruding 20μm from the node edge (Figure 4.4.E.).

Fabrication Techniques

Master Die on a Silicon Wafer

Rongyu Tang (Department of Electronics and Engineering, University of Glasgow) designed and fabricated the photomask from which all structures used in this study were fabricated. The mask was designed to include all patterns to be investigated. The patterns were incorporated into the circular regions, as shown in Figure 4.5, and were identified be the given labelled (A-*Jude*, B-*hex 20*, C-*hex 40*, D-*sun*, E-*oak*, F-*lattice)*. The mask pattern was created on a 4 inch silicon wafer using an MA6 mask aligner (SÜSS MicroTech Inc, Vermont, USA). See Chapter 3, *Materials and Methods*, for a detailed description of the fabrication process.

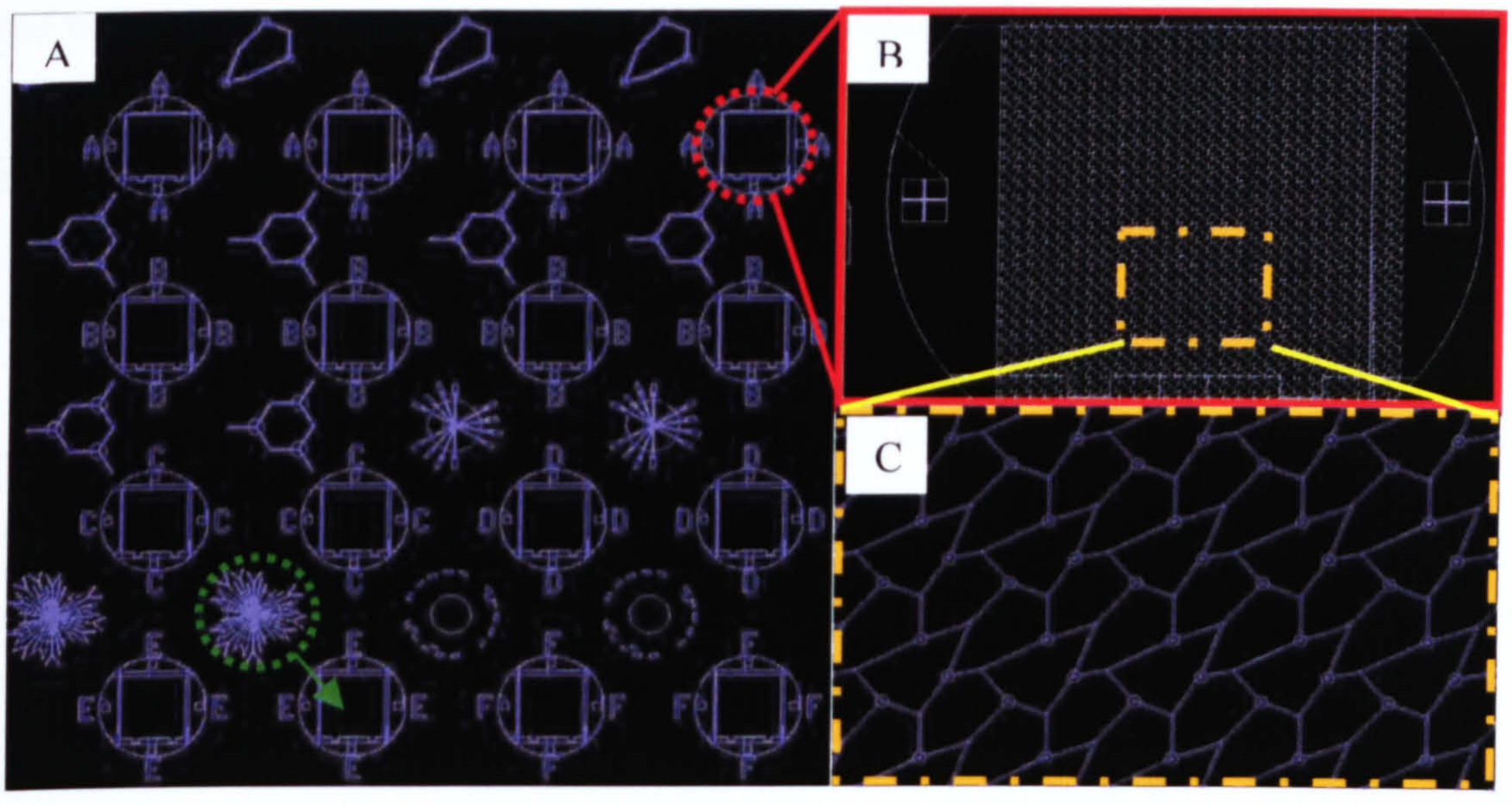

Figure 4.5. Images showing master die design used to fabricate silicon wafers carrying the Jude pattern and hexagonal patterns (A). In image A the node diagram (highlighted in green) indicates the corresponding network pattern. Image B shows the location of the network pattern, and image C shows this area magnified.

Fabrication of Stamp Structure

All stamps for this study were fabricated using stamp fabrication method C (see Chapter 3, *Materials and Methods, Method Development*). Stamps were labelled according to the network design, the location of the patterned region of the silicon wafer and the replication number. For example the region highlighted in Figure 4.6 would be labelled A1.J.01; A1 determines the column location on the silicon wafer, J (*Jude*) the network pattern, and 01 the cast number.

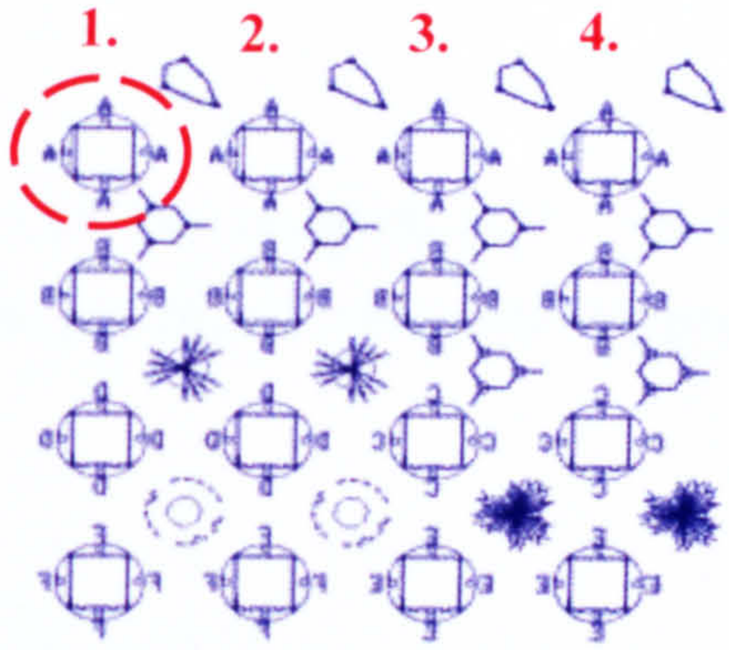

Figure 4.6. Image showing the label system used to identify each stamp structure. The numbers indicate the column location of the pattern.

Structure Analysis

By Scanning Electron Microscopy

All structures were analysed using a Hitachi S4700 scanning electron microscope. The silicon wafers were loaded directly into the chamber, without metal coating as no charge removal was required. The patterned face of the all silicone stamps was removed using a no.10 scalpel blade, this created a structure (approximately 1mm in depth) that was compatible with the SEM mounting requirements. It was necessary to splutter coat all silicone structures with 10nm of gold palladium, creating a conductive surface for viewing in the SEM.

By Immunofluorescent labelling

For immunofluorescence imaging chemical patterns of each network design was created by chemisorption μCP. For the stamping method and immunostaining descriptions see Chapter 3, *Established Methods- Chemisorption Microcontact Printing*.

Cellular Response to the Network Pattern

Embryonic Cell Culture

Only embryonic (E14) Sprague Dawley spinal cord neurons were used in this study. The culture procedure and methods are described in *Chapter 2, Materials and Methods, Primary Embryonic Spinal Cord Neurons- Established Methods*.

Physisorption Microcontact Printing

Chemical patterns for cell analysis were created by physisorption μCP. For method descriptions see Chapter 3, *Materials and Methods, Established Methods-Physisorption Microcontact Printing*.

Immunocytochemical Staining

The methods used are described in Chapter 2, *Primary Embryonic Spinal Cord Neurons- Established Methods*. Two sets of triple stains were used to identify cells complying to the neural networks. The first set consisted of primary antibodies (1° ABs) β-tubulin, GFAP and AA3, and the second set of 1° ABs β-tubulin, Smi31 and synaptophysin. The antibody (AB) staining combinations are listed below in Table 4.3.A. and 4.3.B.

A.

SET 1			
1° AB	Dilution	**2° AB**	Dilution
β-tubulin	1:100	**FITC goat anti-mouse (IgG_{2b})**	1:100
GFAP	1:100	**Cascade Blue goat anti-mouse (IgG_1)**	1:100
AA3	1:10	**TRITC goat anti-rat IgM**	1:100

B.

SET 2			
1° AB	Dilution	**2° AB**	Dilution
β-tubulin	1:100	**FITC goat anti-mouse (IgG_{2b})**	1:100
Smi31	1:1500	**Cascade Blue goat anti-mouse (IgG_1)**	1:100
synaptophysin	1:100	**TRITC goat anti-rabbit IgM**	1:100

Table 4.3. Table showing the antibody staining sets used to identify the cellular response to the network pattern. Table A lists the antibodies used in fluorescence labelling SET 1, and Table B lists those used in SET 2. Dilutions are also given (all 1° AB and 2° AB were diluted with a modified PBS solution: 0.3 M NaCl PBS, 0.3% Triton X).

SEM Imaging

All imaging was carried out on cells grown on μCP polystyrene structures. Cells were kept under normal culture conditions until required. Once removed from incubation, cells were washed (3 times for 2 minutes) in 0.1M (pH 7.4) PIperazine-NN'-bis-2-ethane sulphonic acid (PIPES) to remove all growth media. Samples were then fixed with 2.5% glutaraldehyde in 0.1M PIPES (pH 7.4) for 5 minutes at room temperature. Once fixed samples were given to Margaret Mullin (Electron Microscopy Unit, Institute of Biomedical and Life Sciences, University of Glasgow) who prepared all samples for SEM by freeze drying. Her methods are as follows:

1. Fix samples (2.5% glutaraldehyde in 0.1M PIPES (pH 7.4) for 5 minutes at room temperature).
2. Rinse three times with 0.1M sodium cacodylate buffer.
3. Incubate sample in 1% osmium tetroxide for 1 hour.
4. Rinse in RO water (six 10 minutes washes).
5. Plunge samples into 1/3 propane/ 2/3 isopentane mix at –180°C (Reichert-Jung KF80 Plunger).
6. Keep samples in liquid nitrogen at –80°C under vacuum (10^{-6} bar) overnight.
7. The following day, gradually warm samples by 10°C every 30 mins until they reach 25-30°C.

Once prepared samples were then splutter coated with gold palladium, creating a conductive surface for viewing in the SEM.

Results

Structure Analysis

Patterned Structures in Silicon

The results of etch process RYT1 was continually monitored throughout the duration of this thesis. Figure 4.7 shows SEM images of the silicon wafer taken after the final cleaning step in the fabrication process. Image A, C and E show the node region of hexagonal patterns *sun*, *oak* and *lattice* respectively. Images B, D and F show these region at a higher magnification, focusing on the sidewall deformations, which may be due to the switching of processing gases from etch to protection, to etch and so forth, during dry etching.

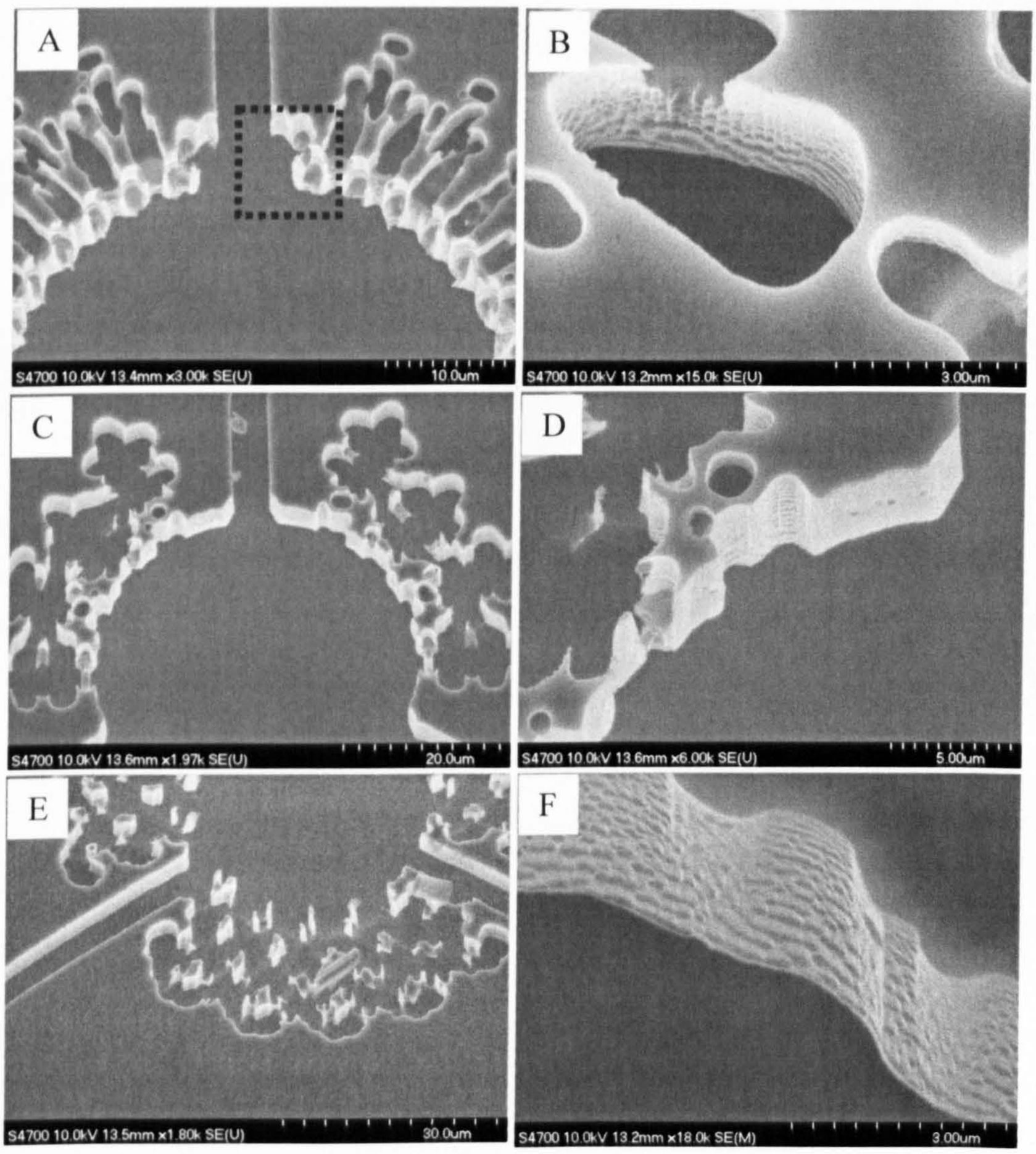

Figure 4.7. Images showing the varying nodal designs of hexagonal patterns hex 20 (A), Hex 40 (B), sun (C), oak (D) and lattice (E).

Pattern Replication in Silicone Polymer

A PDMS (Sylgard 184) replica of the network pattern was cast from the silicon wafer. SEM analysis showed pattern dimensions were maintained in the PDMS replica, with no structural defects observed across the whole patterned area. Figure 4.8. shows the nodal region of each network pattern. From the SEM images the depth of the network pattern was measured at 10μm.

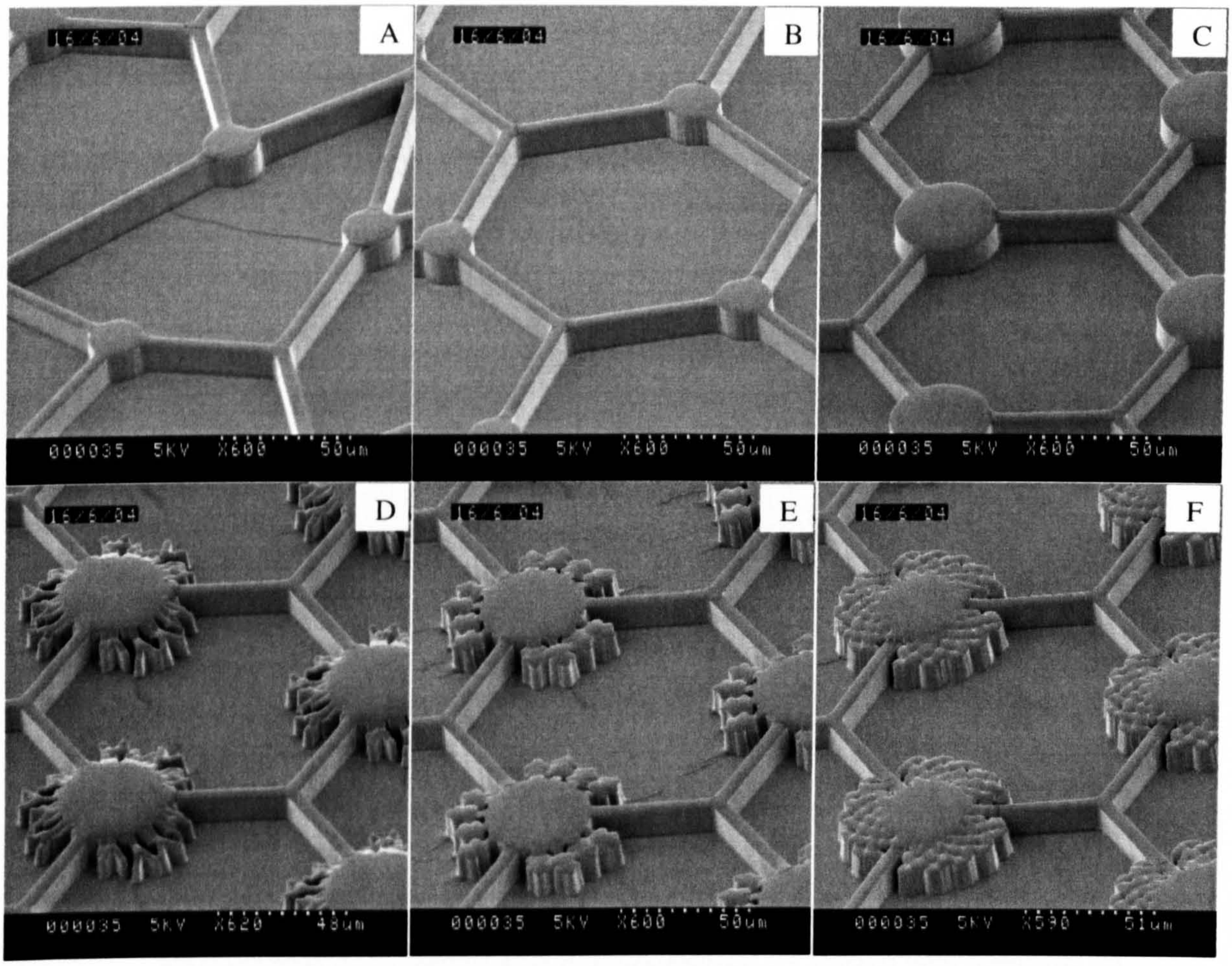

Figure 4.8. SEM images of the PDMS stamp showing network patterns Jude (A), hex 20 (B), hex 40 (C), sun (D), oak (E), and lattice (F). Each image shows the nodal region of the pattern.

Evaluation of Pattern Transfer

Immunofluorescence staining was carried out to determine whether it possible to reproduce the network pattern as a chemical pattern by chemisorption μCP methods. Figure 4.9 (A2-E2) shows a fluorescence micrograph of each pattern, plus a schematic representation of the pattern design (A1-E1).

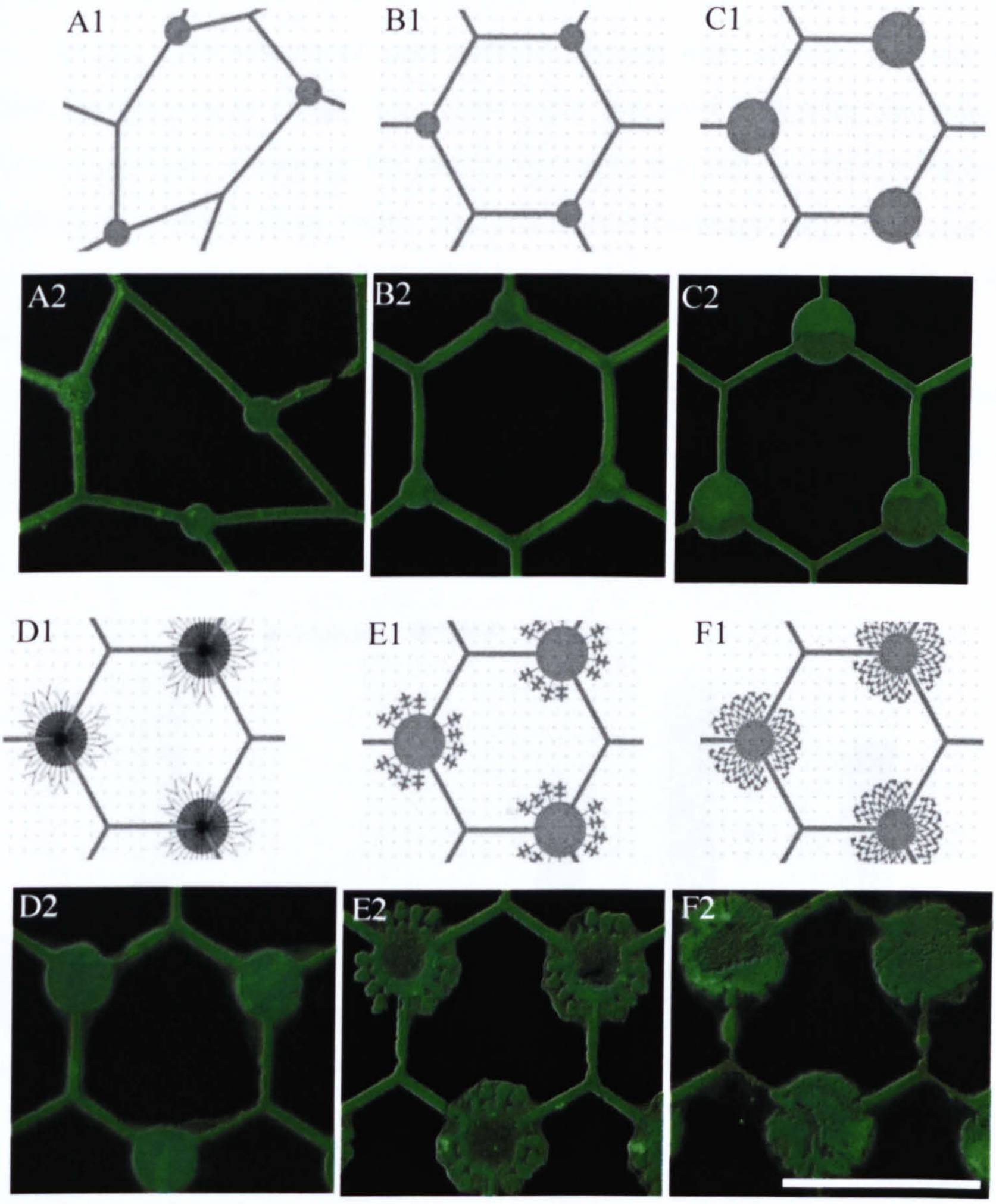

Figure 4.9. Immunofluorescence images of glass cover slips μCP with laminin by chemisorption μCP methods (A2-E2). Images are of each network pattern, focusing on 3 nodal regions. Images A1-E1 are schematic diagrams identifying the network design in each case. Scale bar is 100μm

Cellular Response to the Network Pattern

Classification of Network Population

The proportion of living neurons, glia and oligodendrocytes growing within the various patterns was determined by immunocytochemical staining. Embryonic spinal cord cells, plated at 6000 cells/mm^2, were grown on stamped structures for 2 weeks, then fixed and labelled for cytoskeletal markers β-tubulin (neurons), GFAP (glia) and AA3 (oligodendrocytes). Images were taken at random from 4 different stamped areas (see Figures 4.10.- 4.12.). Four images of each network pattern were used to produce the numerical data summarised in Graph 4.1. Only cells that were following the pattern were counted for this study. However, the percentage value was calculated from the total number of cells within the field of view. For example on average only 50% of cells complied with the *Jude* pattern, with 21% of those staining positive for β-tubulin, 19% staining positive for GFAP and 9% for AA3. *Hex 20* had the highest percentage of neurons growing within the pattern, with over 70% of cells complying to the pattern staining positive for β-tubulin. This network pattern also had the fewest number of GFAP positive glial cells growing within the network compared to any other design.

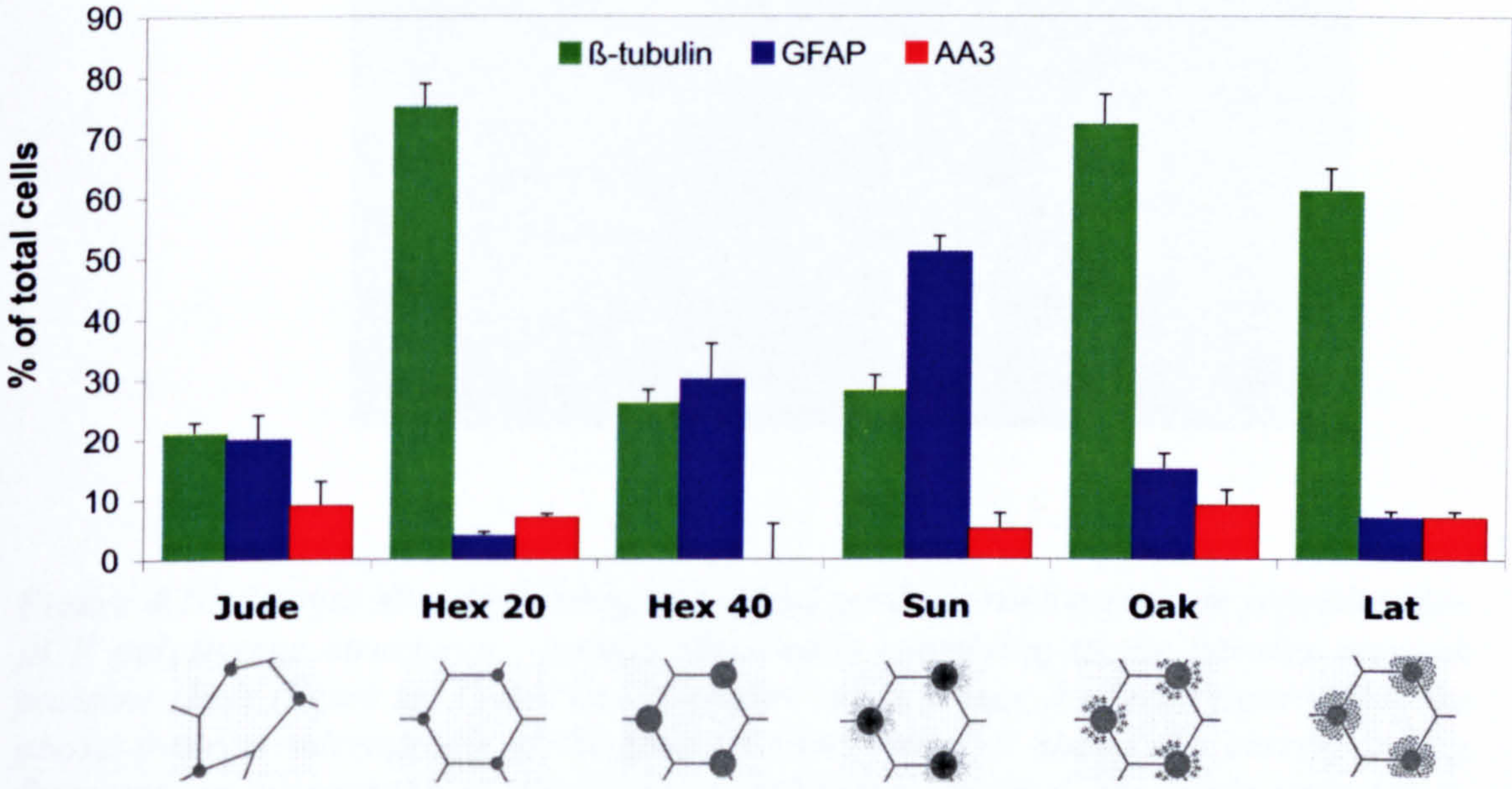

Graph 4.1. Graph shows the percentage of different cell types found growing within the network patterns ± standard deviation. Cell types were identified by immuocytochemical staining for the ß-tubulin (neurons) , GFAP (glia) and AA3 (oligodendrocytes).

1. Jude

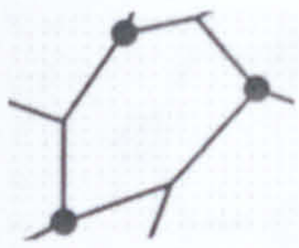

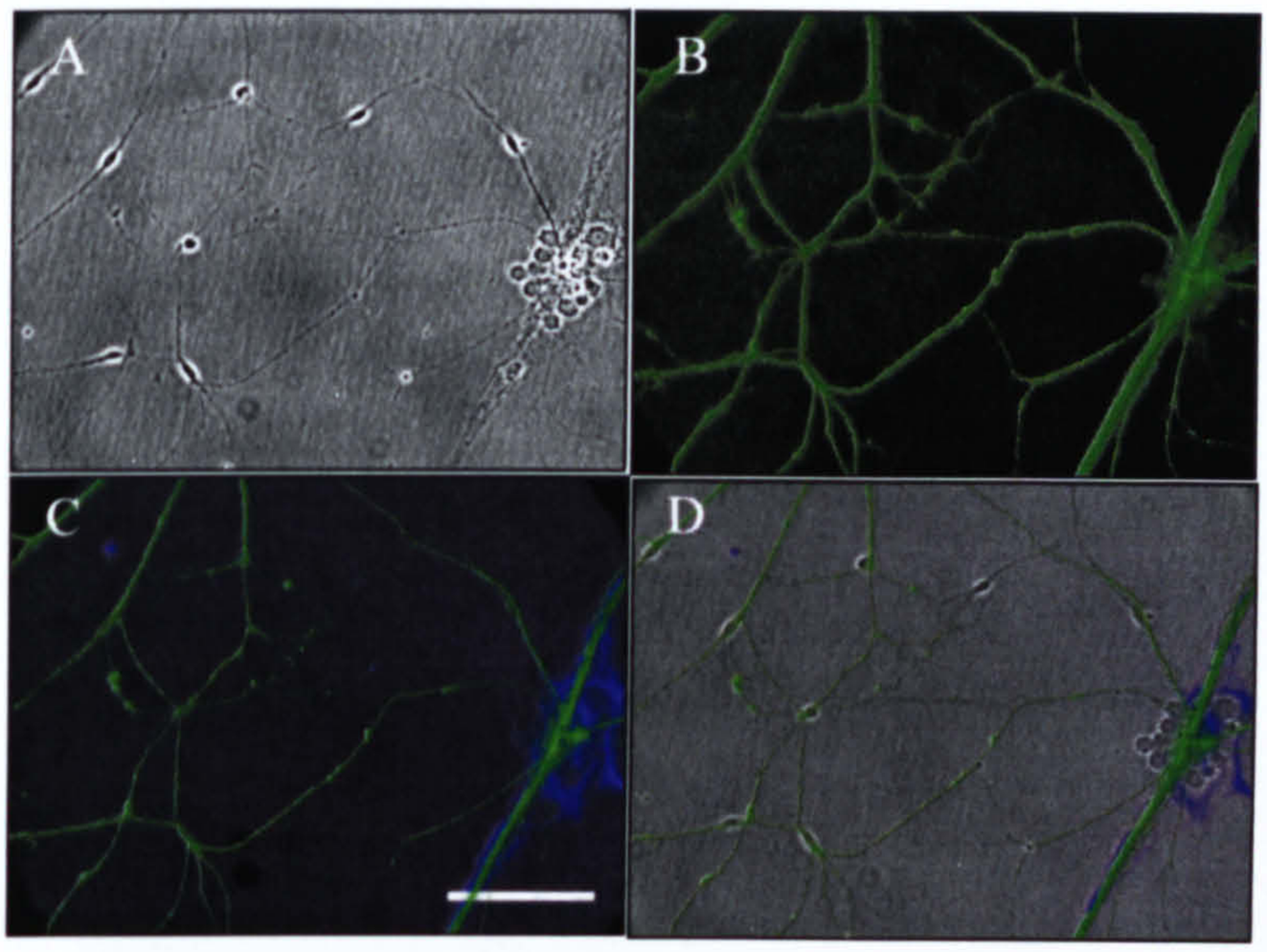

2. Hex 20

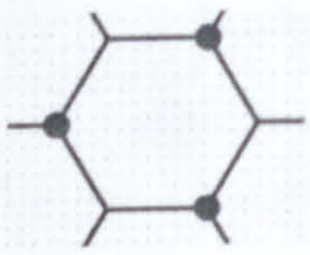

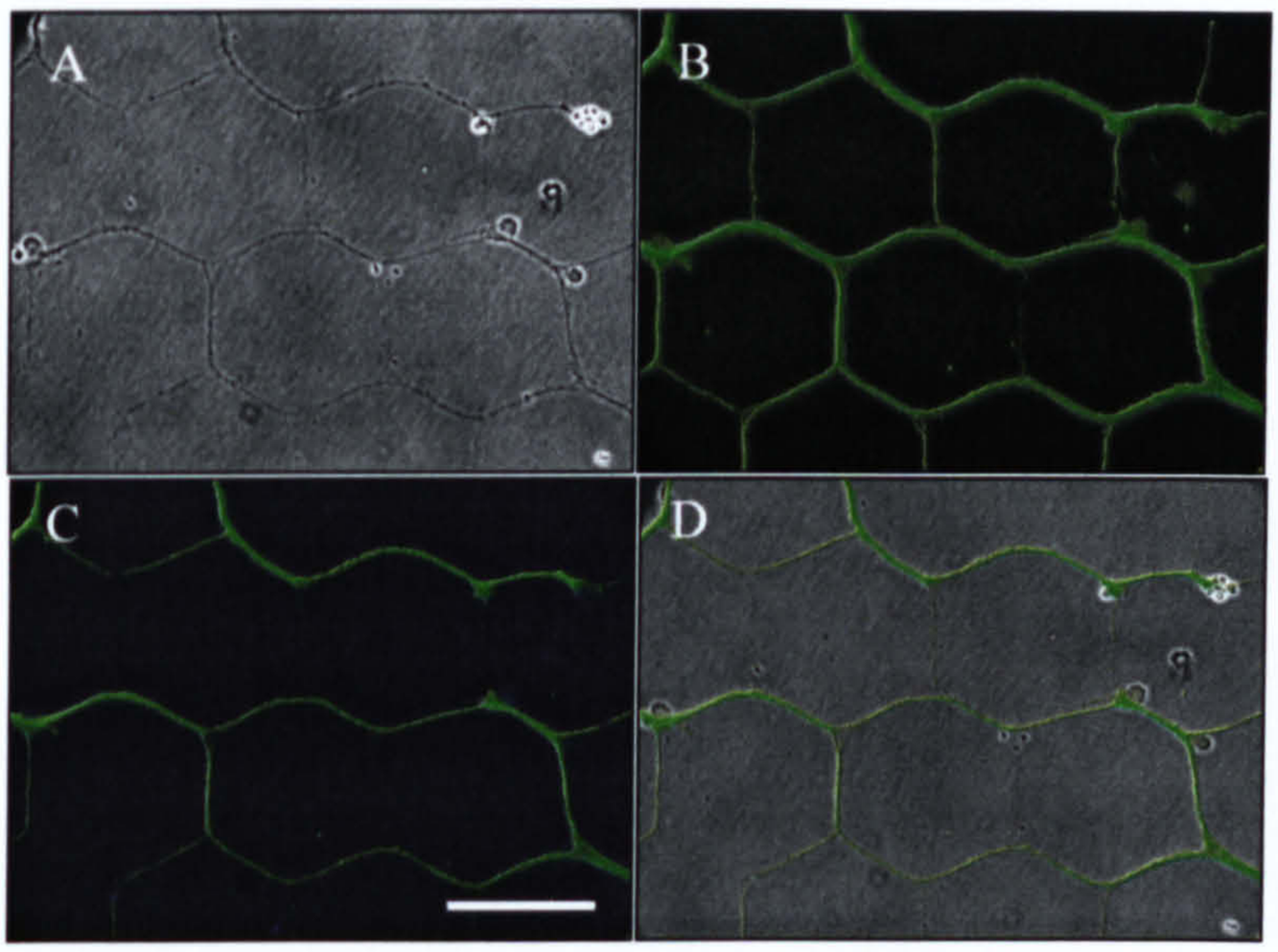

Figure 4.10. Images showing embryonic spinal cord neurons grown on physisorption μCP polystyrene structures. Images show cells complying to the various network patterns; Jude (figure set 1) and hex 20 (figure set 2). Image A of each figure set is the phase contrast micrograph of the field of view, image B shows the corresponding fluorescence micrograph of the ß-tubulin stain only, image C the triple stain for ß-tubulin, GFAP and AA3 and image D is image A (phase) with image C superimposed. Scale bar is 50μm and is the same for all images.

1. Hex 40

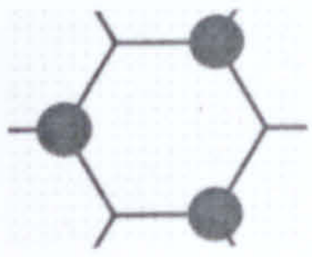

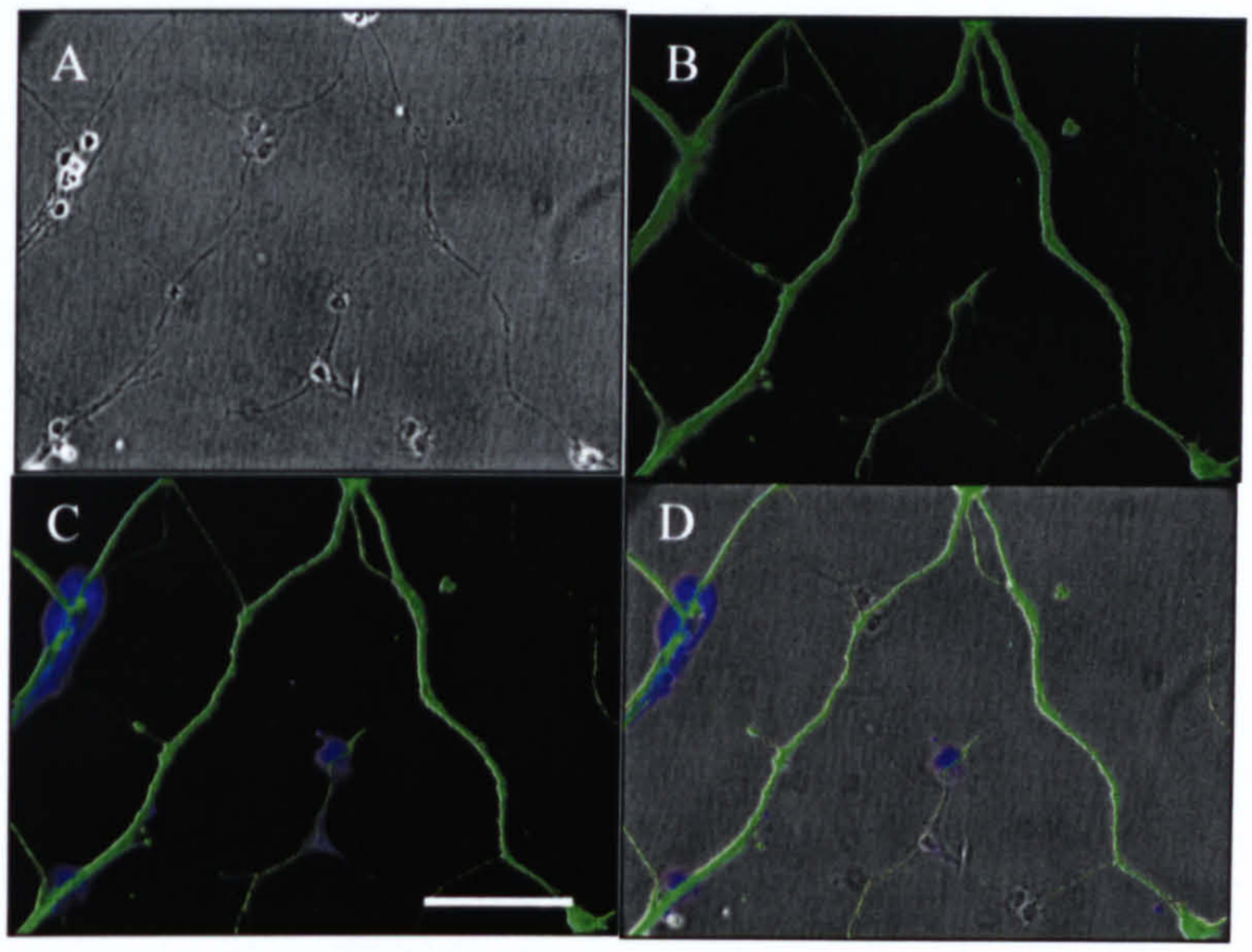

2. Sun

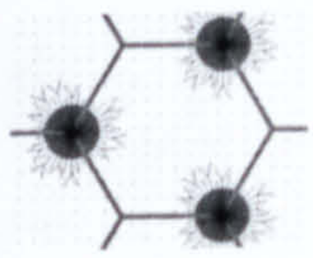

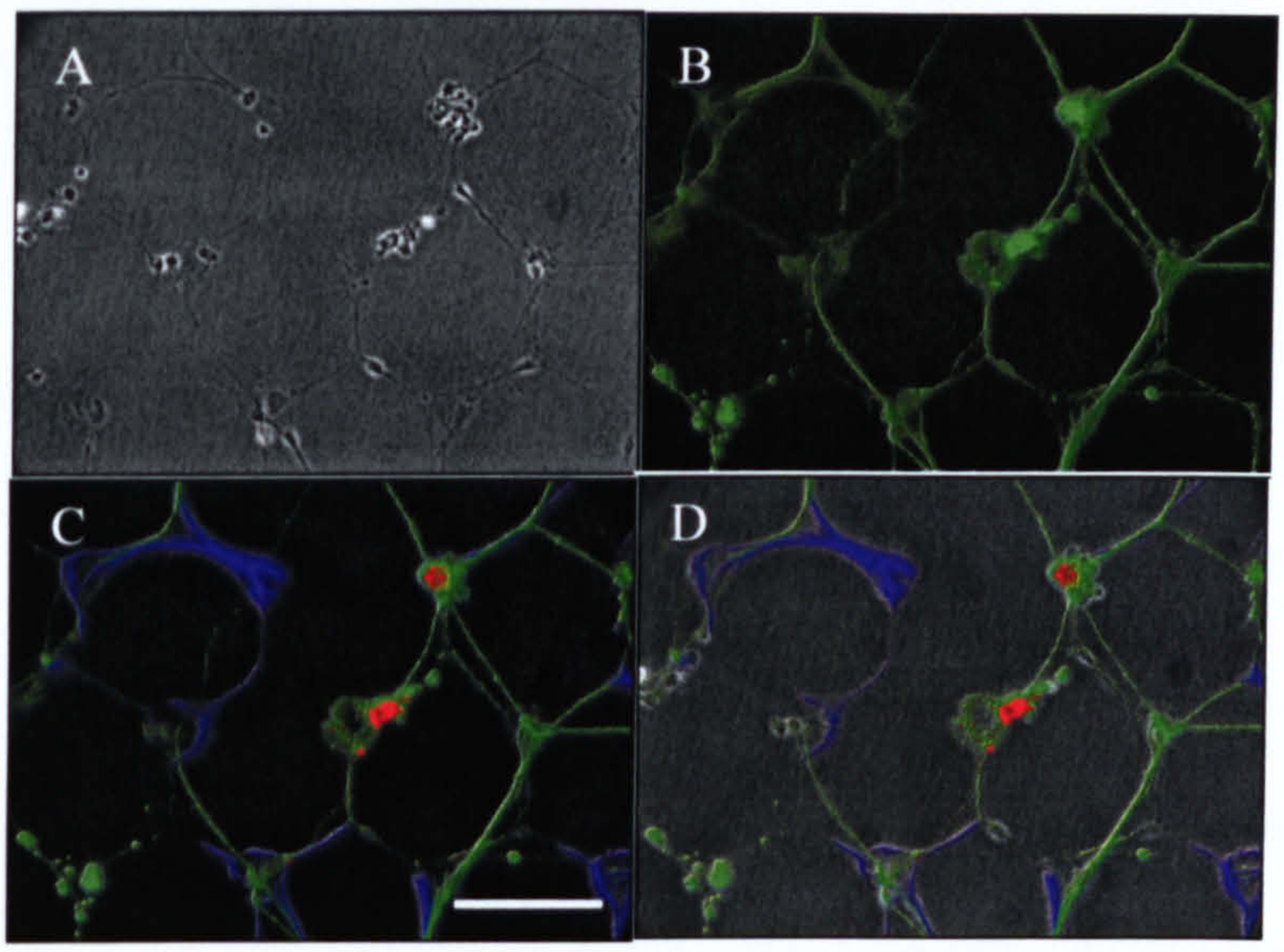

Figure 4.11. Images showing embryonic spinal cord neurons grown on physisorption μCP polystyrene structures. Images show cells complying to the various network patterns; hex 40 (figure set 1) and sun (figure set 2). Image A of each figure set is the phase contrast micrograph of the field of view, image B shows the corresponding fluorescence micrograph of the ß-tubulin stain only, image C the triple stain for ß-tubulin, GFAP and AA3 and image D is image A (phase) with image C superimposed. Scale bar is 50μm and is the same for all images.

1. Oak

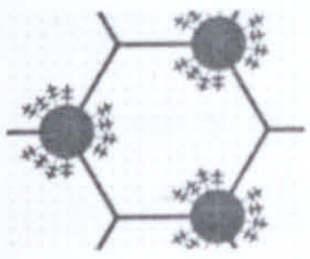

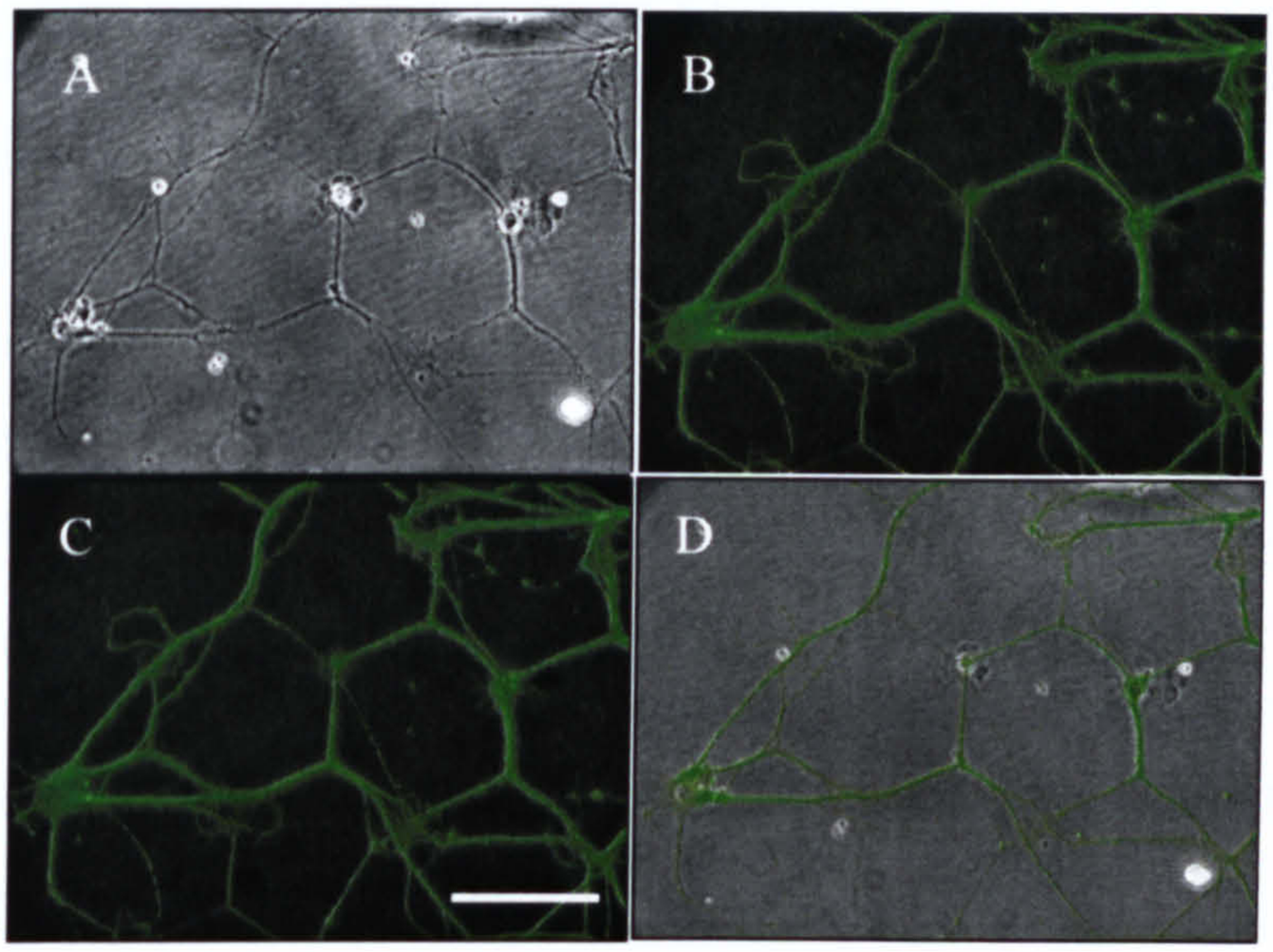

2. Lattice

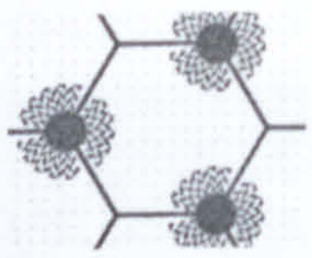

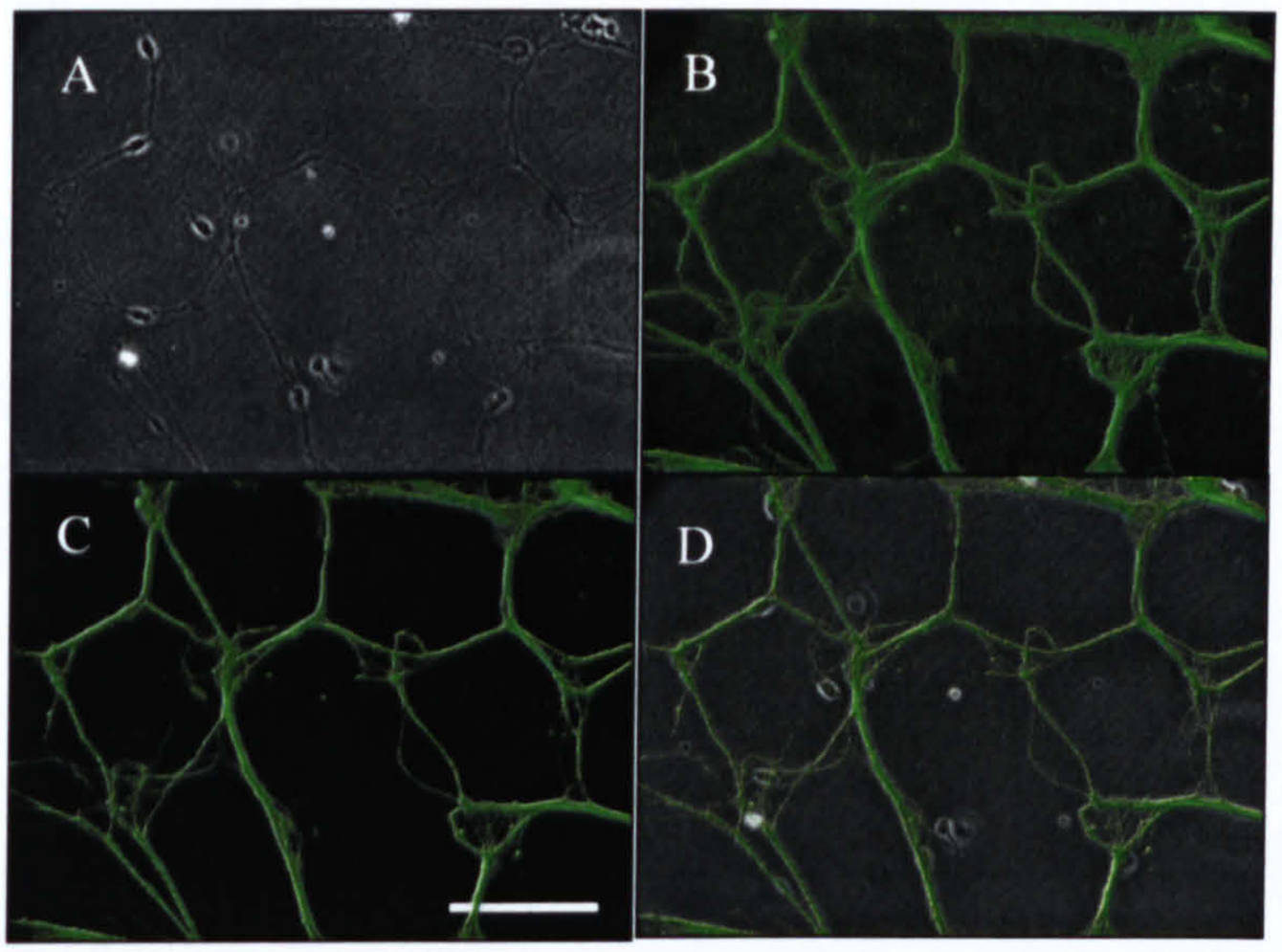

Figure 4.12. Images showing embryonic spinal cord neurons grown on physisorption μCP polystyrene structures. Images show cells complying to the various network patterns; oak (figure set 1) and lattice (figure set 2). Image A of each figure set is the phase contrast micrograph of the field of view, image B shows the corresponding fluorescence micrograph of the ß-tubulin stain only, image C the triple stain for ß-tubulin, GFAP and AA3 and image D is image A (phase) with image C superimposed. Scale bar is 50μm and is the same for all images.

Characterisation of Neural Networks

The effect of the network pattern on neuron connectivity and structural morphology was investigated by means of immunocytochemical staining. Embryonic spinal cord neurons (E14), plated at 6000 cells/mm^2, were grown μCP structures for 2 weeks, then fixed and stained for β-tubulin, synaptophysin and Smi31. Results are based on observations of the fluorescence micrographs (see Figure 4.13.-4.18.). In each figure set the phase contrast image of the network area is shown (D), plus the fluorescence micrograph of each antibody stain (A-C). Image F is a compilation of the 3 immunofluorescence images, with image E showing this superimposed over the phase contrast micrograph. The cytoskeletal, neuron specific stain β-tubulin highlights the neuron growth within the pattern. From these images, difference in cell morphology across the network patterns can be determined. The Smi31 stain highlights the presence and location of axonal processes within the network, with synaptophysin staining showing the network connectivity throughout the pattern

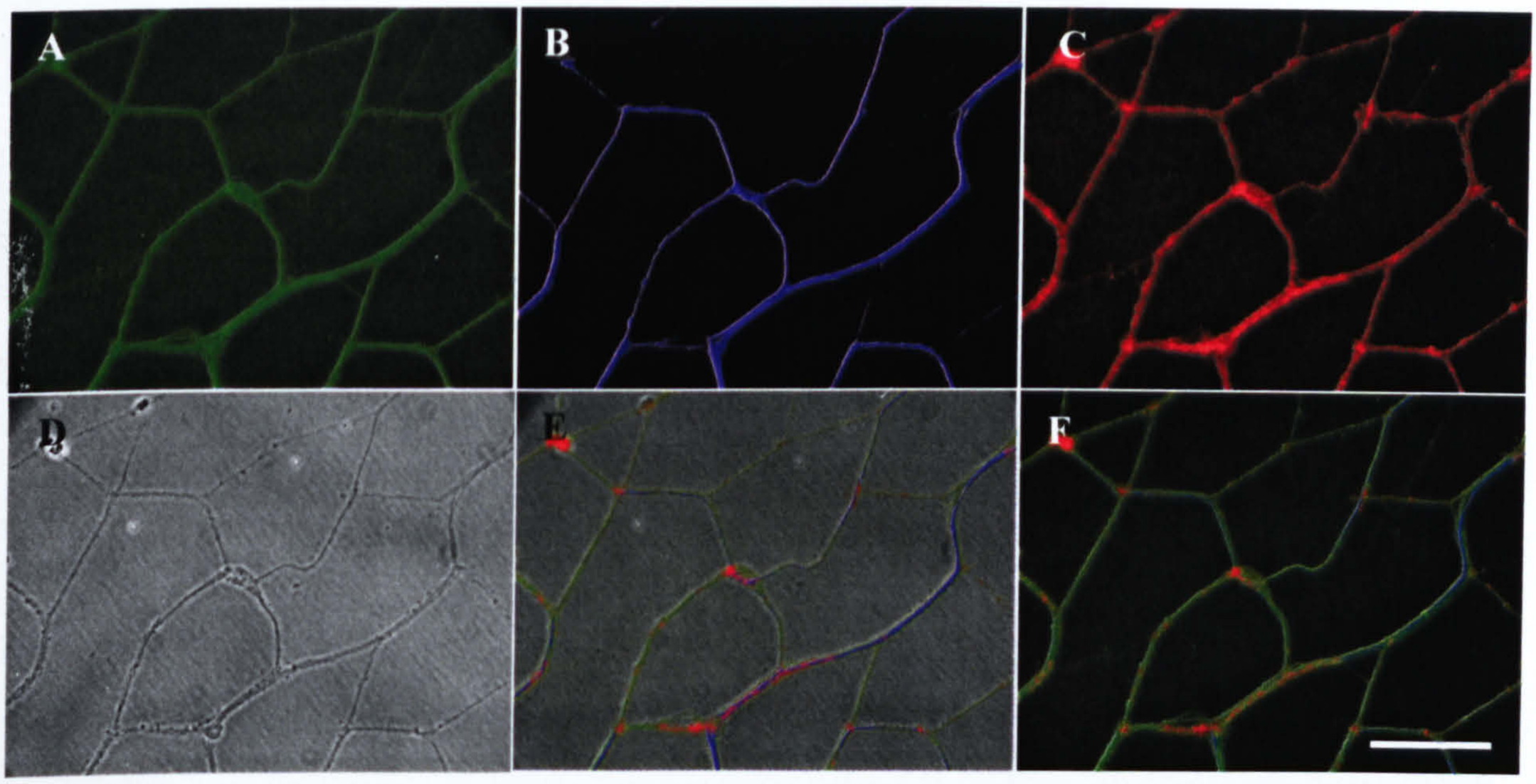

Figure 4.13. Images showing embryonic spinal cord neurons complying to the Jude network pattern. Fluorescence images A-C are of the antibody labelling for ß-tubulin, Smi31 and synaptophysin respectively. Image F is a compilation of these 3 images, with image D showing the corresponding phase contrast micrograph, and image E with the triple stain superimposed. The scale bar is 50µm and is the same for all images.

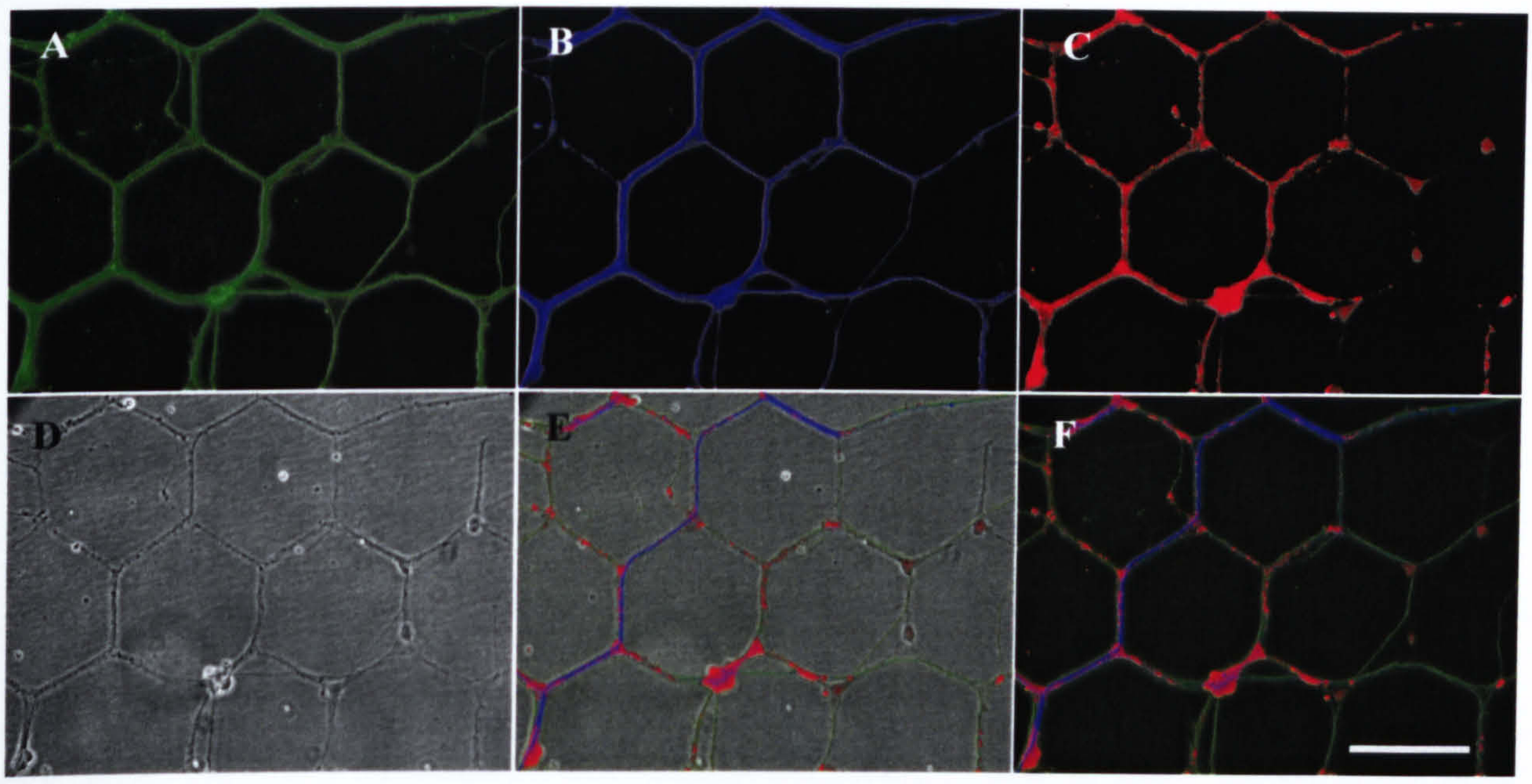

Figure 4.14. Images showing embryonic spinal cord neurons complying to the hex 20 network pattern. Fluorescence images A-C are of the antibody labelling for ß-tubulin, Smi31 and synaptophysin respectively. Image F is a compilation of these 3 images, with image D showing the corresponding phase contrast micrograph, and image E with the triple stain superimposed. The scale bar is 50µm and is the same for all images.

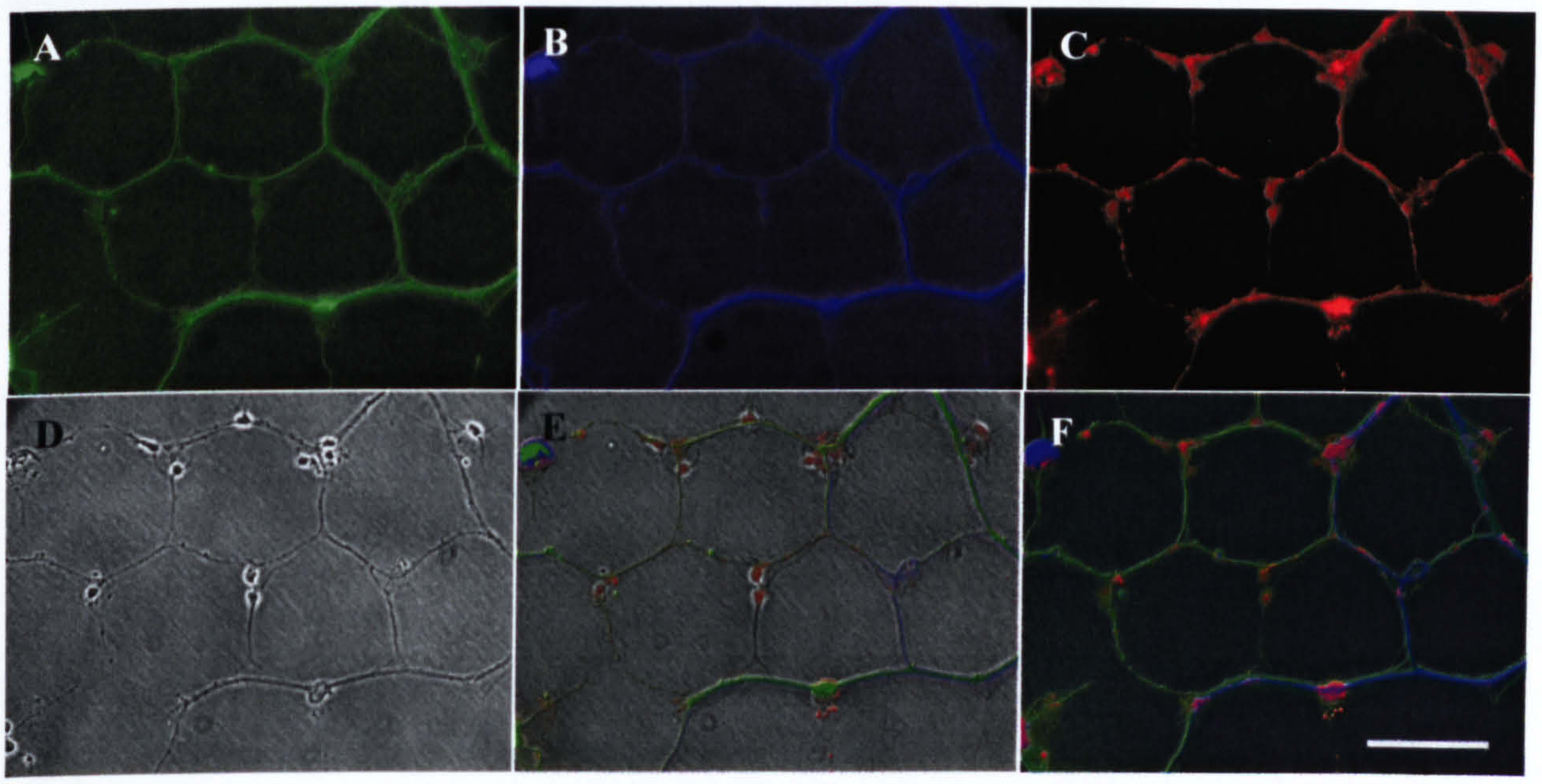

Figure 4.15. Images showing embryonic spinal cord neurons complying to the hex 40 network pattern. Fluorescence images A-C are of the antibody labelling for ß-tubulin, Smi31 and synaptophysin respectively. Image F is a compilation of these 3 images, with image D showing the corresponding phase contrast micrograph, and image E with the triple stain superimposed. The scale bar is 50µm and is the same for all images.

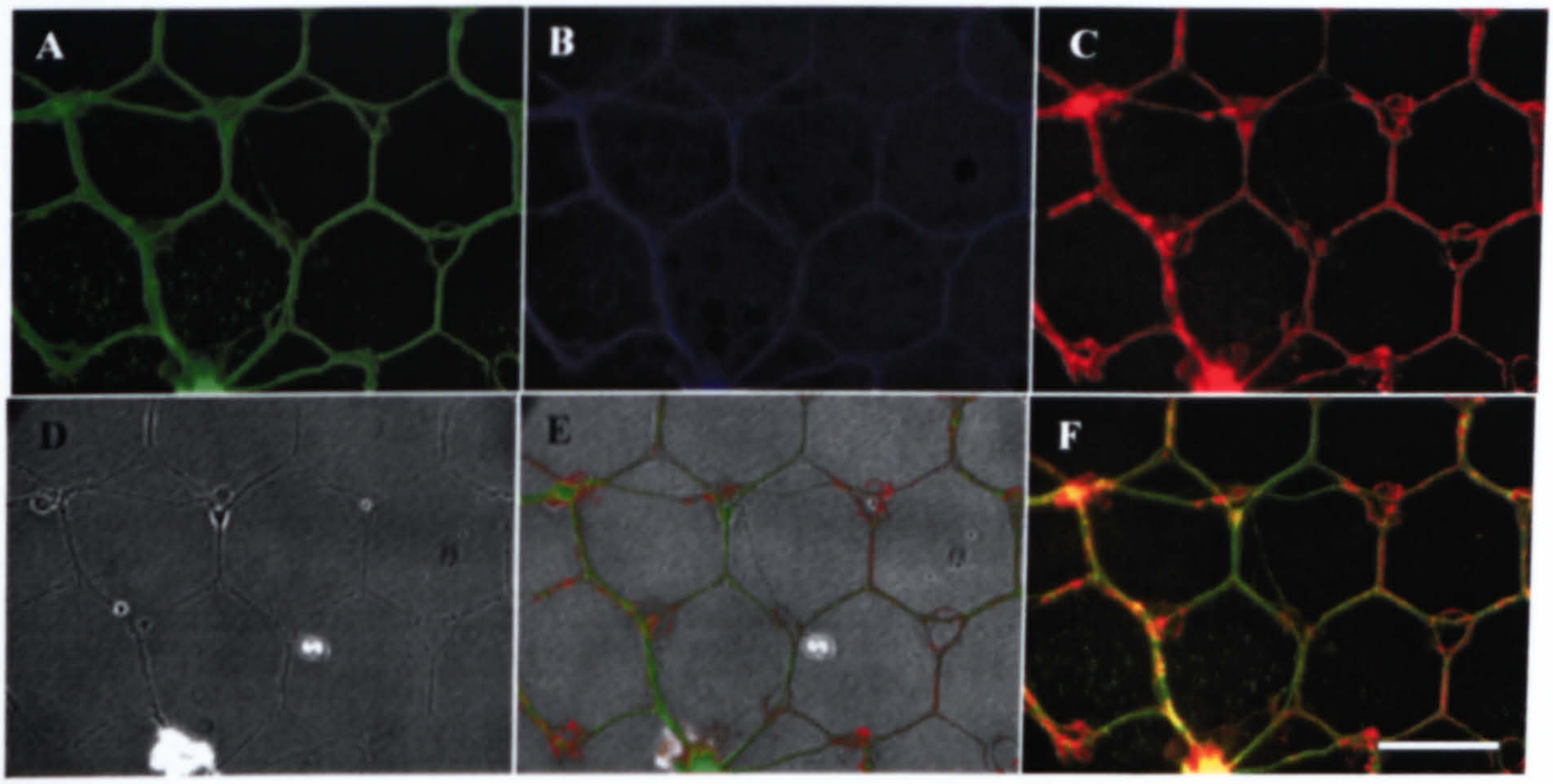

Figure 4.16. Images showing embryonic spinal cord neurons complying to the sun network pattern. Fluorescence images A-C are of the antibody labelling for ß-tubulin, Smi31 and synaptophysin respectively. Image F is a compilation of these 3 images, with image D showing the corresponding phase contrast micrograph, and image E with the triple stain superimposed. The scale bar is 50µm and is the same for all images.

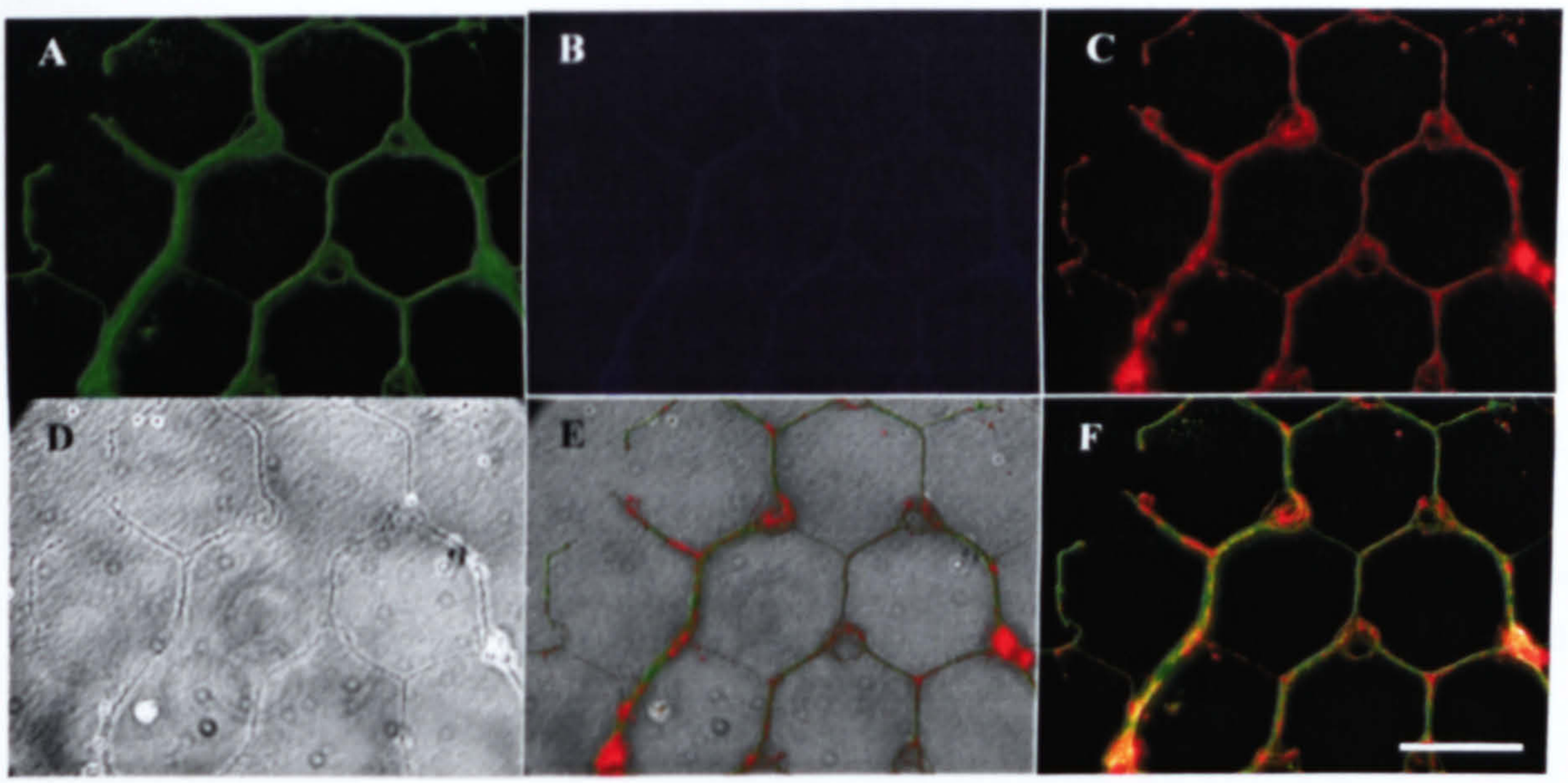

Figure 4.17. Images showing embryonic spinal cord neurons complying to the oak network pattern. Fluorescence images A-C are of the antibody labelling for ß-tubulin, Smi31 and synaptophysin respectively. Image F is a compilation of these 3 images, with image D showing the corresponding phase contrast micrograph, and image E with the triple stain superimposed. The scale bar is 50µm and is the same for all images.

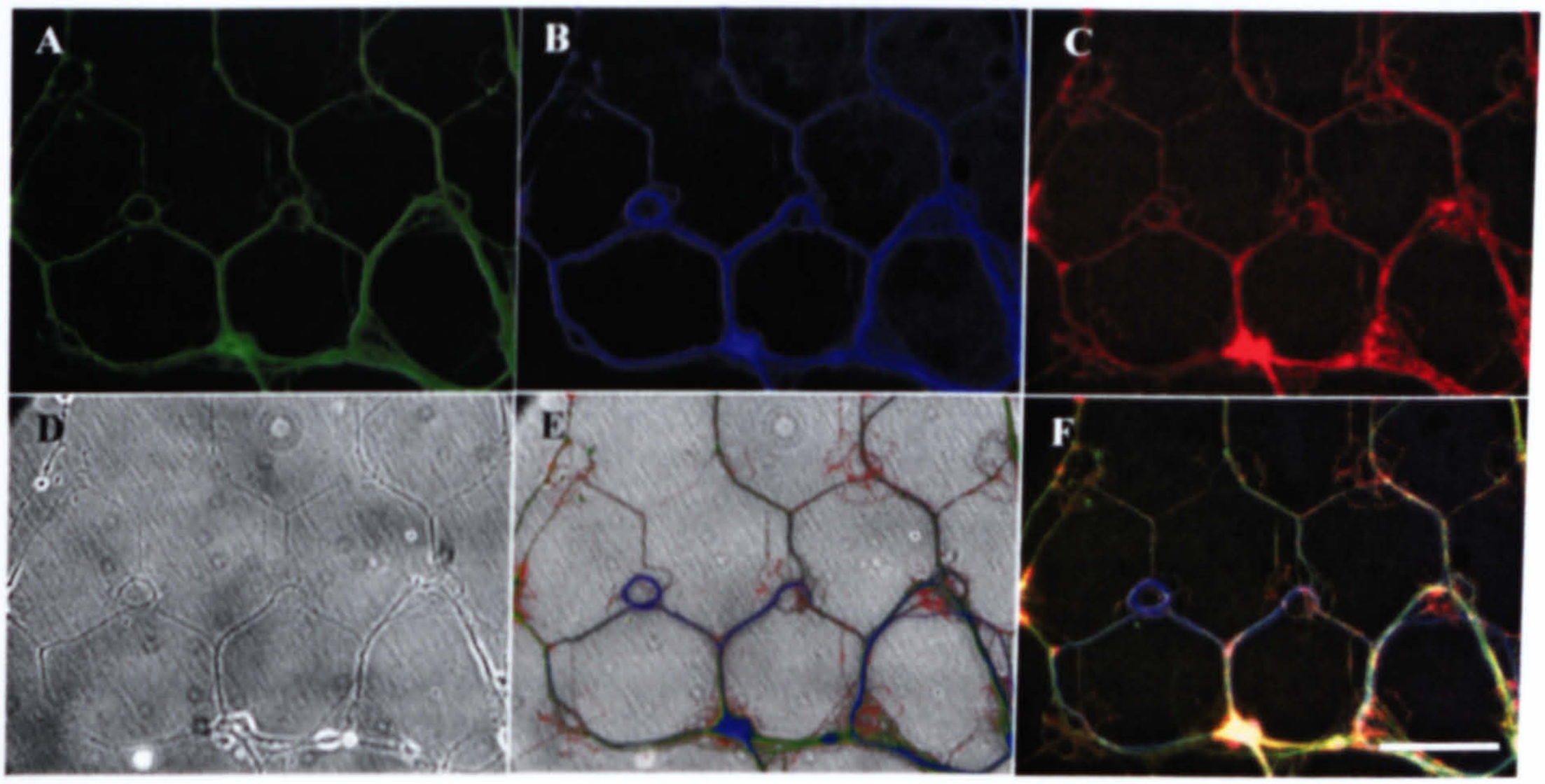

Figure 4.18. Images showing embryonic spinal cord neurons complying to the lattice network pattern. Fluorescence images A-C are of the antibody labelling for ß-tubulin, Smi31 and synaptophysin respectively. Image F is a compilation of these 3 images, with image D showing the corresponding phase contrast micrograph, and image E with the triple stain superimposed. The scale bar is 50µm and is the same for all images.

Investigation of Network Pattern on Neuron Compliance

Using the images collected for the *Characterisation of Neural Networks* study, the effect of the pattern design on network configuration was investigated, by analysing the following parameters: cell bodies located in nodes, cells located on lines and cells off the pattern completely. To determine exactly where cells were lying within the pattern, it was necessary to overlay each acquired image with the outline of the pattern in question (see Figure 4.19). From this it was possible to correctly identify the location of the node site and therefore determine whether the cells that were aligning to the patterns were situated on a node or on the interconnecting tracks. The reason for this being that not every line intersection contained a soma attachment site.

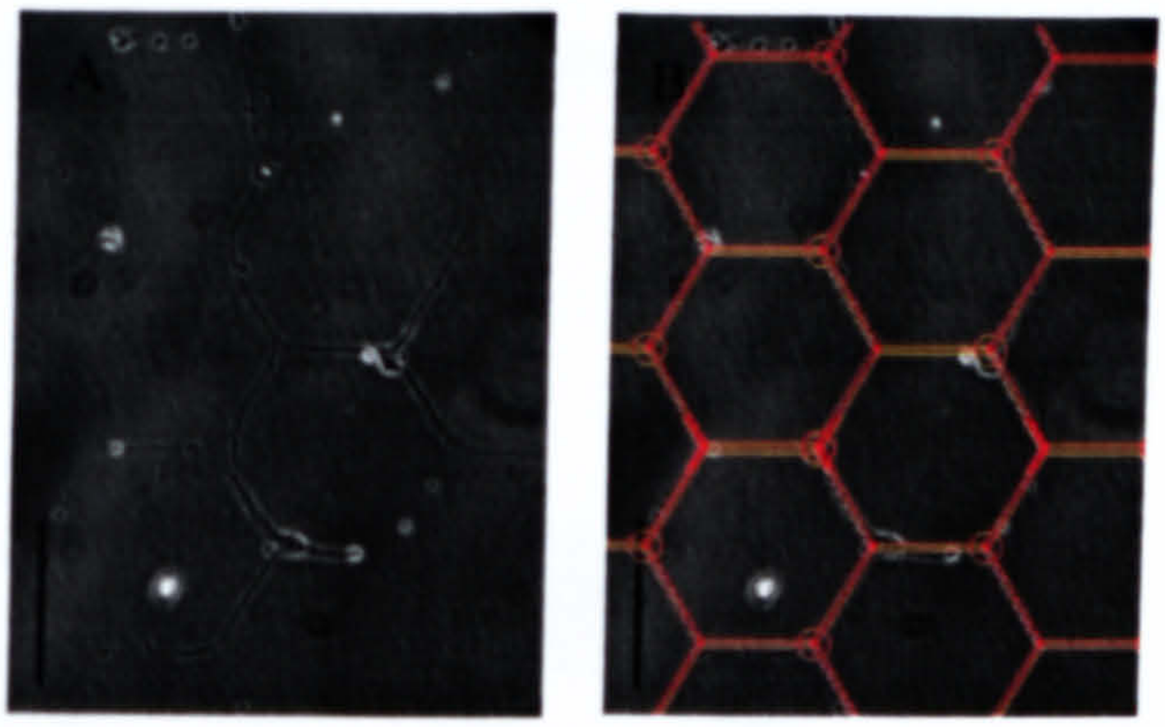

Figure 4.19. Showing an example of the method used to determine cell compliance to the network patterns. Image A shows a phase contrast micrograph of cells growing within the hex 20 network pattern. Image B shows image A with the pattern outline superimposed. Scale bar is 100μm

Of the 6 patterns under investigation only those with the same nodal dimensions were compared for statistical evaluation (*Jude and hex 20*, *hex 40* and *sun*, *hex 40* and *oak*, *hex 40* and *lattice*) using the Student's *t-test*. We initially hypothesised that a greater percentage of cells plated on the *Jude* pattern would be located in the line sections of the network, due to the unequal distribution of tensile forces. Although a significant ($p<0.05$) number of cells did not comply at all to this pattern (Graph 4.2.A), there were significantly less cells located on the line sections (Graph 4.2.B), in comparison to the hexagonal pattern of equal nodal size (*hex 20*). It was also noted that less cells adhered to the nodal sites of the *Jude* compared to *hex 20* (Graph 4.2.C), although this result was not statistically significant at either the 0.01 or 0.05 level of significance, the overall finding suggest a direct correlation between the angle of line intersection and cell compliance. The impact of dendritic architecture on cell compliance was evaluated by comparing the descriptive nodal patterns (*sun, oak, lattice*) to the hexagonal pattern of equal nodal dimensions (*hex 40*). All patterns with a descriptive node design had a greater percentage of cell bodies located on the nodal regions in comparison to the remaining three patterns (*Jude, hex 20 and hex 40*). However, this result was not statistically significant for any comparison. Of all the designs investigated, only the hexagonal pattern of 40μm nodes showed 100% cell compliance to the network. In this case a greater percentage of cells were located on the line sections than on the nodes (see Figure 4.2).

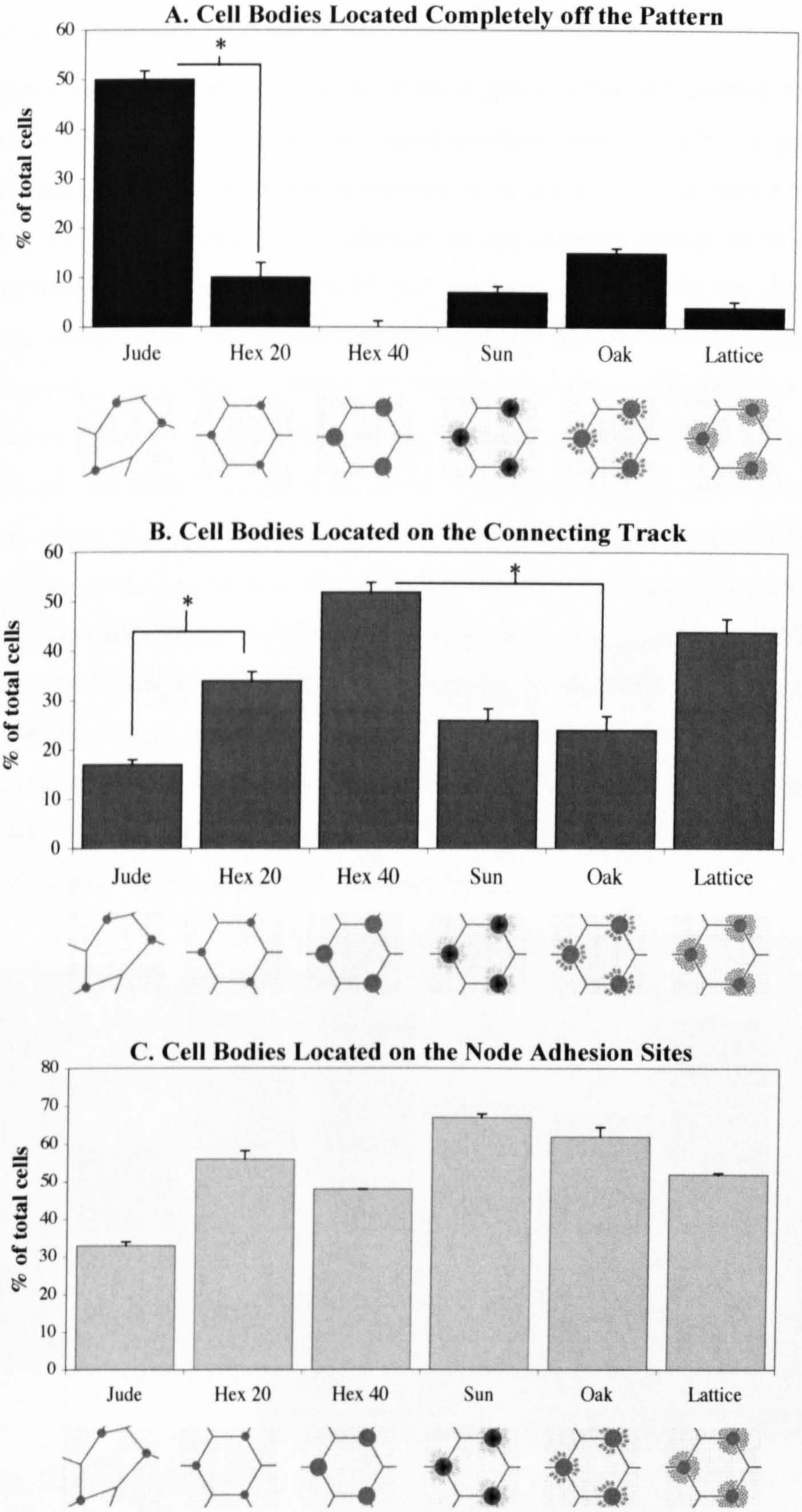

*Graph 4.2. Graphs showing parameters of cell compliance to networks patterns: percentage of cells off the pattern (A), located on line sections (B) and localised to nodal sites (C). Results are the mean value± standard deviation, * denotes significance between related patterns* ($p<0.05$).

SEM Analysis of Neuron Compliance

To investigate how cells were reacting to smallest detail of the μCP pattern scanning electron microscopy was applied. The results are based on observations of SEM images of embryonic spinal cord neurons grown on structures stamped with *hex 40, sun* and *lattice* network patterns following 2 weeks in culture (due to difficulties encountered during SEM preparation and processing, network patterns *Jude, hex 20* and *oak* are not shown, see the chapter *Discussion* for details). Image 4.20 shows cells complying to the *hex 40* network pattern. From this image it is evident that pattern transfer has been highly successful, with the pattern outline easily identified, however, stamp shifting has occurred. Only 2 of the 11 soma attachment sites shown are occupied. Image 4.21 shows 3 soma attachment sites and the connecting intersection of the same network pattern (*hex 40*) but at a higher magnification. From this image it is evident that nodes free of cell bodies are in fact occupied by a dense network of fine neural processes. Figure 4.22 shows cells grown on the *sun* pattern. In image A stamp shifting is also obvious, although cells are complying firmly to the original pattern as shown in the magnified area in image B. The dendritic structures of this pattern do not appear to have been successfully transferred to the receiving substrate. The node design of the *lattice* pattern, however, did transfer as shown in Figure 4.23, with no stamp shifting evident, although cell clumping has occurred at the node sites.

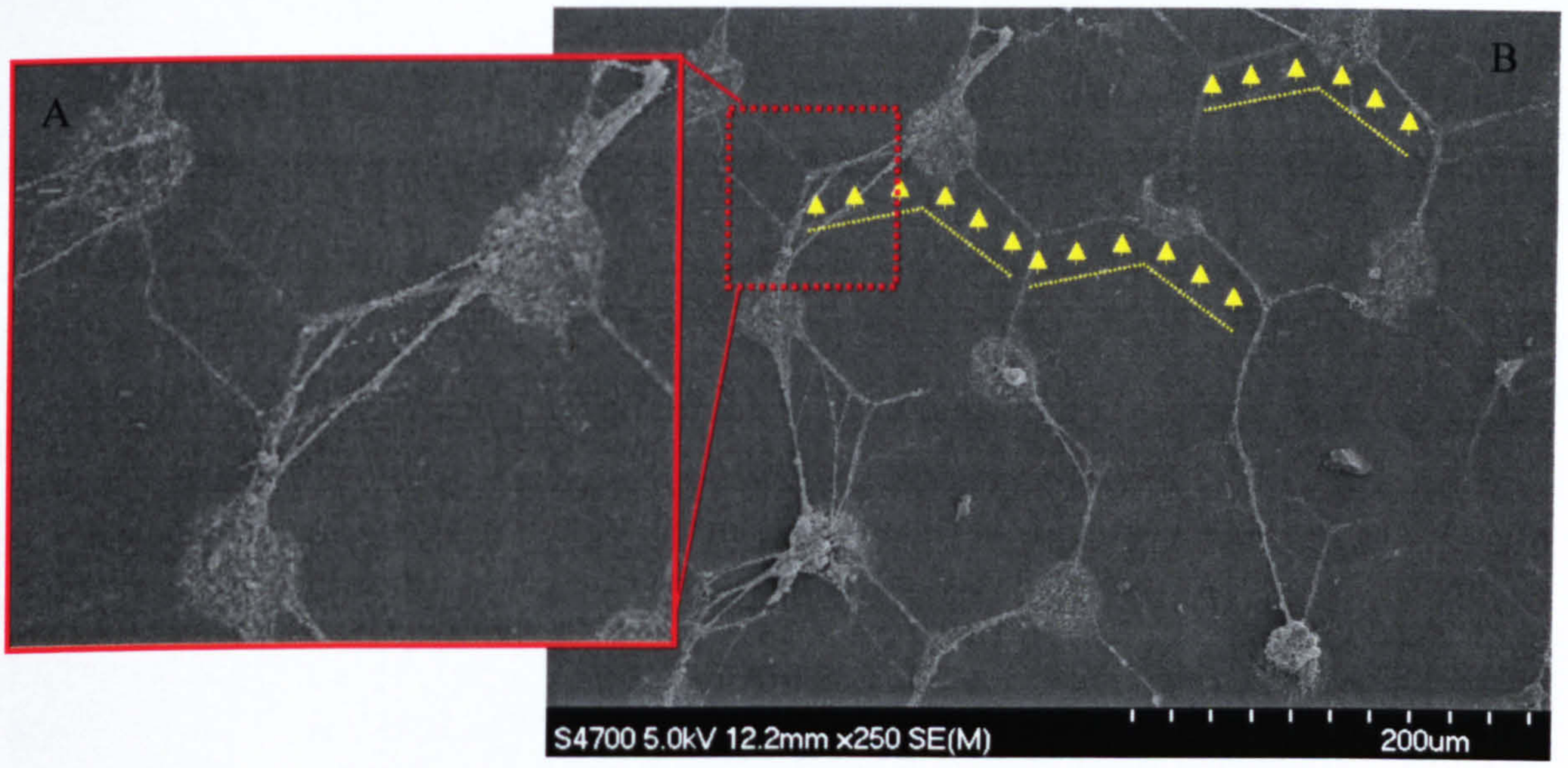

Figure 4.20. SEM micrograph of embryonic spinal cord neurons following the hex 40 network pattern. Cells fixed after 2 weeks in culture and prepared by freeze drying techniques. The yellows arrows in image B indicate the direction of stamp shifting and the yellow hashed lines the resultant underlying pattern. Image A is the highlighted section in image B magnified.

A.

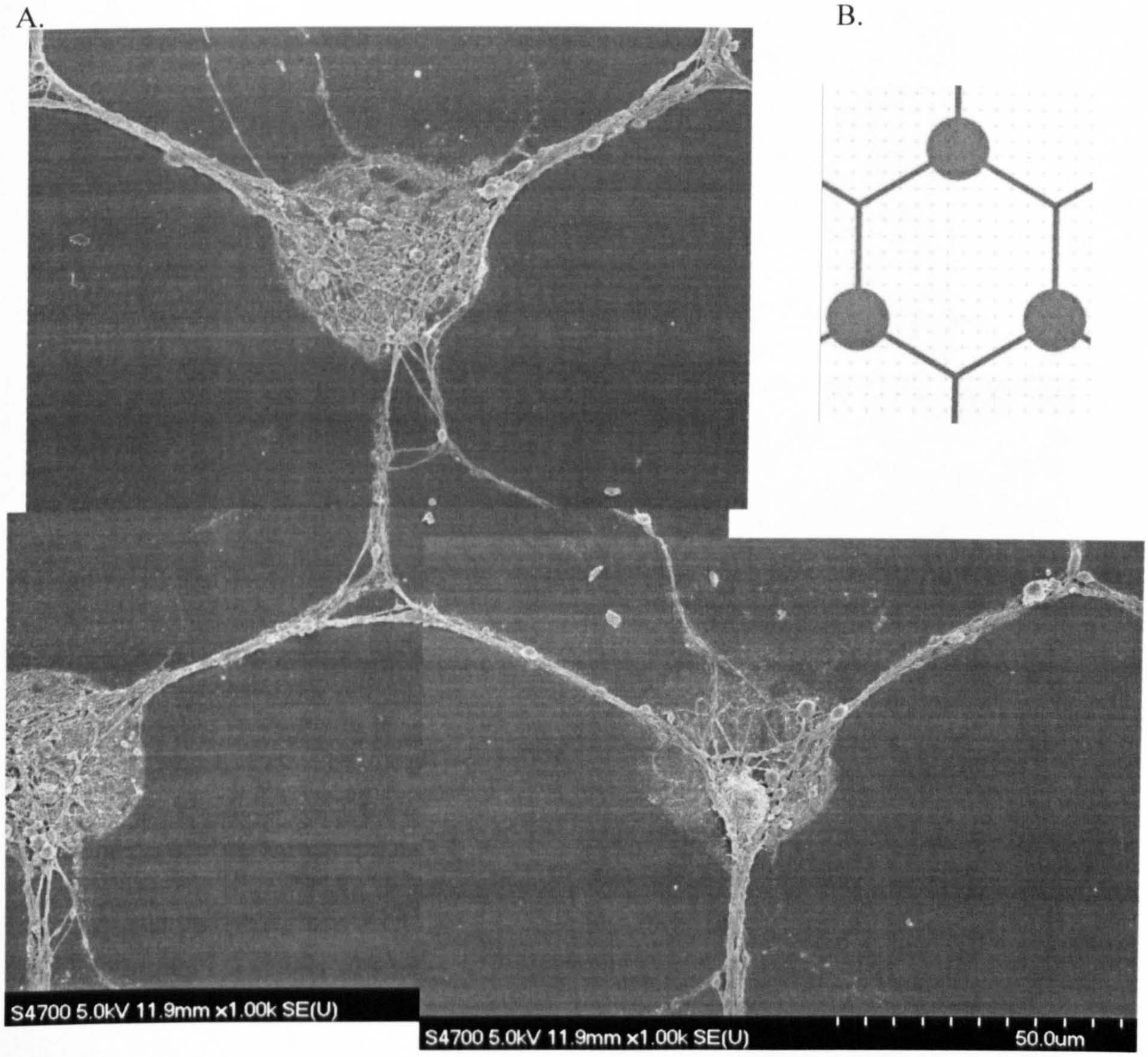

B.

Figure 4.21. Images complied of three SEM micrographs focusing on the intersection between three soma attachment sites. Images are of 2 week old embryonic spinal cord cultures grown on μCP Hex 40 network pattern (A) and a schematic representation of network pattern (B).

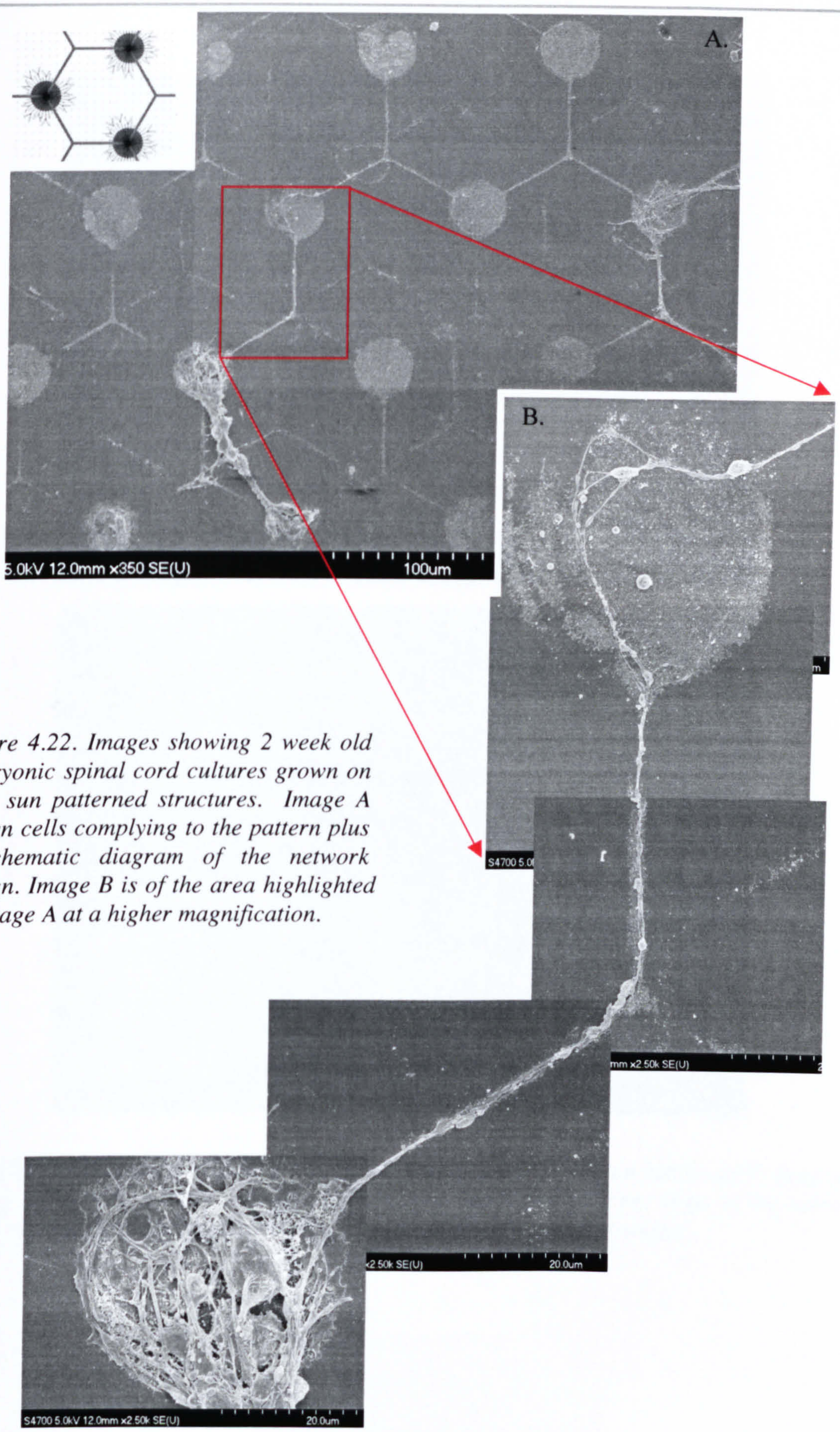

Figure 4.22. Images showing 2 week old embryonic spinal cord cultures grown on μCP sun patterned structures. Image A shown cells complying to the pattern plus a schematic diagram of the network design. Image B is of the area highlighted in image A at a higher magnification.

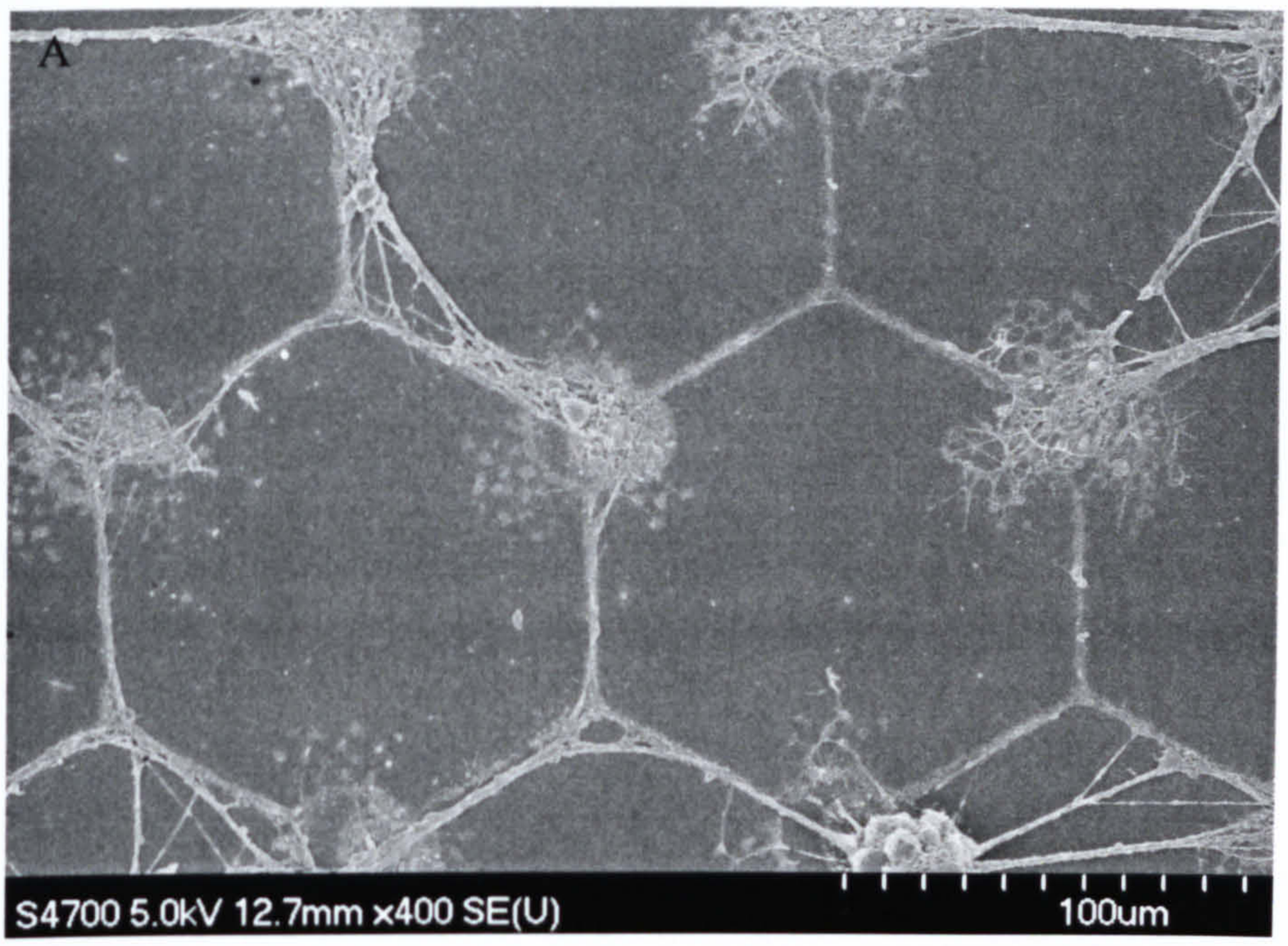

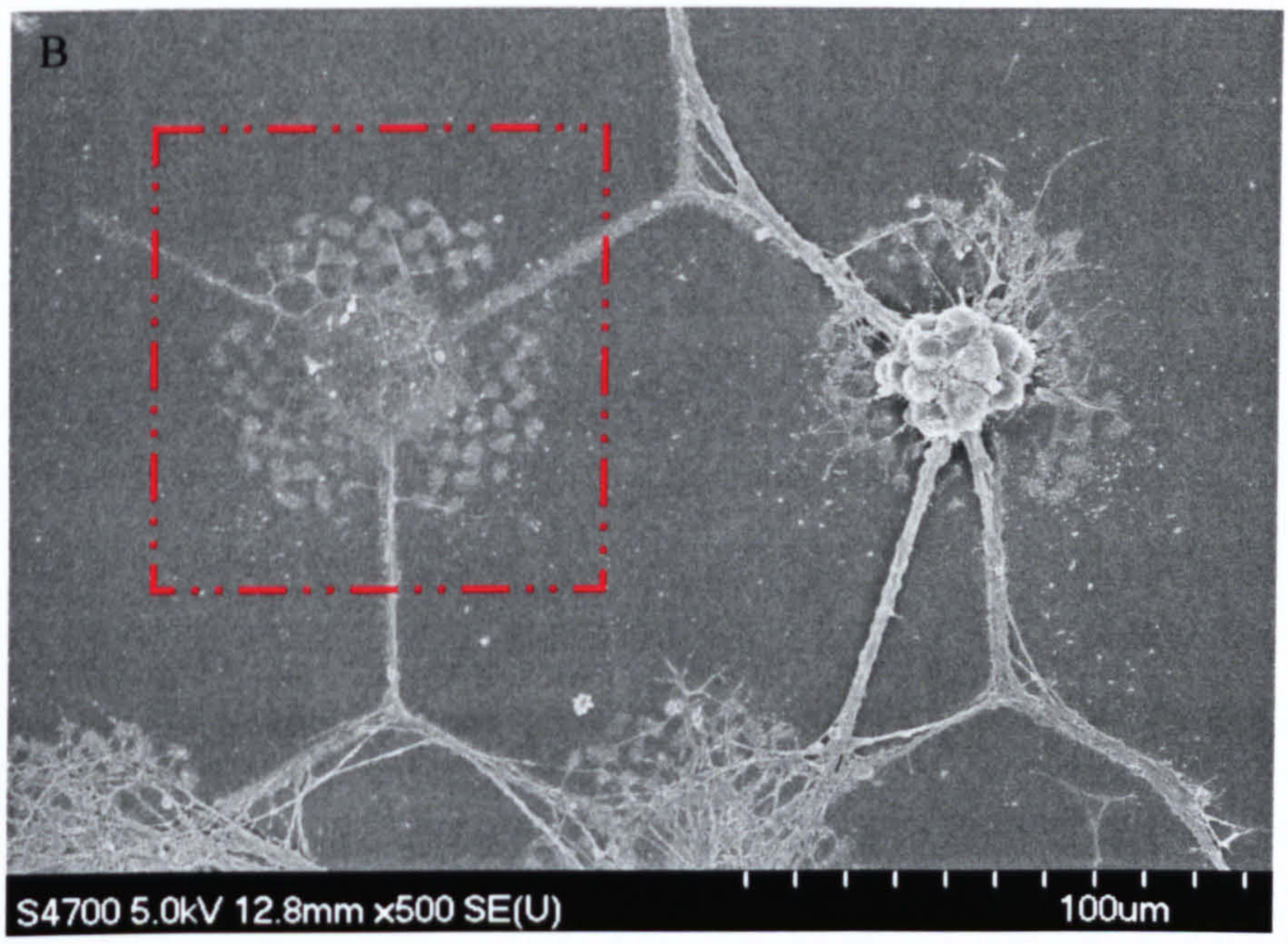

Figure 4.23. SEM images of embryonic spinal cord neurons grown on lattice μCP structures following 2 weeks in culture. Image A shows cell complying to large area of the pattern. Image B highlights an excellent example of a successful node pattern transfer.

Summary

Although the descriptive node designs of *sun, oak* and *lattice* patterns did not affect the morphology of individual cells, they did appear to be having a direct effect on overall neural network compliance. Cell body localisation to the node site was increased compared to the network patterns *Jude, hex 20* and *hex 40*, as was the accumulation of highly connected neurite processes at the node sites free of cell bodies as shown by SEM imaging and synaptophysin staining. These results suggest changes in network geometry can affect network characteristics and therefore network behaviour.

Discussion

Introducing geometric constraints to nerve cell culture can present a number of challenges. If the growth limitations introduced have not been entirely successful, cell migration is often observed as well as neurite wandering. This chapter aimed to investigate the role of the network geometry on controlling cell adhesion and neurite outgrowth within the pattern, and what effect this may have on network behaviour. The patterns investigated have been designed for network construction and have taken into consideration various factors based on observation of cells under normal culture conditions; soma localisation, dendritic modelling and tension distribution. Immediately after plating, cells are spherical but within hours begin to develop neurite process. By introducing an array of projections at the soma adhesion site, we aimed to reduce the tensile pull from the projecting axon that contributes to cell migration and soma misplacement. It is anticipated that dendritic growth into the areas provided would counter balance this phenomenon, by anchoring the soma and allowing varying dendritic architectures to be included in the design of the network. By drastically changing the morphology of the cell, and therefore the network as a whole, I predicted that network characteristics and behaviour may be affected.

Structure Analysis

Patterned Structures in Silicon

SEM analysis of the silicon wafer aimed to determine how effective the dry etch process had been at creating the intricate designs of patterns *sun*, *oak* and *lattice*. Observations of each network pattern at low magnification revealed the fundamental outline had been successfully replicated in silicon. Although the resulting node structure was not a perfect representation of the initial design, it was anticipated that the structure was sufficient to produce a polymer stamp of equal dimensions that would translate the network into a chemical pattern. On closer inspection of the each node feature it was evident that two major defects had occurred: i) the node protrusions of the *sun* design did not appear to have been completely etched away, leaving a step between the centre of the node and dendritic structures, ii) it was also noted that the face of sidewalls in each pattern was rippled, suggesting an error had occurred during the reactive ion etching stage. The un-switching etch recipe RYT1, was developed by Rongyu Tang to create a smooth side wall in the silicon wafer ideally suited for casting applications. However, this type of defect is due to gas switching, suggesting etch parameters were wrong. The etch settings were revised and

more structures fabricated. This removed the rippled effect from the sidewalls but the step feature seen in the *sun* pattern could not be improved.

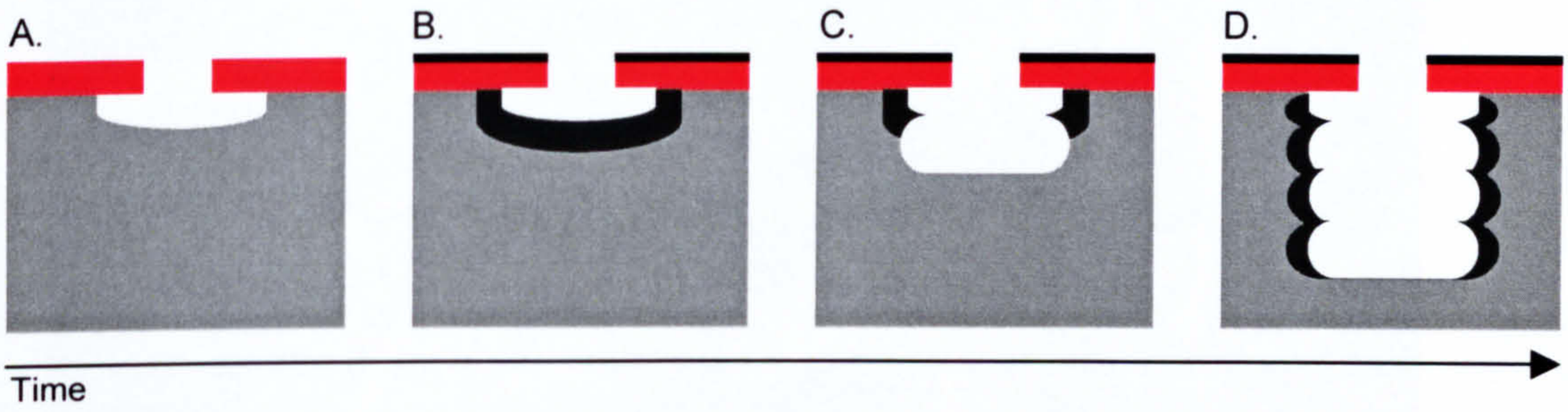

Figure 4.24. Schematic diagram showing the gasphase etch (A, C) and the gasphase deposition (B, D) steps that occur during deep reactive ion etching. This gas switching process can create a rippled effect on the sidewall of the etched substrate as seen on the early patterned silicon wafers. This diagram has been taken from CCE lecture notes written by Dr. Mathis Riehle.

Patterned Replication in Silicone Polymer

In Chapter 3, *Method Development, Stamp Fabrication* the problems encountered during the development of the stamp fabrication protocol, and the resulting methods to resolve these are described. However this study had been carried out using the *Jude* pattern only, which consisted of tracks 5μm in width and 5μm in height with circular nodes of 20μm. Where as the *oak, sun* and *lattice* patterns consisted of intricate node designs with connecting tracks 5μm in width and by 10μm in height that completed the network. Although the SEM imaging of the silicon wafers provided some supportive evidence to suggest replication of the patterns would be possible, it was not known if similar problems to those that had been encountered during Chapter 3 would occur. In particular, stamp binding to the silicon was anticipated due to the small island structures seem in SEM of designs *sun, oak* and *lattice* (Figure 4.7). It was also thought that the dimension of the track intersections would not withstand the force exerted during stamp releasing process. It was quite possible these structures would tear or buckle due to their increased height from 5μm to 10μm. The SEM images shown in Figure 4.8 show that none of these defects occurred. All stamps were of a sound structure, with all track features intact. Only one defect was encountered, this was with the dendritic structures of the *sun* pattern. As expected the step feature seen in the silicon wafer of this pattern had replicated into the stamp. All dendritic structures in this pattern were therefore lying approximately 3μm lower than the centre node (see Figure 4.25).

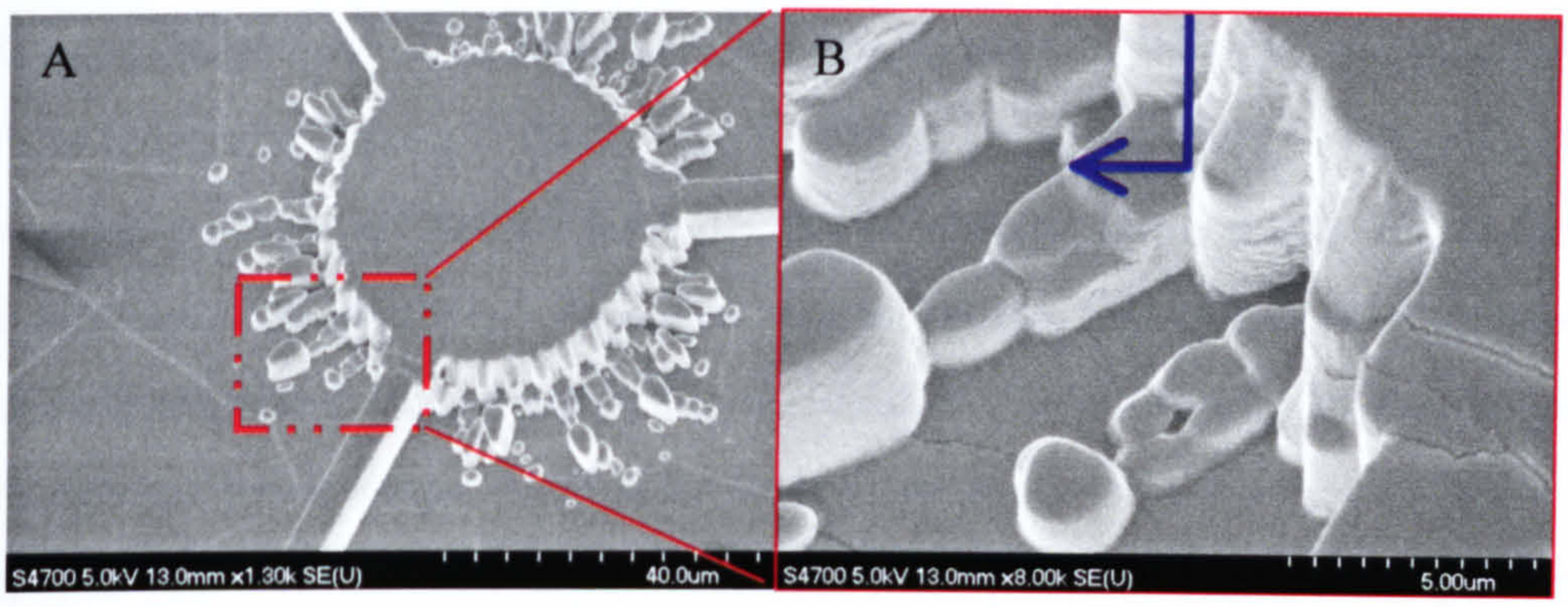

Figure 4.25. SEM images of the node region of the sun pattern. Image A show the whole node feature, with a step region highlighted. Image B is of this region at higher magnification. The blue arrow indicates the extent of the step feature from the centre node to the dendritic protrusions.

Evaluation of Pattern Transfer

Although the SEM analysis of the polymer stamps showed all but one pattern had been successfully replicated, further experiments were required to determine if it would be possible to create a chemical pattern from these stamps. Since the cells would respond primarily to this pattern and not a structural pattern, it was essential that the extent of pattern transfer was evaluated. Immunocytochemical images of the each pattern transfer are shown in Figure 4.9. As expected all the patterns with a circular node feature were replicated without any loss of structural integrity across the whole network. Despite SEM results showing that both the silicon and the polymer stamp were to some effect defective, it was hypothesised that it would be possible to overcome the structural defects of this network pattern if a greater force was applied during stamp application. However fluorescence imaging results proved this not to be the case. The *sun* node details would not transfer, creating a pattern not too different from that of the *hex 40* network. Both the *oak* and *lattice* node details did transfer, although images collected were slightly blurred. It is quite possible this could be due to overloading of the either the primary or secondary antibody during the staining process (if not both), rather than the initial chemical transfer created by μCP.

Cellular Response to the Network Patterns

Classification of the Network Population

For this experiment cells were stained for the neuron marker *β*-tubulin, the glial cell marker GFAP and the oligodendrocyte marker AA3. The aim was to identify what cell types, other than neurons, were complying to the network pattern, and what, if any, effect this had on overall network configuration. Although it was known from previous experiments that other cells types would be present within the culture, it was hoped that the complexity of the pattern would discourage these cells from growing in the network. Glia are a robust cell type, which can adhere to, and survive on substrates that are non-permissive for neurons or oligodendrocytes. It was hypothesised that these cells could adhere and proliferate on the areas outwith the chemical pattern and thus would ideally not interfere with neuron compliance. Since oligodendrocytes, like neurons require an optimal growth environment it was anticipated these cells would not survive after initial plating, reducing the likelihood of their incorporation into the network.

Of the 6 patterns investigated, *hex 20* appeared to be the most effective pattern for neuron compliance, and at the same time the least effective for oligodendrocyte or glial growth. Over 70% of cells within the pattern were *β*-tubulin positive. From the images in Figure 4.10.2 it is evident that cell guidance has been accurately controlled with no evidence of other cell types within the pattern, or neurons lying outwith the pattern. The *Jude* pattern appeared to be the least effective, with only 21% of the cells complying to the pattern identified as being neurons. Both the *sun* and *hex 40* patterns (see Figure 4.11) had a greater percentage of glial cells complying to the pattern than neurons. This is possibly due to larger node area available for cell adhesion. It was hypothesised that presence of glia could provide a preferential area for neuron adhesion and also an alternative route for neurite outgrowth, resulting in a reduced number of neurons growing within the chemical pattern. Because the dendritic structures of the *sun* pattern failed to print, the resulting chemical pattern was of the same dimensions as the *hex 40* pattern, accounting for the similarities in these results. Although patterns *oak* and *lattice* show similar results to the *hex 20* pattern in Graph 4.1, analysis of the images presented in Figure 4.10 and 4.12 highlight the fundamental differences between the patterns. In each case neuron cell bodies are adhering and growing within the patterns, it is the characteristics of neurite growth that varies dramatically. In both the *oak* and *lattice* patterns there are many more processes present throughout the network. Although these processes are following the network to

some extent, they are not tightly aligned as seen in the *hex 20* pattern. It is highly likely, that this difference is due to the variations in node structure between the *hex 20* pattern and the *oak* and *lattice* patterns.

Characterisation of the Neural Networks

This study aimed to determine the changes in cell morphology across the network patterns and what affect this had on network connectivity. Fluorescence labelling with β-tubulin antibody identified the neuron population and the connections between the cells were highlighted by the use of synaptophysin staining. An attempt was made to determine how the axonal processes were responding to each network pattern by labelling cells with Smi 31, a marker of phosphorylated neurofilament proteins present in the axons of mature neurons (Letournel *et al.* 2006). However because these images were taken at random not all network patterns have axon highlighted.

The β-tubulin staining highlights the differences in neuron morphology between the 6 network patterns. Although the *Jude* and *hex 20* patterns are visually different, both have been designed using the same dimension: 20μm nodes with 5μm wide connecting lines. Cells that are complying to these networks appear to have developed three main processes, with synaptophysin evenly distributed throughout (see Figure 4.13 and 4.14). As described previously, cells growing on the patterns with the larger node dimensions (*hex 40, sun, oak* and *lattice*) have developed many more processes, not all of which are complying to the network. It is quite clear that the larger area is allowing neurite wandering to occur within the node region. From observations of images presented in Figure 4.15 to 4.18 it is evident that processes are actively searching for a permissive path. Figure 4.26 shows an example of this occurring in patterns *hex 40* and *lattice*. From these magnified images the direction of axon movement and growth can be identified. It is possible that this activity is causing the neurites to find alterative routes caused by imperfections in the pattern transfer. Although node size is contributing to differences in network configuration, the different descriptive node patterns do not appear to be affecting neuron morphology consistently as hypothesised.

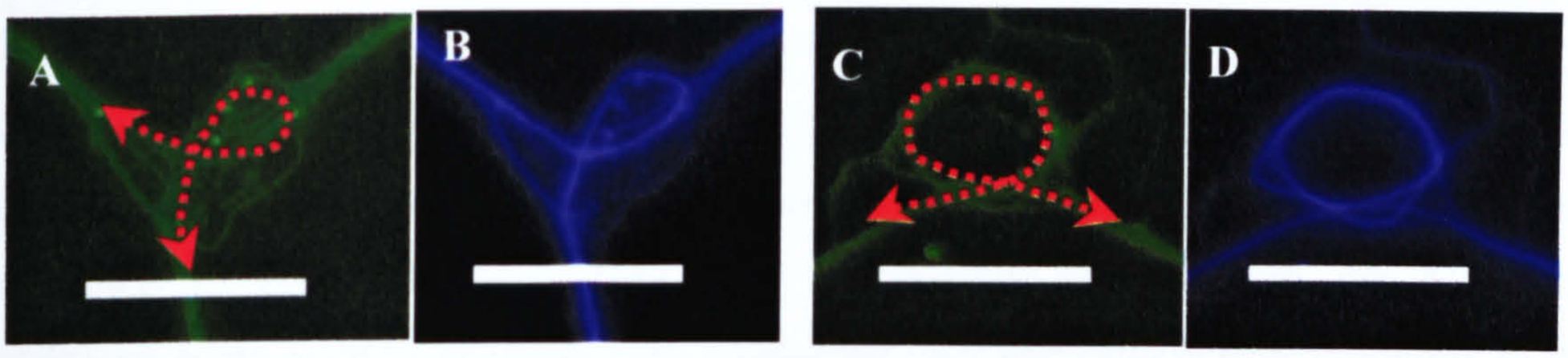

Figure 4.26. Magnified images of node region of hex 40 (A, B) and lattice (C, D) patterns. Image A and C are of the ß-tubulin stain and images B and D highlight the path of the axonal process. The arrow indicated the direction of axon proliferation. The scale bar is 40µm in all images.

Due to the defects in the *sun* polymer stamp, it was not expected that this pattern would differ from the *hex 40* pattern. However, it was anticipated that a difference would exist between *oak* and *lattice* patterns, and the *hex 40* pattern. No obvious difference in cell morphology can be seen in the *oak* pattern. However both the synaptophysin and ß-tubulin staining results of the *lattice* pattern suggests fine processes are responding to the node design (see Figure 4.27). The synaptophysin staining in this case is also very different to those obtained from patterns of smaller node dimensions. In contrast to the *hex 20* and *Jude* patterns, synaptophysin appears localised to the node regions in the lattice patterns, rather than being spread evenly throughout the network. Figure 4.27 compares the ß-tubulin and synaptophysin of patterns *hex 20*, *hex 40* and *lattice* as it occurs at the node region. In the *hex 40* pattern the synaptophysin staining is much more intense as there is an abundance of neurite processes accumulating at this site, whereas in the lattice pattern the synaptophysin stain is radiating outwards from the central node region.

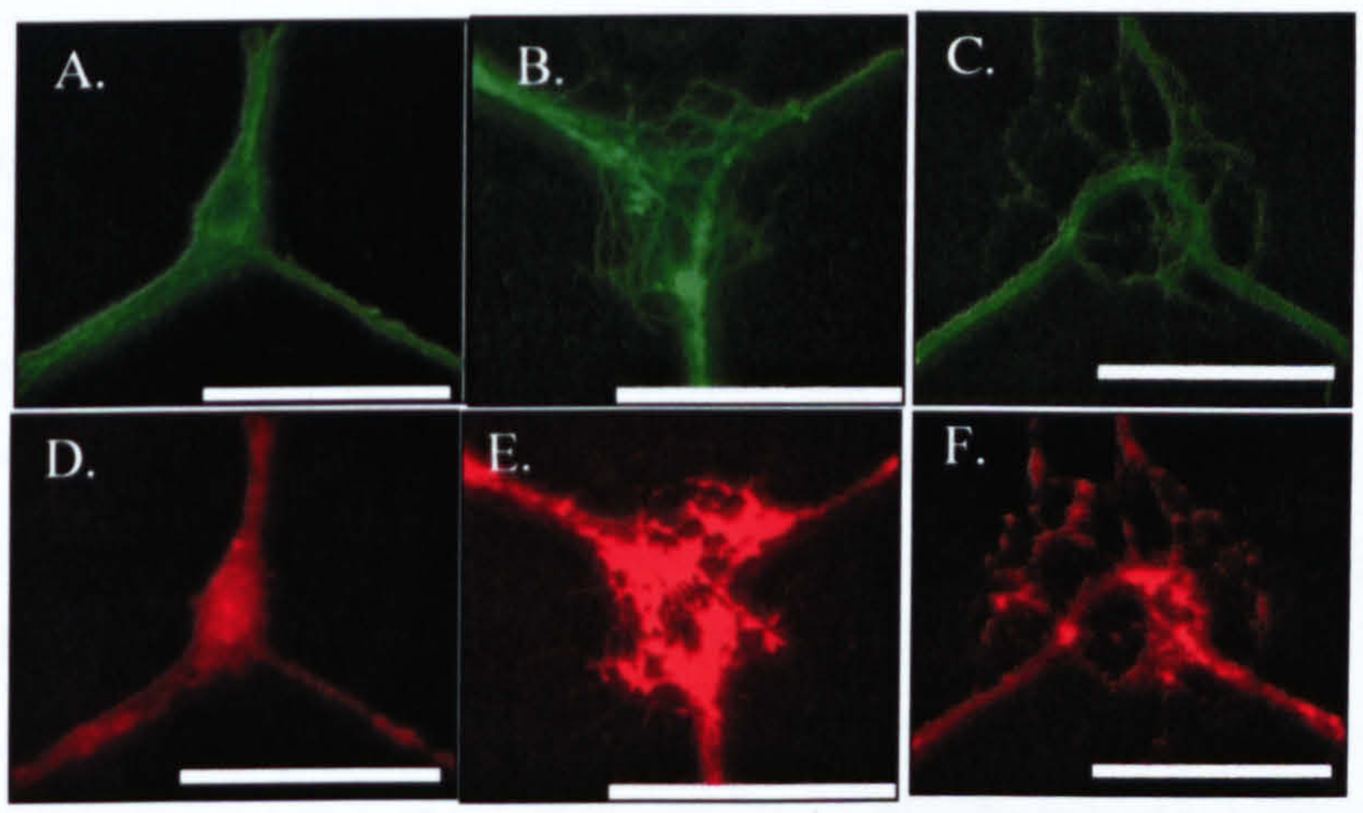

Figure 4.27. Magnified images of the node region of hex 20 (A, D), hex 40 (B, E) and lattice patterns (C, F). Images A, B and C shown neurite processes stained for ß-tubulin, and images D, E and F show the corresponding synaptophysin stain. The scale bar is 50µm in all images.

Investigation of Network Pattern on Neuron Compliance

The effect of network pattern on cell compliance was investigated using the images collected for the previous experiment (*Characterisation of Neural Networks*). Cell compliance to each network pattern was investigated according to the following parameters; soma-node localisation, cells located on lines and cells failing to comply to the pattern at all. Only the cells that stained positive for *ß*-tubulin were used in this study. The statistical significance of the results was determined using the Student's *t*-test. Graph 4.2.A shows the percentage of cells located off the pattern for each network design. These results are very closely correlated to those presented in Graph 4.1, *Classification of Network Population* section, despite the fact that the data in this section has been collected from a different source (images of cells stained for *ß*-tubulin, GFAP and AA3). This close relationship between these two sets of results suggests that cell compliance is a direct result of the network pattern, as the same trend in results has been produced with different cultures, and not due to coincidence. As hypothesised there is a significantly higher percentage of non-compliance to the *Jude* pattern than any other network. Only the *hex 40* pattern had 100% compliance to the network pattern, however over 50% of cells were located on the line intersections rather than the desired soma attachment sites. The network patterns with the greater node dimensions all had on average a higher percentage of cells complying to the node sites than the smaller node pattern. This result is most likely due to more than one cell body adhering to the node, as evident in the phase contrast images of shown in Figures 4.13 to 4.18.

SEM Analysis of Neuron Compliance

Observation of the stamped areas by SEM aimed to identify the finer processes of the neural networks, and how these responded to the chemical pattern. As all μCP in this study was performed on plastic Petri dishes, all samples used for the investigation of fine neurite compliance had to be prepared by freezing drying methods for SEM analysis. For samples to fit into the liquid nitrogen chamber they had to cleaved to less than 1cm^2. This modification of the substrate presented a number of problems. If the material was cut prior to μCP and culturing using a Dremel circular saw (DREMEL, Uxbridge, UK), the debris that was produced during cutting contaminated the surface. If a heated cutting device was used (in this case a scalpel blade), although almost no debris was produced, the melted plastic created a ridge surrounding the area for μCP, which prevented the stamp from

coming into contact with the substrate. Therefore all samples were cleaved after μCP and cell culturing, taking great care not to destroy the neural networks. However not all attempts were successful and so patterns *Jude*, *hex 20* and *oak* are missing from this analysis. However, the author believes that the results previously presented in this chapter are sufficient to support statements and conclusions drawn from this study. From those patterns that were successfully processed (*hex 40*, *sun* and *lattice*), the initial observation made from the SEM images is that many of the node sites are free of cells bodies, and those that were occupied had more than one cell present. This was true for all three patterns (see Figures 4.20-4.23). A closer inspection of the 'cell-free' nodes confirmed that these were in fact occupied by a dense network of neurite processes, as shown by *ß*-tubulin and synaptophysin staining (see Figure 4.28). SEM analysis of the *sun* pattern concluded that the dendritic node details were not, in any form, being translated into a chemical pattern. Surprisingly the node detail of the lattice pattern was clearly visible by SEM, and almost completely accurate in its dimensions (see Figure 4.22), despite the poor immunochemical staining result shown in Figure 4.9. The finer processes of cells growing in this pattern were responding to the smallest detail of the node design.

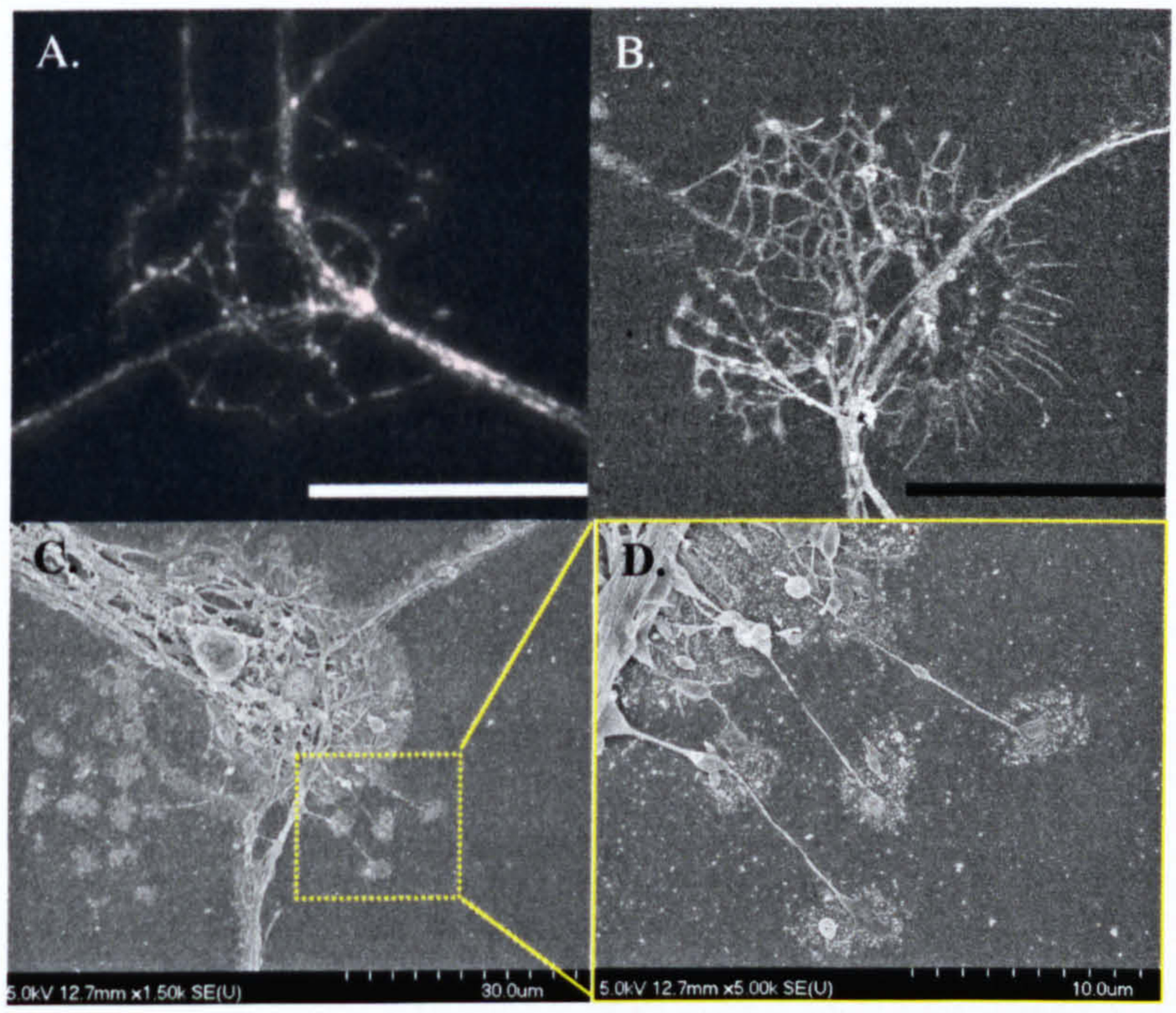

Figure 4.28. Images showing the response of fine neurite processes to the node design of the lattice network pattern. Image A is an unprocessed fluorescent micrograph of synpatophysin staining, where the highlighted areas are positive for synaptophysin (the scale bar is 50μm). Images B and C are SEM images showing fine processes responding to the node design, and image D is the highlighted area in image C at a higher magnification.

Conclusion

From the observations of the results presented in this chapter it is concluded that the geometry of a network pattern can influence the overall characteristics of that neural network. An increase in node size has an effect on cell compliance, and can also encourage activity hot-spots where mass connections are formed. Although the patterns designed for introducing dendritic arborisations did not produce the change in cell morphology that was hypothesised, the intricate design of the *lattice* pattern was shown to be guiding the finer neurite processes. This suggests the principles of this study have been achieved albeit the pattern designs used need to be revised if dendritic arborisations are to be introduced to the network pattern.

Chapter 5.

Nerve Cell Responses to Micrometric and Nanometric Topography

Abstract

It is well documented that cells respond to structural topography. Therefore micrometric grooved structures were used to create organised cultures on the PDMS Neuro-chip substrate (a cell containment chip designed to combine neural networks with planar multi-electrode recording systems). However, observations made using SEM imaging showed that cells were not aligning to the micrometric topography as expected. Therefore it was necessary to investigate other topographical guidance mechanisms that would be compatible with the Neuro-chip concept. Nanopillared topography was applied to this study. Coomassie blue staining showed that this topography reduced cell adhesion. However, when cells did adhere, they displayed longer processes in comparison to those grown on flat structures. SEM analysis revealed that the nanometric pillars were causing processes to form linear networks. Although the mechanisms through which this phenomenon was occurring was not deciphered, this result suggests nanopillared topography could provide a means for both guiding and stimulating neurite growth.

Introduction

The precise formation of neuronal connections is an essential process during early development of the nervous system (Hivert *et al.* 2002). During this period of growth cell synapses, and therefore neural networks, are not formed at random but are driven into place by guiding forces that exist in the cells environment. These forces exist in the form of chemical cues, such as secreted factors like netrin-1, and physical cues such as cell adhesion molecules present on the surface of surrounding cells (Aubert *et al.* 1995, Dodd & Jessell 1988, Stoeckli & Landmesser 1998). Over the last decade the advancements made in micro- and nano-fabrication industry has provided a means for scientists to manipulate the cells immediate environment by creating diverse biomaterials with varying topographies and chemistries. Such studies have shown changes in substrate topography can alter cell adhesion, movement and morphology, apoptosis, lead to macrophage activation and gene expression, all of which are essential mechanisms for tissue repair (Dalby *et al.* 2004c). In the case of neurophysiology, studies investigating the interaction of cells with biomaterials have been partly driven by the desire to construct a brain-machine interface, capable of correcting both sensory and motor defects that can occur in the nervous system after disease or injury (Fan *et al.* 2002b, Fromherz 2003, He & Bellankonde 2005, Krause *et al.* 2006, Sorribas *et al.* 2002), while other groups have focused their attentions on developing a 'smart' scaffold capable of bridging the dense disorganised and non-permissive tissue that forms around a lesion site to allow regeneration (Mahoney & Seth 2006, Novikov *et al.* 2002, Stokols & Tuszynski 2004, Yang *et al.* 2004, Yang *et al.* 2005). In each case the adhesion of the cell, and the fine control of the axonal position and growth, are essential components for a successful result. Therefore the correct topographical pattern and the most effective dimensions (micro- or nano-) must be investigated.

Micrometric Topography- Neuro-chip

To understand the effect of pattern geometry on network behaviour one must investigate the electrical activity of the cells within the neural network. To do so requires the coming together of cell patterning techniques and multi-electrode

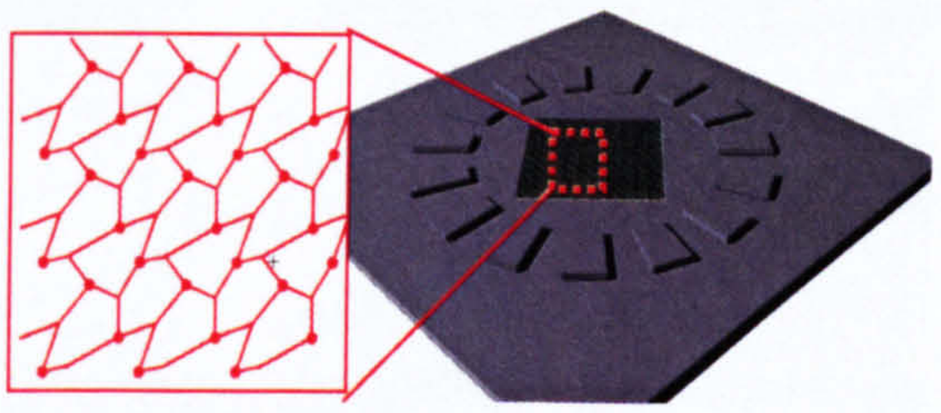

Figure 5.1. Schematic drawing showing the Neuro-chip fabrication cell containment device

(MEA) recording devices. The Neuro-chip is a cell containment device, which has been designed to do just that (see Chapter 6). The idea was to create a structure, which would bring a network of cells into contact with an array of electrodes, without having to grow the cells directly onto the MEA device. Using such a device topographical patterning could be introduced without having to incorporate complex procedures during electrode fabrication (Curtis *et al.* 1992), or introduced stamp alignment methods that would be necessary with μCP (Lauer *et al.* 2001). It was hypothesised this method of separating long term cell culture from the recording device would increase the lifetime of the electrodes, as cells would not be growing directly onto the array, therefore cell trypinsation or other vigorous cleaning methods would not be required. The geometric design of the network pattern is described in the introduction of Chapter 4. The micrometric dimension of the pattern are based on results from the classical ridge-groove alignment publications which have shown nerve cells respond to grooved topography (Clark *et al.* 1987, 1990, Curtis & Wilkinson 1997). By using this device we can employ electrophysiological methods to further our understanding of network behaviour and investigate network response to pattern geometry.

Nanometric Topography- Nanopillars

Nanotechnology, the fabrication of structures and devices of nanometric scale, is emerging as a new and exciting tool in bioengineering. The size of such structures is comparable to the molecular level of matter, and therefore has profound implications on the level of finite control that can be employed within a biological model. (Barbucci *et al.* 2003, Curtis & Riehle 2001, Curtis & Wilkinson 2001, Dalby *et al.* 2004a, Dalby *et al.* 2004b, Gallagher *et al.* 2002). In the case of nerve cell growth and guidance, for example, there are various extracellular matrix molecules, such as laminin, which are of nano-metric dimensions. Using nano-fabrication technology it may be possible to further investigate the exact roles such molecules play in network development by recreating their dimensions within an artificial environment. This may also provide insight into the interaction that occurs between advancing neurite processes and underlying nano-metric environment that exists in-vivo. To date only a handful of studies have investigated the response of neurons grown on structures with nanotopographies (Cyster *et al.* 2004, Fan *et al.* 2002a, Fan *et al.* 2002b, Johansson *et al.* 2006, Khan *et al.* 2005). In 2002 Fan *et al.* (Fan *et al.* 2002a) set out to investigate the surface requirements of biosensor devices fabricated from silicon, with the aim of determining what effect the nano-scale surface topography had on neuron adhesion.

The nanotopography investigated was a by-product of the surface fabrication process, which created a surface of varying *'roughness'* (measured by AFM, having a Ra of 2-810nm depending on etching conditions). The results from this study showed that neurons preferentially adhered to substrates of a higher Ra value. Based on this data, Fan *et al* attempted to introduce a patterned topography by varying the roughness of the surface (creating a grid-like area of adhesion). However this again only highlighted the surface adhesion preference of the neurons as shown in Figure 5.2 (Fan *et al.* 2002b).

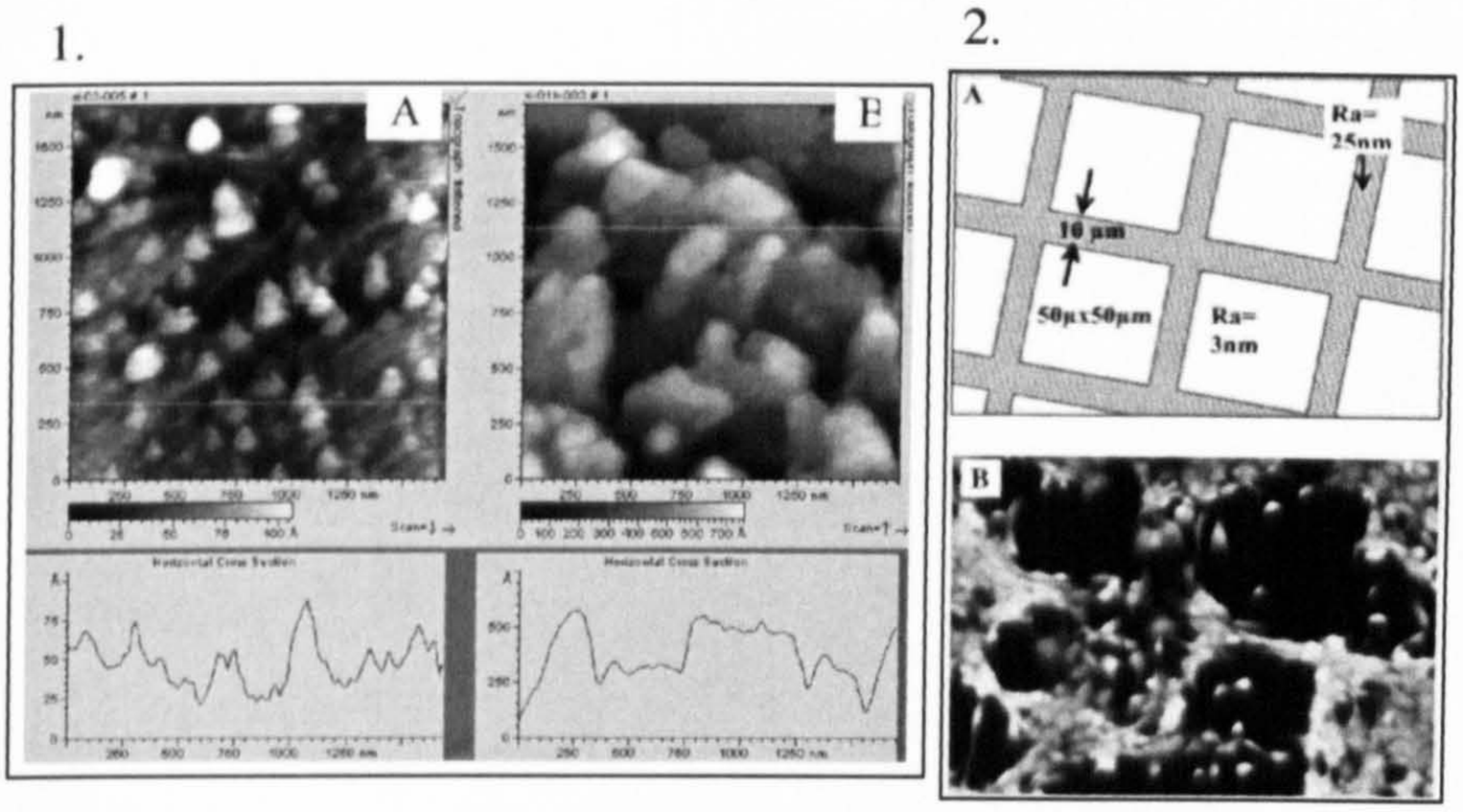

Figure 5.2. Images taken from Fan 2002 publication (Fan et al. 2002b). Image 1 shows the AFM micrograph of the three-dimensional nano-scale topography of the silicon substrate (A: Ra=2.2nm, B: Ra=25nm). Image 2 shows the dimensions of the patterned surface, and resultant alignment of substantia nigra cells.

The studies conducted by Cyster (Cyster *et al.* 2004) and Khan (Khan & Auner 2005) also considered random surface roughness on cell adhesion, and so provide little insight into the response of nerve cells, in particular their fine neurite processes, to a geometrically defined nanotopography. However, an example of such has been found within the 2006 publication by Johansson, Carlberg, Danielsen, Montelius and Kanje. In this paper (Johansson *et al.* 2006), explant cultures of dorsal root ganglia were grown on grooved nano-patterns of varying dimensions (ranging from width: 100-400nm, and pitch: 200nm-1200nm). Although this study has shown that neurons will align to a topography of nano-dimensions, by using a groove/ridge topography (a topography that has been studied extensively at the micrometric level) they have failed to explore possible alternatives to the topographical dimensions, and the possible effects, other than alignment, they may have on neurite growth. It is for this reason we will investigate the effects of a pillared nanotopography.

Summary

Here we will consider the fabrication methods used to create the Neuro-chip device. The ability to grow and align cells to the network pattern incorporated into the Neuro-chip device will be investigated using fluorescence and scanning electron microscopy. The cellular response to a nanopillared topography of linear pitch will be investigated, in terms of process alignment and proliferation, again using fluorescence and scanning electron microscopy.

Materials and Methods

Micrometric Topography- Neuro-chip

Fabrication of the Master Die on a Silicon Wafer

All silicon wafers were fabricated by Rongyu Tang following the two-step dry etch process. Step 1, which is described in Chapter 3, *Materials and Methods,* involves the etching of the network pattern into the silicon wafer. Only Step 2, the creation of the supporting structures, will be described here. These methods were applied directly after Step 1.

Cleaning and Photolithography

1. Clean wafer by sonicating in acetone for five minutes. Rinse with RO water.
2. Clean wafer in Piranha Acid (7 parts sulphuric acid, 1 part hydrogen peroxide) to remove remains of the photoresist, then blow dry with particle free nitrogen following final rinse.
3. Bake the wafer at 100 °C for 15 minutes.
4. Spin Shipley AZ4562 onto sample at 4000 rpm for 30 seconds (see diagram (e), Figure 5.3).
5. Bake the sample at 90 °C for 30 minutes or alternatively bake on a hotplate at 90 °C for 5 minutes.
6. Let the sample cool down to room temperature.
7. Load circular support pattern mask onto mask aligner (SUSS MicroTec MA6) and expose sample to UV light for 5 seconds (200W Hg) (see diagram (f), Figure 5.3).
8. Develop the sample in Microposit® concentrate and RO water solution (1:1) for 60 seconds.

Dry Etching

Dry etch wafer with recipe RYT1 in ICP for seven minutes (see diagram (g), Figure 5.3). This creates 5 micron deep supporting structures (see diagram (h), Figure 5.3).

Final cleaning

1. Clean wafer by sonicating in acetone for five minutes. Rinse with RO water.
2. Clean wafer in Caro's Acid (7 parts sulphuric acid, 1 part hydrogen peroxide) to remove remains of the photoresist. Rinse in RO water, then blow dry with particle free nitrogen following final rinse.

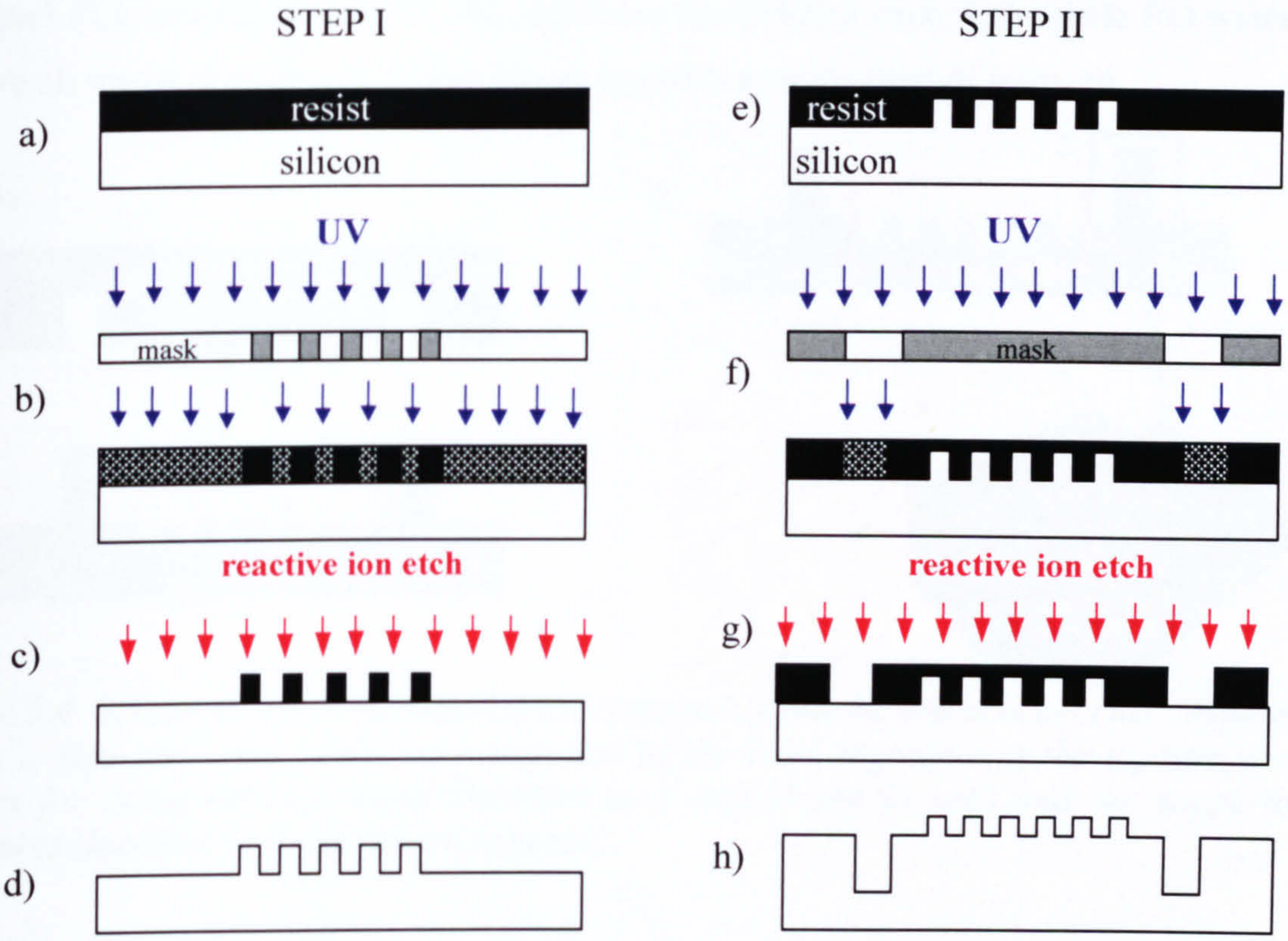

Figure 5.3. Schematic Diagram illustrating the two-step dry etch process used to create the Neuro-chip structure from a master die onto a silicon wafer. The first diagram (Step I-a, Step II-e) represents the silicon wafer spin coated with resist. This is brought into contact with the master die and exposed to UV (Step I-b, Step II-f). The exposed silicon is dry etched (Step I-c, Step II-g) using etch recipe RYT1 to create the final structure (Step I-g, Step II-h).

Fabrication of PDMS Neuro-chip

The neural chip was fabricated using the commercially available polymer Sylgard 184 as it is known to be oxygen permeable. The polymer was stirred for 5 minutes before being mixed with the curing agent at a ratio of 1:10. The uncured polymer solution was placed in a suction chamber for 20 minutes to remove all air bubbles, then dispensed onto the silicon wafer using a 5 ml syringe (no backing structure or mold was used to contain the polymer, which was allowed to spread over the whole of the wafer, creating a thin film approximately 1 mm thick). The polymer-coated wafer was placed in the oven preheated to 75°C and left overnight. Once cured each of the six Neuro-chip structures was gently removed from the silicon wafer using a scalpel blade and tweezers, then cut to roughly the same size as a 13 diameter cover slip: this was to ensure the structure was compatible with the required culture vessels and the planar MEA device for which it was designed. The structures were then sterilised in 70% ethanol, washed in sterile RO water then incubated in

12 μg/ml PLL overnight at 37°C. All structures were rinsed once with sterile RO water to remove all traces of excess PLL then blown dry with a sterile flow of nitrogen.

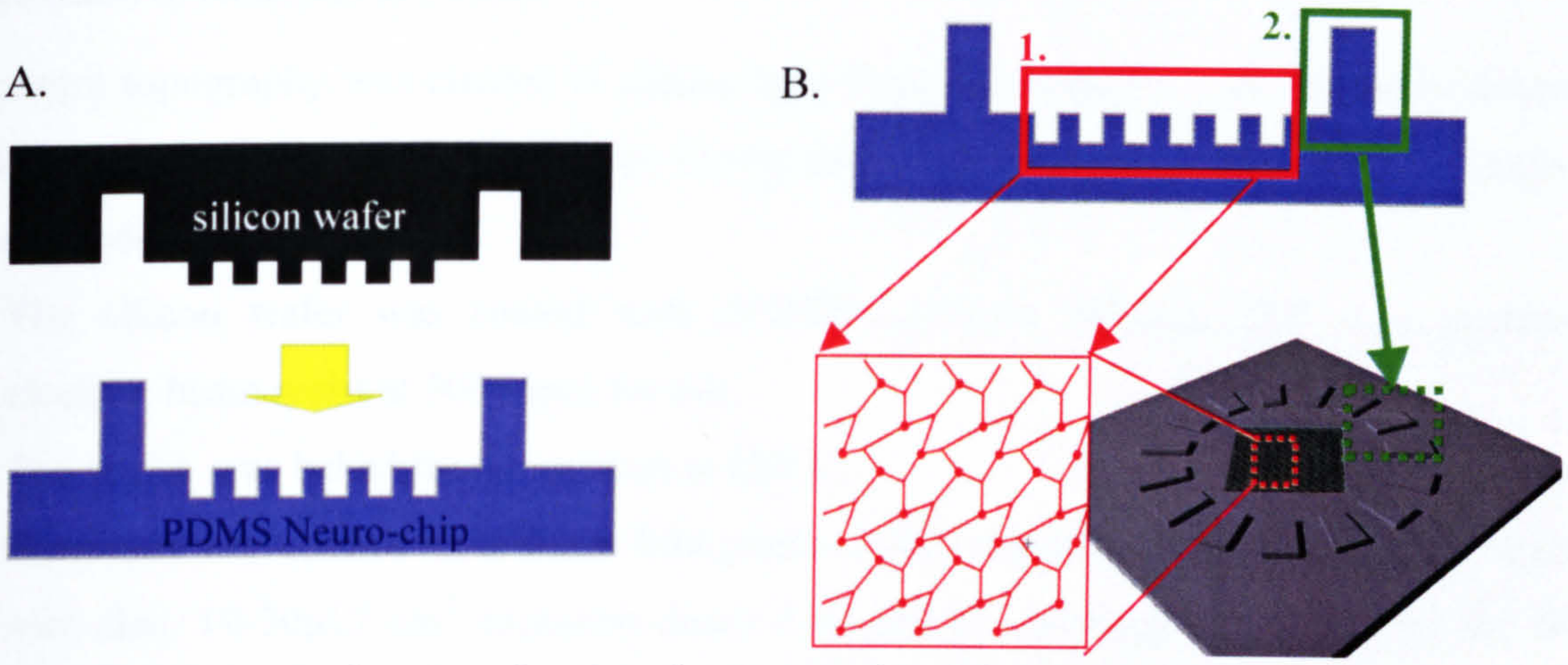

Figure 5.4. Schematic drawing showing the Neuro-chip fabrication process (A). Figure B shows a side view and aerial representation of the chip, highlighting the topographical pattern for nerve cell alignment (labelled no.1 and shown in red) and the supporting structures (labelled no.2 and shown in green).

Cell Culture

Both rat postnatal (P1) and embryonic (E14) spinal cord neurons were used in this study. The culture procedure and methods are described in Chapter 2, *Materials and Methods, Established Methods*. Cells were plated at 3000 cells/cm^2 in all experiments within this section.

Immunofluorescent labelling

The methods used are described in Chapter 2, *Primary Postnatal Spinal Cord Neurons-Established Methods*. Cell were stained first for primary antibody MAP2 (1:100) and then secondary antibody TRITC goat anti-mouse (1:100).

Scanning Electron Microscopy

All imaging was carried out on cells grown on PDMS polymer structures. Cells were kept under normal culture conditions until required. For a description of the SEM preparation procedure please refer to Chapter 4, *Materials and Methods, SEM Imaging*.

Nanometric Topography- Nanopillars

Fabrication of Nanopits in Silicon

A nanopit topography was created in silicon by e-beam lithography. All master structures used were fabricated by Kris Seunarine, Centre for Cell Engineering, Glasgow University. His methods are listed below:

1. The silicon wafer was coated with ZEP520A:anisole (40:60), ZEP is a positive electron-beam resist at 5000 rpm for 60s.
2. The wafer was baked for 60 minutes at 180°C.
3. The resist was opened by E-beam lithography (50kv accelerating voltage, 40-80 beam spot size, 10-30μC/ cm^2 exposure dose) followed by development in xylene for 60 seconds. The resulting pattern in the resist was a square array of openings 150nm in diameter, with 300nm spacing (centre to centre).
4. The resist coated silicon substrate was etched in an Inductively Coupled Plasma (ICP) using un-switched gases.

   Etch parameters: Flow rate: C_4F_8/SF_6 = 120 sccm/40 sccm

   Chamber pressure: 10 mTorr

   Coil Power/platen power: 18 W/525 W

   Process time: 10nm/min

Fabrication of PCL Nanopillar Replica

Sheets of Poly-Caprolactone (PCL) polymer were made by placing commercially available PCL beads (Sigma, Poole, UK) in a 20cm^2 grid with 1cm spacing between 2 sheets of glass. The glass was clamped together, then placed in a preheated oven at 70°C and left for 2 hours, or until the beads had melted and formed a single sheet. After this time the glass/PCL/glass construct was removed and allowed to cool until the PCL sheet had turned white. The PCL sheet was then removed and cut into 1 cm^2 sections, discarding any deformed areas where air bubbles had formed or PCL beads had not met. The PCL replicas of the nanopit silicon wafer were fabricated using a standard hot plate preheated to 75°C. The silicon wafer was placed in the centre of the hotplate and allowed to heat-up for 1 minute, the 1 cm^2 section of PCL was then placed on top and backed with a microscope slide. Once the PCL sheet had melted, this was evident by a change in PCL from being translucent (white) to transparent (clear), slight pressure was applied to the back of the microscope slide, spreading the molten polymer over the silicon wafer. The polymer, with

both the silicon and slide still bound, was then removed from the hotplate and placed in a container of RO water to cool for 5 minutes. If the polymer did not release from the silicon wafer during this time, a sterile particle-free air flow was used to gently pry the PCL replica from the silicon. PCL replicas, flat PCL sections and 13 diameter glass cover slips were sterilised in 70% ethanol, then rinsed in sterile RO water before being incubated in 12 μg/ml PLL overnight at 37˚C.

Embryonic Cell Culture

Only Embryonic Spinal cord neurons were used in this study. The culture procedure and methods are described in Chapter 2, *Materials and Methods, Primary Embryonic Spinal Cord Neurons, Established Methods*. Cells were plated at 3000 cells/cm^2 in all experiments within this section.

Coomassie Blue Staining

Cells were washed in 1x PBS (warmed to 37˚C prior to use) to remove all traces of growth media then fixed with 4% formal saline at 37˚C for 15 minutes. Cells were incubated in commassie blue (a non-specific protein stain) for 5 minutes then rinsed with RO water (3x 5 minutes). All images were taken using a Scion camera (model CFW-1310M, supplied by Alrad Instruments Ltd, Newbury, UK) mounted on a Zeiss Axiovert-25 microscope (Ziess Ltd, Hertfordshire, UK), and acquired using Image Pro-plus software (MediaCybernetics, Workingham, UK).

Immunocytochemical Staining

The methods used are described in Chapter 2, *Primary Embryonic Spinal Cord Neurons, Established Methods*. Cell were double stained first for primary antibody ß-tubulin and then stained for the secondary antibody FITC goat anti-mouse (IgG_{2b}). PCL structures were mounted cells down, onto a microscope slide with a 50μl droplet of mounting medium (also containing nuclei stain). The structures were not sealed with clear nail polish. All images were taken using a Evolution QEi camera (MediaCybernetics, Workingham, UK) mounted onto a Zeiss Axiovert-200M microscope, and acquired using Image pro-plus software (MediaCybernetics, Workingham, UK).

Scanning Electron Microscopy

All imaging was carried out on cells grown on PCL polymer structures. Cells were kept under normal culture conditions until required. For a description of the SEM preparation procedure please refer to Chapter 4, *Materials and Methods, SEM Imaging.*

Results

Micrometric Topography for Cell Guidance- The Neuro-chip

Structure Analysis

The master die for the Neuro-chip was created in silicon by a two step-etch process. The resulting silicon wafer is shown in Figure 5.5.A. This structure is the inverse of the Neuro-chip design, with the larger supporting structures etched into the silicon and the tracks of the network patterns standing proud. From this the silicon Neuro-chip structure was cast in PDMS. This was approximately 1-2 mm thick and was then cut to approximately the same size as a 13 diameter cover slip, therefore making it compatible with a 12 well culture plate. Image B in Figure 5.5. shows the PDMS Neuro-chip structure inverted onto a glass microscope slide. Image B1 shows the contact points of the supporting structures on the microscope slide (B2 shows this image inverted using Photoshop imaging software). The area containing the network pattern is not visible, as it does not come into contact with the glass. However in image B3, slight pressure was applied to the structure bringing the network pattern into contact with the microscope slide (B4 the inverted image), making the array of the pattern visible. SEM imaging showed that the dimensions of both the supporting structures of the Neuro-chip and the network pattern were maintained following the release from the silicon mold.

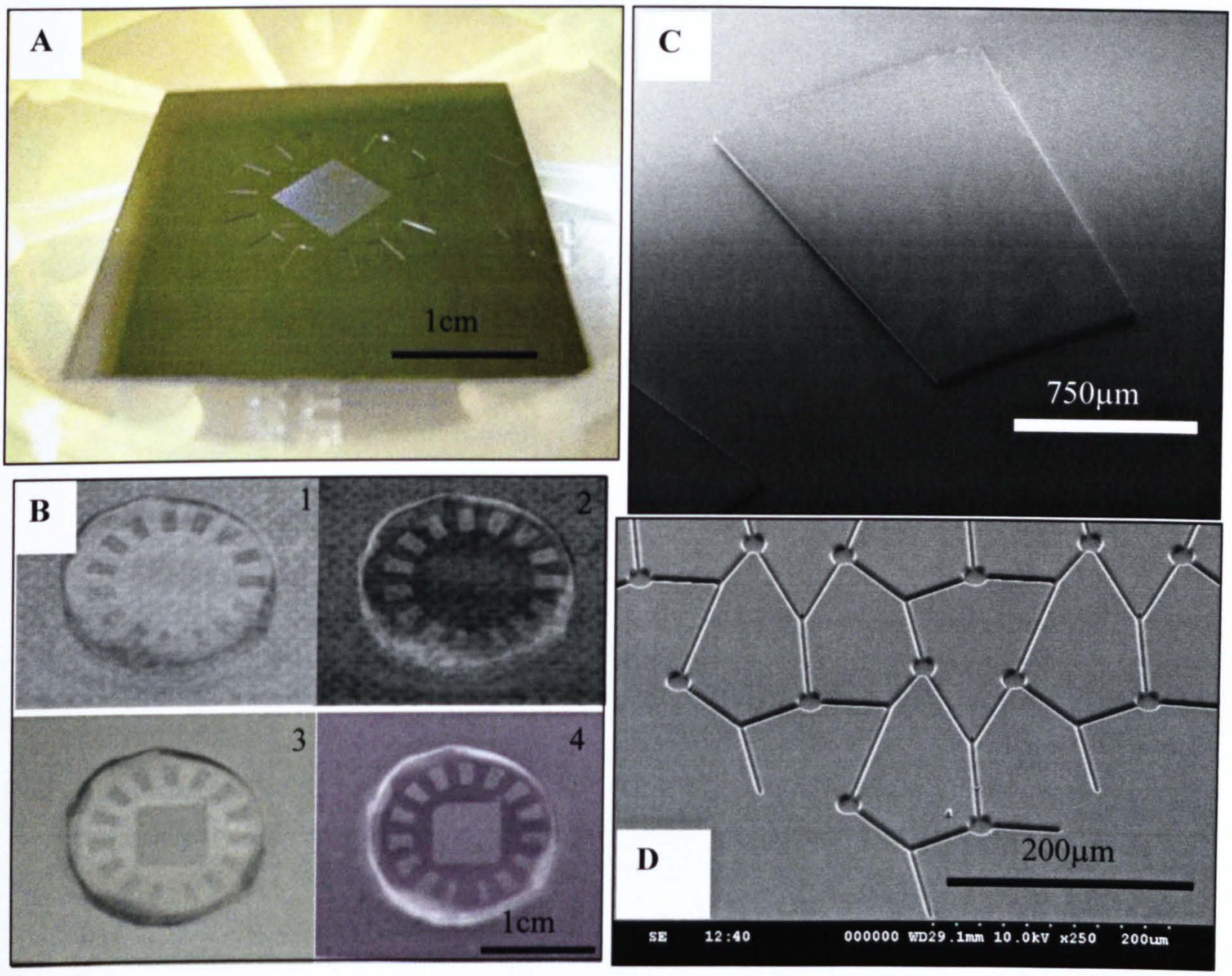

Figure 5.5. Figure showing the Neuro-chip structure. Image A is of the silicon wafer, fabricated from a master die by a two-step dry etch process and image B shows the resulting silicone structure cast from this. Images C and D are SEM micrographs of the supporting structure and the network pattern respectively.

Cellular Reaction to the Micrometric Topography

Postnatal (P1) spinal cord neurons were plated at 3000 cells/mm^2 onto each construct (5 in total) and maintained in culture for up to 20 days. Cells were fixed and stained for MAP2. The results are both phase and fluorescent images of cells grown on the Neuro-chip at this time point. From the phase image, shown in Figure 5.6.A, both cells and the grooved network pattern are visible. The corresponding fluorescence image is shown in Figure 5.6.B. Image C shows a 3 node intersection of the network pattern at a higher magnification, and image D is the corresponding fluorescence image. This experiment was repeated three times, testing a total of 15 structures. In all cases there was no evidence of cell compliance to the grooved network pattern, although some cell bodies did adhere to the node regions, however this did not occur frequently (see Figure 5.6, image C).

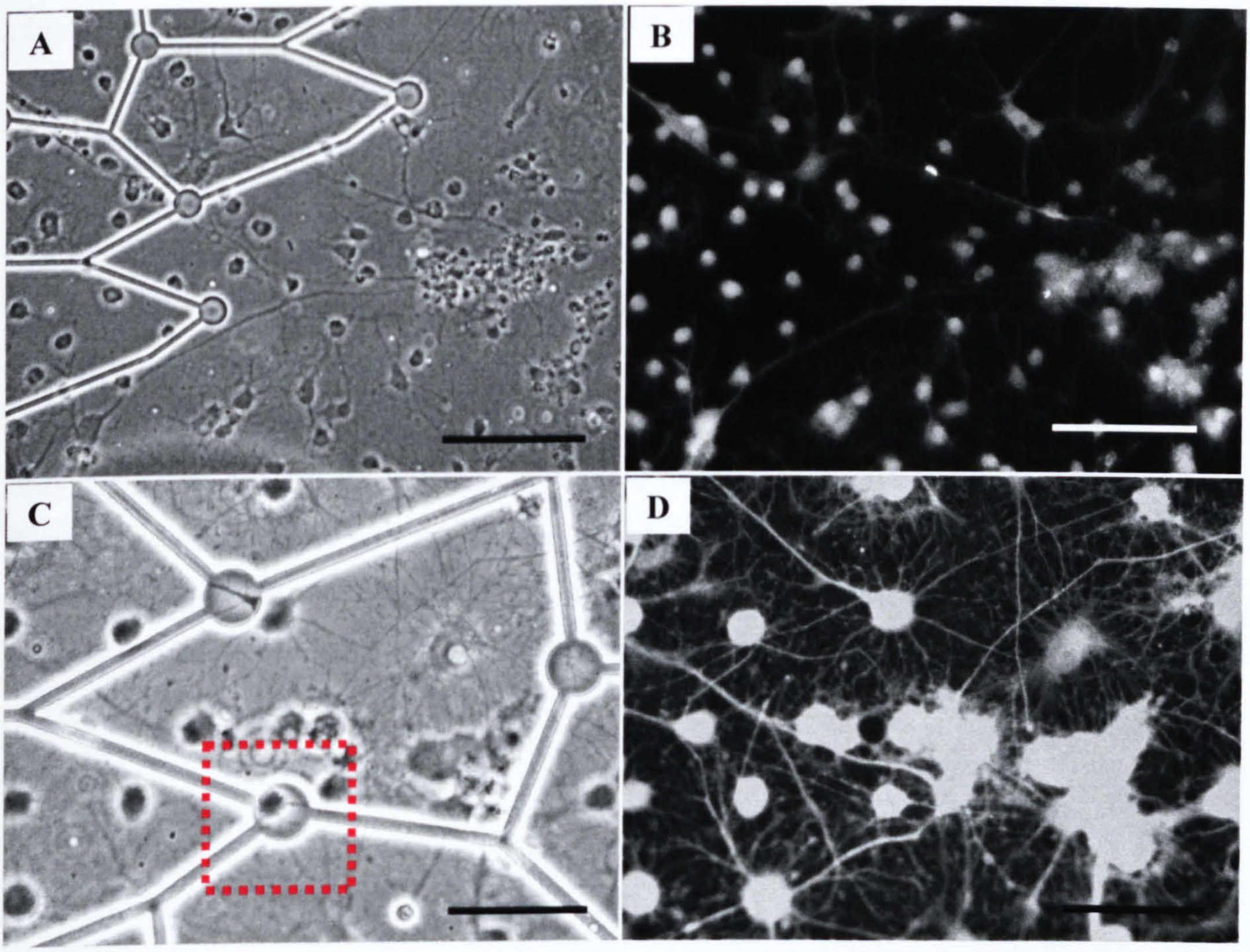

Figure 5.6. Images showing postnatal spinal cord neurons grown on the PDMS Neuro-chip. Image A is a phase contrast micrograph showing the edge of the Jude pattern, and image B the corresponding fluorescence image. Image C is phase at higher magnification showing a 3 node intersection (highlighting a cell located in the node region), and image D the corresponding fluorescence image. The scale bar is images A and B is 100μm, where as in images C and D the scale bar is 50μm.

SEM Analysis of Cellular Reaction to the Micrometric Topography

Of the five different samples analysed by SEM, not one structure had cell bodies or neurite processes growing in the grooves and therefore complying to the network pattern. It may thus be concluded that, although cells were growing over the entire face of the network pattern, they were not responding to the micrometric topography. The structures were analysed at a low magnification, so that both cells and their advancing processes could be visualised, as well as at a high magnification in order to determine how the smallest feature of the cell was responding to the topography. From images taken at a lower magnification, the path of an advancing process could be determined, as shown in Figure 5.7. In this image the process in the centre of the field of view appears to have actively changed its direction of growth, moving away from the 'cliff edge' of the pattern. However, at the next 'cliff edge' encountered by this process, it seems the leading edge of the process has identified the groove and is preparing to respond, in some way, to the topography. A closer inspection of the patterned area at a higher magnification revealed that a number of cell processes were bridging the 5μm wide grooved tracks as well as the 20μm in diameter circular nodes (see Figure 5.9), suggesting that the response anticipated in Figure 5.7 is not one of alignment. Figure 5.8 shows a neurite process spanning the entire 5μm width of a grooved track, although this process appears to be aligning to the cliff edge thereafter, this is just an artefact caused by the freeze drying process (unfortunately cell and surface cracking is evident in all images, this is due to the freeze drying process, and has occurred after the cells were fixed). In Figure 5.9 three examples are given of processes spanning the nodal regions of the pattern. Image A and C are of the same process, with image C showing the path of a branched neurite. It is quite clear from this figure set that both small neuritis and larger processes are avoiding the grooved area of the pattern.

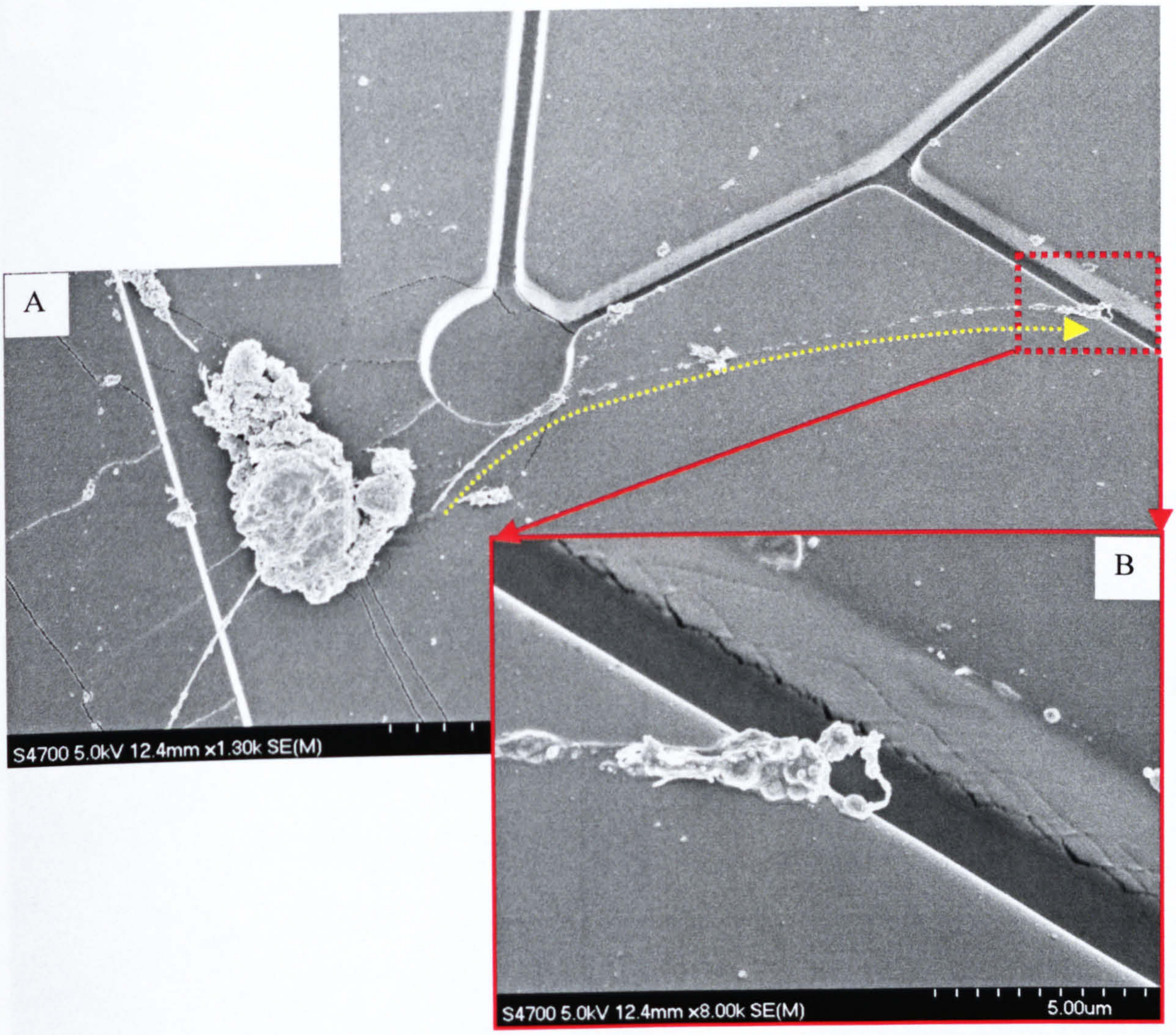

Figure 5.7. SEM image showing embryonic spinal cord neuron growing over the network pattern but not aligning to the grooves. Image A shows the neurite avoiding the grooved node section, with path of process highlighted in yellow. Image B is the area outlined in image A at higher magnification. This appears to show a process in the verge on splitting, with one vertex aligning to the wall edge and the other growing towards the groove canyon.

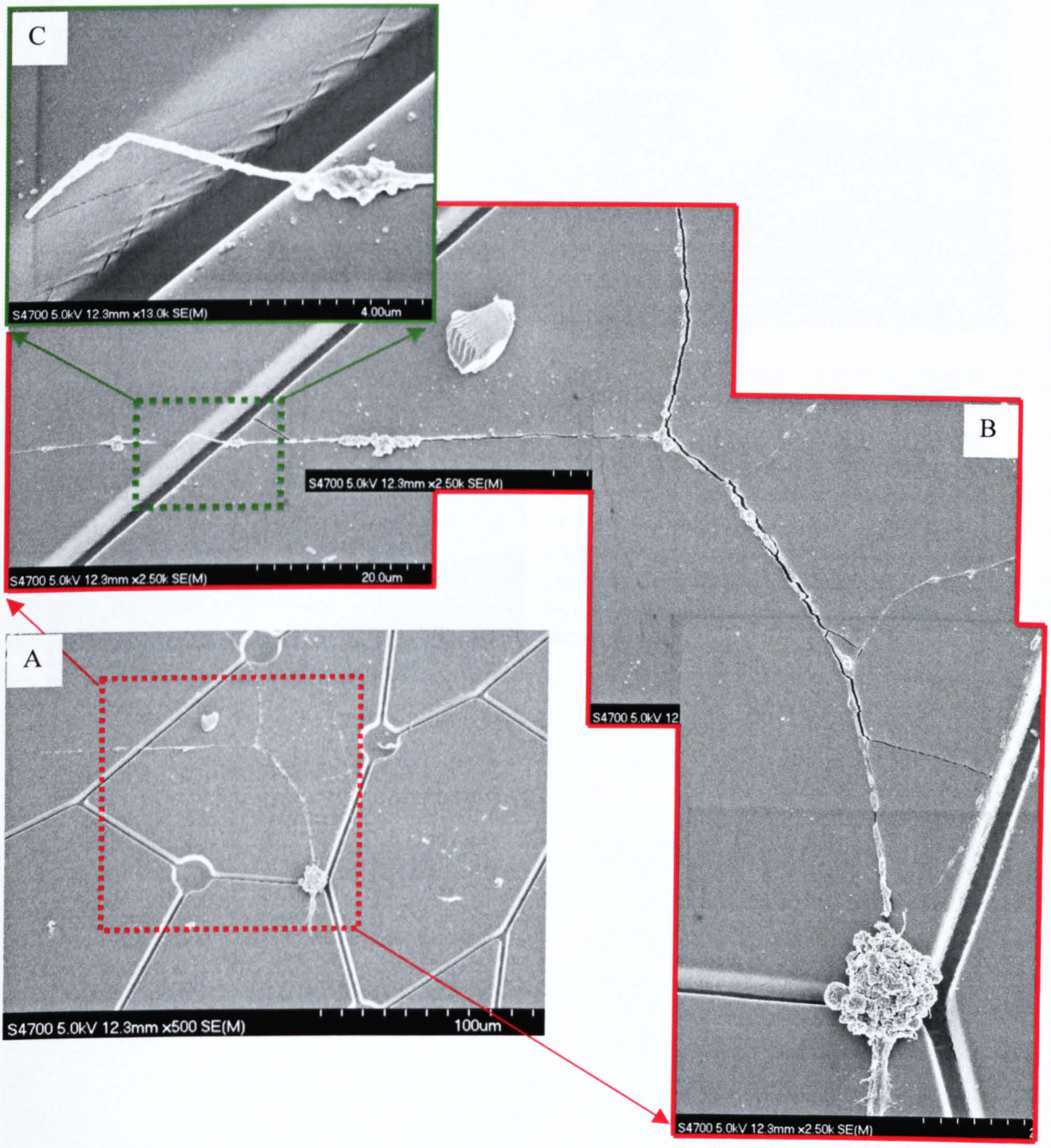

Figure 5.8. SEM image showing embryonic spinal cord neuron growing over the network pattern but not aligning to the grooves. Image C (the highlighted section in image B at higher magnification) shows the neurite extensions bridging the pattern groove. Although this process appears to be aligning to the ridge of the groove track, image B shows this is most likely due to the process breaking during the freeze drying procedure.

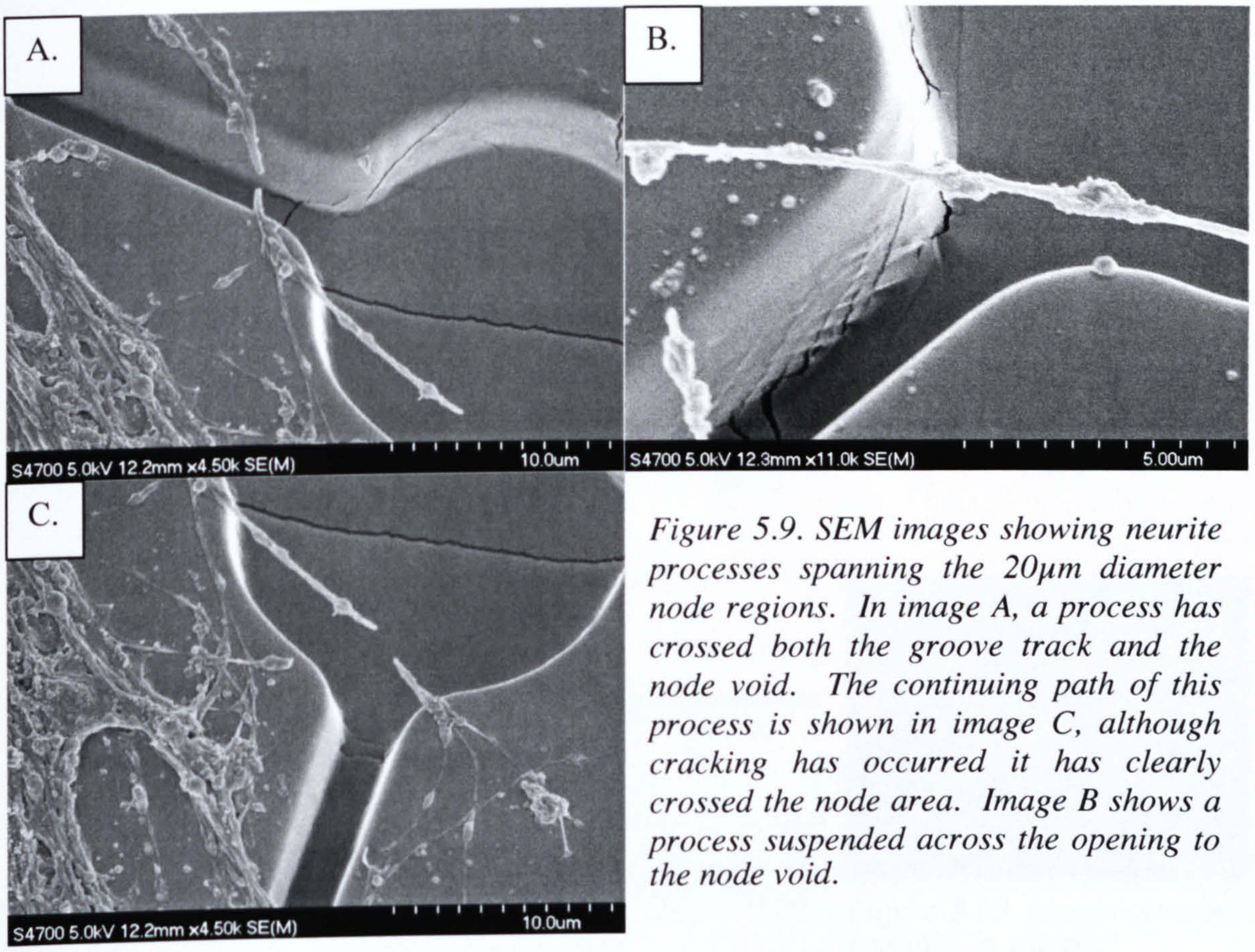

Figure 5.9. SEM images showing neurite processes spanning the 20µm diameter node regions. In image A, a process has crossed both the groove track and the node void. The continuing path of this process is shown in image C, although cracking has occurred it has clearly crossed the node area. Image B shows a process suspended across the opening to the node void.

Nanometric Topography- Nanopillars

Structure Analysis

Nanopits in Silicon

The silicon wafer used in this study was fabricated by Kris Seunarine, Department of Electronics and Electrical Engineering, Glasgow University. The dimensions of the pits on the nanoimprint die were calculated from 6 different SEM images (results are presented in Table 5.1). These measurements were made by Elena Martinez, Centre for Cell Engineering, Glasgow University (Martines, E. *et al.* 2005).

	DIAMETER		DEPTH	SPACING
	BOTTOM	TOP		
MEAN	138 nm	205 nm	141 nm	300 nm
STDV	7	8	1	1

Table 5.1 Table showing the dimensions of the nanopits in silicon. Calculations were made from 6 different silicon wafers

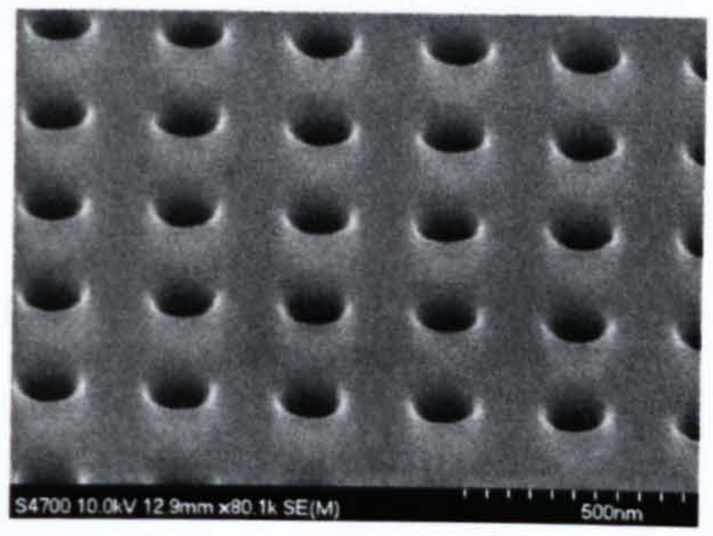

Figure 5.10. Image showing nanopits in silicon.

Nanopillars - PCL Replicas of the Silicon Wafer

The PCL structures created from the silicon wafer were a reverse of the silicon topography, thus the pits in silicon were creating an array of nanopillars on PCL. The SEM image in Figure 5.11 shows a typical example of the nanopillar structure, the dimensions of which were measured to be 115 nm in height with a base diameter of 105 nm. These measurements were made from 10 different PCL structures by Elena Martinez.

	BASE -dia	HEIGHT	SPACING
MEAN	105 nm	116 nm	300 nm
STDV	4	5	1

Table 5.2. Table showing the dimension of the nanopillars in PCL. Calculations were made from 10 different structures.

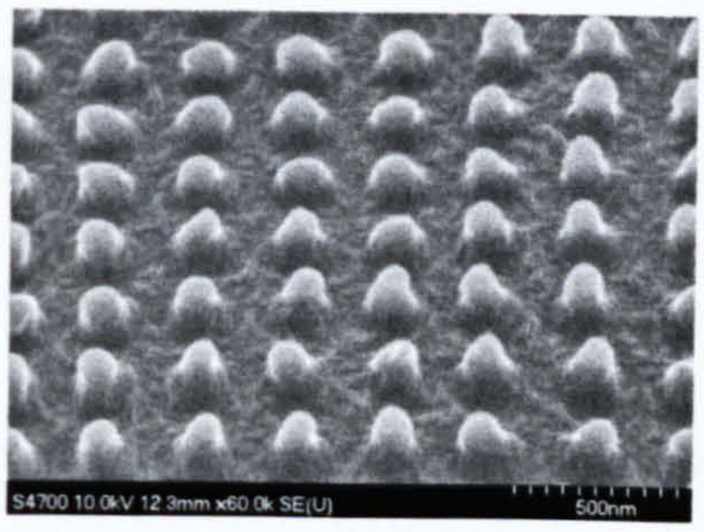

Figure 5.11. Image showing nanopillars in PCL.

Cellular Response to Nanopillar Topography

Investigation of Cell Adhesion

Embryonic (E14) spinal cord neurons were grown under normal culture conditions for 1 week on nanopillared PCL structures, flat PCL sections and 13 diameter glass cover slips. Samples were fixed and stained at this time point with Coomassie blue or for the cytoskeletal cell markers *ß*-tubulin (neuron) and GFAP (glia). From the Coomassie blue stained structures it was evident that the nanopillar topography reduced cell adhesion. In Figure 5.12 the area of nanopillar topography (highlighted red in image B) is free of the Coomassie blue stain, with an obvious border occurring between the topography and the surrounding flat area as shown by thresholding (image B). From immunocytochemical staining it was evident that both the neuronal population and the glial population of the cell culture had been affected (see Figure 5.13), with an abundance of *ß*-tubulin and GFAP positive cells located on the flat topography in comparison to the clearly reduced cell numbers on the nanopillared area. A quantification of cell distribution across the topography was calculated using the nuclear DAPI stain shown in Figure 5.13.C. The image was divided at the topographical border and both areas were processed by thresholding, and then counting the particles highlighted, which were separated by double *'erode'*, single *'dilute'* processing in the image analysis programme Image J (see Figure 5.14 for examples). The results of the cell count presented in bar chart G, Figure 5.14, show a significant difference in the number of cells adhering to the flat PCL than compared to the nanopillar topography. These results support the observations made using the Coomassie blue stain.

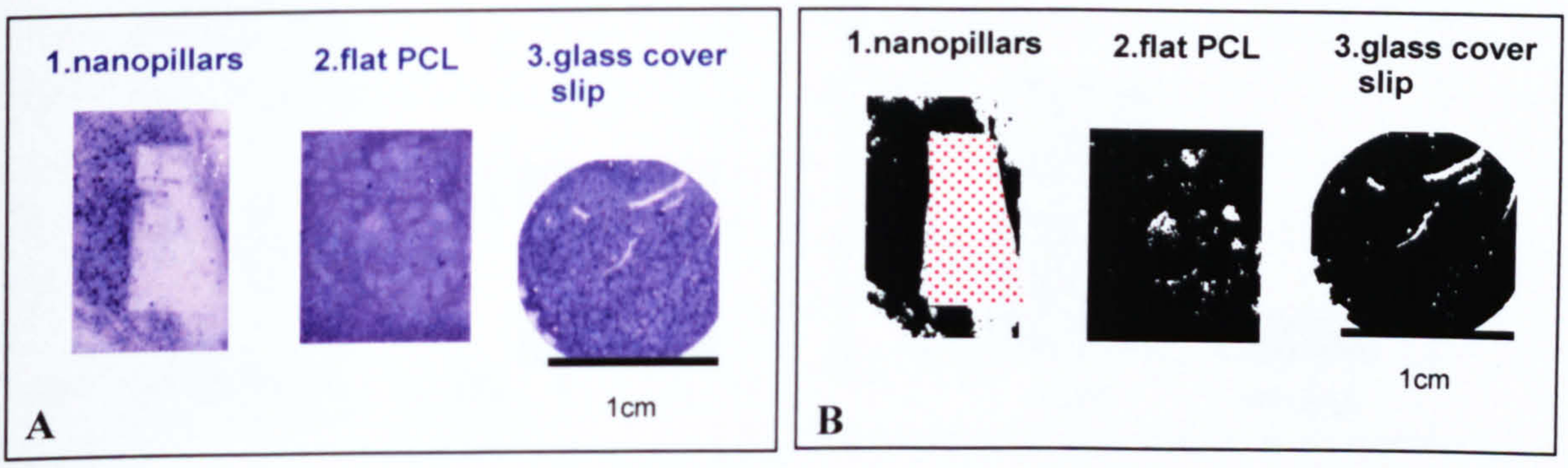

Figure 5.12. (A) Overview photograph of Coomassie blue stained structures (1. nanopillars, 2. flat PCL and 3. 13 diameter glass cover slip); areas of cell adhesion are stained blue. Image B shows image A after thresholding with the area of nanopillar topography highlighted in red.

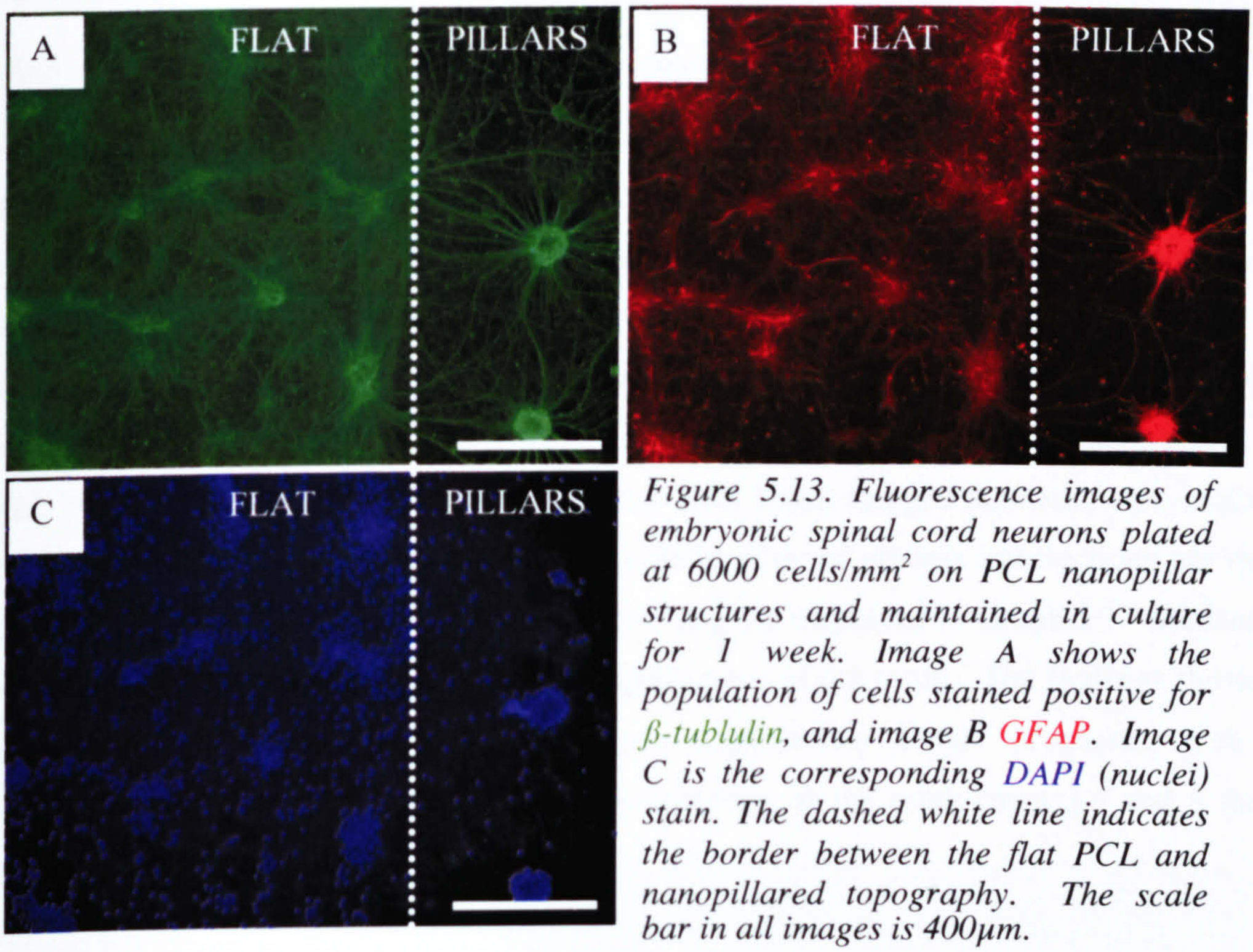

Figure 5.13. Fluorescence images of embryonic spinal cord neurons plated at 6000 cells/mm^2 on PCL nanopillar structures and maintained in culture for 1 week. Image A shows the population of cells stained positive for ß-tublulin, and image B GFAP. Image C is the corresponding DAPI (nuclei) stain. The dashed white line indicates the border between the flat PCL and nanopillared topography. The scale bar in all images is 400µm.

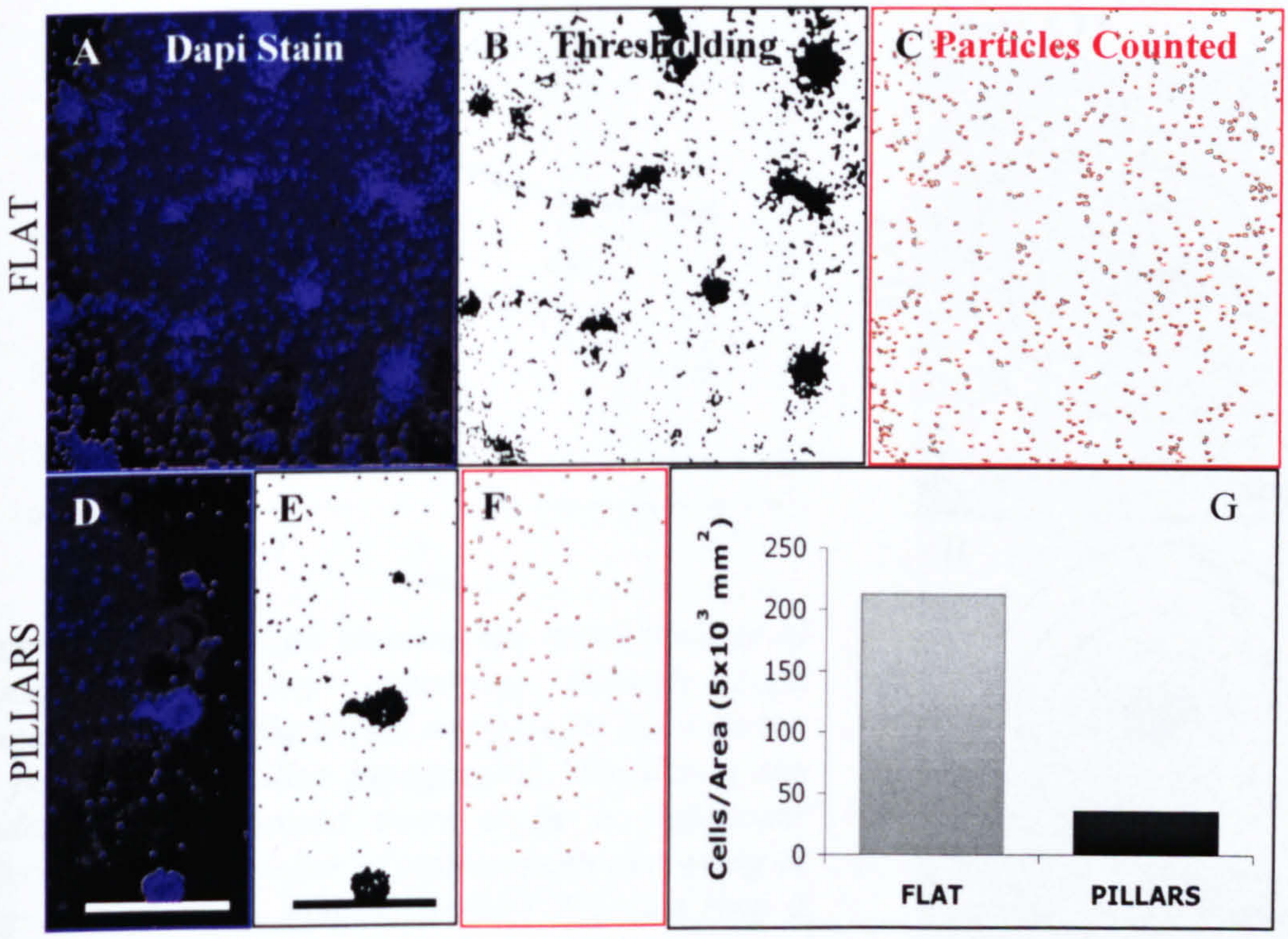

Figure 5.14. Quantification of cell adhesion on flat PCL structures compared to the PCL nanopillars. Image A and D show the nuclei stain for the flat and nanopillar PCL respectively, the corresponding thresholded image (B and E) and from this the particles counted (C, F,). Only particles 150 pixels or less were considered, the larger clusters of cells were discarded from this analysis. The scale bar is 400µm and is the same for all images. The results of the particle count are presented in bar chart G.

Effect of Nanotopography on Neurite Morphology

Results presented in this section were obtained from images of cultures grown on flat and nanopillars structures, fixed and stained with Coomassie blue after 3 days. Ten cells grown on each topographical substrate were selected at random for analysis. Cells grown on PCL flat structures had visibly more primary processes, which were observed to be shorter in length than those found of cells grown on PCL nanopillars. Neurite branching was investigated using a modified Scholl analysis technique (see Figure 5.15) (Mahoney, M. J. *et al.* 2005). A series of Scholl concentric rings with 10μm stepped diameter were centred around the cell body of the selected cell, and the number of process intersections per ring counted. The mean number of intersections per ring are displayed in Graph 5.1. Student's t-test was used to investigate the statistical significance of the result. The findings showed that cells cultured on PCL nanopillars grew significantly longer processes, with a significantly greater number of intersections occurring at the outer rings 3,4 and 5 than those grown on flat PCL.

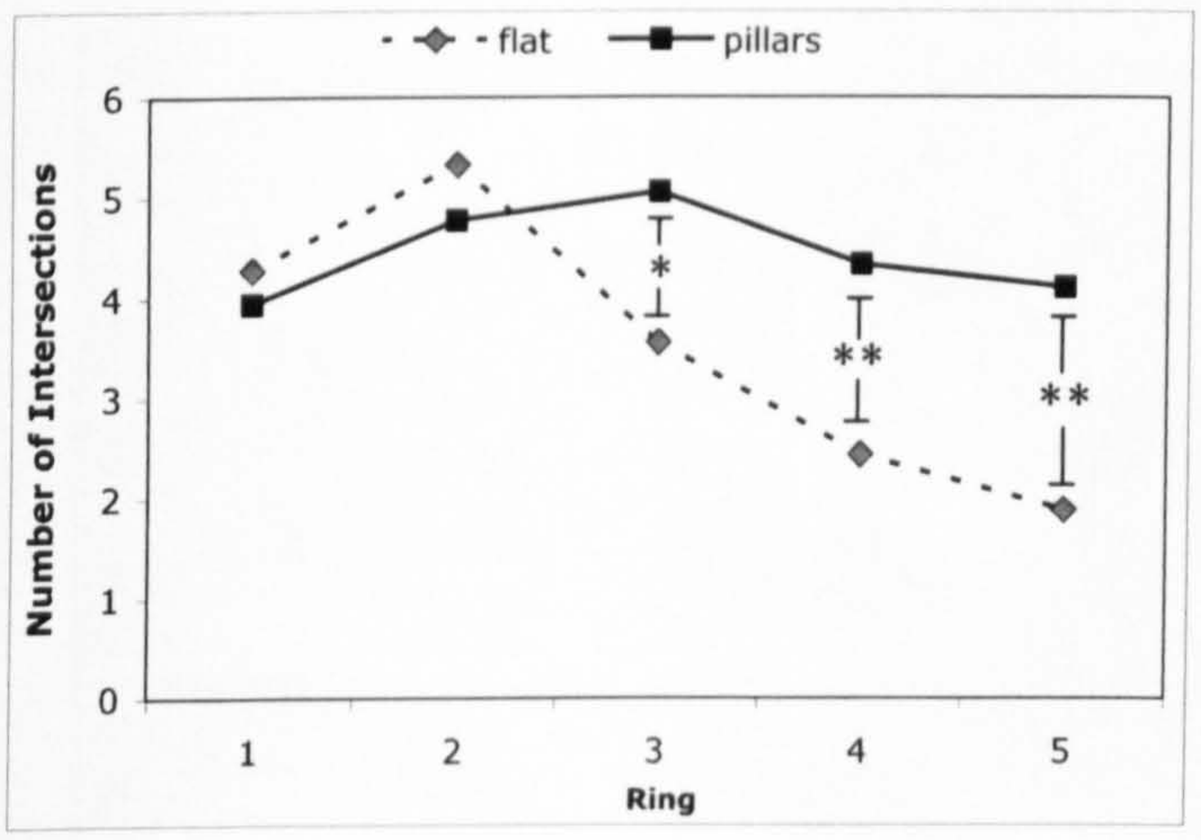

*Graph 5.1. Line graph showing the mean number of process intersections occurring through each concentric ring of the Scholl analysis for cells grown on flat and nanopillar topography. Results of the Student's t-test showed there to be a significant difference in the number of intersections occurring at ring 3 ($p<0.05$ *), ring 4 ($p<0.01$ **) and ring 5 ($p<0.01$ **) between the two topographies.*

Figure 5.15.

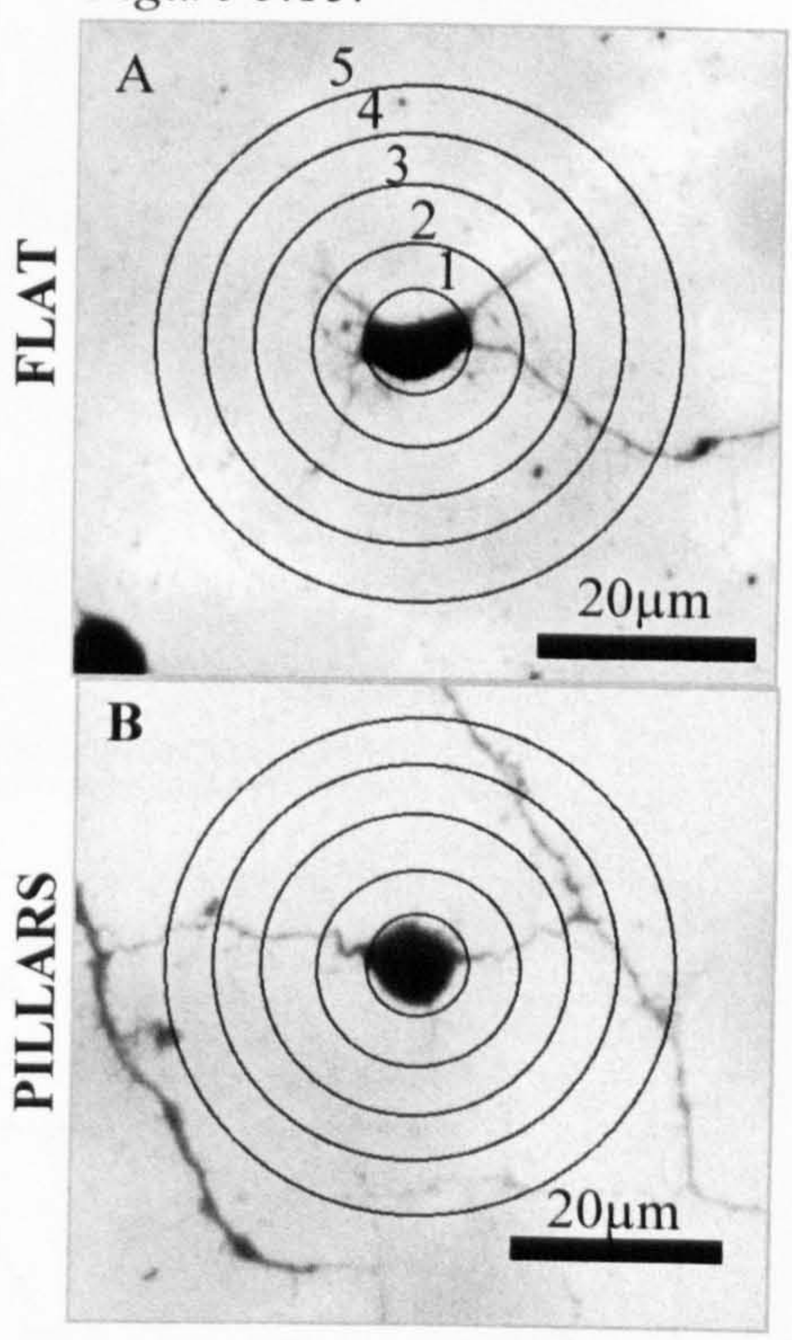

Figure 5.15. Coomassie blue stained embryonic spinal cord neurons grown on flat (A) and nanopillared (B) PCL structures. Superimposed over each image is a schematic diagram of the 5 concentric rings used in the modified Scholl analysis approach.

Effect of Nanotopography on Neurite Length

The length of the longest process emerging from the axon hillock, a conical element of the nerve cell body (Levitan & Kaczmarek 2002, Pannese 1994), was compared on each topographical substrate (see Figure 5.16). The length of all visible branches and segments of this process, limited by the optical resolution of the image acquisition system used (Scion camera, model CFW-1310M, mounted on a Zeiss Axiovert-25 microscope) were considered, and the total length recorded as the neurite length (Figure 5.16, image C). Ten cells grown on each topographical substrate were selected at random, and the processes measured (results are shown in Graph 5.2). Cells grown on the nanopillars had a mean process length of 120μm compared to 75μm for cells grown on flat PCL. Using Student's t-test the difference in mean value was found to be statistically significant at the 0.01 level of probability.

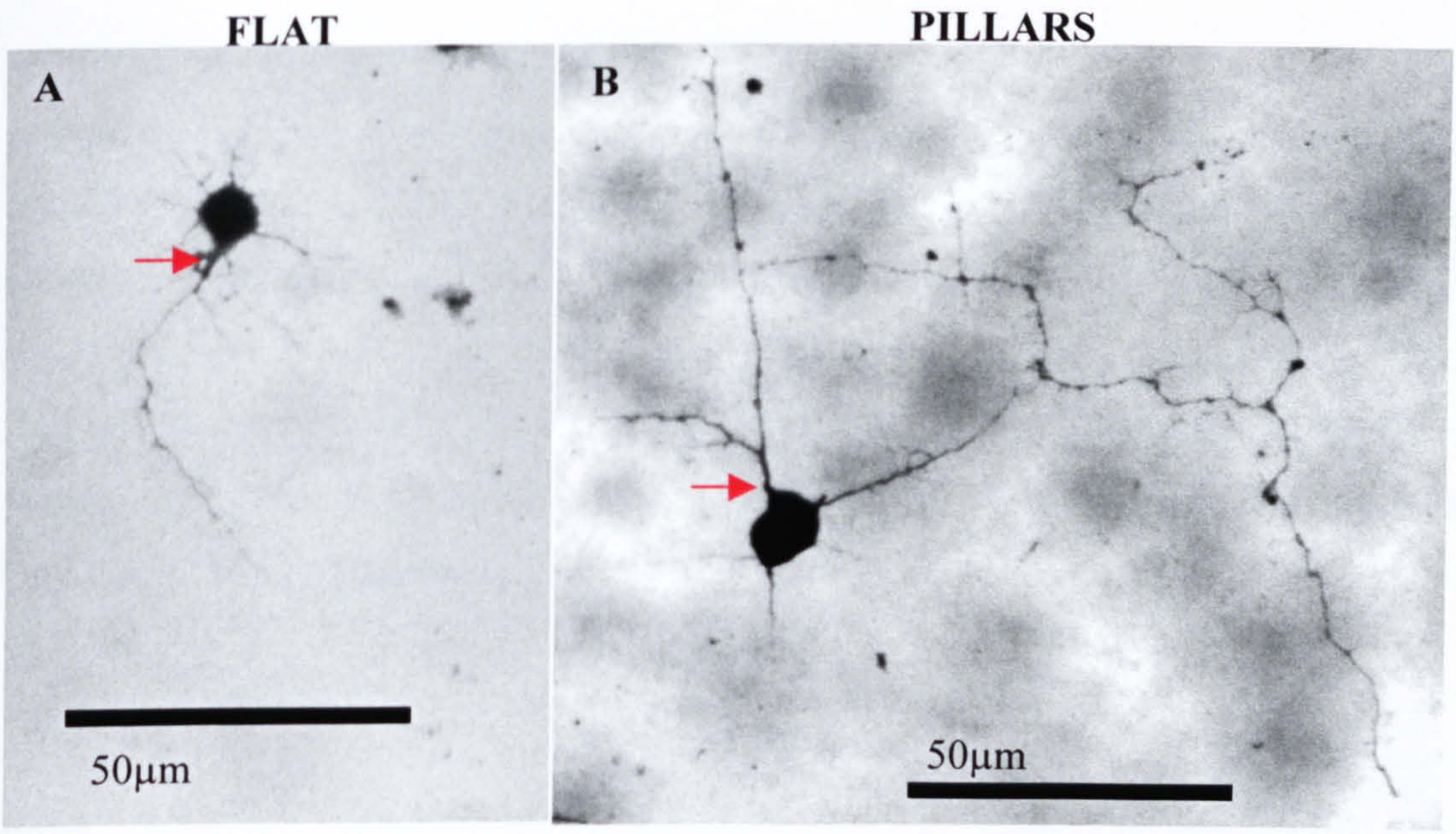

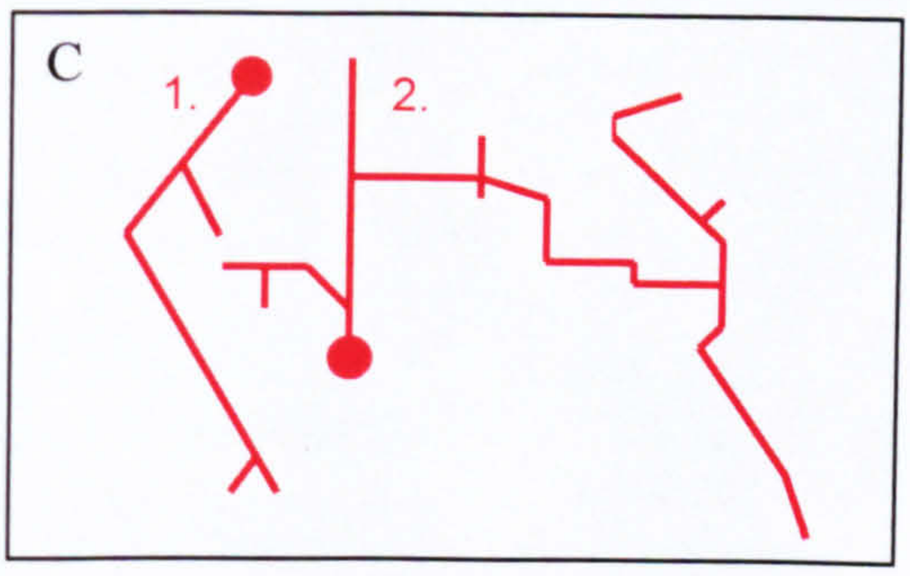

Figure 5.16. Coomassie blue stained embryonic spinal cord neurons grown on flat (A) and nanopillared (B) PCL structures after 3 days in culture. The arrows in each image indicate the location of the axon hillock. Image C is a schematic diagram of the neurites measured in images A (C.1) and B (C.2).

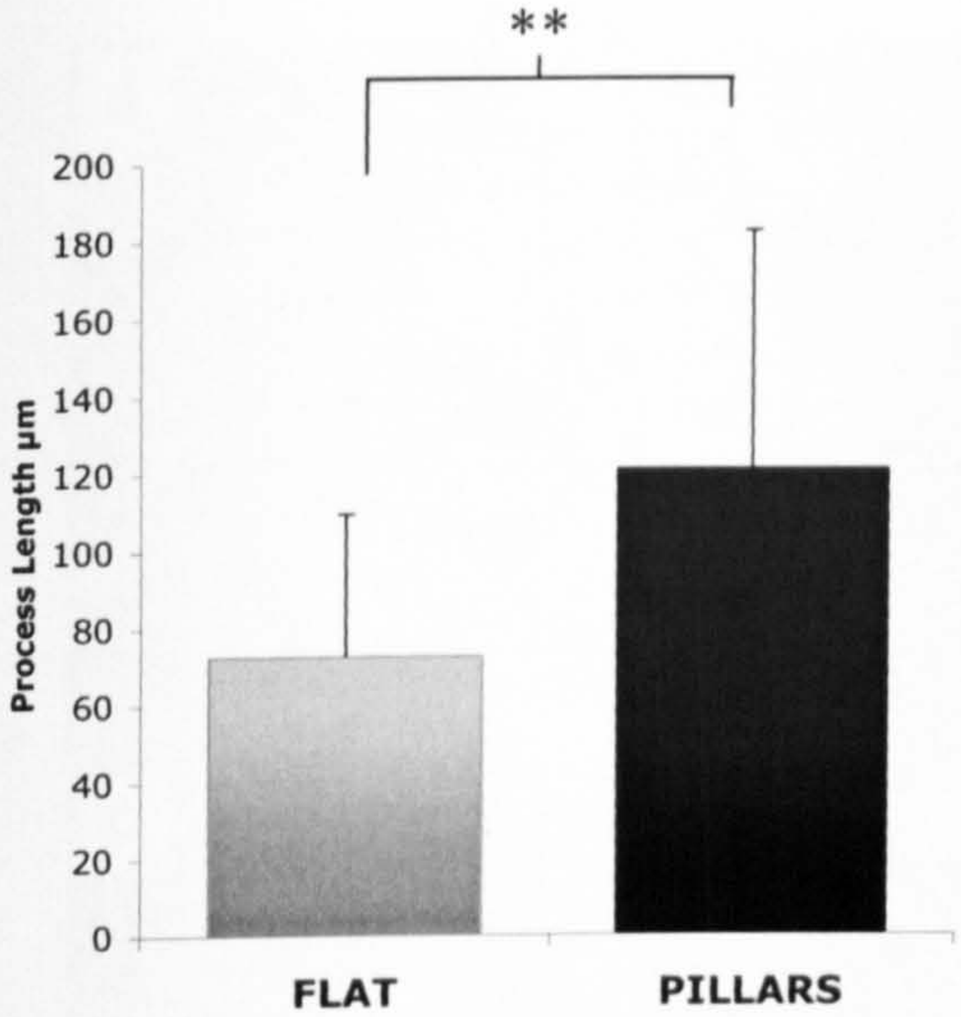

*Graph 5.2. Bar chart showing the mean process length (µm) of cells grown on flat PCL structures in comparison to those grown on PCL nanopillars after 1 week in culture. Results are mean value ± standard deviation, ** denotes a significant different in the result at the 0.01 level of significance as determined by the Student's t-test.*

Investigation of Cell Alignment- Using Coomassie Blue Staining

Embryonic spinal cord neurons were maintained in culture for 1 week, then fixed and stained with Coomassie blue. The angle of process intersection between two overlapping processes was measured. Only the smallest angle created at this junction was used to produce the results presented in Graph 5.3. It is evident from the Coomassie blue staining (see Figure 5.17) that cells grown on PCL pillars are aligning both vertically and horizontally to the underlying lattice matrix, with the average angle of intersection calculated to be 84° ± a standard deviation of 4°.

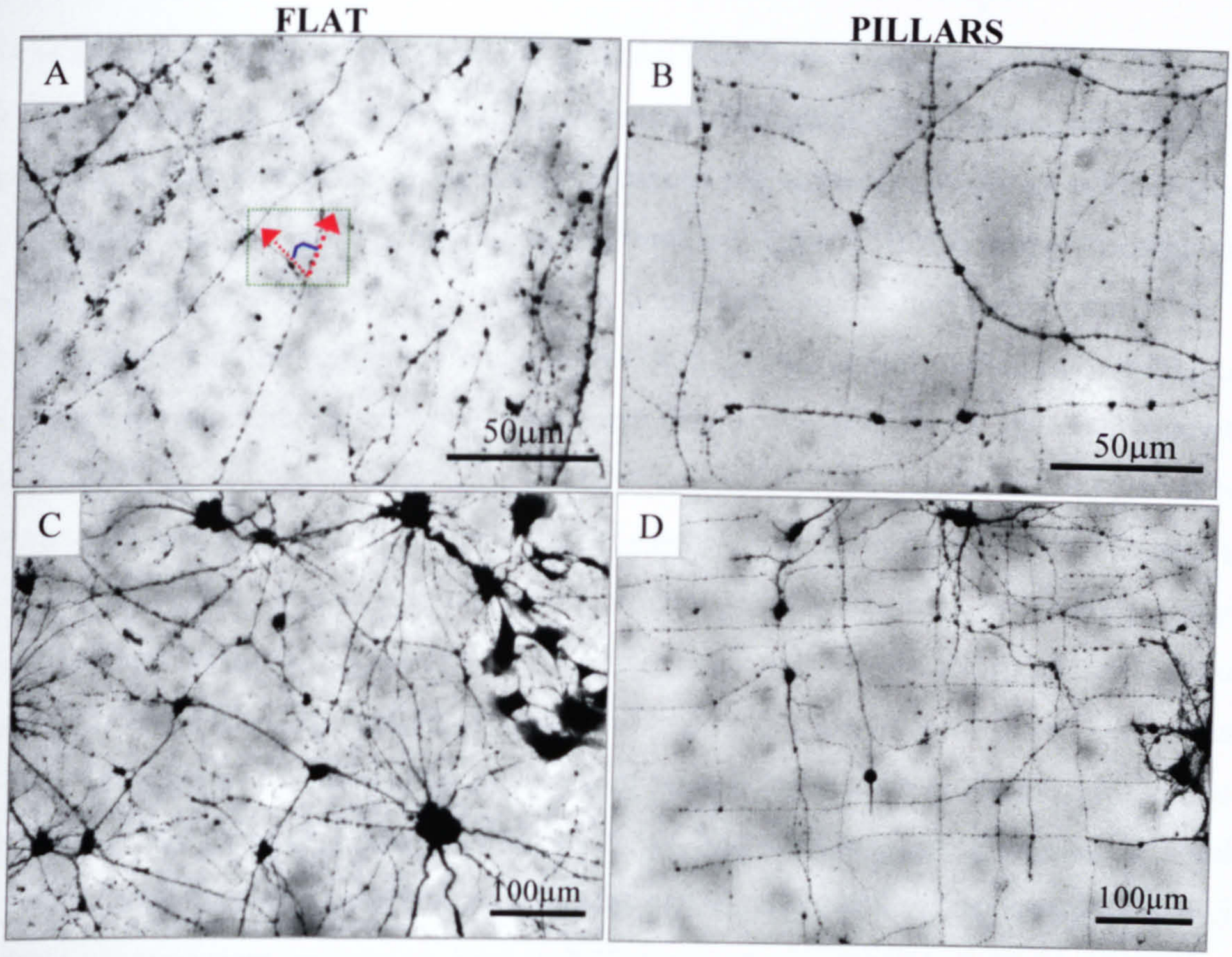

Figure 5.17. Images of embryonic (E14) grown on PCL structures, fixed and stained with Coomassie blue after 1 week in culture. The highlighted area shows an example of the acute angles measured.

.

*Graph 5.3. Bar chart showing the mean angle of process intersection for cells grown on flat PCL structures in comparison to those grown on PCL nanopillars after 1 week in culture. Results are mean value ± standard deviation, ** denotes a significant different in the result at the 0.01 level of probability as determined by Student's t-test.*

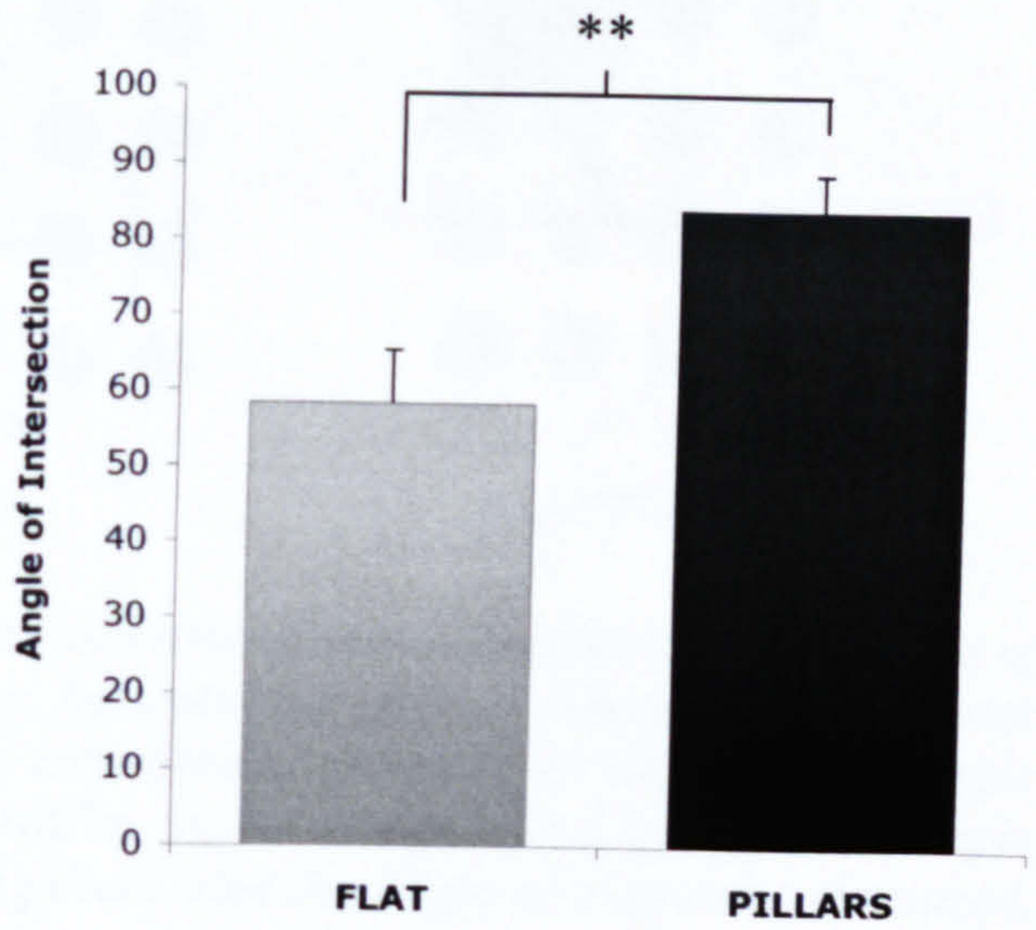

Investigation of Process Alignment- Using Scanning Electron Microscopy

This study aimed to determine how the smallest elements of cell morphology (the fine, short filopodia-like processes, that are often present protruding from larger neurites) were responding to the nanopillar topography. Because the smallest processes evident from SEM imaging were no wider than 300nm, as shown in Figure 5.19.D, a size restriction was applied and only neurites less than 300nm in width were considered for this analysis. It was anticipated that the results presented here would provide more detailed information on how neurons were interacting with the nanotopography, adding to the data already accumulated. SEM images were taken of embryonic (E14) spinal cord neurons grown on PCL nanopillared structures for 1 week. The results are calculated from 20 SEM images at 10kv, 12mm x 30.0k. The proportion of each process growing on top or between the pillars was considered separately (see Figure 5.19.C), a proportion being defined as a section of the process that is growing straight, regardless of the length, discarding all sections that are curved. The angle of alignment and the length of each segment were measured with respect to the axes of the nanopillar array (see Figure 5.18), and the results are presented in Graph 5.4. The results show that over 50% of segments are aligning between the nanopillars, with an angle of alignment measuring 88.6 ± 2.7° (mean ± standard deviation). Segments aligning between the nanopillars were significantly shorter in length (mean length = 899 ± 580 nm) than those aligning on top (mean length = 1356 ± 620nm).

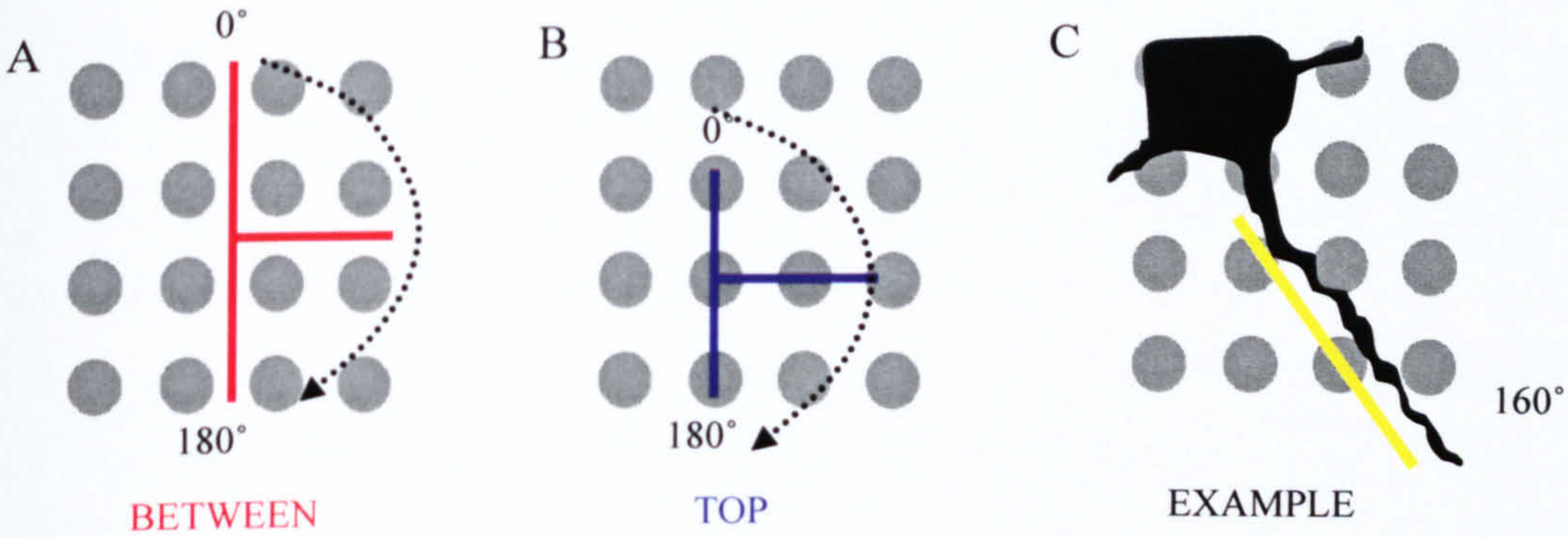

Figure 5.18. Schematic diagram showing the main axis of the nanopattern. The segments of filopodia-like processes that were aligning between the pillars (image A) and those aligning on top of the pillars (image B) were considered separately. In each case the angle of alignment was measured between 0° and 180°as shown. Image C is a schematic example of a process (in black) aligning between the pillars, and the angle of alignment measured, in this case 160°.

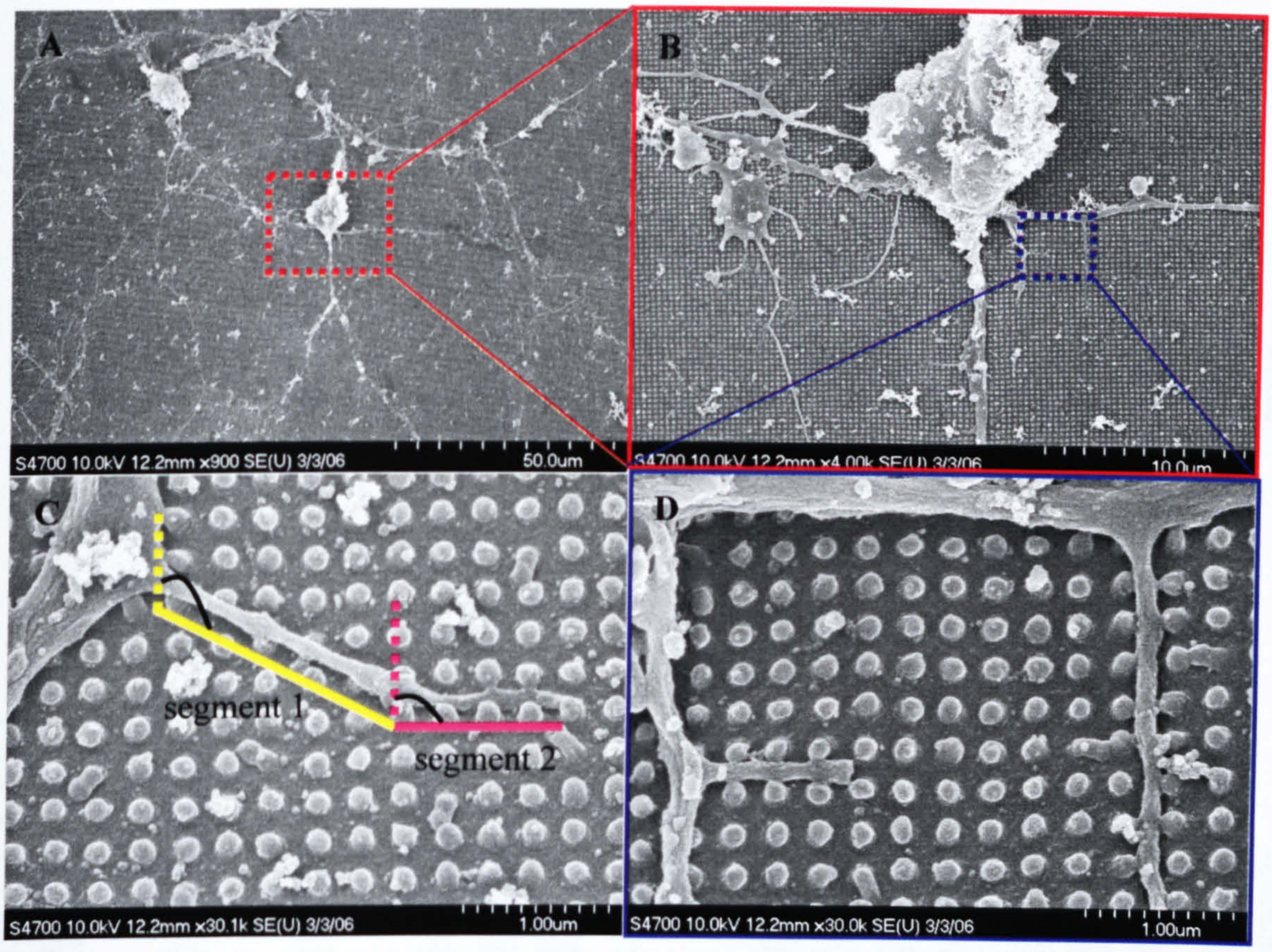

Figure 5.19. SEM images showing neurites aligning to the nanopillar topography. Image C highlights the methods used to produce the results presented in Graph 5.4. Each aligning segment of the neurite was considered separately.

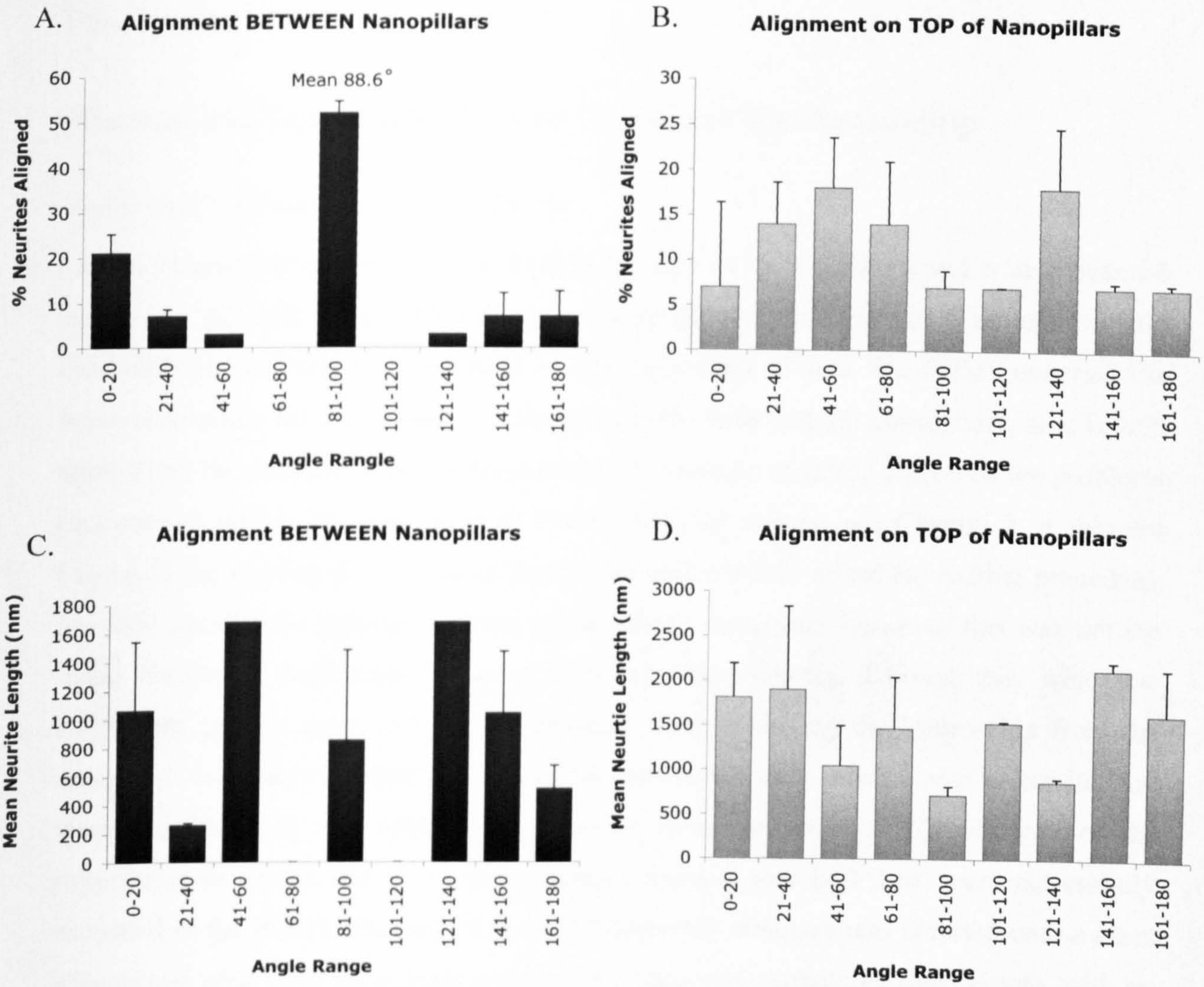

Graph 5.4. Bar charts showing the results calculated from the SEM images. In each bar chart the angle of alignment ranges from 0-180°. The results have been categorised into 9 bins of 20° steps and the mean calculated (± standard deviation). Chart A and C show the results of neurite segments aligning between the pillars, and charts B and D show the results of those aligning on top.

Summary

The Neuro-chip structure, including the micrometric detail of the network pattern, was successfully created in PDMS silicone. Although nerve cells were not aligning to the micrometric grooved topography as predicted, the bridging response that was observed is a very interesting result in itself. Cells did however show a very pronounced response to the nanopillared topography, suggesting a combination of this type of topography with the basic principle of the Neuro-chip may be required if this concept is to be used for neural network studies.

Discussion

Micrometric Topography for Cell Guidance- The Neuro-chip

Neuro-chip Fabrication in PDMS Silicone

For the Neuro-chip design to be functionally possible, it must be fabricated from a material that is gas permeable, as cells grown on the surface of the Neuro-chip structure would eventually be inverted, and maintained so for long periods of time. The PDMS material was selected to allow for the diffusion of O_2 between the cells and the atmosphere, as it is well known that this material is gas permeable (Liu & Sheardown 2005). Based on the problems encountered during the fabrication of PDMS polymer stamps, see Chapter 3, it was not known if the varying dimensions of the master wafer would affect the casting procedure, possibly causing the polymer to bond to the silicon structure. However this was not the case. Structures were easily removed from the silicon master, although they were also easily torn, and so great care had to be taken when removing the Neuro-chip from the master. It was observed that structures 1mm or thicker were much easier to handle, and were less likely to tear when being removed from the wafer. SEM analysis of the supporting structures and the network pattern showed that both had been successfully recreated in the PDMS silicone. When the Neuro-chip structure was inverted onto a glass microscope slide only the contact points of the supporting structures were visible, with no other area of the chip coming into contact with the underlying structure. The idea for developing this cell containment system was that if cells adhered to, and proliferated within the grooved network, the combined dimension of the Neuro-chip supports (5μm height) and the network grooves (5μm depth) would be adequate to provide enough free space for the flow of media between cells and the MEA base, but close enough to make a tight seal between the neurons and the electrodes possible (see Figure 5.20, and Figure 6.11, Chapter 6, for IRM results).

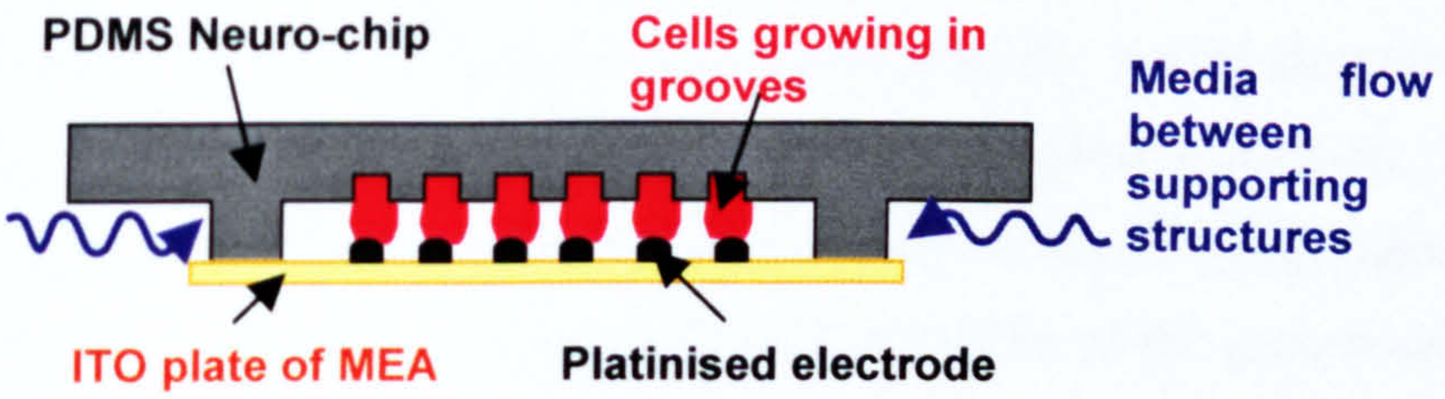

Figure 5.20. Schematic diagram illustrating the proximity between neurons, lying in grooves, and the platinised electrode heads of the MEA device.

Cellular Reaction to the Micrometric Topography

The effect of linear groove and ridge micrometric structures on cell orientation is well documented (Barbucci *et al.* 2003, Clark *et al.* 1990, Clark *et al.* 1991, Curtis & Wilkinson 1997, Mahoney *et al.* 2005, Rajnicek *et al.* 1997, Recknor *et al.* 2006). However, it was not possible to recreate such a result with the PDMS structures. Following the immunocytochemical staining results (see Figure 5.6) it was first thought that the grooved structures of the network pattern had not been successfully created in the PDMS. It was hypothesised that during the release of the Neuro–chip from the silicon master the walls of the pattern had collapsed, sealing the grooves and preventing cells from aligning (Figure 5.21).

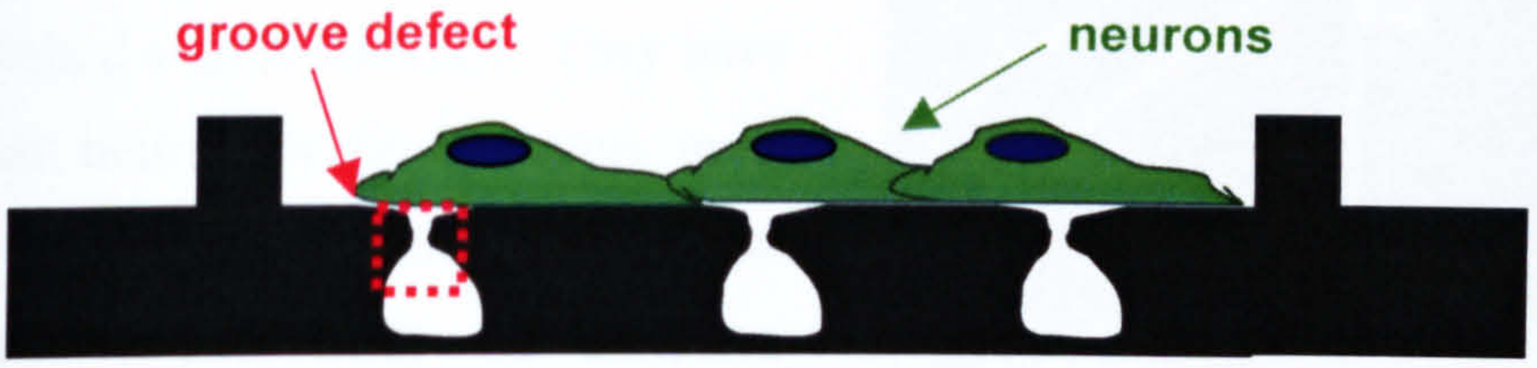

Figure 5.21. Schematic diagram illustrating the possible defect (highlighted in red) that occurred during the fabrication of the PDMS Neuro-chip structure, which would explain the immunocytochemical staining result shown in Figure 5.6.

However SEM analysis of the network pattern in PDMS disproved this theory, as the walled structures of the pattern were clearly open, with no structural defects evident. Although the grooved structures of the pattern were accessible to the cells, it was evident from the SEM analysis that cells were not responding to the topography. In some cases cells appeared to be actively avoiding the grooved area. In Figure 5.7, the process highlighted appears to have proliferated away from the pattern at a point where it has clearly had the opportunity to enter the grooved area, a surprising result considering the observation made in the publications mentioned above. The fact that cell processes were actually bridging the grooved structures was even more surprising. However, it is quite possible that this response is a direct result of the PLL coating. It is feasible that the PLL solution is only coming into contact with the upper section of the walled structures, leaving the lower sections and the floor of the grooves free from any adhesive solution. If the PLL solution failed to penetrate this area, possibly due to air bubbles forming, then it is quite probable that an advancing neurite could not adhere to the floor of the groove causing it to climb back up the wall of the track and span the void, as depicted in Figure 5.22, rather than align within the network pattern.

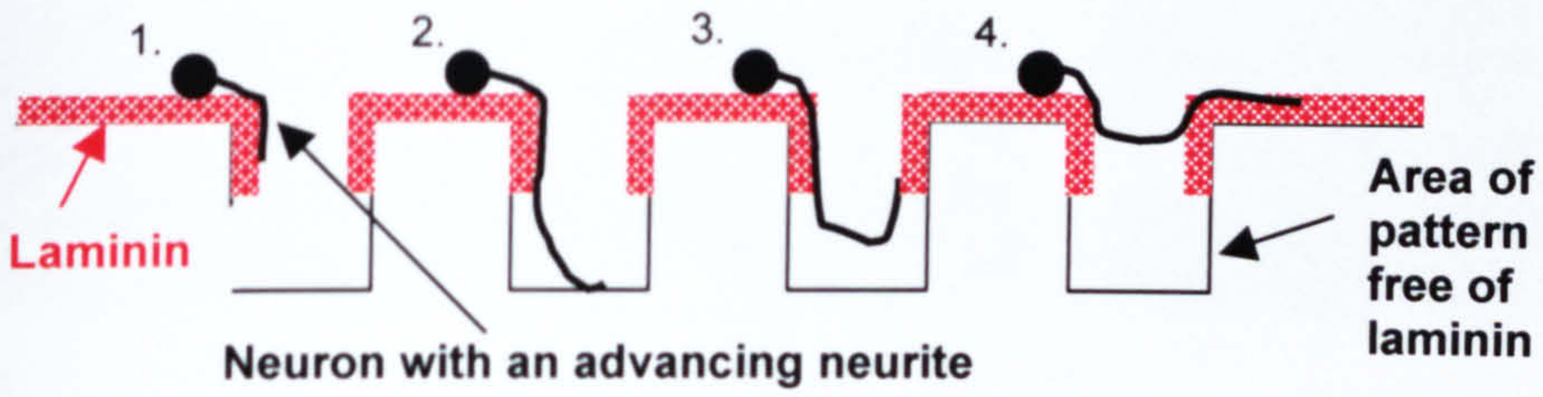

Figure 5.22. Schematic diagram illustrating the possible limitation of the PLL coating. Each step of the diagram shows an advancing neurite and demonstrates the hypothesised cause of neurite bridging.

However in a recent paper, Goldner *et al* have published similar findings. They have shown that neurite bridging occurs even when the floor of the grooves has been successfully coated with an adhesive solution. Although it should be mentioned that in this case the grooved structures were considerably wider, with the width ranging from 30μm to 1000μm (Goldner *et al.* 2006). It was noted that the structure used in this study was similar to the patterned network of the Neuro-chip in the fact that the grooves were lying below the face of the structure, and did not run continuously to the edge of the array (see Figure 5.23.). It could be that this common feature of the two structures could be causing the neurites to form bridges. Considering the majority of cells are adhering to the plateau regions above the grooves, cells landing within the grooves are being driven (possibly by chemotactic mechanisms) towards an area where the probability of forming synaptic connections is much greater due to the increase in cell numbers. Another possibility is that there is a subtle difference in fabrication process used to create the groove/ridge structure in this study and that of Goldner et al, compared to the methods used in the previously mentioned publications. In both the Mahoney (Mahoney & Anseth 2006) and Recknor (Recknor *et al.* 2006) papers a micrograph of the structure edge is given (see Figure 5.24); this is clearly different from structures shown in Figure 5.23. This leads to the question, can cells respond differently to a 'ridged' structure, like that shown in Figures 5.24 and 5.25.A, compared to the 'grooved' structures shown in Figures 5.23 and 5.25.B, the structure used in this study and that of Goldner?

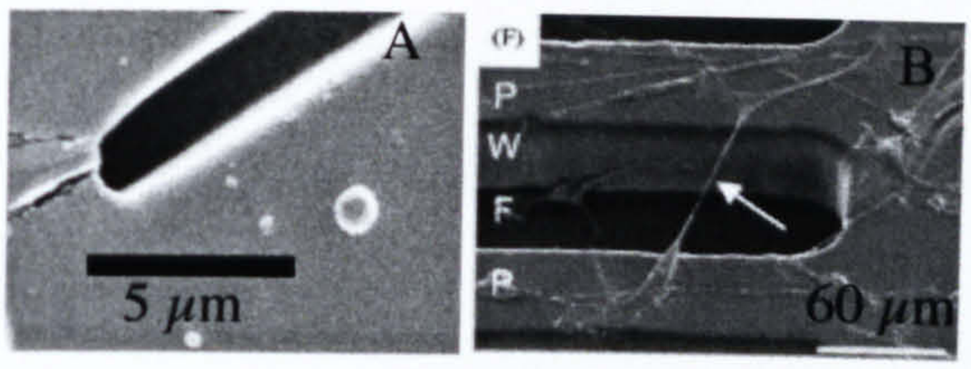

Figure 5.23. SEM image of the edge of the network pattern of the Neuro-chip (A). Note that the groove does not run to the end of the structure. Image B is taken from Goldner et al. 2006 and shows the edge of the structure in their study.

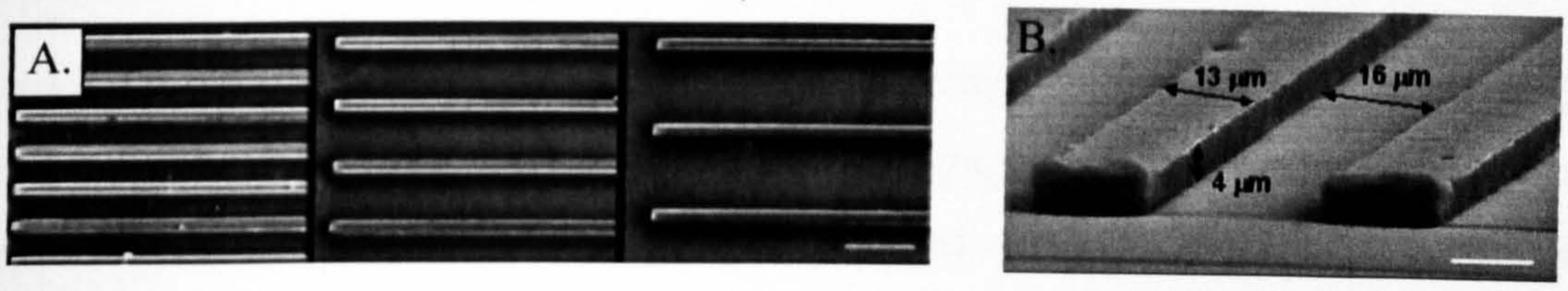

Figure 5.24. SEM images showing the edge groove/ridge structure used in the studies conducted by Mahoney & Anseth 2006 (A) and Recknor et al, 2006. The channels have been created by series of parallel tracks protruding from the surface of the structure. The scale bar in image A is 50µm and in image B, 10µm.

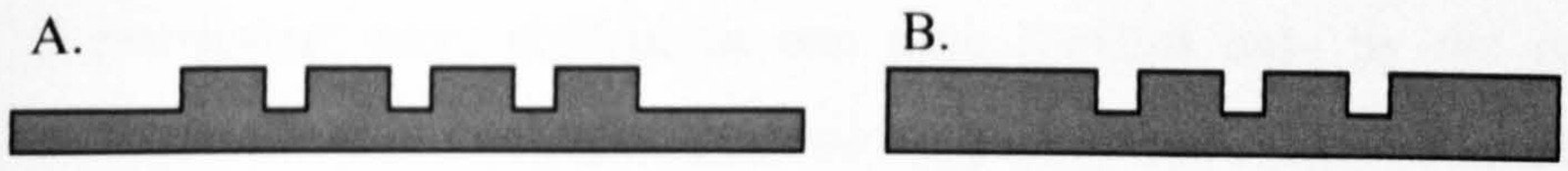

Figure 5.25. A schematic diagram showing the different ways to fabricate a simple groove/ridge structure.

However regardless of the formation of the grooves/ridge structure the ability of processes to span the grooves, and even wider node areas, has profound implications on the future of the groove/ridge construct as the foundation of 3-dimensional scaffolds for the tissue engineering approach to axon guidance. The fact that this fundamental groove/ridge design is the primary pattern that has carried over into the 3-dimensional neurite guidance studies, the viability of such structures is questionable. With the case of neurons, is a more detailed design, where cells can occupy a 3-dimensional space more akin to their arrangement observed *in-vivo,* required?

Conclusion

Despite the dimensions of the micro-metric grooved structure having been derived from previous publications that have shown neuron alignment, no such results were produced from this study. Cells, nor their processes grew within the patterned tracks; the processes that did encounter the grooved topography did not align to it, but extended over the void to the plateau region beyond.

Nanometeric Topography- Nanopillars

Given that cells were not responding to the micrometric topography, it was decided to investigate the response of cells to nanometric topography with the aim of introducing this to the Neuro-chip structure if a successful result was obtained. Based on results recently published by other members of the CCE group (Martines *et al.* 2005, Seunarine *et al.* 2006), I investigated the cellular response to a regular nanopattern of pillared topography.

Fabrication of Nanopillars in PCL

The technique used to fabricate the PCL nanopillared structures was a cheap and quick method of embossing many replicas at one time (limited only by the cooling period required to release the master sample, approximately 20 structures could be replicated in 20 minutes). However, SEM imaging showed the resulting structure was not 100% accurate with, on average, 30% of the topographical area having some structural defects. Although this left a substantial area of the nanopattern available for cell analysis, if further experiments were to be conducted it is advised that a more refined method of embossing is developed.

Effect of Nanopillars on Cell Adhesion

Coomassie blue staining was used in this study as a quick and simple method of investigating large areas of cell adhesion. From the overview photographs it was obvious that the area covered with nanopillar topography was almost completely free of staining, and hence protein or cells. A total of 10 structures were tested in this manner, all of which produced the same response (see Figure 5.12). An attempt was made to use immunocytochemical staining to identify the relative percentage of neuron and glial adhering to each topographical area. However image analysis of the stained structures proved difficult due to the varying thickness and dimensions of each individual PCL structure (all samples were not uniform, with varying degrees of 'thickness' across the entire structure). Due to this nature of the structures it was difficult to focus on a selected area, and during the time it took to focus on the cells in question, the lack of mounting sealant made the fading of the fluorescent stain a limiting factor. However, from observation made during fluorescence microscopy and from the only useable image captured, it was apparent that the adhesion of both the neurons and glial was reduced within

the area of the nanotopography. From these images, a quantification of cell adhesion on the nanopattern (as shown in Figure 5.14) was made using a cell count based on identifying cell nuclei by means of the DAPI stain. The bar chart in Figure 5.14 shows that a greater number of cells/area are adhering to the flat PCL in comparison to the nanopillars. This anecdotal evidence is in support of the results obtained using Coomassie blue staining and on its own is not being considered as significant.

Effect of Nanotopography on Neuron Morphology

Due to the fact that the results obtained with immunocytochemical staining were very limited, Coomassie blue staining was used in this study to identify the effects of nanotopography on gross neuron morphology. It was quite obvious from the Coomassie blue staining that the PCL topography was affecting the overall dimensions of the neuron structure. Cells grown on the flat PCL were displayed neuronal morphology typical of primary cultured neurons, showing highly branched dendritic processes, and a longer distinctive axon (as determined by the presence of the conical region of the axon hillock, (Levitan & Kaczmarek 2002, Pannese 1994). Cells grown on the nanopillars had developed relatively the same number of initial processes, however they did display less dendritic branching. This changed the overall morphology of the cells considerably. As well as the dendritic structure being affected, the axons of cells grown on the nanopillars had developed differently, by growing significantly longer compared to that of cells grown on the flat PCL (see Figure 5.16). It is well documented that cells grown in the presence or absence of neurite growth promoting proteins, such as laminin, Robo and N-cadherin, exhibit different cell morphologies similar to the results obtained in this study (Bixby & Jhabvala 1990, Hivert *et al.* 2002, Matsuzawa *et al.* 1996, Sobeih & Corfas 2002, Stoeckli *et al.* 1991). One possible explanation for the result presented here, is that, although the topography itself was reducing overall cell adhesion, the nanopillar array was in fact increasing the overall surface area to which PLL could bind to. It could be that the increase in the polycation binding to anionic sites on glycoproteins and proteoglycans that are present on the cell surface, is facilitating neurite proliferation (Sorribas *et al.* 2001), although future studies should aim to correctly identify the exact mechanisms through which this result is occurring. However, the physical interaction between the small neurites and the nanopillars, which is highly evident in the high magnification SEM images (see Figure 5.26), suggests various other adhesion-mediated signalling pathways are possibly being activated.

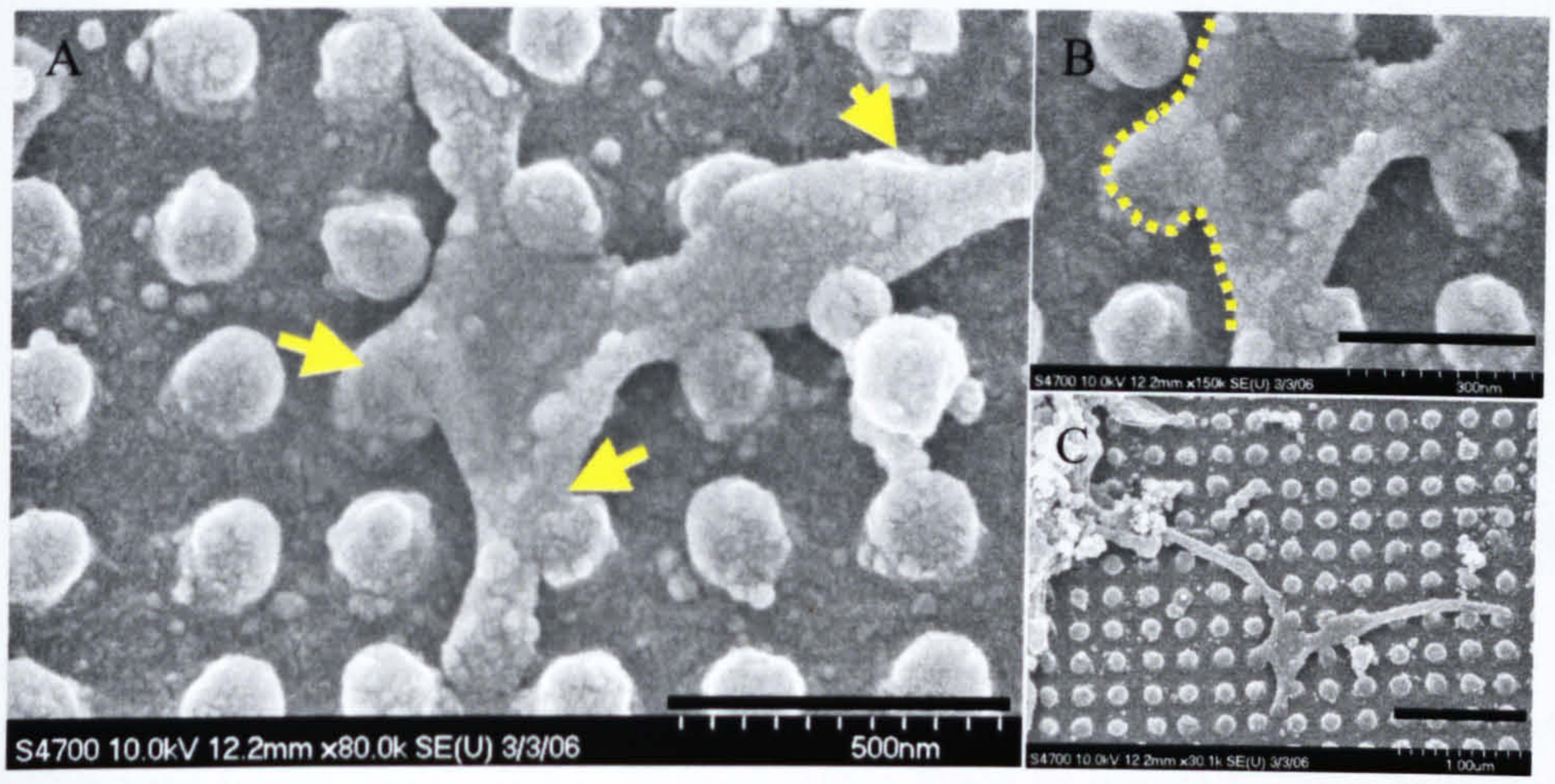

Figure 5.26. SEM images showing the physical interaction between an advancing neurite and the nanopillar topography. The arrows in image A indicate a cell and pillar associations. Image B highlights the edge of the neurite membrane overlying a nanopillar and image C shows the process at a lower magnification. Scale bars are 500nm (A), 300nm (B) and 1μm (C).

Cell Alignment to the Nanopillar Topography

The qualitative and quantitative results presented in this study, are highly supportive of the fact that cells are aligning to the linear array of the nanopattern. Taking only the smallest angle into account, the average angle of process intersection (where two processes meet) was calculated to be 84° for cells grown on the nanopillars, only 6 degrees off a perfect 90° alignment. This result was determined from the Coomassie blue stained images at x20 magnification; therefore this is a measurement of large processes of micrometric scale. Since the topography is of nanometric dimensions the mechanisms through which the larger processes are aligning could be attributed to simple cell adhesion properties. It has been well established that formation of focal contacts, specialised adhesion sites formed between cells and the underlying extracelluar matrix, can be influenced by altering the cell surrounding nano-environment (Dalby *et al.* 2004b). Such associations occur in neurons through the interaction of cell adhesion molecules (CAMs) to components of the extracellular matrix (ECM) or cell adhesion sites on neighbouring cells (Bixby & Jhabvala 1990, Rader *et al.* 1993, Skaper *et al.* 2001, Sobeih & Corfas 2002, Suter *et al.* 1998). It could be that as the process or axon advances along the substrate, focal adhesions are occurring as the cell encounters the nanopillars with the effect of aligning the process to the nanopattern (see Figure 5.27.) resulting in the effect shown in Figure 5.17. However, the mechanisms through which these focal contacts are occurring must be further investigated.

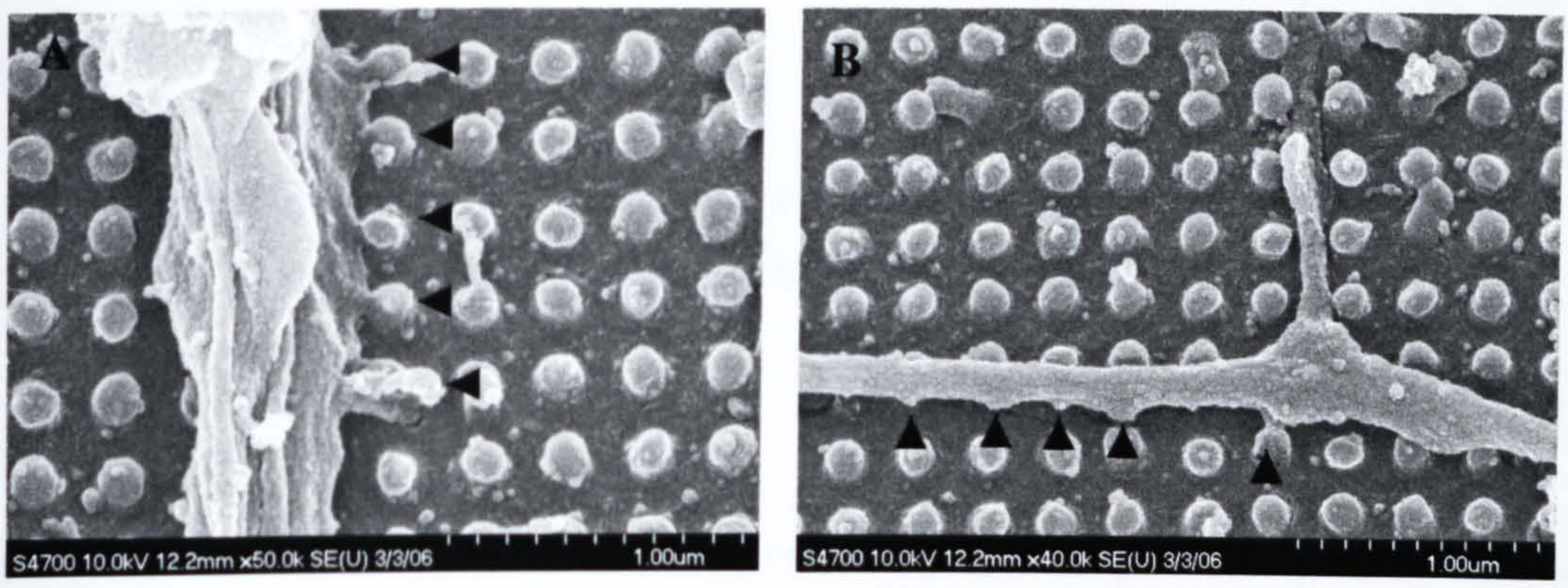

Figure 5.27. SEM images showing the alignment of a larger processes to the edge of the nanopillar array. The arrows in each image indicate what appears to be the formation of focal adhesions to the nanopillars. It is possible those in image B have been broken during the freeze drying process.

Not only were large processes observed to be aligning to the nanopattern but also small filopodia-like processes, identified by scanning electron microscopy. Extending from both dendrites and axons, these structures (approximately 100-200nm in width) were aligning both between, and on top of the rows of nanopillars. It would be interesting to investigate whether the presence of the nanopillared topography was in fact increasing the number of the filopodia-like processes seen in this study, as it has been suggested that these processes actively initiate synapse formation by being precursors for dendritic spines. (Annies *et al.* 2006, Takahashi *et al.* 2003). Further studies investigating the effect of nanopatterns of vary geometries on spine configuration may also yield interesting results, as there is now growing evidence to support the theory that dendritic spine geometry is a major determinant of synaptic transmission at excitable synapses (Roelandse *et al.* 2003).

Conclusion

Although this study has produced conclusive results as to the response of spinal cord neurons to nanopillared topography, there are still many questioned that need answered: the biological mechanism and signalling pathways through which this response is occurring is paramount in determining what future such a topography has in neural tissue engineering.

Chapter 6.

The Application of Multi-electrode Recording Devices to Investigate Neural Network Behaviour

Abstract

Information is conveyed within a neural network by alterations in signal transmission. Signal firing rate and amplitude are key components of the network code. To understand how such elements contribute to network function multi-electrode array (MEA) devices were used to record activity from randomly distributed neural networks, with the aim of comparing their activity to networks growing within a spatially organised pattern. Two devices were tested, the flexible MEA, which records cells from above, and the planar MEA, which records cells from below. Random network cultures were found to be spontaneously actively, and displaying rhythmic burst firing patterns. Unfortunately good signals could not be obtained from cultures grown in geometric patterns, and therefore a comparison of firing activity in random networks, and organised networks, could not be made.

Introduction

Electrophysiology refers to the recording of the electrical properties of living cells and tissues. There are two major types of electrophysiological recording systems, intracellular electrophysiology and extracellular electrophysiology, which are classified by the position of the electrode in relation to the neuron during recording (Kuffler *et al.* 1984). Intracellular electrophysiology, which includes the voltage clamp and patch clamp systems, involves the use of micro-electrodes that penetrate the cell, where as extracellular electrophysiology consists of the recording of electrical activity by electrodes placed outside the cell.

Intracellular electrophysiology has been the predominant recording system in the history of neurophysiology. The voltage clamp was the method used in the pioneering work conducted by Hodgkin and Huxley in the UK in 1939, and Curtis and Cole in the USA in 1940, to determine the ionic mechanisms responsible for generating nerve impulses (Brown 1991). Using this method the cell membrane potential can be maintained at a particular voltage allowing ionic current flow to be investigated. This system has been fundamental in characterising the sodium and potassium currents that are responsible for the action potential waveform as shown below (see Figure 6.1).

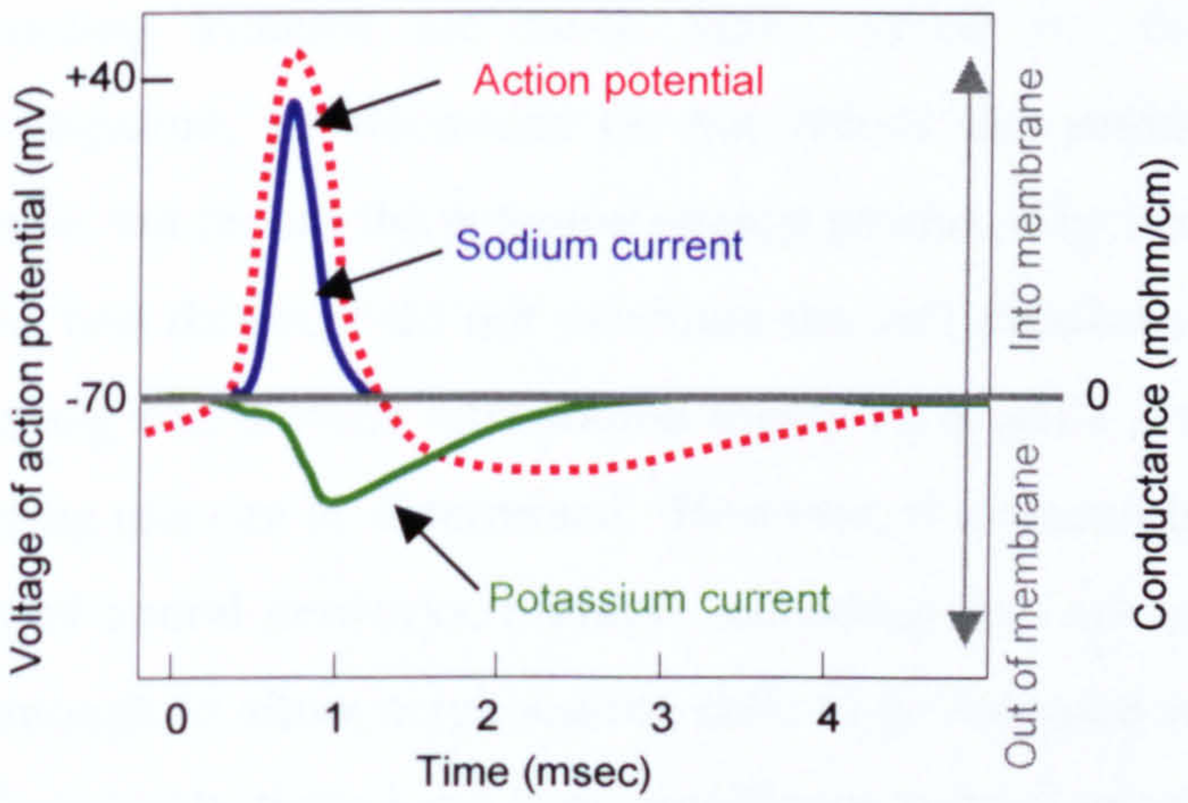

Figure 6.1. Schematic diagram showing the sodium and potassium currents that are responsible for the action potential wave form.

Using the patch clamp technique the ionic conductance through individual ion channels can be investigated. This method differs from voltage clamp, as slightly larger electrodes are employed, and once in contact with the cell, gentle suction is applied drawing a section of

the membrane into the electrode pore. This results in creating a high resistance seal between electrode and cell (see Figure 6.2). Unlike voltage clamp, this method creates a circuit with the small section of the membrane rather than the cell as a whole (although whole-cell configurations can also be formed), allowing the investigator to study single ion channel physiology. Both these intracellular recording methods have played a significant role in the study of pharmacological compounds and the effects these have on both membrane and channel conductance. However in both set-ups there is a limit as to how many cells can be studied simultaneously and for how long experiments can be conducted, as the physical damage caused by the intracellular electrode can kill the cell within an hour of starting the experiment (Curtis *et al.* 1994). Although studies investigating network activity have used intercellular recording methods to identify network activity (Vogt *et al.* 2005), such limitations rule out this type of elctrophysiology for the study of multiple cells over long periods of time.

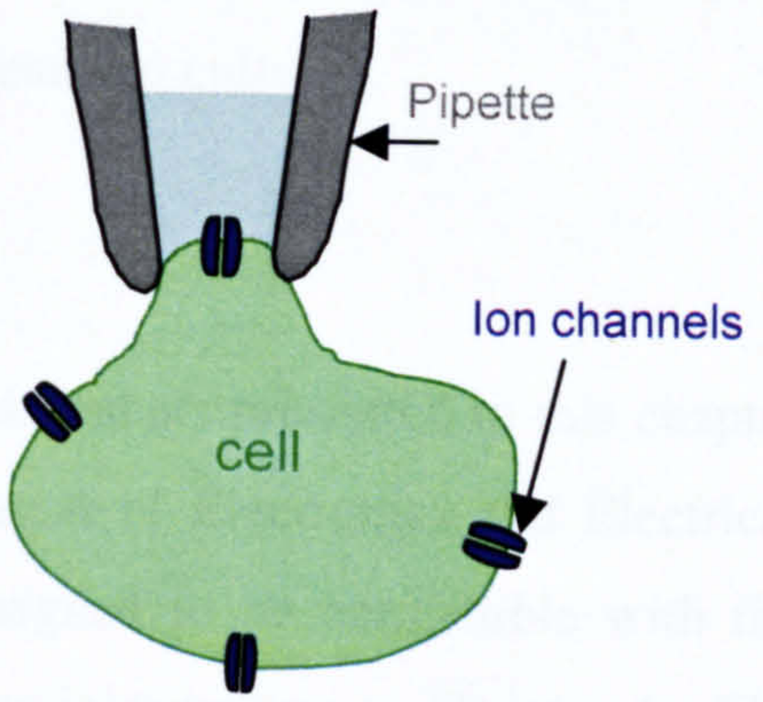

Figure 6.2. Schematic diagram illustrating the patch clamp principles. Once the pipette is in contact with the cell, suction is applied through the electrode creating a seal.

Extracellular recording systems are much better suited for this particular area of neuroscience investigation, as electrodes do not record the potential change occurring across the membrane, but record the potential change produced by local currents outside the active cell or fibre, and therefore do not penetrate the cell membrane (Curtis *et al.* 1992). This type of recording can provide information regarding a cell's active state, and if a cell is activated, the firing rate can be determined. However, if extracellular electrodes are to be used for the study of neural networks, multiple recording sites are required and electrodes have to be small enough to allow neighbouring cells to be recorded without electrode cross talk occurring. Fortunately there have been significant technological advancements in the microelectronics industry since the first design for the multi-electrode devices surfaced 20 years ago. Electrodes can now be fabricated to submicron dimensions (Kashimura *et al.* 2003), can have both stimulatory and excitatory properties (Jimbo *et al.* 2003), and can be of varying array designs (Berdondini *et al.* 2005, Hempel *et al.* 2002, James *et al.* 2004) and electronic concepts (Fromherz 2003, Jahnsen *et al.* 1999, Spence *et al.* 2003). At The

Centre For Cell Engineering we fabricated two very distinct electrode arrays, both of which have been specifically designed to work with patterned neuronal cultures.

The Planar Multi-Electrode Array

The planar multi-electrode array (MEA) used for the experiments presented in this chapter was designed and fabricated by Rongyu Tang, Department of Electronics and Electrical Engineering, Glasgow University. The device was designed to be compatible with the original '*Jude*' network pattern, which is described in the introduction to Chapter 4. The array consists of 64 electrodes, which have been spatially arranged to directly correspond with a cell body adhesion site (node region) when the network pattern is superimposed as shown in Figure 6.3.A.

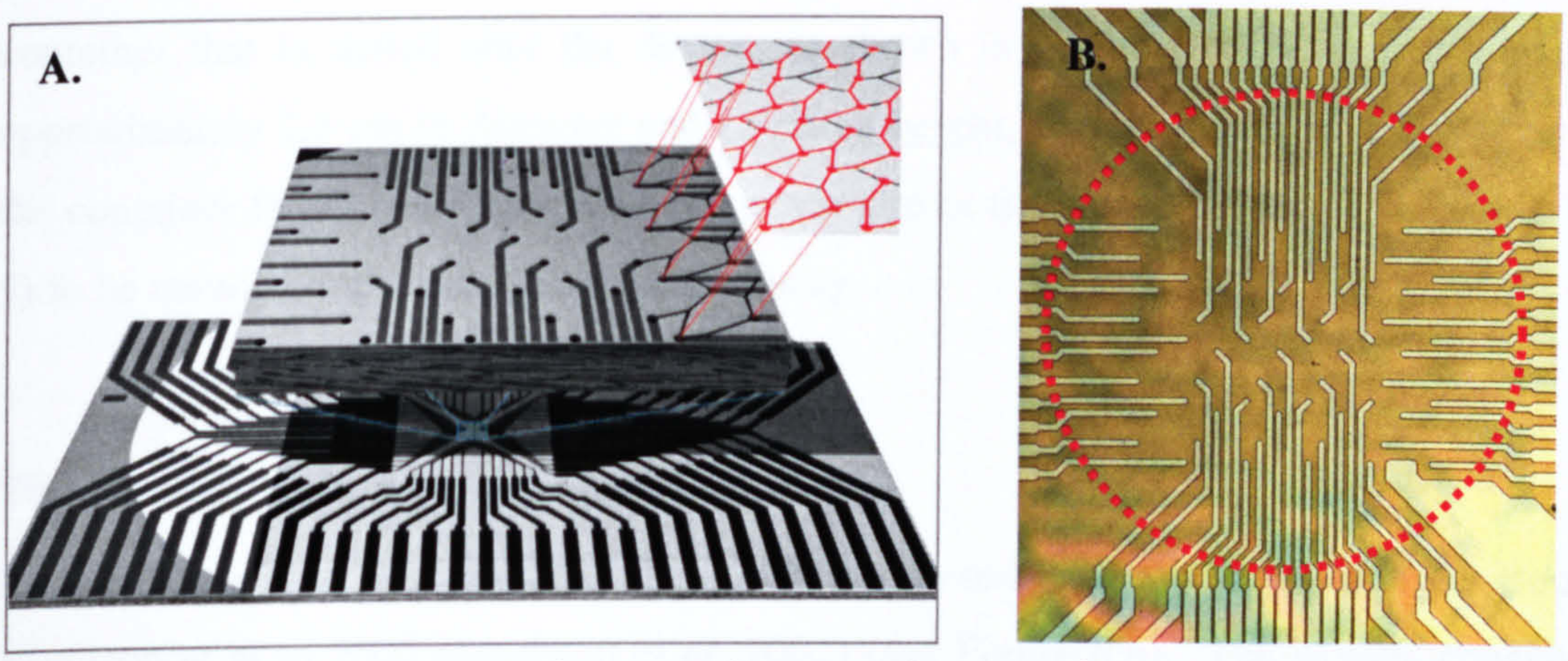

Figure 6.3. Image A is a schematic diagram showing the correlation between the neural network 'Jude' pattern and the design of electrode array on the planar MEA device. Once the pattern is superimposed, each electrode will lie directly bellow a node region. Image B is a phase contrast pictograph of the fabricated array, with the red highlighted area showing the cell container.

Image 6.3.B shows an example of the unfinished electrode array taken during the fabrication process, prior to the platinising of the electrode heads. The lines extending into the centre of the array are the gold wires, which have been deposited onto the substrate through a resist mask, and then defined by lift-off. The underlying quartz substrate has been coated with a thin layer of silicon nitride resulting in a transparent device that allows the positioning of cells to be closely monitored. Each gold wire finishes in a platinised electrode head approximately 20μm in diameter (Figure 6.4).

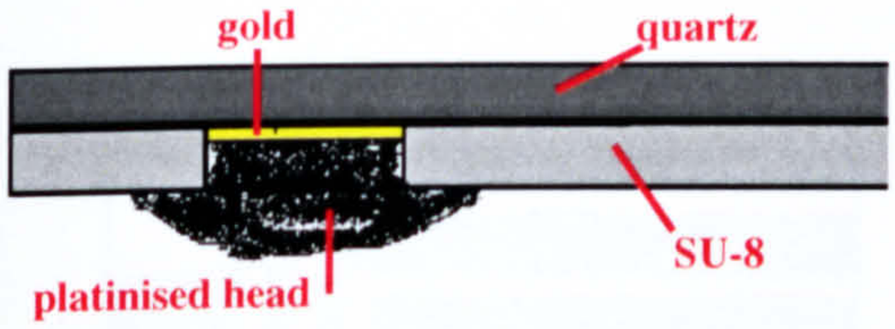

Figure 6.4. Schematic Diagram showing a cross section of platinised electrode head. The top layer of the diagram depicts the quartz substrate, and the lower grey layer is the SU-8 insulator. The yellow layer is the gold wire with the platonised electrode head shown in black.

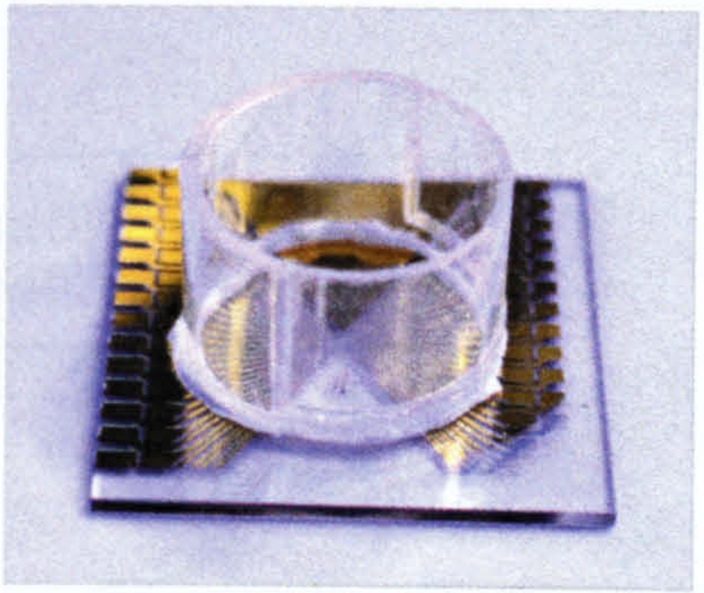

Figure 6.5. Photograph showing the MEA with the cell container sealed onto the device.

The electrode array (highlighted in Figure 6.3.B) is surrounded by a circular plastic cell container that is sealed onto the device, as shown in Figure 6.5. This cell container is approximately 2.5 cm in diameter and 1.5cm in height, providing enough free space within the container to allow a 13mm diameter cover slip or the Neuro-chip structure (see Chapter 5) to be manoeuvred across the electrode array.

The Flexible Multi-Electrode Array

Rongyu Tang also fabricated the flexible MEA, based on the initial design developed by Sandison et al in 2002 (Sandison *et al.* 2002) (see Figure 6.6). The device, consisting of eight electrodes connected by gold wires, has been fabricated onto a polyimide film. This device has been designed for the recording of cells from above, and has been mounted onto a micromanipulator allowing it to be positioned above an area of interest. Flexible polyimide film has been bent and fixed into a crescent, with the electrodes at the lowest point (see Figure 6.6.C). This ensures a tight seal can be made at the electrode-cell interface without damaging the cells or the device as the electrodes are brought into contact with the cells.

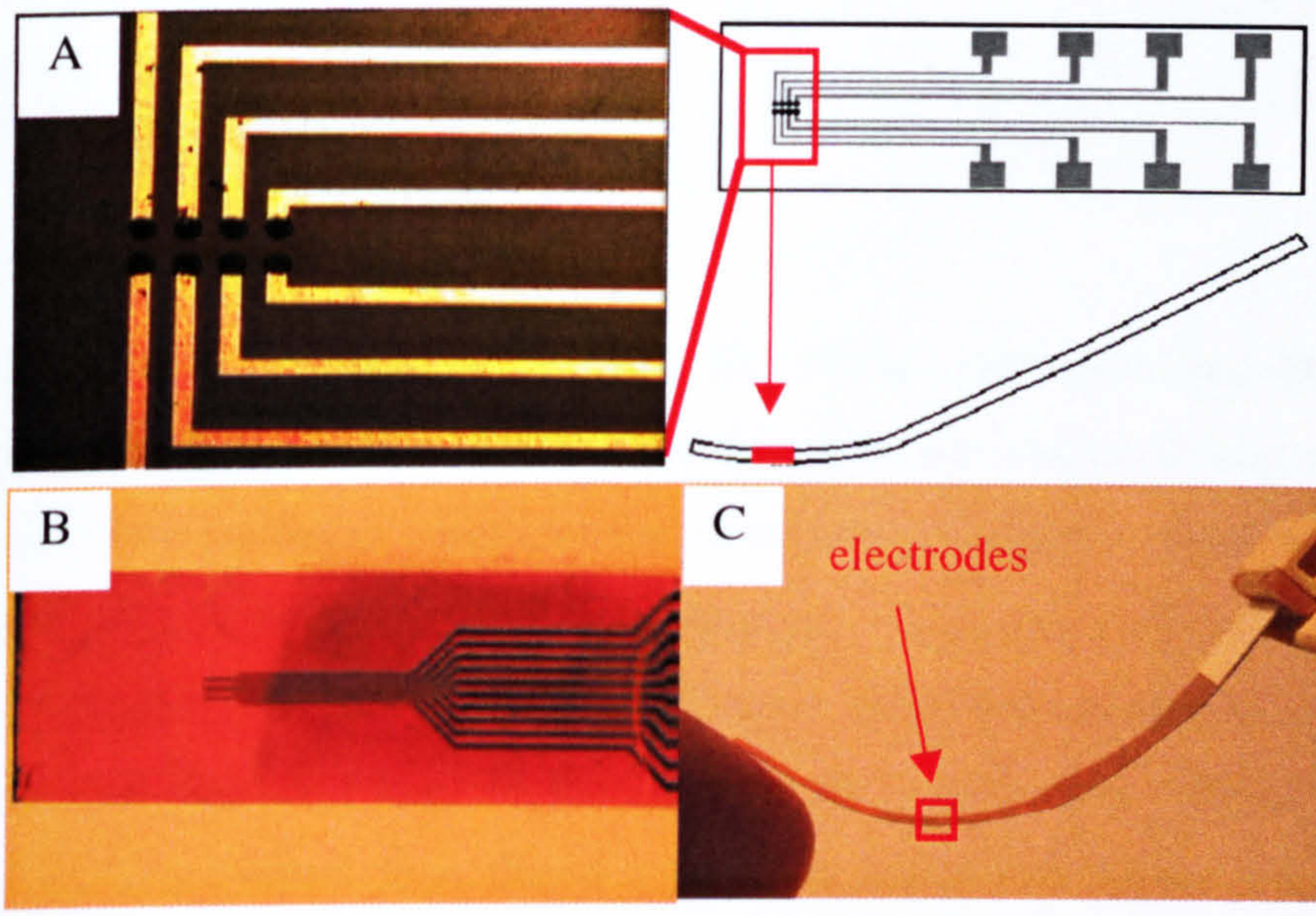

Figure 6.6. Image A is a phase contrast image arrangement of the eight electrodes and a schematic diagram showing where they are located on the device. Image B is an overview photograph of the polyimide film and Image C the crescent shape it is mounted into for recording.

Summary

Dissociated cardiomyocyte cultures will be used to test both MEA recording systems. Once optimised, both systems will be used to record the spontaneous electrical activity of random spinal cord cultures, with the aim of comparing this to the activity of organised networks.

Materials and Methods

Cardiomyocyte Cultures

Substrate Preparation

Cells were grown on glass cover slips, flat PDMS substrates and PDMS Neuro-chip structures. Glass cover slips (13mm dia) were cleaned in Caro's acid (3 parts sulphuric acid, 1 part 30% hydrogen peroxide) for 15 minutes, washed 3 times in sterile RO water before being stored in 70% ethanol until required. To remove all traces of ethanol, cover slips were stored in sterile RO water for 48 hours, then blow-dried with sterile particle-free compressed air and then kept in the oven at 60°C overnight. PDMS structures were sterilised in 70% ethanol then rinsed 3 times in sterile RO water. All substrates were coated with 100 μg/ml fibronectin (made up with sterile PBS) for 1 hour at room temperature, then washed once with sterile RO water to remove all unbound protein.

Cell Isolation

For each preparation four neonatal Sprague Dawley rat pups aged between 1-3 days (supplied by Biological Services) were killed by barbiturate overdose according to Home Office guidelines. Each pup was pinned face up on a dissection board, then washed in 70% ethanol to minimise contamination. The rib cage was removed using dissecting scissors, and the exposed heart was isolated using a sterile scalpel blade to severe all connecting vessels. The hearts were collected in a Petri dish (stored on ice) containing ice cold HEPES saline. Once the last heart had been isolated, all were washed 3 times using HEPES saline to remove all erythrocytes. The collected hearts were then transferred to a fresh Petri dish (containing no solution), where they were finely chopped using a sterile scalpel blade (No.10 blade). The chopped tissue was then digested in 0.25% trypsin solution for 15 minutes at 37°C. Five millilitres of 10% foetal calf serum (FCS) solution was added to stop enzymatic digestion, cells were then centrifuged at 1500 rpm for 4 minutes and the pellet resuspended in growth media (86mls DMEM, 10ml FCS, 2ml antibiotics solution, 2ml insulin transferrin selenite (ITS)). The cell suspension was triturated approximately 10 times to break up remaining tissue fragments, then left to stand for 2 minutes allowing un-dissociated tissue fragments to settle (which were then removed using a Pasteur pipette, and then discarded). Cells were plated, at a density of 3000 cells/mm^2, and left to adhere for 1

hour at 37°C. After this time all unstuck cells were removed by exchanging the media twice. Cells were then returned to culture in 2 ml fresh Growth media, at 37°C in 5% $C0_2$, with growth media changed every 5 days. Cultures were maintained until cells were visibly contracting, and then used for electrophysiological experiments.

Video Microscopy

Cardiomyocytes activity was monitored using video microscopy. The cells were viewed using a Zeiss Axiovert 25 microscope (Ziess Ltd, Hertfordshire, UK) and activity was recorded at real time using a CCD video camera (model CV-M50 supplied by Alrad Instruments Ltd, Newbury, UK) connected to a Panasonic AG-6730 Time Lapse Video Recorder (Panasonic, Berkshire, UK), run in the 3h mode.

Spinal Cord Cultures

For a detailed description of spinal cord culture methods please refer to Chapter 2. Cells used for electrophysiology were cultured on PDMS Neurochip structures (with and without topographical guidance); see Chapter 5, *Materials and Methods, Fabrication of PDMS Neurochip* for method descriptions.

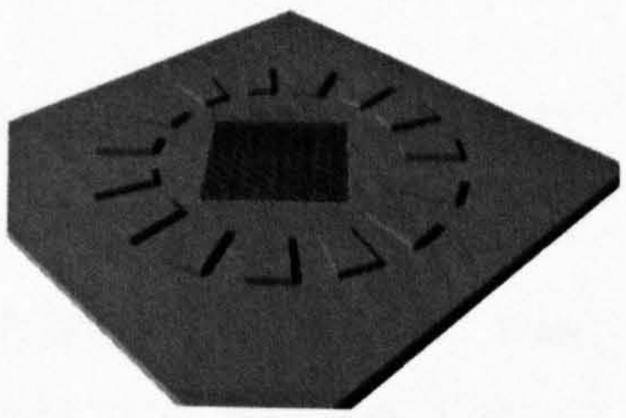

Figure 6.7. Image illustrating the design of the Neuro-chip structure, which was fabricated in PDMS

Electrophysiological Recording

Cell Preparation

The methods used to prepare neuronal and cardiomyocyte cultures for electrophysiological experiments were the same. Firstly, the extra-cellular recording solution (see Table 6.1) was preheated to 37°C in a warm bath. Cells were removed from incubation and then washed twice with recording solution to remove all traces of growth media before being incubated in 2ml of recording solution for 30 minutes at 37°C. After this time cells were ready for electrophysiology. During experiments the recording solution was exchanged every 30 minutes.

Table 6.1. Table listing the reagent composition of the recording solution used in all electrophysiological experiments. The reagents were dissolved in sterile RO water, mixed for 5 mins then brought to a pH of 7.3 using 1M NaOH.

REAGENT	Conc. (mM)
KCl	5
NaCl	150
Magnesium Chloride ($MgCl_2$)	1
HEPES	10
Calcium Chloride ($CaCl_2$)	2.5
Glucose	10

Recording Set-up

Both recording devices were designed and fabricated by Rongyu Tang, Department of Electronics and Engineering, University of Glasgow. Fabrication Methods will not be described here but will be available for reference in his thesis, which will be submitted to The Department of Electronics and Electrical Engineering.

i. Planar MEA Device

The electrode device, mounted onto a Motic AE31 microscope (Motic Instruments Inc. BC, Canada) was connected to a PC (Viglen "Genie" Pentium 4) via a Digidata 1322A digitiser (Axon Instruments, Molecular Devices Ltd, Berkshire, UK). The recording chamber was rinsed once with 70% ethanol for sterilaisation, then rinsed 3 times with RO water, then once with recording solution leaving 2ml of recording solution in the chamber. Cells used in conjunction with this system were grown on PDMS structures, which were then inverted onto the array for recording purposes. During recording, cells were maintained at 37°C using a hot-air system (this was built by the Departmental workshop, IBLS Support Services). After each session the cells were removed and chamber washed with RO water, then 70% ethanol and then covered with parafilm.

ii. Flexible MEA Device

The Flexible electrode was mounted onto the stage of the microscope using a micromanipulator. The device was connected to a PC via the Digidata 1322A digitiser. Once all recording equipment was switched on, the MEA was submerged in a Petri dish containing recording solution and noise levels optimised. Cells were grown on glass cover slips, and were kept in a Petri dish for the experiments, during which cells were maintained at 37°C using a heat stage (Link Am Scientific Instruments, Surrey, UK). The electrodes were brought into contact with the cells using the manipulator, and guided into position by observing the progress through the phase microscope on which the devise was mounted.

Results

Planar and Flexible MEA Testing

Cardiomyocyte Cultures

Actively and spontaneously contracting cardiomyocytes were successfully maintained in culture for up to 2 weeks on glass cover slips, flat PDMS structures and the PDMS Neuro-chip. After 2 days, cells were beginning to show contractile activity and therefore ready for electrophysiological recordings. Cells maintained for longer than 5 days would begin to form a confluent monolayer as shown in Figure 6.8 (This movie can be found on the DVD that accompanies this thesis).

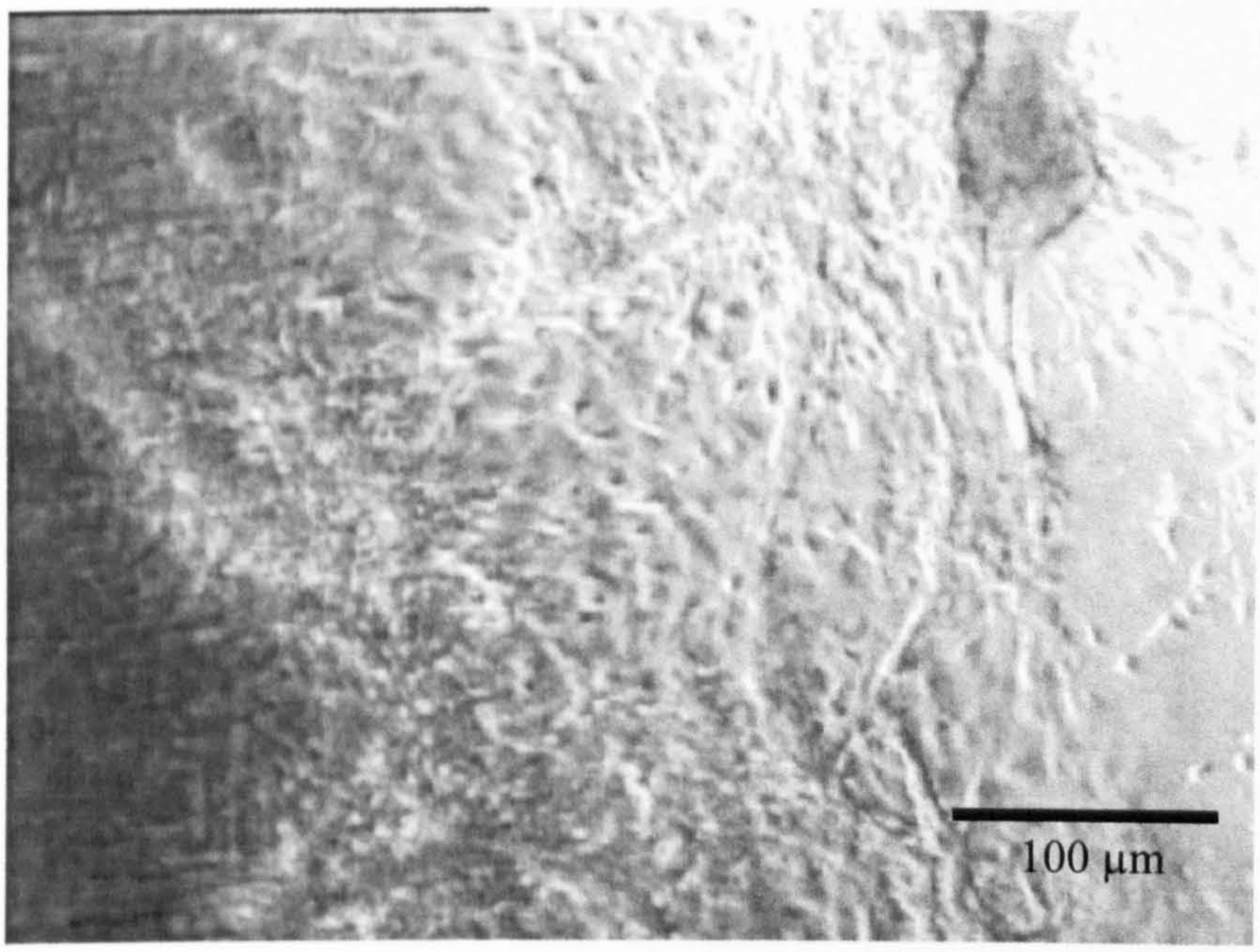

Figure 6.8. Movie showing a cardiomyoctye culture after 5 days in-vitro taken using a phase contrast microscope. Cells have formed a confluent monolayer due to the proliferation of fibroblastic cells within the culture.

Recording of Cardiomyocyte Activity using Planar MEA

The contractile activity of 5 day old cardiomyocytes cultures was recorded using the planar MEA device. The recording system was set to a 5KHz readout rate, at a 100x amplification gain. Cells grown on PDMS structures were inverted onto the electrode array and maintained under recording conditions for 2 hours. Spontaneous contractile events, observed through the microscope on which the device had been mounted, were time-locked

to the action potentials recorded using the Planar MEA set-up. Examples of the spontaneous electrical activity recorded are shown in Figure 6.9. These graphs have been created from the raw data by copying the x,y coordinates of each response into an Excel spread sheet. In each graph the individual coloured trace corresponds to the electrical activity recorded by an electrode on the array. In Graph A, three electrodes have been activated, all of which have detected seven contractile events. Although the signals are similar in waveform they appear to be of varying amplitudes. In Graph B, only one electrode has been activated, solely recording the three events that have occurred. Cells were found to be highly active within the first 30 minutes of the experiment, with contractile activity decreasing over time. Two hours after the start of the recording experiment cells were almost completely inactive.

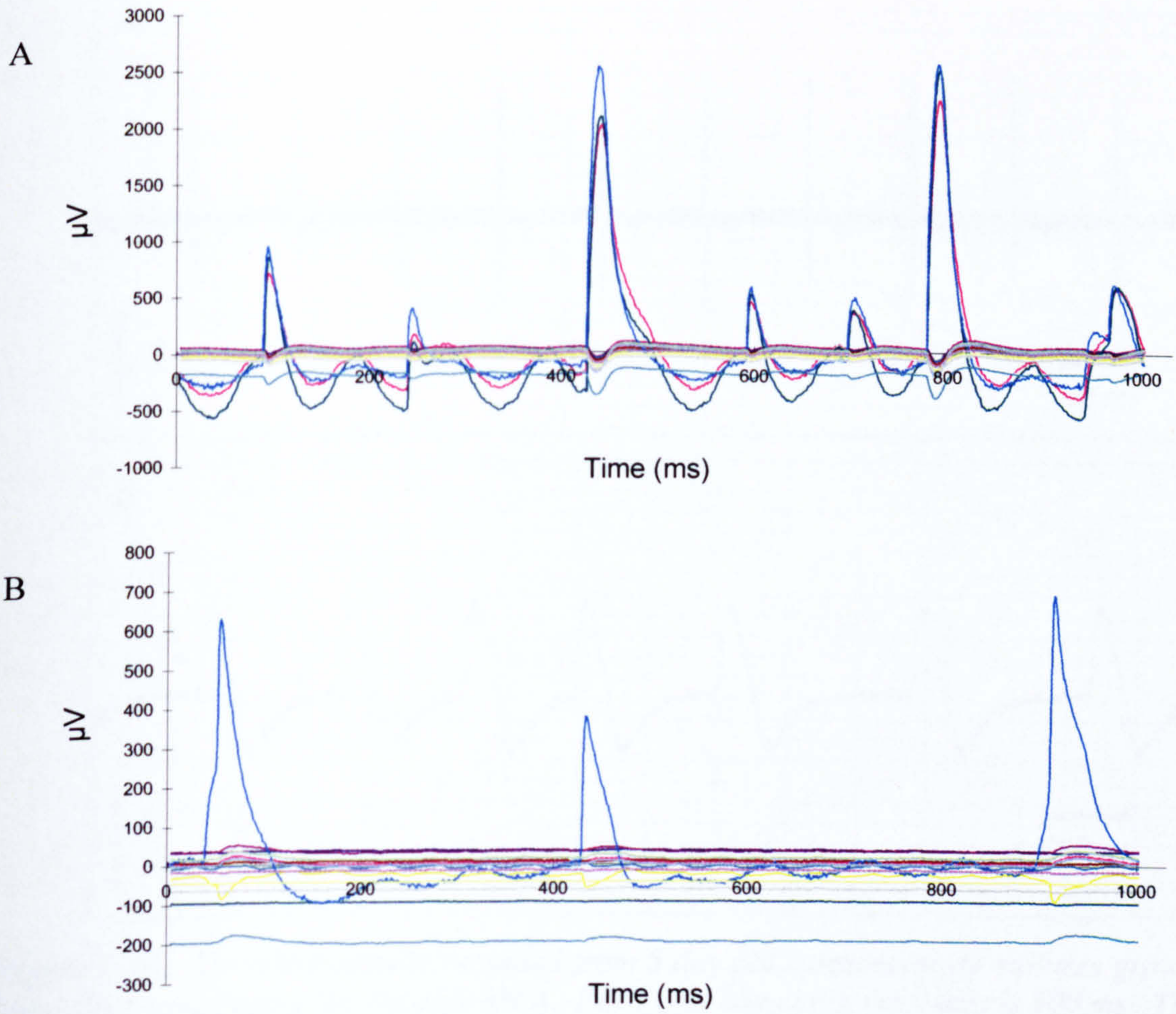

Figure 6.9. Electrophysiologcal recordings of cardiomyocyte activity recorded using the planar MEA device. Cells used in this example have been cultures for 5 days prior to the experiment. Events shown in graph A were recorded after the 10 minutes into the 2 hour experiment and events in graph B were recorded after 20 minutes

Recording of Cardiomyocyte Activity using Flexible MEA

The first flexible electrode arrays available for electrophysiological experiments had only one of the eight electrodes active; therefore the test recordings on cardiomyocytes show only one trace. Five-day-old cardiomyocytes cultures grown on glass cover slips were used in this experiment. Figure 6.10 shows two examples of the spontaneous contractile activity recoded using the flexible array. Trace A, is an example of electrical activity that is recorded when the electrodes were in close proximity to the cells. As the electrodes were moved away from the cells, the signal waveforms altered due to current leakage (see Trace B). These traces are screen captures of the original traces recorded using the axoscope software.

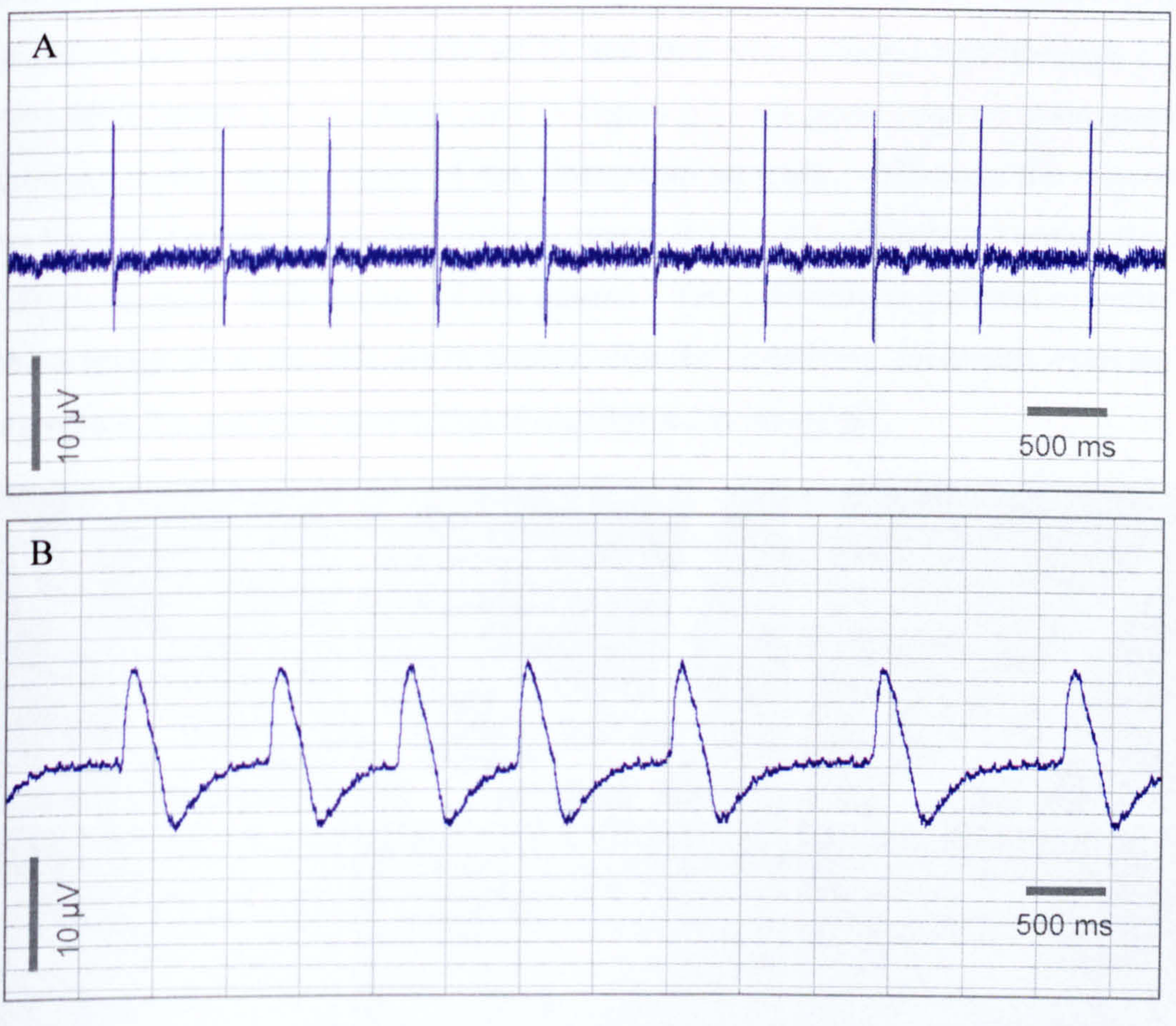

Figure 6.10. Electrical activity recorded from 5 day old cardiomyocyte cultures grown on glass cover slips using the Flexible MEA. Each grid box along the x-axis is 500 ms. The Y-scale in both images is 10 µV. Trace shows the typical signals recorded from cardiomyocytes when the electrode was in close contact with the cells, trace B is an example of the signals recoded when the electrode was not in contact with the cells.

Neural Network Activity

Each electrophysiological experiment using spinal cord cultures was carried out over a 2 hour period. No electrical or chemical stimulants were used to obtain the results presented in this chapter.

Neuro-chip and Planar MEA Compatibility

Interference reflection microscopy (IRM) was carried out to ensure that the cells growing on the Neuro-chip structures were close enough to the electrodes for changes in current flow to be detected. Cells were maintained in culture for seven days on the Neuro-chip structures. Structures were inverted onto a 60 x 60 mm cover slip, then mounted on a Zeiss Axiovert 200M microscope and observed through an oil-immersion x60 objective, first in phase contrast (see Figure 6.11, image set 1), and then with reflected light through a green excitation filter (Image set 2). Image set 1 in Figure 6.11 are phase contrast micrographs of cells growing in the central region of the Neuro-chip structure. Although the majority of cells are located outwith the grooved pattern, image B shows a cell adhered within the 5μm deep, 20μm diameter node region of the pattern. The interference patterns recorded for each phase image show all cells are in contact with the underlying cover slip, even the cell growing within the grooved pattern, that is highlighted in image B1.

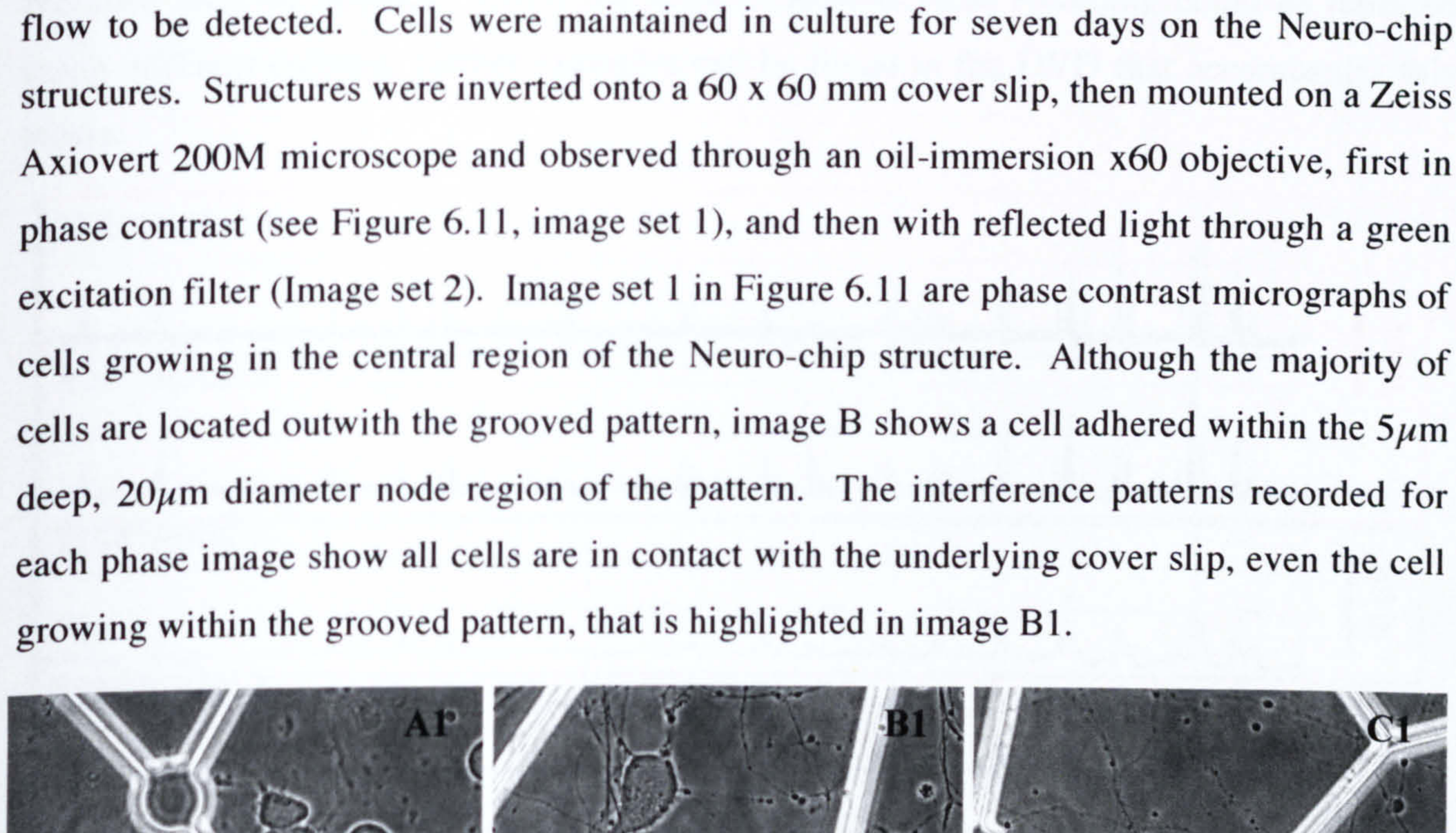

Figure 6.11. IRM images of embryonic spinal cord neurons growing on the PDMS Neuro-chip structure, then inverted onto a glass cover slip. Image set A1-3 are phase contrast micrographs, and image set B1-3 are the corresponding interference patterns. The scale bar in all images is 20μm.

Recording of Neural Network Activity using Planar MEA

The results presented in this section have been recorded from embryonic spinal cord neurons, grown on PDMS Neuro-chip structures, after 2 weeks in culture. Cells were relatively quiet during the first ten minutes, with no spontaneous activity observed until after 5 minutes into the recording period. Figure 6.12 shows a typical example of the type of activity seen in neuron cultures using the planar MEA device. These signals were recorded 15 minutes into the experiment, with this trend in activity lasting for 30 minutes. After this time the spontaneous network activity decreased, with almost no signals being recorded after 40 minutes. Under the same conditions these recording could be repeated using different cultures, further examples can be found in the DVD that accompanies this thesis.

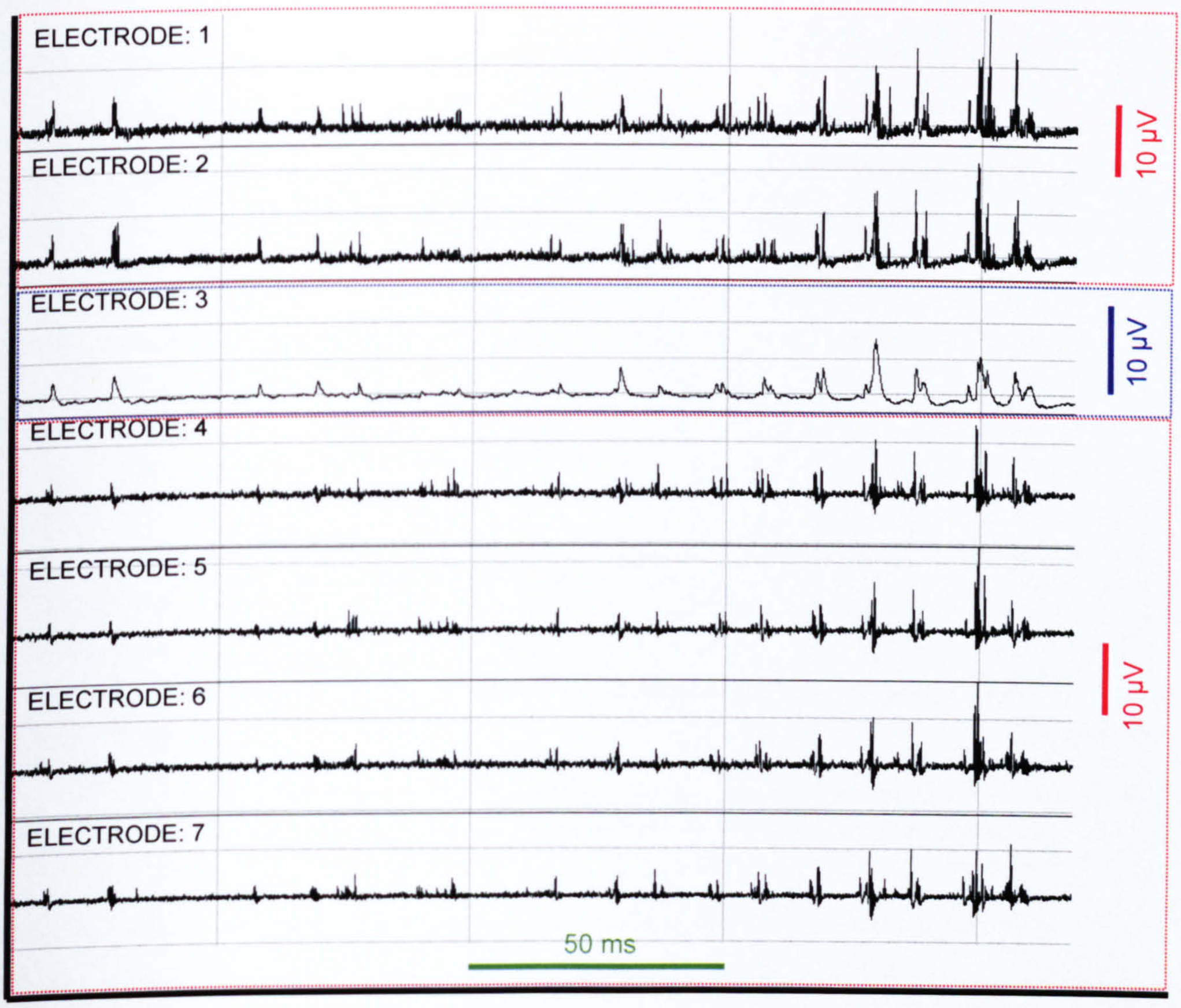

Figure 6.12. Spontaneous electrical activity recorded from 2 week old embryonic spinal cord cultures using the planar MEA device. The cultures were grown on the Neuro-chip structures. The Y scale bar is in µV and is the same for electrodes 1, 2 and 4-7.

Recording of Neural Network Activity using Flexible MEA

The results presented here have been recorded from embryonic spinal cord neurons grown on glass cover slips and maintained in culture for 2 weeks. In this case cells were spontaneously active from the start of the experiment, with bursts of activity being observed almost immediately (see Figure 6.13). Between these periods of high activity cells remained relatively quite, however this pattern of activity changed over the course of the experiment. After 15 minutes of recording the duration of the bursts decreased and network activity became less aggressive, with smaller events occurring more frequently. Again, similar activity patterns were repeatedly reproduced with different cultures and are presented in the accompanying DVD.

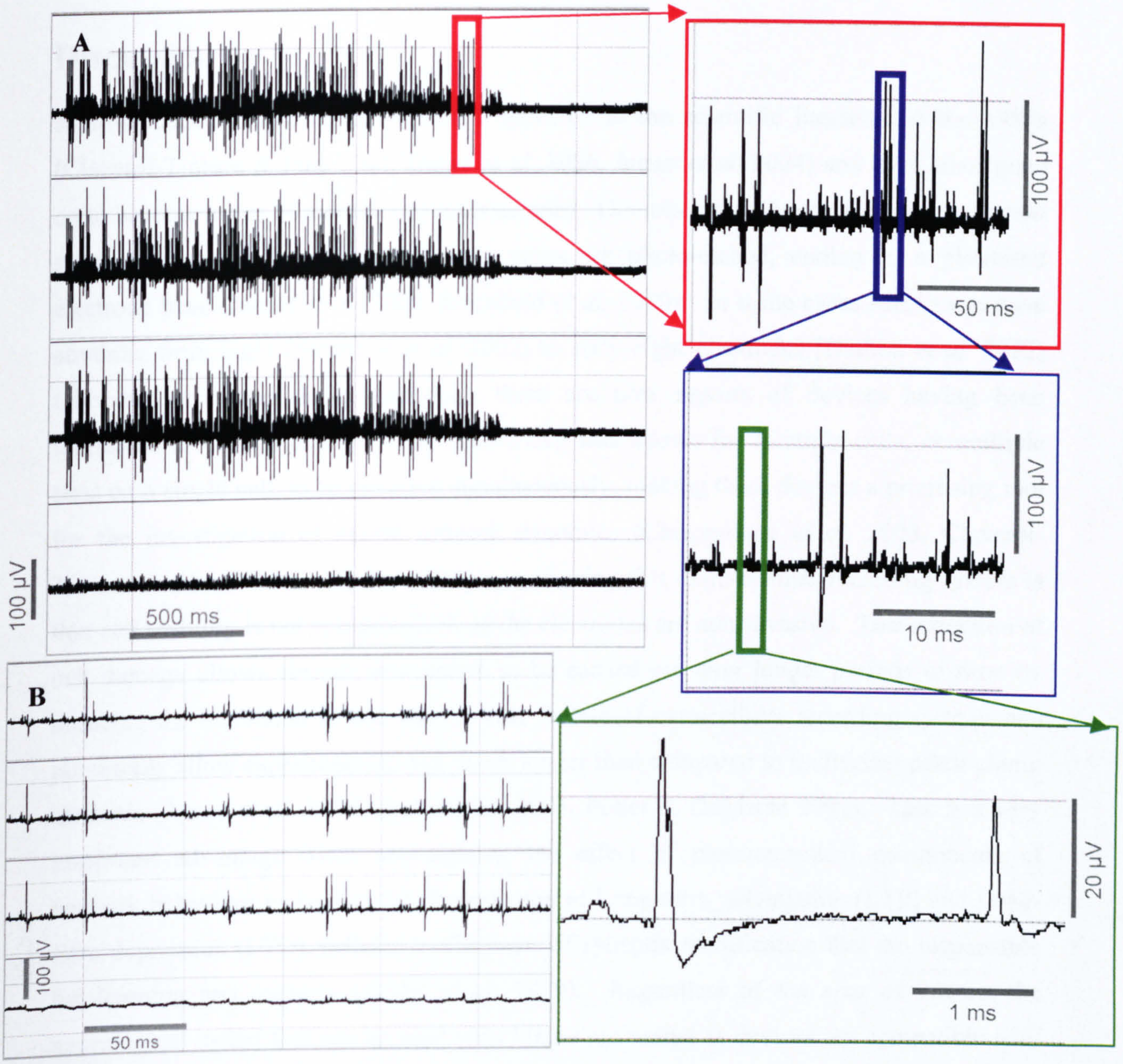

Figure 6.13. Spontaneous electrical activity recorded from 2 week old embryonic spinal cord neurons grown on glass cover slips, using the flexible MEA device. Trace A shows burst activity recorded at the start of the experiment and Trace B shows an example of activity recorded after 15 minutes. This trend in activity was repeatedly reproduced with different cultures.

Summary

Both MEA devices proved to have been successfully fabricated, as real nerve impulses were recorded using each array. Random nerve cell cultures were displaying spontaneous rhythmic burst, firing patterns typical of spinal cord cultures. This trend in activity was reproduced with a number of different cultures.

Discussion

Multi-electrode recording devices first appeared in the scientific literature in the 1980s (Claverol-Tinture & Pine 2002, Droge *et al.* 1986, James *et al.* 2004) and have since gone on to become a part of modern day neuroscience. Devices normally consist of a transparent substrate into which micrometric gold wires are photo-etched, ending in a platinised electrode head (James *et al.* 2004, Morefield *et al.* 2000). In some cases MEAs can have anything from eight (Sandison *et al.* 2002) to sixty-eight electrodes (Darbon *et al.* 2002) fabricated into one device (although there are now reports of devices having been fabricated to consist of over 1000 electrodes); this allows for multiple cells, or multiple sites on a single cell, to be recorded simultaneously, making these devices a promising tool for the investigation of neural network dynamics (Chiappalone *et al.* 2003, Claverol-Tinture & Pine 2002). Another advantage of using this extra-cellular recording system is that cell viability is not compromised, as the electrodes are non-invasive. This reduction of cell damage allows chronic stimulation to be carried out over longer periods of time by reducing the likelihood of cell death. This feature of extracellular recording systems can potentially allow experiments to last much longer than compared to traditional patch-clamp methods (James *et al.* 2000, Jimbo *et al.* 2003, Potter & DeMarse 2001). This is a very important advantage when investigating the effect of pharmaceutical components of network behaviour as well as the phenomenon of Long-term potentiation (LTP) and Long-term depression (LTD), cellular mechanisms of synaptic modification that are responsible for learning and memory (Jimbo *et al.* 1999). Regardless of the area of interest the neurological model that can be used with MEAs are varied as devices are compatible with brain slices, high density cultures, or spatially organised cultures of a defined geometric pattern.

As scientific interest in neural network processing has risen, there has also been a parallel increase in the development and fabrication of these multiple-electrode recording devices. MEAs are now commercially available from companies such as Multi Channel Systems© (Martinoia *et al.* 2005, Wagenaar *et al.* 2005). However, the attraction to many groups is the possibility to design and fabricate their own device, custom built to suit their research needs. Of the groups that have fabricated their own MEAs few have considered an alternative approach to contemporary 64 electrode array design (Bendonin *et al.* 2005). At

CCE we fabricated two very distinct electrode arrays, both of which have been specifically designed to work with patterned neuronal cultures.

As mentioned previously in this thesis, it is hypothesised that variations in cell morphology correspond to alteration in firing patterns. Multielectrode systems are an excellent system for investigating this phenomenon, as to fully understand the effects of pattern geometry and cell morphology on network communication requires electrophysiological recording of the entire network (Spence *et al.* 2003), focusing on the areas of the network where synapses are most likely to occur. The design of the MEAs used in this study has taken this factor into consideration, and therefore have been custom built to suit the geometric pattern of the neural networks.

Principles of the MEAs Designed and Fabricated at CCE

Planar MEA

The spatial distribution of the electrodes within the planar array were set to correspond with the *Jude* network pattern, with each electrode head being positioned directly below a node adhesion site when the network pattern was positioned over the array. The diameter of the cell container (shown in Figure 6.5) was greater than that of the Neuro-chip, this provided enough free space within the container for the chip to be manoeuvred around the electrodes. Although the planar device consisted of 64 electrodes within the array, only seven of these electrodes had been activated for the preliminary tests presented in this thesis. This was simply to reduce the data recorded and therefore simplify the testing procedure.

Flexible MEA

The flexible array was originally designed on the hypothesis that ion channels of neurons, growing on a substrate *in-vitro*, migrate to the area of the membrane that is not in contact with the substratum (Sandison *et al.* 2002). Therefore to successfully record network activity using extracellular electrodes it is necessary to record from above. The flexible array, which consists of two rows of four electrodes, is compatible with both random dissociated cultures and organised networks created by μCP methods. Unlike the planar array, this device benefits from the fact that it is not fixed, and using a micromanipulator,

the electrodes can be positioned above any area within the network. When working with the μCP networks this feature proved most beneficial as certain areas of the pattern displayed better cell compliance than others, and were therefore of preference for electrophysiological recordings.

MEA Testing with Cardiomyocytes

Cardiomyocytes were used to test both MEA set-ups, as these cells are known to physically contract when activated, allowing cell activity to be time-locked to the electrical recording (Igelmund *et al.* 1999, Sprossler *et al.* 2001). Using both MEA devices, real spontaneous cardiomyocyte activity was recorded. These electrical impulses were recorded simultaneously with the contractile events that were observed within the culture. The spike trends shown in Figures 6.9 and 6.10 correspond to those recorded by Igelmund *et al.* (1999), with spike amplitude ranging from 200μV to 2 mV. It should be noted that different wave forms recorded with the Flexible array that are shown in Figure 6.10 are a result of the position of the electrode in relation to the cell during recording. If the electrode is in close proximity to the cell, the local current flow is concentrated to the area surrounding the electrode. However, if the electrode is further away from the cell the current flow diffuses into the culture media and can distribute away from the electrode, resulting the alteration in waveform shown in Figure 6.10, Trace B.

However, not only were the MEA devices tested using this biological model, but also the concept of the Neuro-chip structure. For this structure to be effective, cells must be able to survive inverted on the electrodes for long periods of time. Although it was well known that PDMS material is gas permeable, it was not known if the diffusion rate would be sufficient to supply these highly metabolic cells with the atmospheric conditions they require. Also it was questionable if the dimensions of the supporting structures would be high enough to allow media exchange throughout the cultures, while being low enough for the current flow to be recorded the electrodes.

To test these conjectures cardiomyocytes were grown on flat PDMS sections and the Neuro-chip structures. Cells on the flat PDMS were inverted onto the planar MEA device and both electrical and physical activity was monitored. Cells were found to spontaneously active for over 30 minutes under these conditions, without exchanging the recording

solution or adding any stimulating compounds. This result suggests that not only would the PDMS material be effective, but also the design and dimensions of the Neuo-chip, as cell survival was not compromised on the flat inverted structure. Cells grown on the Neuro-chip structure, and inverted onto the planar MEA, were observed to be actively contracting, and this activity lasted for approximately 2 hours without stimulation or exchange of the recording solution. This result proved that the design of the Neuro-chip is effective is maintaining a suitable environment for electrically active cells, although if longer experiments are to be carried out it might be necessary to use a flow system which would continuously exchange the recording solution (removing waste and bring fresh nutrients), and make the this set-up compatible with testing pharmacological compounds.

Neural Network Activity

Neuro-chip and Planar MEA Compatibility

Although electrical activity was recorded from cardiomyocytes grown on the Neuro-chip, it necessary to determine whether neurons growing within the grooved pattern were close enough to the electrodes for current flow to be detected. Interference reflection microscopy (IRM) was applied here to investigate the distance between cells in the grooves and the surface of the planar electrode array (Curtis 1964, Verschueren 1985). To perform this evaluation it was necessary to substitute the MEA substrate for a glass cover slip, therefore the protruding electrode heads have not been considered in this test. However, the interference reflection patterns, shown in Figure 6.11, clearly demonstrate that cells growing within the 5μm deep grooved pattern, set within the cell containment chip, make contact with the substrate onto which they are inverted. If the platinised electrode heads are taken into consideration, then it is feasible to suggest that a relatively tight seal can be made at the cell-electrode interface. Unfortunately neurons did not respond to the grooved patterns as hypothesised (see Chapter 5), and therefore organised neural networks could not be created in this way. However, it is believed the Neuro-chip design is still a promising tool for investigating and characterising network behaviour if a suitable topography for aligning cell growth is identified.

Understanding Random Neural Network Activity

The main objective in this study was to determine how network activity of spatially organised cultures differed from that of random cultures. Therefore the first step was to characterise firing patterns of random cultures grown on substrates that had no growth modifying topography. For this experiment Neuro-chip structures were created without guidance topography. However, as described in Chapter 5, cells did not respond to the grooved pattern and so the Neuro-chip with the grooved pattern was used for all experiments, as cells remained randomly distributed across the chip substrate. For the experiments with the flexible array, cells were grown on glass cover slips. Approximately twenty different cultures were tested for both planar and flexible MEA experiments. At no point were any stimulants, pharmaceutical, electrical or otherwise, used in any of the experiments, therefore all the spikes recorded were truly spontaneous.

Because spike burst or clusters are a prominent feature of network activity, the description of activity at the bursting level can provide a vast amount on information on network behaviour without having to deal with complex single spike analysis (Harsch *et al.* 1997). Therefore only bursting activity will be discussed. The data presented in Figure 6.12, shows the typical spontaneous activity recorded from dissociated spinal cord neurons using the planar array, and Figure 6.13.B is an example of the typical activity recorded with the flexible array. In each case, cells are showing distinctive bursting patterns of activity. Spike bursts ranged from approximately 2 ms in duration to 7 ms, and appeared to be following a rhythmic pattern as would be expected with spinal cord cultures (Bracci *et al.* 1996, Chiappalone *et al.* 2003, Darbon *et al.* 2002, Harsch *et al.* 1997, Novellino *et al.* 2003, Streit 2001). It was not known which cells were responsible for this patterned activity but it is quite possible pacemaker cells within the network were evoking it. As the duration of the spike bursts increased, the amplitude of the recorded spikes also increased. In Figure 6.13.A an example of tetanic burst activity that was recorded at the beginning of an experiment using the flexible array in shown. This type of network activity was only ever witnessed at the beginning of experiments and was rarely recorded thereafter. This is most promising, as such activity can have a depressing effect on network activity as a whole, and could compromise the overall understanding of network behaviour (Darbon *et al.* 2002, Streit *et al.* 2001).

Organised Neural Network Activity

An attempt was made to record from spatially organised neural networks using both MEA set-ups. To combat the problem of non-compliance to the grooved topography of the Neuro-chip, flat chips were fabricated and geometrical patterns were created on the structure by μCP techniques. However, cells would not adhere to the substrates prepared in this way, and the cells that did adhere were not forming patterns. An attempt was also made to create the patterns by μCP on cover slips, with the aim of inverting these onto the planar array. However the glass background was too hydrophilic, and cell growth spread across the entire substrate. Patterned neural networks, successfully created on polystyrene Petri dishes by μCP methods (as shown in Chapter 4), were used for studies conducted using the flexible array. Although networks created in this way were known to be synaptically active and in good health (as shown by immunofluorescence staining), no viable recording were obtained. Approximately 10 different cultures were tested in this way, however at no point was any spontaneous electrical activity recorded. It could be that cells were simply not active, or that the network signals were too weak to be detected by the electrodes.

Conclusion

Spontaneous electrical activity from dissociated cultures was recorded using both MEA devices. Although this proved both devices had been successfully fabricated for their purpose, there are some significant improvements that could be made to this set-up if it is to be used for future experiments. Firstly, a flow system should be incorporated into each set-up so that pharmaceutical compounds can be introduced to the experiments. Secondly, MEA devices should be fabricated incorporating stimulatory electrodes within each array, this would be beneficial for invoking network activity, especially when working with spatially arranged networks of fewer cells.

Chapter 7.

Final Discussion

In this thesis a number of different aspects of cell engineering have been applied with the aim of increasing our understanding of neural network configuration and behaviour. I have applied both chemical surface modification and varying surface topographies to create organised networks, which I have attempted to analyse using microscopical methods and electrophysiological recordings.

Primary Cell Culture of Spinal Cord Tissue

Spinal cord tissue was chosen as a biological model for all experiments during the course of this research. The main reason for choosing this tissue type is that the neural networks that exist within spinal cord are probably the most defined of all within the CNS. Also it was anticipated that observations made during the work conducted on topographical biomaterials might lead the way to further experiments on axon growth that would contribute to the current experimental research that already exists within the field of spinal regeneration. Understanding the mechanisms through which axon proliferation can occur is paramount to this area of investigative research; therefore an in-depth understanding of the growth requirements of this cell type, and the effect varying topographies can have on axon proliferation, can only be advantageous for further development of biomaterials for this purpose. There is also growing evidence to suggest that neural networks in the spinal cord are capable of anatomical and functional recovery after physical injury (de Leon *et al.* 2001, Edgerton *et al.* 2004), suggesting that the amalgamation of spinal cord neural network investigations and topographical guidance studies is potentially the future of spinal regeneration research. Therefore it is arguable that the investigation of cellular responses to guidance structures, whether structural or chemical, must be carried out with both embryonic cultures (to investigate network formation during development), and postnatal cultures (to investigate the phenomenon of plasticity following injury). Therefore the switch from postnatal rats to embryonic cultures, although not one of choice, is not believed to be have been detrimental to this study. However, it would be interesting to investigate the response of postnatal cultures to the same experimental conditions tested on embryonic cultures, and compare the cellular responses.

When establishing the best protocol for extraction, growth and maintenance of both postnatal and embryonic cultures, attempts were made to identify the different types of neurons that exist with the networks of this tissue by staining for their specific neurotransmitters. Cells were labelled for markers against glycine, GABA, glutamine, and acetylcholine (Beattie, unpublished). However, no conclusive staining results were obtained, a disappointing result considering the information this could have provided on the how random networks form *in-vitro*, and how this might have compared to those influenced by chemical and/or structural modification of the substrate.

Can Cell Morphology Effect Network Behaviour?

μCP has been shown to be highly successful in containing neurite outgrowth within a desired pattern, yet there still appears to be little control over neuron polarity. Nerve cells *in-vivo* are highly polarised structurally and functionally as individual cells, and as elements in neural circuitry (Stenger *et al.* 1998). As described in the main Introduction to this thesis, axons differ from dendrites, with axons being long, relatively unbranched and specialised for neurotransmitter release, whereas dendrites are highly branched and express postsynaptic receptors for signal reception. Unfortunately, without the complex, fine scale molecular cues present *in-vivo*, axon and dendrites extend in random directions within the patterned culture. Thus, the viability of patterned cell culture, as a tool for further understanding the neural network function, remains questionable. Without being able to control cell-cell synaptic connections, it is arguable that these networks remain random and are no different from normal cell culture. Only recently have research groups addressed the question of directing neurite polarity (Corey & Feldman 2003, Stenger *et al.* 1998, Vogt *et al.* 2003). However, few have considered the implications of neuron morphology on network behaviour.

Understanding the relationship between structure and function is a classic biological problem. The structure-function correlation of the neuron is probably one of the most puzzling in nature. Although each neuron has a defined structure, the different variations of this are endless, making it almost impossible to categorise and classify all that exist within the nervous system. Dendrites alone can differ in length, diameter, branching complexity and surface smoothness (Connors & Regehr 1996). It is this diversity in neuron structure that has lead scientists towards the theory that nerve cell morphology plays a predominant

role in cell, and therefore network function. The complexity of tasks that are preformed by the CNS reflects the complexity of cell shape, network geometry and brain design (Chklovskii 2004). But how could neuron shape affect network function? The key to this relationship appears to exist within the structure of the dendritic tree, as it is believed that dendrites are responsible for collecting and integrating complex spatio-temporal patterns of postsynaptic potentials and controlling the generation of time-structured action potentials (Segev & London 2000) . The different firing patterns initiated in the neuron are essential components of the network circuitry. Recent studies, using computer simulated models to recreate known, *in-vivo* morphologically and functionally complex neuron structures *in-silico*, now suggest that cell firing is influenced by the morphological complexity of dendritic arborisations (Connors & Regehr 1996, van Ooyen *et al.* 2002, van Pelt *et al.* 2001, Vetter *et al.* 2001). Especially interesting in this context is the model developed by van Ooyen *et al* (2002), who equalised all varying factors that would normally contribute to the differences in individual nerves cells (such as ion channel density, and branch diameter), allowing only differences in morphology to be investigated. Results from this study demonstrated that not only did tree length but also tree symmetry have an effect on pattern firing pattern, suggesting that if one is to try and investigate network behaviour in an *in-vitro* model, then it is necessary to maintain the fundamental structures of the cell that are major determinants of network activity. Although it could be argued that restriction of the cell morphology would also be beneficial to this study, suggesting a comparison between networks that restrict cell morphology (allowing only controlled number of processes to develop) and those that do not, is required.

Although my attempts to introduce different dendritic architecture into the neural networks in culture were successful in the fact that cell morphology was visibly altered, it is arguable that to create such defined structures (replicating the natural characteristics of a neuron) requires a more defined element of control. It could be that to truly obtain a morphologically defined network would require μCP with specific growth promoting molecules (such as neurotrophins), which would stimulate dendrite proliferation within the desired locations of the network pattern (Miller & Kaplan 2003). Combining such efforts with the geometric patterns used in this thesis could provide further insight into the guidance mechanisms that drive network construction as well as the relationship between network structure and function.

Understanding Network Circuitry: A Role for the MEA

Neural networks in vitro exhibit spontaneous and complex spatio-temporal spike patterns (Morefield *et al.* 2000). In order to understand how these electrical patterns relate to network function requires the electrophysiological understanding of the network as a whole. This in turn requires the ability to record from sites throughout the cell network. Some studies have used patch clamp techniques to investigate network activity with success (Vogt *et al.* 2005b), however this method is limited by the number of cells that can be stimulated, or recorded from, simultaneously. MEA recording systems have been designed to do just that, with devices consisting of multiple recording and stimulation sites which can simultaneously activate and record from the network (Jimbo *et al.* 2003).

Investigating the Relationship Between Network Organisation, Firing Patterns and Network Function

Network communication is a direct result of the synaptic connections that occur within a circuit and it is now accepted that synaptic connectivity is highly adaptive to changes in the network activity (Jimbo *et al.* 1999). It has been suggested that such correlated activity plays a crucial role in the brain function. However, little is known as to how modifications in synaptic strength and firing rate directly relate back to the network function (Shahaf & Marom 2001, Tateno *et al.* 2002). Using dissociated cultures and brain slices, attempts have been made to investigate this grey area within neuroscience (Novellino *et al.* 2003), although some researchers believe in order to fully understand network function requires a more controlled approach in terms of the biological model applied (Chang *et al.* 2001). Slice cultures have the advantage of retaining some of the connectivity that exist *in-vivo*. However, cells that are migrating out of a slice do form random connections. Cultures of dissociated neurons also form random, though highly complex, network arrangements. It is arguable that these systems are still far too complex and an approach is necessary to obtain more simplified networks (Lauer *et al.* 2002).

Growing neurons in geometrically defined network patterns is one way to overcome this problem. This has the effect of greatly simplifying the network by limiting the adhesion of neurons to specific area on a substrate surface as seen when using chemical and topographical techniques. By reducing the cell number within a network the electrical activity between cells can be closely scrutinised as the volume of recorded data is

potentially reduced, and the firing patterns of individual cells can be easily distinguished, as can their signal direction and location within the network. Also the introduction of pattern formation within a nerve cell culture could be used to reinstate some of the organisation that is lost during dissociation (James *et al.* 2004). This control over network orientation can ensure that cells and /or their processes are in close proximately to the electrodes, an essential feature of extracellular recording systems. μCP has the potential of being an excellent tool for the study of both network formation and network function when applied to this bio-sensing set-up. However, this method of integrating cell patterning and electrophysiological recording does present a number of challenges, in particular the alignment of the micrometric pattern to the electrode array (Connolly *et al.* 1990). It is for this reason the cell containment device described in Chapter 5 was designed. This chip is compatible with μCP techniques as well as topographical patterning. Although it was not established whether network pattern does in fact affect network behaviour in this thesis, the criteria for tackling this question has been identified and optimised.

Nanotopography as a Means of Creating Organised Neural Networks

Although the initial reason for turning to nanometric topography was to provide a substitute for the grooved structures of the Neuro-chip, the cellular response to topography was in itself very interesting, with important implications on the use of nanometric topography in the study of neuro-engineering. The development of nerve tissue engineering technologies has the potential of transforming the lives of many individuals who are victims of physical damage to the CNS. Spinal cord injuries in particular cannot be detected or prevented prior to their occurrence, and can therefore have devastating effects on all those affected. As mentioned previously in this thesis, the majority of mature neurons in the CNS cannot regenerate, therefore the treatment of injured, or diseased nervous tissue is a challenge to the medical profession. One promising method is to introduce a cell support system that can encourage both cell growth and guidance (Moore *et al.* 2006). It is well documented that, although cell death is a major cause in the loss of function at the lesion site, it is the chemical and structural composition of the area surrounding a lesion that is responsible for the inability for nerve tissue to regenerate (Novikov *et al.* 2002). Therefore a scaffold capable of bridging this area devoid of adhesive and growth promoting stimuli is required if nerve regeneration is to occur.

From the results presented in Chapter 5 it is evident that the pillared nanotopography influences cell morphology, by appearing to encourage axon proliferation. This suggests that the nanometric pillars are stimulating cellular pathways that initiate axon growth. Although the exact mechanisms through which this phenomenon is occurring has not been established here, other studies have suggested that the biomaterials of nanometric dimension can be interpreted by a nerve cell as naturally occurring ECM (Yang *et al.* 2004). There also exists evidence, collected using other cell types, that supports this theory (Dalby *et al.* 2004a, Dalby *et al.* 2004b, Dalby *et al.* 2004c, Dalby *et al.* 2004d, Dalby *et al.* 2004e, Dalby *et al.* 2004f, Dalby *et al.* 2004g, Dalby 2004h). Dalby *et al.* have shown that fibroblastic cells can alter their cell morphology in response to varying nano-environments, and this response has been attributed to notable shifts in fibroblast gene regulation, with changes in the areas of cell proliferation, signal transduction and extracellular matrix production (Dalby *et al.* 2004g). However the exact reaction of a cell depends entirely on the dimensions of the underlying topography, as some studies have shown nanotopography can also be non-adhesive to cells (Gallagher *et al.* 2002). Regardless of the nanotopographical features of a substrate, and the cellular response that it can induce, it is feasible to suggest that nanotopography can have a finer level of control over neurite growth in comparison to micrometric dimensions.

Closing Remarks- Nano or Micro?

During the course of this project organised neural networks have been successfully created using μCP techniques (see Chapter 4). However, neurite wandering has persisted throughout. It is possible that the micrometric dimensions of the polymer stamps have contributed to the neurites diverting from the chemical path, by providing an adhesive area much greater than that that is required for an advancing process. This suggests that an increase in the level of compliance that is necessary for controlling cell morphology within a network pattern, would require a topography (chemical or structural) of nanometric dimensions. The results presented in Chapter 5 support this theory, as both larger processes (approximately 1μm in width) and filopodia-like processes (approximately 300nm in width) were aligning to the nanotopography. Using such nanometric dimensions it may yet be possible to incorporate the dendritic patterns that were envisaged in Chapter 4, and potentially reduce the non-compliance that was observed within the network patterns with descriptive node designs. By applying this change in the experimental design, cell

morphology could be precisely controlled, therefore furthering the potential to investigate the relationship between cell shape, network configuration and network behaviour that could not be fully determined in this study.

Future Work

Although the main objective of this thesis, *the creation of organised neural networks in culture,* has been achieved, the fundamental question *can network morphology affect network function,* remains unanswered. However, within this thesis a number of shortcomings in the experimental methods and/or design have been identified.

To alter cell morphology precisely the use of nanometric patterns, at the descriptive node adhesion sites (*sun, oak* and *lattice*), is recommended. It is suggested that the width of the dendritic protrusions in each pattern is reduced to 1μm or less.

It would be interesting to investigate the effect of μCP on the nanopillared topography. However, to fully understand this response would require a thorough investigation into the signalling pathways that are being stimulated by the nanopillared topography itself.

Networks should be characterised to identify the different subclasses of neurons that exists within a random dissociated network, and if the percentage of the population differs when cells are grown in a geometrically defined network arrangement. It would be interesting to determine if pattern geometry can affect network characteristics in this respect.

If a means by which cells morphology can be precisely determined and maintained, the effect of cell shape on cell activity could easily be investigated using patch clamp techniques. This could provide some insight into the possible role of cell morphology on network behaviour.

A comparison of the electrophysiological activity of defined networks to those of random distribution could complete this study. The Neuro-chip design is an excellent method for incorporating patterned networks and MEA recording systems, although desired patterns should be created by μCP methods or by using a different structural topography such as the nanopillars.

At no point in this study has the role of glia in network formation and function been considered. Future studies involving this cell type could provide interesting results, and could potentially be the key to fully understanding neural networks.

Conclusion

The development of neural networks and their functional role in neuronal processing is considered the bane of modern day neuroscience. Although the work presented in this thesis has in some way contributed to the on going research within this field, there is still a long way to go until we fully understand the mechanisms through which these phenomenon occur. It is quite possible that the experimental technology required to address the questions that remain unanswered within neuroscience today does not yet exist. Therefore it is essential that investigative experiments which attempt to test possible theories, such as those described here, are continuously preformed.

Appendix I: Media, Reagents and Solutions

Throughout this thesis there is reference to various medias, reagents and solutions, some of which are described within each Chapter. Those that are not are listed here.

Antibiotics Mix

A supplement added to growth media containing 150 ml L-glutamine (Gibco), 100 ml Pen/Strep (Gibco) and Amphotericin B (Gibco), stored in 20ml aliquots at -20°C.

Coomassie Blue

A non-specific protein stain used to label cells. To make up 1 litre add 1g Coomassie Brilliant blue to 430 ml RO water, 500 ml methanol and 70 ml acetic acid. Stir for 5 minutes to ensure solution is thoroughly mixed and particles dissolved, then filter through Whatmans no.1 filter paper. This stock has a shelf life of 3 months.

Fibroblastic Growth Factor (FGF)

Used as a growth supplement, 10μg of b-FGF (Invitrogen) was dissolved in 2 ml sterile PBS and used at a final concentration of 5ng/ml.

Foetal Calf Serum Media (10%)

This solution was used to block enzymatic digestion of postnatal spinal cord cells and contained only 9 mls of Neuro Basal A media (Gibco) and 1 ml of FCS (Gibco). When used in the preparation of cardiomyocytes, NBA media was substituted for DMEM (Gibco).

Formal Saline (4%)

10ml formaldehyde (38%) was added to 90ml PBS. This solution was used to fix cells for immunofluorescence and Coomassie Blue staining.

HEPES Saline

Reagents were dissolved in 1L RO water, mixed and adjusted to 7.4 pH by adding droplets of 1M sodium hydroxide, and finally autoclaved to sterilise. If it was felt the sterility of this solution had been compromised at anytime, the solution was sterile filtered through a 0.22μm syringe filter.

REAGENT	Conc. (mM)	Grams/L
Sodium Chloride (NaCl)	140	8
Potassium Chloride (KCl)	5	0.4
HEPES	10	2.38
d-Glucose	5	1
Phenol Red	0.001	0.1

Insulin Transferrin Selenite Solution

The stock solution was prepared by Technical staff at CCE to give a final concentration of 5μg/ml for Insulin and Transferrin, and 5ng/ml for Selenite when diluted 1:200.

Permeablising Buffer

10.3g sucrose, 0.292g NaCl, 0.06g $MgCl_2$ (hexahydrate), 0.476g HEPES was added to 100ml PBS. The solution was mixed and then adjusted pH to 7.2 by adding droplets of 1M sodium hydroxide, then 0.5ml Triton X was added and the solution thoroughly mixed.

Phosphate Buffered Salt Solution (x10)

Reagents were dissolved in 1L RO water to make a 10 times concentrated stock solution at a pH of 7.4. All PBS solutions used in this thesis have been diluted 1 in 10 form this 10x stock. If a sterile PBS solution of 100ml or more was required the solution was sterilised by autoclaving. If only a small sterile volume was required, the solution was sterilised by filtration through a 0.22μm syringe filter.

REAGENT	Conc. (mM)	Grams/L
Sodium Chloride (NaCl)	1368.9	80
Potassium Chloride (KCl)	26.8	2
di-Sodium Hydrogen Phosphate (Na_2HPO_4)	73.7	11.5
Potassium di-Hydrogen Phosphate (KH_2PO_4)	14.7	2

PBS Modified for Immunocytochemistry

A 0.3M NaCL PBS solution was used to dilute all antibodies used to label embryonic spinal cord neurons. This solution also contained 0.3% Triton X-100 (Sigma). This composition of this solution was used designed by Annette Sorensen from The Glial Biology Group at the The Beatson Institute, Glasgow University.

Plating Media for Embryonic Cell Cultures

Embryonic cultures were plated in media containing 20% horse serum, 2mM L-glutamine, 5ml HBSS W/O Ca^{2+} and Mg^{2+} (Gibco) and 9.8 mls DMEM for 2 hours to allows neurons to adhere.

Poly-l-lysine Solution

PLL (Sigma) in powder form was dissolved in sterile RO water to the required concentration, then sterile filtered through a 0.22μm syringe filter.

RO Water

Water was purified using a Milli-RO15 Millipore Pure Water Systems (Millipore Ltd, Watford, UK) then autoclaved to sterilise.

SBTI-DNAse Solution

The following components, 0.52mg/ml soybean trypsin inhibitor (Sigma), 3.0 mg/ml BSA, 0.04mg/ml bovine pancreas DNAse, were dissolved in 25ml Leibovitzs L15 media (Gibco) supplemented with 1.25μl gentamycin (Sigma). Once all reagents were dissolved the solution was sterile filtered through a 0.22μm syringe filter.

Trypsin Solution (0.25%)

This enzymatic solution, consisting of 1ml of Trypsin (2.5%) (Gibco) in 9ml HEPES saline was used to digest the connective tissue surrounding postnatal spinal cord cells.

Trypsin Solution (Containing Collagenase)

200μl of Trypsin (2.5%) (Gibco) and 200μl of collagenase (5%) (MP Biomedicals, Stretton, UK) was added to 1.6 mls of HBSS W/O Ca^{2+} and Mg^{2+}.

Tween 20 Buffer

This solution was made up to 100ml with 99.5ml of PBS (1x) and 0.5ml Tween 20 buffer (Promega, Southampton, UK) and was used to remove excess antibodies during immunocytochemical staining.

Appendix II: *Abstracts*

List of abstracts accepted for oral or poster presentation relating to this PhD study.

Oral Presentations

Beattie, A.J., Tang, R. *Comparison of Microset with polydimethylsiloxane as a new polymer for microcontact printing* (2003) Kelvin Nanotechnology Conference, Glasgow.

Beattie, A.J., Tang, R. *Scaffolds for nerve tissue engineering* (2004) Engineering in Regenerative Medicine, UK Focus for Biomedical Engineering, Liverpool

Beattie, A.J., Gadegaard, N. *Nanotopography and microcontact printing-will this combination be the answer to creating neural nets in culture*? (2004) 1st UK-Cuba Conference on Nanoscience, Havana, Cuba.

Beattie, A.J., Tang, R. *Understanding Spinal Plasticity* (2005) Neural Networks and Adaptive Properties Workshop, Newcastle.

Poster Presentations

Beattie, A.J., Tang, R. *Creating organised neural networks* (2004) 4th International Meeting on Substrate Integrated Micro Electrode Arrays, Reutlingen, Germany.

References

Abu-Akel, A. 2003. A Neurobiological Mapping of Theory of Mind. *Brain Res Brain Res Rev.* 43: 29-40

Ai, H., Meng, H., Ichinose, I., Jones, S.A., Mills, D.K., et al. 2003. Biocompatibility of Layer-by-Layer Self-Assembled Nanofilm on Silicone Rubber for Neurons. *J Neurosci Methods.* 128: 1-8

Alberts, B., Bray, D., Lewis, L., Raff, M., Roberts, K., Watsn, J. D. 1994. *Molecular Biology of the Cell.* New York: Garland Publishings Inc.

Andres-Barquin, P.J. 2002. Santiago Ramon Y Cajal and the Spanish School of Neurology. *Lancet Neurol.* 1: 445-52

Annies, M., Bittcher, G., Ramseger, R., Loschinger, J., Woll, S., et al. 2006. Clustering Transmembrane-Agrin Induces Filopodia-Like Processes on Axons and Dendrites. *Mol Cell Neurosci.* 31: 515-24

Aubert, I., Ridet, J.L., Gage, F.H. 1995. Regeneration in the Adult Mammalian Cns: Guided by Development. *Curr Opin Neurobiol.* 5: 625-35

Banker, G., Goslin, K. 1998. *Culturing Nerve Cells.* London: The MIT Press

Barbucci, R., Pasqui, D., Wirsen, A., Affrossman, S., Curtis, A., Tetta, C. 2003. Micro and Nano-Structured Surfaces. *J Mater Sci Mater Med.* 14: 721-5

Bear, M.F., Connors, B.W., Paradiso, M.A. 2001. *Neuroscience: Exploring the Brain.* Baltimore: Lippincott Williams and Wilkins

Bendonin, L., Chiappalone, M., van der Wal, P.D., Imfeld, K., de Rooij, N.F., et al. 2005. A Microelectrode Array (Mea) Integrated with Clustering Structures for Investigating in Vitro Neurodynamics in Confined Interconnected Sub-Populations of Neurons. *Sensors and Actuators B.* 114: 530-41

Berdondini, L., van der Wal, P.D., Guenat, O., de Rooij, N.F., Koudelka-Hep, M., et al. 2005. High-Density Electrode Array for Imaging in Vitro Electrophysiological Activity. *Biosens Bioelectron.* 21: 167-74

Berg, D.K., Fischbach, G.D. 1978. Enrichment of Spinal Cord Cell Cultures with Motoneurons. *J Cell Biol.* 77: 83-98

Biederer, T., Sara, Y., Mozhayeva, M., Atasoy, D., Liu, X., et al. 2002. Syncam, a Synaptic Adhesion Molecule That Drives Synapse Assembly. *Science.* 297: 1525-31

Bixby, J.L., Jhabvala, P. 1990. Extracellular Matrix Molecules and Cell Adhesion Molecules Induce Neurites through Different Mechanisms. *J Cell Biol.* 111: 2725-32

Bracci, E., Ballerini, L., Nistri, A. 1996. Spontaneous Rhythmic Bursts Induced by Pharmacological Block of Inhibition in Lumbar Motoneurons of the Neonatal Rat Spinal Cord. *J Neurophysiol.* 75: 640-7

Branch, D.W., Wheeler, B.C., Brewer, G.J., Leckband, D.E. 2000. Long-Term Maintenance of Patterns of Hippocampal Pyramidal Cells on Substrates of Polyethylene Glycol and Microstamped Polylysine. *IEEE Trans Biomed Eng.* 47: 290-300

Brandt, R. 2001. Cytoskeletal Mechanisms of Neuronal Morphogenesis. *Zoology (Jena).* 104: 221-7

Brandt, R., Hundelt, M., Shahani, N. 2005. Tau Alteration and Neuronal Degeneration in Tauopathies: Mechanisms and Models. *Biochim Biophys Acta.* 1739: 331-54

Bray, D. 1979. Mechanical Tension Produced by Nerve Cells in Tissue Culture. *J Cell Sci.* 37: 391-410

Brewer, G.J. 1997. Isolation and Culture of Adult Rat Hippocampal Neurons. *J Neurosci Methods.* 71: 143-55

Brewer, G.J., Cotman, C.W. 1989. Survival and Growth of Hippocampal Neurons in Defined Medium at Low Density:Advantages of a Sandwich Culture Technique or Low Oxygen. *Brain Research.* 494: 65-74

Brewer, G.J., Torricelli, J.R., Evege, E.K., Price, P.J. 1993. Optimized Survival of Hippocampal Neurons in B27-Supplemented Neurobasal, a New Serum-Free Medium Combination. *J Neurosci Res.* 35: 567-76

Brown, A.G. 1991. *Nerve Cells and Nervous Systems*. London: Springer-Verlag Limited

Capaday, C. 2002. The Special Nature of Human Walking and Its Neural Control. *Trends Neurosci.* 25: 370-6

Chang, J.C., Brewer, G.J., Wheeler, B.C. 2003. A Modified Microstamping Technique Enhances Polylysine Transfer and Neuronal Cell Patterning. *Biomaterials.* 24: 2863-70

Chang, J.C., Gregory, J.B., Wheeler, B.C. 2001. Modulation of Neural Network Activity by Patterning. *Biosensors & Bioelectronics.* 16: 527–33

Chen, Z.J., Negra, M., Levine, A., Ughrin, Y., Levine, J.M. 2002a. Oligodendrocyte Precursor Cells: Reactive Cells That Inhibit Axon Growth and Regeneration. *J Neurocytol.* 31: 481-95

Chen, Z.J., Ughrin, Y., Levine, J.M. 2002b. Inhibition of Axon Growth by Oligodendrocyte Precursor Cells. *Mol Cell Neurosci.* 20: 125-39

Chevalier-Larsen, E., Holzbaur, E.L. 2006. Axonal Transport and Neurodegenerative Disease. *Biochim Biophys Acta.*

Chiappalone, M., Vato, A., Tedesco, M.B., Marcoli, M., Davide, F., Martinoia, S. 2003. Networks of Neurons Coupled to Microelectrode Arrays: A Neuronal Sensory System for Pharmacological Applications. *Biosens Bioelectron.* 18: 627-34

Chklovskii, D.B. 2004. Synaptic Connectivity and Neuronal Morphology: Two Sides of the Same Coin. *Neuron.* 43: 609-17

Clark, P., Britland, S., Connolly, P. 1993. Growth Cone Guidance and Neuron Morphology on Micropatterned Laminin Surfaces. *Journal of Cell Science.* 105: 203-12

Clark, P., Connolly, P., Curtis, A.S., Dow, J.A., Wilkinson, C.D. 1987. Topographical Control of Cell Behaviour. I. Simple Step Cues. *Development.* 99: 439-48

Clark, P., Connolly, P., Curtis, A.S., Dow, J.A., Wilkinson, C.D. 1990. Topographical Control of Cell Behaviour: Ii. Multiple Grooved Substrata. *Development.* 108: 635-44

Clark, P., Connolly, P., Curtis, A.S., Dow, J.A., Wilkinson, C.D. 1991. Cell Guidance by Ultrafine Topography in Vitro. *J Cell Sci.* 99 (Pt 1): 73-7

Claverol-Tinture, E., Pine, J. 2002. Extracellular Potentials in Low-Density Dissociated Neuronal Cultures. *J Neurosci Methods.* 117: 13-21

Connolly, P., Clark, P., Curtis, A.S., Dow, J.A., Wilkinson, C.D. 1990. An Extracellular Microelectrode Array for Monitoring Electrogenic Cells in Culture. *Biosens Bioelectron.* 5: 223-34

Connors, B.W., Regehr, W.G. 1996. Neuronal Firing: Does Function Follow Form? *Curr Biol.* 6: 1560-2

Corey, J.M., Feldman, E.L. 2003. Substrate Patterning: An Emerging Technology for the Study of Neuronal Behavior. *Exp Neurol.* 184 Suppl 1: S89-96

Cornish, T., Branch, D.W., Wheeler, B.C., Campanelli, J.T. 2002. Microcontact Printing: A Versatile Technique for the Study of Synaptogenic Molecules. *Mol Cell Neurosci.* 20: 140-53

Craighead, H.G., James, C.D., Turner, A.M.P. 2001. Chemical and Topographical Patterning for Directed Cell Attachment. *Current Opinion in Solid State and Material Science.* 5: 177-84

Curtis, A.S. 1964. The Mechanism of Adhesion of Cells to Glass. A Study by Interference Reflection Microscopy. *J Cell Biol.* 20: 199-215

Curtis, A.S., Breckenridge, L., Connolly, P., Dow, J.A., Wildinson, C.D., Wilson, R. 1992. Making Real Neural Nets: Design Criteria. *Med Biol Eng Comput.* 30: CE33-6

Curtis, A., Wilkinson, C., Breckenridge, L. 1994. *In Enabling Technologies for Cultured Neural Networks.* San Diego: Academic Press. pp. 99-120. pp.

Curtis, A., Wilkinson, C. 1997. Topographical Control of Cells. *Biomaterials.* 18: 1573-83

Curtis, A.S., Wilkinson, C.D. 1998. Reactions of Cells to Topography. *J Biomater Sci Polym Ed.* 9: 1313-29

Curtis, A., Riehle, M. 2001. Tissue Engineering: The Biophysical Background. *Phys Med Biol.* 46: R47-65

Curtis, A., Wilkinson, C. 2001. Nantotechniques and Approaches in Biotechnology. *Trends Biotechnol.* 19: 97-101

Curtis, A.S., Casey, B., Gallagher, J.O., Pasqui, D., Wood, M.A., Wilkinson, C.D. 2001c. Substratum Nanotopography and the Adhesion of Biological Cells. Are Symmetry or Regularity of Nanotopography Important? *Biophys Chem.* 94: 275-83

Cyster, L.A., Parker, K.G., Parker, T.L., Grant, D.M. 2004. The Effect of Surface Chemistry and Nanotopography of Titanium Nitride (Tin) Films on Primary Hippocampal Neurones. *Biomaterials.* 25: 97-107

Dalby, M.J., Berry, C.C., Riehle, M.O., Sutherland, D.S., Agheli, H., Curtis, A.S. 2004a. Attempted Endocytosis of Nano-Environment Produced by Colloidal Lithography by Human Fibroblasts. *Exp Cell Res.* 295: 387-94

Dalby, M.J., Gadegaard, N., Riehle, M.O., Wilkinson, C.D., Curtis, A.S. 2004b. Investigating Filopodia Sensing Using Arrays of Defined Nano-Pits Down to 35 Nm Diameter in Size. *Int J Biochem Cell Biol.* 36: 2005-15

Dalby, M.J., Giannaras, D., Riehle, M.O., Gadegaard, N., Affrossman, S., Curtis, A.S. 2004c. Rapid Fibroblast Adhesion to 27nm High Polymer Demixed Nano-Topography. *Biomaterials.* 25: 77-83

Dalby, M.J., Pasqui, D., Affrossman, S. 2004d. Cell Response to Nano-Islands Produced by Polymer Demixing: A Brief Review. *IEE Proc Nanobiotechnol.* 151: 53-61

Dalby, M.J., Riehle, M.O., Johnstone, H., Affrossman, S., Curtis, A.S. 2004e. Investigating the Limits of Filopodial Sensing: A Brief Report Using Sem to Image the Interaction between 10 Nm High Nano-Topography and Fibroblast Filopodia. *Cell Biol Int.* 28: 229-36

Dalby, M.J., Riehle, M.O., Sutherland, D.S., Agheli, H., Curtis, A.S. 2004f. Changes in Fibroblast Morphology in Response to Nano-Columns Produced by Colloidal Lithography. *Biomaterials.* 25: 5415-22

Dalby, M.J., Riehle, M.O., Sutherland, D.S., Agheli, H., Curtis, A.S. 2004g. Fibroblast Response to a Controlled Nanoenvironment Produced by Colloidal Lithography. *J Biomed Mater Res A.* 69: 314-22

Dalby, M.J., Riehle, M.O., Sutherland, D.S., Agheli, H., Curtis, A.S. 2004h. Use of Nanotopography to Study Mechanotransduction in Fibroblasts--Methods and Perspectives. *Eur J Cell Biol.* 83: 159-69

Dalby, M.J., Riehle, M.O., Sutherland, D. S., Agheli, H., Curtis, A. S. G. 2004. Fibroblast Response to a Controlled Nanoenvironment Produced by Colloidal Lithography. *Journal of Biomedical Materials Research.* 69: 314-22

Darbon, P., Scicluna, L., Tscherter, A., Streit, J. 2002. Mechanisms Controlling Bursting Activity Induced by Disinhibition in Spinal Cord Networks. *European Journal of Neuroscience.* 15: 671-83

de Leon, R.D., Roy, R.R., Edgerton, V.R. 2001. Is the Recovery of Stepping Following Spinal Cord Injury Mediated by Modifying Existing Neural Pathways or by Generating New Pathways? A Perspective. *Phys Ther.* 81: 1904-11

Detrait, E., Lhoest, J.B., Knoops, B., Bertrand, P., van den Bosch de Aguilar, P. 1998. Orientation of Cell Adhesion and Growth on Patterned Heterogeneous Polystyrene Surface. *J Neurosci Methods.* 84: 193-204

Diaz-Nido, J., Ulloa, L., Sanchez, C., Avelia, J. 1996. The Role of the Cytoskeleton in the Morphological Changes Occuring During Neuronal Differentiation. *Cell and Developmental Biology.* 7: 733-9

Dodd, J., Jessell, T.M. 1988. Axon Guidance and the Patterning of Neuronal Projections in Vertebrates. *Science.* 242: 692-9

Droge, M.H., Gross, G.W., Hightower, M.H., Czisny, L.E. 1986. Multielectrode Analysis of Coordinated, Multisite, Rhythmic Bursting in Cultured Cns Monolayer Networks. *J Neurosci.* 6: 1583-92

Edgerton, V.R., Tillakaratne, N.J., Bigbee, A.J., de Leon, R.D., Roy, R.R. 2004. Plasticity of the Spinal Neural Circuitry after Injury. *Annu Rev Neurosci.* 27: 145-67

Engel, J. 1992. Laminins and Other Strange Proteins? *Biochemistry.* 31: 10643-51

Fan, Y.W., Cui, F.Z., Chen, L.N., Zhai, Y., Xu., Q.Y., Lee, I.-S. 2002a. Adhesion of Neural Cells on Silicon Wafer with Nano-Topographic Surface. *Applied Surface Science.* 187: 313-8

Fan, Y.W., Cui, F.Z., Hou, S.P., Xu, Q.Y., Chen, L.N., Lee, I.S. 2002b. Culture of Neural Cells on Silicon Wafers with Nano-Scale Surface Topograph. *J Neurosci Methods.* 120: 17-23

Forscher, P., Smith, S.J. 1988. Actions of Cytochalasins on the Organization of Actin Filaments and Microtubules in a Neuronal Growth Cone. *J Cell Biol.* 107: 1505-16

Fromherz, P. 2003. Semiconductor Chips with Ion Channels, Nerve Cells and Brain. *Physica E.* 16: 24–34

Gallagher, J.O., McGhee, K.F., Wilkinson, C.D., Riehle, M.O. 2002. Interaction of Animal Cells with Ordered Nanotopography. *IEEE Trans Nanobioscience.* 1: 24-8

Goldner, J.S., Bruder, J.M., Li, G., Gazzola, D., Hoffman-Kim, D. 2006. Neurite Bridging across Micropatterned Grooves. *Biomaterials.* 27: 460-72

Gross, G.W., Harsch, A., Rhoades, B.K., Gopel, W. 1997. Odor, Drug and Toxin Analysis with Neuronal Networks in Vitro: Extracellular Array Recording of Network Responses. *Biosens Bioelectron.* 12: 373-93

Grunwald, I.C., Klein, R. 2002. Axon Guidance: Receptor Complexes and Signaling Mechanisms. *Curr Opin Neurobiol.* 12: 250-9

Guthrie, S. 2001. Axon Guidance: Robos Make the Rules. *Curr Biol.* 11: R300-3

Gutierrez-Galvez, A., Gutierrez-Osuna, R. 2003. Pattern Completion through Phase Coding in Population Neurodynamics. *Neural Netw.* 16: 649-56

Haastert, K., Grosskreutz, J., Jaeckel, M., Laderer, C., Bufler, J., et al. 2005. Rat Embryonic Motoneurons in Long-Term Co-Culture with Schwann Cells-a System to Investigate Motoneuron Diseases on a Cellular Level in Vitro. *J Neurosci Methods.* 142: 275-84

Harsch, A., Ziegler, C., Gopel, W. 1997. Strychnine Analysis with Neuronal Networks in Vitro: Extracellular Array Recording of Network Responses. *Biosens Bioelectron.* 12: 827-35

He, W., Bellamkonda, R.V. 2005. Nanoscale Neuro-Integrative Coatings for Neural Implants. *Biomaterials.* 26: 2983-90

Heller, D.A., Garga, V., Kelleher, K.J., Lee, T.C., Mahbubani, S., et al. 2005. Patterned Networks of Mouse Hippocampal Neurons on Peptide-Coated Gold Surfaces. *Biomaterials.* 26: 883-9

Hempel, C.M., Sugino, K., Nelson, S.B. 2002. Multi-Unit Spike-Triggered Averaging: A Method for Probing the Physiology of Central Synapses. *J Neurosci Methods.* 120: 121-9

Hivert, B., Liu, Z., Chuang, C.Y., Doherty, P., Sundaresan, V. 2002. Robo1 and Robo2 Are Homophilic Binding Molecules That Promote Axonal Growth. *Mol Cell Neurosci.* 21: 534-45

Holmes, O. 1990. *Human Neurophysiology: A Student Text. 2nd Ed.* London: Chapman & Hall Medical

Igelmund, P., Fleischmann, B.K., Fischer, I.R., Soest, J., Gryshchenko, O., et al. 1999. Action Potential Propagation Failures in Long-Term Recordings from Embryonic Stem Cell-Derived Cardiomyocytes in Tissue Culture. *Pflugers Arch.* 437: 669-79

Jahnsen, H., Kristensen, B.W., Thiebaud, P., Noraberg, J., Jakobsen, B., et al. 1999. Coupling of Organotypic Brain Slice Cultures to Silicon-Based Arrays of Electrodes. *Methods.* 18: 160-72

James, C.D., Davis, R.C., Kam, L., Craighead, H.G., Isaacson, M., et al. 1998. Patterned Protein Layers on Solid Substrates by Thin Stamp Microcontact Printing. *Langmuir.* 14: 741-4

James, C.D., Davis, R., Meyer, M., Turner, A., Turner, S., et al. 2000. Aligned Microcontact Printing of Micrometer-Scale Poly-L-Lysine Structures for Controlled Growth of Cultured Neurons on Planar Microelectrode Arrays. *IEEE Trans Biomed Eng.* 47: 17-21

James, C.D., Spence, A.J., Dowell-Mesfin, N.M., Hussain, R.J., Smith, K.L., et al. 2004. Extracellular Recordings from Patterned Neuronal Networks Using Planar Microelectrode Arrays. *IEEE Trans Biomed Eng.* 51: 1640-8

Jessen, K.R. 2004. Glial Cells. *Int J Biochem Cell Biol.* 36: 1861-7

Jimbo, Y., Kasai, N., Torimitsu, K., Tateno, T., Robinson, H.P. 2003. A System for Mea-Based Multisite Stimulation. *IEEE Trans Biomed Eng.* 50: 241-8

Jimbo, Y., Tateno, T., Robinson, H.P. 1999. Simultaneous Induction of Pathway-Specific Potentiation and Depression in Networks of Cortical Neurons. *Biophys J.* 76: 670-8

Johansson, F., Carlberg, P., Danielsen, N., Montelius, L., Kanje, M. 2006. Axonal Outgrowth on Nano-Imprinted Patterns. *Biomaterials.* 27: 1251-8

Kam, L., Boxer, S.G. 2001. Cell Adhesion to Protein-Micropatterned-Supported Lipid Bilayer Membranes. *J Biomed Mater Res.* 55: 487-95

Kane, R.S., Takayama, S., Ostuni, E., Ingber, D.E., Whitesides, G.E. 1999. Patterning Proteins and Cells Using Soft Lithography. *Biomaterials.* 20: 2363-76

Kashimura, Y., Nakashima, H., Furukawa, K., Torimitsu, K. 2003. Fabrication of Nano-Gap Electrodes Using Electroplating Technique. *Thin Solid Films.* 438 –439: 317–21

Kendal, E.R., Schwartz, J.H., Jessell, T.M. 2000. Principles of Neuroscience.

Khan, S.P., Auner, G.G., Newaz, G.M. 2005. Influence of Nanoscale Surface Roughness on Attachment on Silicon. *Nanomedicine.* 1: 125-9

Kingsley, R.E. 2000. *Concise Text of Neuroscience*. Philadelphia: Lippincott Williams and Wilkins

Kleinfield, D., Kahler, K.H., Hockberger, P.E. 1988. Controlled Growth of Dissociated Neurons on Patterned Substrates. *J Neurosci.* 8: 4098-120

Kobbert, C., Appsb, R., Bechmannc, I., Lanciegod, J.L., Meye, J., Thanosa, S. . 2000. Current Concepts in Neuroanatomical Tracing. *Progress in Neurobiology.* 62: 327-51

Krause, G., Lehmann, S., Lehmann, M., Freund, I., Schreiber, E., Baumann, W. 2006. Measurement of Electrical Activity of Long-Term Mammalian Neuronal Networks on Semiconductor Neurosensor Chips and Comparison with Conventional Microelectrode Arrays. *Biosens Bioelectron.* 21: 1272-82

Kuffler, S.K., Nicholls, J.G., Martin, A.R. 1984. *From Neuron to Brain.* Sunderland, Massachusetts: Sinauer Associates Inc.

Lacquaniti, F., Grasso, R., Zago, M. 1999. Motor Patterns in Walking. *News Physiol Sci.* 14: 168-74

Latham, P.E., Richmond, B.J., Nirenberg, S., Nelson, P.G. 2000. Intrinsic Dynamics in Neuronal Networks. Ii. Experiment. *J. Neurophysiol.* 83: 828–35

Lauer, L., Klein , C., Offenhausser, A. 2001a. Spot Compliant Neuronal Networks by Structure Optimized Micro-Contact Printing. *Biomaterials.* 22: 1925-32

Lauer, L., Ingebrandt, S., Scholl, M., Offenhausser, A. 2001b. Aligned Microcontact Printing of Biomolecules on Microelectronic Device Surfaces. *IEEE Trans Biomed Eng.* 48: 838-42

Lauer, L., Vogt, A., Yeung, C.K., Knoll, W., Offenhausser, A. 2002. Electrophysiological Recordings of Patterned Rat Brain Stem Slice Neurons. *Biomaterials.* 23: 3123-30

Lavedan, C., Buchholtz, S., Nussbaum, R.L., Albin, R.L., Polymeropoulos, M.H. 2002. A Mutation in the Human Neurofilament M Gene in Parkinson's Disease That Suggests a Role for the Cytoskeleton in Neuronal Degeneration. *Neurosci Lett.* 322: 57-61

Le Roux, P.D., Reh, T.A. 1994. Regional Differences in Glial-Derived Factors That Promote Dendritic Outgrowth from Mouse Cortical Neurons in Vitro. *J Neurosci.* 14: 4639-55

Le Roux, P.D., Reh, T.A. 1995. Independent Regulation of Primary Dendritic and Axonal Growth by Maturing Astrocytes in Vitro. *Neurosci Lett.* 198: 5-8

Letournel, F., Bocquet, A., Perrot, R., Dechaume, A., Guinut, F., et al. 2006. Neurofilament High Molecular Weight-Green Fluorescent Protein Fusion Is Normally Expressed in Neurons and Transported in Axons: A Neuronal Marker to Investigate the Biology of Neurofilaments. *Neuroscience.* 137: 103-11

Levitan, I.B., Kaczmarek, L. K. 2002 *The Neuron: Cell and Molecular Biology.* New York: Oxford University Press

Lewis, A.K., Bridgman, P.C. 1992. Nerve Growth Cone Lamellipodia Contain Two Populations of Actin Filaments That Differ in Organization and Polarity. *J Cell Biol.* 119: 1219-43

Liu, L., Sheardown, H. 2005. Glucose Permeable Poly (Dimethyl Siloxane) Poly (N-Isopropyl Acrylamide) Interpenetrating Networks as Ophthalmic Biomaterials. *Biomaterials.* 26: 233-44

Luo, L. 2002. Actin Cytoskeleton Regulation in Neuronalmorphogenisis and Structural Plasticity. *Annu. Rev. Cell Dev. Biol.* 18: 601–35

Mahoney, M.J., Anseth, K.S. 2006. Three-Dimensional Growth and Function of Neural Tissue in Degradable Polyethylene Glycol Hydrogels. *Biomaterials.* 27: 2265-74

Mahoney, M.J., Chen, R.R., Tan, J., Saltzman, W.M. 2005. The Influence of Microchannels on Neurite Growth and Architecture. *Biomaterials.* 26: 771-8

Mallavarapu, A., Mitchison, T. 1999. Regulated Actin Cytoskeleton Assembly at Filopodium Tips Controls Their Extension and Retraction. *J Cell Biol.* 146: 1097-106

Martines, E., Seunarine, K., Morgan, H., Gadegaard, N., Wilkinson, C.D., Riehle, M.O. 2005. Superhydrophobicity and Superhydrophilicity of Regular Nanopatterns. *Nano Lett.* 5: 2097-103

Martinoia, S., Bonzano, L., Chiappalone, M., Tedesco, M. 2005. Electrophysiological Activity Modulation by Chemical Stimulation in Netorks of Cortical Neurons Coupled to Microelectrode Arrays:A Biosensor for Neuropharmacological Applications. *Sensors and Actuators B.* 108: 589-69

Matsuzawa, M., Liesi, P., Knoll, W. 1996. Chemically Modifying Glass Surfaces to Study Substratum-Guided Neurite Outgrowth in Culture. *J Neurosci Methods.* 69: 189-96

Miller, C., Shanks, H., Witt, A., Rutkowski, G., Mallapragada, S. 2001. Oriented Schwann Cell Growth on Micropatterned Biodegradable Polymer Substrates. *Biomaterials.* 22: 1263-9

Miller, F.D., Kaplan, D.R. 2003. Signaling Mechanisms Underlying Dendrite Formation. *Current Opinion in Neurobiology.* 13: 391–8

Moore, M.J., Friedman, J.A., Lewellyn, E.B., Mantila, S.M., Krych, A.J., et al. 2006. Multiple-Channel Scaffolds to Promote Spinal Cord Axon Regeneration. *Biomaterials.* 27: 419-29

Morefield, S.I., Keefer, E.W., Chapman, K.D., Gross, G.W. 2000. Drug Evaluations Using Neuronal Networks Cultured on Microelectrode Arrays. *Biosens Bioelectron.* 15: 383-96

Mueller, B.K. 1999. Growth Cone Guidance: First Steps Towards a Deeper Understanding. *Annu Rev Neurosci.* 22: 351-88

Muller, H.W., Junghans, U., Kappler, J. 1995. Astroglial Neurotrophic and Neurite-Promoting Factors. *Pharmacol Ther.* 65: 1-18

Novellino, A., Chiappalone, M., Vato, A., Bove, M., Tedesco, M.B., Martinoia, S. 2003. Behaviours from an Electrically Stimulated Spinal Cord Neural Network Cultured on Microelectrode Arrays. *Neurocomputing.* 52-54: 661-9

Novikov, L.N., Novikova, L.N., Mosahebi, A., Wiberg, M., Terenghi, G., Kellerth, J.O. 2002. A Novel Biodegradable Implant for Neuronal Rescue and Regeneration after Spinal Cord Injury. *Biomaterials.* 23: 3369-76

Orike, N., Thrasivoulou, C., Cowen, T. 2001. Serum-Free Culture of Dissociated, Purified Adult and Aged Sympathetic Neurons and Quantitative Assays of Growth and Survival. *J Neurosci Methods.* 106: 153-60

Pannese, E. 1994. *Neurocytology- the Fine Structure of Neurons, Nerve Processes and Neuroglial Cells.* Stuttgart: Thieme Medical Publishers Inc.

Parsons, A.M., el-Fakahany, E.E., Seybold, V.S. 1995. Tachykinins Alter Inositol Phosphate Formation, but Not Cyclic Amp Levels, in Primary Cultures of Neonatal Rat Spinal Neurons through Activation of Neurokinin Receptors. *Neuroscience.* 68: 855-65

Pasterkamp, R.J., Kolodkin, A.L. 2003. Semaphorin Junction: Making Tracks toward Neural Connectivity. *Curr Opin Neurobiol.* 13: 79-89

Pfrieger, F.W., Barres, B.A. 1996. New Views on Synapse-Glia Interactions. *Curr Opin Neurobiol.* 6: 615-21

Phillips, C.A., Gallimore, J.J., Hendershot, D.M. 1995. Walking When Utilizing a Sensory Feedback System and an Electrical Muscle Stimulation Gait Orthosis. *Med Eng Phys.* 17: 507-13

Potember, R., Matsuzawa, M., Liesi, P. 1998. Conducting Networks from Cultures Cells on Self Assembled Monolayers. *Synthetic Metals.* 1997-9

Potter, S.M., DeMarse, T.B. 2001. A New Approach to Neural Cell Culture for Long-Term Studies. *Journal of Neuroscience Methods.* 110: 17–24

Powell, E.M., Meiners, S., DiProspero, N.A., Geller, H.M. 1997. Mechanisms of Astrocyte-Directed Neurite Guidance. *Cell Tissue Res.* 290: 385-93

Quist, A.P., Pavlovic, E., Oscarsson, S. 2005. Recent Advances in Microcontact Printing. *Anal Bioanal Chem.* 381: 591-600

Rader, C., Stoeckli, E.T., Ziegler, U., Osterwalder, T., Kunz, B., Sonderegger, P. 1993. Cell-Cell Adhesion by Homophilic Interaction of the Neuronal Recognition Molecule Axonin-1. *Eur J Biochem.* 215: 133-41

Rajnicek, A., Britland, S., McCaig, C. 1997. Contact Guidance of Cns Neurites on Grooved Quartz: Influence of Groove Dimensions, Neuronal Age and Cell Type. *J Cell Sci.* 110 (Pt 23): 2905-13

Ramrus, D.A., Berg, J.C. 2006. Enhancement of Adhesion to Heterogeneously Patterned Substrates. *Colloids and Surfaces A: Physiochem.Eng.Aspects.* 273: 84-9

Ravenscroft, M.S., Bateman, K.E., Shaffer, K.M., Schessler, H.M., Jung, D.R., et al. 1998. Developmental Neurobiology Implications from Fabrication and Analysis of Hippocampal Neuronal Networks on Patterned Silane-Modified Surfaces. *J. Am. Chem. Society.* 120: 12169-77

Recknor, J.B., Sakaguchi, D.S., Mallapragada, S.K. 2006. Directed Growth and Selective Differentiation of Neural Progenitor Cells on Micropatterned Polymer Substrates. *Biomaterials.* 27: 4098-108

Roelandse, M., Welman, A., Wagner, U., Hagmann, J., Matus, A. 2003. Focal Motility Determines the Geometry of Dendritic Spines. *Neuroscience.* 121: 39-49

Roll, E.T., Treves, A. 1998. Neural Networks and Brain Function. New York: Oxford University Press

Sanchez, C., Diaz-Nido, J., Avila, J. 2000. Phosphorylation of Microtubule-Associated Protein 2 (Map2) and Its Relevance for the Regulation of the Neuronal Cytoskeleton Function. *Prog Neurobiol.* 61: 133-68

Sandison, M., Curtis, A.S., Wilkinson, C.D. 2002. Effective Extra-Cellular Recording from Vertebrate Neurons in Culture Using a New Type of Micro-Electrode Array. *J Neurosci Methods.* 114: 63-71

Schmalenberg, K.E., Buettner, H.M., Uhrich, K.E. 2004. Microcontact Printing of Proteins on Oxygen Plasma-Activated Poly(Methyl Methacrylate). *Biomaterials.* 25: 1851-7

Scholl, M., Sprossler, C., Denyer, M., Krause, M., Nakajima, K., et al. 2000. Ordered Networks of Rat Hippocampal Neurons Attached to Silicon Oxide Surfaces. *J Neurosci Methods.* 104: 65-75

Scholze, A., Gotz, B., Faissner, A. 1996. Glial Cell Interactions with Tenascin-C: Adhesion and Repulsion to Different Tenascin-C Domains Is Cell Type Related. *Int J Dev Neurosci.* 14: 315-29

Segev, I., London, M. 2000. Untangling Dendrites with Quantitative Models. *Science.* 290: 744-50

Selinger, J.V., Pancrazio, J.J., Gross, G.W. 2004. Measuring Synchronization in Neuronal Networks for Biosensor Applications. *Biosens Bioelectron.* 19: 675-83

Seunarine, K., Geadegaard, N., Riehle, M.O., Wilkison, C.D.W. 2006. Opitimal Heating for Short Hot Embossing Cycles. *Microelectronic Engineering.* 83: 859-63

Sgarbi, N., Pisignano, D., Di Benedetto, F., Gigli, G., Cingolani, R., Rinaldi, R. 2004. Self-Assembled Extracellular Matrix Protein Networks by Microcontact Printing. *Biomaterials.* 25: 1349-53

Shahaf, G., Marom, S. 2001. Learning in Networks of Cortical Neurons. *J Neurosci.* 21: 8782-8

Skaper, S.D., Moore, S.E., Walsh, F.S. 2001. Cell Signalling Cascades Regulating Neuronal Growth-Promoting and Inhibitory Cues. *Prog Neurobiol.* 65: 593-608

Smith, A., Gervasi, C., Szaro, B.G. 2006. Neurofilament Content Is Correlated with Branch Length in Developing Collateral Branches of Xenopus Spinal Cord Neurons. *Neurosci Lett.* 403: 283-7

Smith, R., Lewis, P., Weiss, P. 2004. Patterned Self-Assembled Monolayers. *Progress in Surface Science.* 75: 1-68

Sobeih, M.M., Corfas, G. 2002. Extracellular Factors That Regulate Neuronal Migration in the Central Nervous System. *Int J Dev Neurosci.* 20: 349-57

Sorribas, H., Braun, D., Leder, L., Sonderegger, P., Tiefenauer, L. 2001. Adhesion Proteins for a Tight Neuron-Electrode Contact. *J Neurosci Methods.* 104: 133-41

Sorribas, H., Padeste, C., Tiefenauer, L. 2002. Photolithographic Generation of Protein Micropatterns for Neuron Culture Applications. *Biomaterials.* 23: 893-900

Spence, A.J., Hoy, R.R., Isaacson, M.S. 2003. A Micromachined Silicon Multielectrode for Multiunit Recording. *J Neurosci Methods.* 126: 119-26

Sprossler, C., Schollb, M., Denyerc, M.C., Krausea, M., Nakajimac, K., , Maelickeb, A., Knolla, W., Offenhausser, A. 2001. Model Network Architectures in Vitro on Extracellular Recording Systems Using Microcontact Printing. *Synthetic Metals.* 117: 281-3

St John, P.M., Kam, L., Turner, S.W., Craighead, H.G., Issacson, M., et al. 1997. Preferential Glial Cell Attachment to Microcontact Printed Surfaces. *J Neurosci Methods.* 75: 171-7

Stenger, D.A., Hickman, J.J., Bateman, K.E., Ravenscroft, M.S., Ma, W., et al. 1998. Microlithographic Determination of Axonal/Dendritic Polarity in Cultured Hippocampal Neurons. *J Neurosci Methods.* 82: 167-73

Stoeckli, E.T., Kuhn, T.B., Duc, C.O., Ruegg, M.A., Sonderegger, P. 1991. The Axonally Secreted Protein Axonin-1 Is a Potent Substratum for Neurite Growth. *J Cell Biol.* 112: 449-55

Stoeckli, E.T., Landmesser, L.T. 1998. Axon Guidance at Choice Points. *Curr Opin Neurobiol.* 8: 73-9

Stokols, S., Tuszynski, M.H. 2004. The Fabrication and Characterization of Linearly Oriented Nerve Guidance Scaffolds for Spinal Cord Injury. *Biomaterials.* 25: 5839-46

Streit, J., Tscherter, A., Heuschkel, M.O., Renaud, P. 2001. The Generation of Rhythmic Activity in Dissociated Cultures of Rat Spinal Cord. *European Journal of Neuroscience.* 14: 191-202

Suter, D.M., Errante, L.D., Belotserkovsky, V., Forscher, P. 1998. The Ig Superfamily Cell Adhesion Molecule, Apcam, Mediates Growth Cone Steering by Substrate-Cytoskeletal Coupling. *J Cell Biol.* 141: 227-40

Takahashi, H., Sekino, Y., Tanaka, S., Mizui, T., Kishi, S., Shirao, T. 2003. Drebrin-Dependent Actin Clustering in Dendritic Filopodia Governs Synaptic Targeting of Postsynaptic Density-95 and Dendritic Spine Morphogenesis. *J Neurosci.* 23: 6586-95

Tateno, T., Kawana, A., Jimbo, Y. 2002. Analytical Characterization of Spontaneous Firing in Networks of Developing Rat Cultured Cortical Neurons. *Phys Rev E Stat Nonlin Soft Matter Phys.* 65: 051924

Theodosis, D.T., Piet, R., Poulain, D.A., Oliet, S.H. 2004. Neuronal, Glial and Synaptic Remodeling in the Adult Hypothalamus: Functional Consequences and Role of Cell Surface and Extracellular Matrix Adhesion Molecules. *Neurochem Int.* 45: 491-501

Uemura, E., Carriquiry, A., Kliemann, W., Goodwin, J. 1995. Mathematical Modeling of Dendritic Growth in Vitro. *Brain Res.* 671: 187-94

Ullian, E.M., Harris, B.T., Wu, A., Chan, J.R., Barres, B.A. 2004. Schwann Cells and Astrocytes Induce Synapse Formation by Spinal Motor Neurons in Culture. *Mol Cell Neurosci.* 25: 241-51

van Ooyen, A., Duijnhouwer, J., Remme, M.W., van Pelt, J. 2002. The Effect of Dendritic Topology on Firing Patterns in Model Neurons. *Network.* 13: 311-25

van Pelt, J., Schierwagen, A. 2004. Morphological Analysis and Modeling of Neuronal Dendrites. *Math Biosci.* 188: 147-55

van Pelt, J., van Ooyen, A., Uylings, H.B. 2001. The Need for Integrating Neuronal Morphology Databases and Computational Environments in Exploring Neuronal Structure and Function. *Anat Embryol (Berl).* 204: 255-65

Vernadakis, A. 1996. Glia-Neuron Intercommunications and Synaptic Plasticity. *Prog Neurobiol.* 49: 185-214

Verschueren, H. 1985. Interference Reflection Microscopy in Cell Biology: Methodology and Applications. *J Cell Sci.* 75: 279-301

Vetter, P., Roth, A., Hausser, M. 2001. Propagation of Action Potentials in Dendrites Depends on Dendritic Morphology. *J Neurophysiol.* 85: 926-37

Vogt, A.K., Brewer, G.J., Decker, T., Bocker-Meffert, S., Jacobsen, V., et al. 2005a. Independence of Synaptic Specificity from Neuritic Guidance. *Neuroscience.* 134: 783-90

Vogt, A.K., Brewer, G.J., Offenhausser, A. 2005b. Connectivity Patterns in Neuronal Networks of Experimentally Defined Geometry. *Tissue Eng.* 11: 1757-67

Vogt, A.K., Lauer, L., Knoll, W., Offenhausser, A. 2003. Micropatterned Substrates for the Growth of Functional Neuronal Networks of Defined Geometry. *Biotechnol Prog.* 19: 1562-8

Vogt, A.K., Stefani, F.D., Best, A., Nelles, G., Yasuda, A., et al. 2004. Impact of Micropatterned Surfaces on Neuronal Polarity. *J Neurosci Methods.* 134: 191-8

Vogt, A.K., Wrobel, G., Meyer, W., Knoll, W., Offenhausser, A. 2005c. Synaptic Plasticity in Micropatterned Neuronal Networks. *Biomaterials.* 26: 2549-57

Wagenaar, D.A., Madhavan, R., Pine, J., Potter, S.M. 2005. Controlling Bursting in Cortical Cultures with Closed-Loop Multi-Electrode Stimulation. *J Neurosci.* 25: 680-8

Walsh, F.S., Doherty, P. 1996. Cell Adhesion Molecules and Neuronal Regeneration. *Curr Opin Cell Biol.* 8: 707-13

Wheeler, B.C., Corey, J.M., Brewer, G.J., Branch, D.W. 1999. Microcontact Printing for Precise Control of Nerve Cell Growth in Culture. *J Biomech Eng.* 121: 73-8

Wilkinson, C., Curtis, A. 1999. Networks of Living Cells. *Physics World.* 12: 45-8

Wojciak, B., Crossan, J., Curtis, A.S.G., Wilkinson, C.D.W. 1995. Grooved Substrata Facilitate *in Vitro* Healing of Completely Divided Flexor Tendons. *Journal of Materials Science: Materials in Medicine.* 6: 266-71

Yang, F., Murugan, R., Ramakrishna, S., Wang, X., Ma, Y.X., Wang, S. 2004. Fabrication of Nano-Structured Porous Plla Scaffold Intended for Nerve Tissue Engineering. *Biomaterials.* 25: 1891-900

Yang, F., Murugan, R., Wang, S., Ramakrishna, S. 2005. Electrospinning of Nano/Micro Scale Poly(L-Lactic Acid) Aligned Fibers and Their Potential in Neural Tissue Engineering. *Biomaterials.* 26: 2603-10

Yang, H., Xiao, Z.C., Becker, B., Hillenbrand, R., Rougon, G., Schachner, M. 1999. Role for Myelin-Associated Glycoprotein as a Functional Tenascin-R Receptor. *J Neurosci Res.* 55: 687-701

GLASGOW
UNI
LI

THESIS CONTAINS CD/DVD